ANDROGEN RECEPTOR *N*-TERMINAL DOMAIN ANTAGONISTS: SYNTHESIS, SAR, AND ANIMAL STUDIES

by

Daniel Golec

B.A., The University of Alberta, 2014

A THESIS SUBMITTED IN PARTIAL FULFILLMENT OF

THE REQUIREMENTS FOR THE DEGREE OF

MASTER OF SCIENCE

in

THE FACULTY OF GRADUATE AND POSTDOCTORAL STUDIES

(Chemistry)

THE UNIVERSITY OF BRITISH COLUMBIA

(Vancouver)

April 2022

The following individuals certify that they have read, and recommend to the Faculty of Graduate and Postdoctoral Studies for acceptance, the thesis entitled:

Androgen Receptor N-Terminal Domain Antagonists: Synthesis, SAR, and Animal Studies

submitted by   Daniel Golec   in partial fulfilment of the requirements for

the degree of   Master of Science

in   Chemistry

Examining Committee:

Raymond Andersen, Professor, Department of Chemistry, UBC

Supervisor

Katherine Ryan, Professor, Department of Chemistry, UBC

Supervisory Committee Member

Stephen Withers, Professor, Department of Chemistry, UBC

Supervisory Committee Member

Abstract

All current hormone therapies for prostate cancer (PC), including metastatic castration-resistant prostate cancer (mCRPC), target the androgen receptor (AR). The most effective treatments for mCRPC target the C-terminal ligand-binding domain (LBD) of the AR, which ultimately fail with resumed transcriptional activity. Another target, the AR N-terminal domain (NTD) contains activation function-1 (AF-1), which is essential for AR transcriptional activity. Blocking the AR AF-1 has the potential to by-pass AR-resistance mechanisms, including constitutively active AR splice variants (AR-V) that lack the LBD. New anti-androgen drug classes, ralaniten and sintokamides, have been shown to directly interact with the AR AF-1. Fluorination of the bisphenol-A (BPA) bridge allows for a flexible drug design imparting hydrophilicity without compromising the active drug.

Synthesis and biological evaluation of fluorinated ralaniten analogs, BU-86 **(2.24),** BU-87 **(2.25)**, was undertaken in order to investigate the activity of the chlorohydrin side-chain and whether or not the secondary hydroxyl group is necessary for active site drug binding. Fluorinated ralaniten ketone, BU-88 **(2.26),** and its potential degradation product, BU-89 **(2.33),** were investigated as the ketone functionality has the potential for reversible covalent binding. However, its chemical and metabolic stability is questionable, despite clear signs of potency *in vivo*. Sterically hindered tertiary alcohol analogs BU-130 **(2.45),** and BU-170 **(2.46)**, were investigated by introducing a methylated glycidol ether in the hope of achieving greater metabolic stability at no cost to potency. This modification is possible due to the enhanced solubility of bridge fluorinated BPA.

Sintokamide analogs LPY37 **(3.41)** and LPY36 **(3.42)** have previously been shown to inhibit transcription by splice variant driven PC cell lines *in vitro*, reducing the expression of prostate specific antigen (PSA). In order to study them further in an animal model, a scaled-up

synthesis was required. In order to have a more soluble sintokamide inspired drug, LPY80 **(3.51)** and LPY39 **(3.52)** were tested. The evaluation of the most potent ralaniten analog, BU-170 **(2.46)** and the most potent sintokamide analog LPY36 **(3.42)** in combination with enzalutamide is ongoing. These AR-NTD antagonists provide new insights into a novel therapy for the treatment of CRPC.

Lay Summary

The research described herein elaborates on a greater body of drug chemistry targeting the androgen receptor that has proven effectiveness for the treatment of prostate cancer and in particular its terminal form, metastatic castration resistant prostate cancer. The further development of effective drugs for the treatment of terminal prostate cancer has the potential to soften the burden that premature death has on communities and the families who are affected by them. The compounds described in this thesis represent new variations on the ralaniten and sintokamide AR NTD scaffolds that might aid the development of new therapies for prostate cancer. The drug candidates made in this thesis are shown to decrease tumor growth in murine models of mCRPC.

Preface

Chapter 2 is work done at UBC and the BC Cancer Agency. All synthetic routes to obtain ralaniten analogs were done by the author. All synthetic ralaniten compounds were synthesized and characterized by the author, including NMR spectroscopy and mass spectroscopy. The biological activity of the six synthetic analogs were performed and evaluated by Nasrin Mawji and Adrianna Banuelos, under the supervision of Dr. Marianne Sadar at the BC Cancer Agency (BCCA).

Chapter 3 is work done at UBC and the BC Cancer Agency. Previous work, including the synthesis and biological activity has been published. Isolation of Sintokamides A to E was done by Dr. David Williams in the Andersen Lab. All Synthetic routes were planned and executed by the author. All synthetic sintokamide compounds were synthesized and characterized by the author, including NMR spectroscopy. The biological activity for four synthetic analogs were evaluated by Nasrin Mawji and Adrianna Banuelos, under the supervision of Marianne Sadar at the BC Cancer Agency.

Table of Contents

List of Figures

List of Schemes

List of Symbols and Abbreviations

Δv – Chemical Shift Difference

δ – Chemical Shift

% – Percent

(±) – Racemic

µM – Micromole(s)

µm – Micrometer(s)

A.D – Anno Domini

ACE – Angiotensin-Converting Enzyme

ADT – Androgen Deprivation Therapy

ADME – Adsorption, Distribution, Metabolism, Excretion

AF-1 – Activation Function 1

AF-2 – Activation Function 2

AR – Androgen Receptor

ARE – Androgen Response Element

AR-V – Androgen Receptor Splice Variant

BADGE - Bis-phenol A Diglycidal Ether

BBB – Blood-Brain-Barrier

BCCA – British Columbia Cancer Agency

BnEt$_2$NHCl – Benzyldiethylammonium Chloride

BPA – Bisphenol-A

(Boc)$_2$O – Di-tert-butyl Dicarbonate

BrC$_3$H$_6$Cl – 1-Bromo-3-chloropropane

C$_{10}$H$_{12}$O$_3$S – (R)-Glycidyl Tosylate

CBP - CREB-Binding Protein

CDCl$_3$ – Deuterated Chloroform

CeCl$_3$ – Cerium (III) Chloride

CHCl$_3$ – Chloroform

CH$_3$SO$_2$NH$_2$ - Methyl Sulfonamide

ClogP – Octanol-Water Partition Coefficient

ClPh$_2$P - Chlorodiphenyl Phosphine

CRPC – Castration Resistant Prostate Cancer

COCONUTS - The Collection of Open Natural Products Database

Cs$_2$CO$_3$ – Cesium Carbonate

CuSO$_4$ – Copper Sulfate

d – doublet

dd – doublet of doublets

ddd – doublet of doublets of doublets

DCM – Dichloromethane

DIBAL-H – Diisobutylaluminum Hydride

DIEA – Diisopropylethyl Amine

DHT - Dihydrotestosterone

DMAP – 4-Dimethyl Amino Pyridine

DMF – Dimethylformamide

DMSO – Dimethyl Sulfoxide

DMSO-d6 – Deuterated Dimethyl Sulfoxide

DNA – Deoxyribonucleic Acid

DNB – DNA Binding Domain

EDC - 1-Ethyl-3-(3-dimethylaminopropyl) Carbodiimide

EFSA – European Food and Safety Authority

EPI - ESSA Active Pharmaceutical Ingredient

ESI – Electrospray Ionization

ER – Estrogen Receptor

Et$_3$N – Triethylamine

EtOAc – Ethyl Acetate

FL – Full Length

g – gram(s)

GR – Glucocorticoid Receptor

H$_2$O – Water

HBA – Hydrogen Bond Acceptor

HBD – Hydrogen Bond Donor

HCl – Hydrochloric Acid

Hex - Hexane

HNP – Halogenated Natural Product

HR – Hinge Region

HOBt - Hydroxybenzotriazole

HPLC - High Performance Liquid Chromatography

HRMS – High Resolution Mass Spectrometry

HSP – Heat Shock Protein

Hz – Hertz

IC$_{50}$ – Half-Maximal Inhibitory Concentration

ID – Injection Dose

IDR – Intrinsically Disordered Region

IL6 – Interleukin 6

J – Coupling Constant

Kg – Kilogram(s)

LBD – Ligand Binding Domain

LiOH – Lithium Hydroxide

LHRH – Luteinizing-Hormone Releasing-Hormone

LNCaP – Lymph Node Carcinoma of the Prosate

LRMS – Low Resolution Mass Spectrometry

K$_2$CO$_3$ – Potassium Carbonate

M – Mole per liter

m – Multiplet

mCPRC – Metastatic Castration Resistant Prostate Cancer

MeOH – Methanol

MeSH – Methyl Mercaptan

mL – milliliter

mg – Milligram(s)

mmol – millimole(s)

mol – mole(s)

mol/L – mole per liter

MHz – Mega Hertz

MNP – Marine Natural Product

Na₂SO₄ – Sodium Sulfate

NaHCO₃ – Sodium Bicarbonate

NaHSO₃ – Sodium Thiosulfate

NaH – Sodium Hydride

NaOH – Sodium hydroxide

NaOCl – Sodium Hypochlorite

NATH – N-substituted Arylthiohydantoin

NCS – N-chlorosuccinimide

NMR – Nuclear Magnetic Resonance

NP – Natural Product

NSAA – Non-Steroidal Anti-Androgen

NTD – N-Terminal Domain

Nuc – Nucleophile

Oxyma Pure - Ethyl cyano(hydroxyimino)acetate

PC – Prostate Cancer

PKA – Protein Kinase A

PR – Progesterone Receptor

PSA – Prostate Specific Antigen

PyBOP - Benzotriazol-1-yloxytripyrrolidinophosphonium Hexafluorophosphate

q – Quartet

Q-TOF – Quadrupole-Time of Flight

quin – Quintet

s - Singlet

SAR – Structure-Activity-Relationship

SCUBA - Self-contained Underwater Breathing Apparatus

Sc(OTf)₃ – Scandium (III) triflate

SINT1 – Sintokamide A

SM – Secondary Metabolites

SOCl₂ – Thionyl Chloride

STAT3 – Signal Transducer and Activator of Transcription 3

t – Triplet

TBAF – Tetrabutylammonium Fluoride

TFA – Trifluoroacetic Acid

THF - Tetrahydrofuran

TMSCHN₂ – Trimethylsilyldiazomethane

TMSCN – Trimethylsilylcyanide

TS-Cl – 4-Toluenesulfonyl Chloride

Acknowledgements

First and foremost, I'd like to thank my supervisor Dr. Raymond Andersen for giving me the opportunity to study marine natural products and their synthesis. My path to graduate school was not a straight trajectory and was only made possible by Raymond taking a chance on me, first as a technician, and secondly as a student. My fascination of natural products was nurtured under Raymond and my scientific understanding of them will be carried with me well into my future.

Secondly, I have to thank my lab mates, specifically Jack Kunzhong Jian, who was incredibly gracious with his time and knowledge and was always there to discuss synthetic strategy and NMR characterization. I also have to personally thank Benjamin Yeremy and Mostafa Hager who became my closest colleagues to discuss all matter of problems both personal and scientific.

Third, I have to thank my parents, Zbigniew and Elizabeth Golec, thank you for all your support and sacrifice. I would not be here today if not for you and my success it owed wholeheartedly for it. I appreciate all that you have done through thick and thin.

Last, but certainly not least, I have to thank my loving and supportive partner, Ashton Sturm. Her support over the last 11 years my life has been immeasurable and I look forward to many more years of conquering mountains and finally being done all together with graduate school. We finally get to move forward without one of us studying something!

I'm grateful for all your time. Thank you!

Dedication

I dedicate this thesis to the scientific endeavor and those who have contributed to it. Individually we play such a small role in human understanding, but together as one we contribute to its entirety.

Chapter 1: Introduction

1.1 History of Natural Products in Drug Discovery

Harnessing the natural environment to treat ailments and diseases has fascinated the human species throughout history. Speculation of natural product (NP) use dates back to Neanderthals, where an excavation of Shanidar IV (60,000 BCE) unearthed an ancient burial of flower pollen and willow bark.[1] *Cupressus sempervirens* (Cypress) and *Commiphora* species (Myrrh) were described on ancient Mesopotamian (2600 BCE) cuneiform tablets; the oils are still used to treat cough, cold, and inflammation. Morphine, the first industrialized NP, is perhaps the most famous (traced back to 2500 BCE). It was first isolated from *Papaver somniferum L.* (opium poppy) and Merck began commercial distribution in 1826. Subsequently, boiling crude morphine extract with acetic anhydride was used to produce heroin and simple methylation of morphine gave the medically relevant opiate codeine. Bayer produced the first semi-synthetic NP-based drug Aspirin (anti-inflammatory agent) in 1899 by acetylating salicin, an extract from the bark of the willow tree *Salix alba L.* Another highly impactful NP discovery was the antibiotic penicillin from the fungus *Pencillium notatum* by Fleming in 1929, which subsequently saw him share the Nobel prize in Medicine 1945 with Florey and Chain.[2] Quinine and artemisinin are NP anti-malarial drugs with the latter being isolated from *Artemisia annua* in 1972 by Tu Youyou (shared Nobel Prize 2015). Artemisinin has a history of use to treat malarial symptoms dating back to the Eastern Jin Dynasty (317 – 420 AD), first being described in Ge Hong's *Zhouhou Beiji Fang* (Handbook of Prescriptions for Emergencies).[3] Paclitaxel, an antineoplastic agent first isolated from bark of a Pacific Yew tree *Taxus brevifolia* in 1962, is approved for treatment of ovarian, breast, lung, and melanoma cancers. It was successfully

synthesized in 1994 by the Holton and Nicolaou laboratories to circumvent the incredibly inefficient and environmentally unfriendly process used to obtain paclitaxel from rare *T. brevifolia* extracts.[4] However, this synthesis and further 10 distinct synthetic pathways have not been able to achieve better yield output due to the complexity and length of producing Taxol.[5] Currently, its production for clinical use is dependent on the semi-synthesis that relies on the natural product 10-deacetylbaccatin III isolated from the leaves of the European Yew tree *Taxus baccata*.[6] The paclitaxel total and semi-synthesis is a great testament to how sophisticated nature is at synthesizing small molecules, making the laboratory challenge an exciting and difficult endeavor.

1.1.1 Natural Product Sources

The prevalence of the internet has enabled the creation of publicly accessible resource databases that aid the investigation of bio-active NPs with therapeutic potential. Open access to information allows for the rational design of new NPs for drug discovery, rather than the serendipitous discovery, by screening several parameters at once including history, folklore, toxicology, pharmacology, and availability. The latest estimate shows that ~470,000 NPs have been discovered, with the Dictionary of Natural Products database having physiochemical and biological properties, common names, literature references, molecular structures, and origins of ~300,000 NPs. ~195,000 of NPs are considered secondary metabolites (SMs) and 70% derive from plants, followed by animalia and microbial sources, respectively. Most importantly, there are now specific databases for geographical region of origin, disease, or use. This has streamlined researcher knowledge for NP novelty and application, allowing for easy open-source collaboration. The Collection of Open Natural Products Database (COCONUTS), which has

gathered all available NPs from all current open-source databases in one place (**Figure 1.1**), exemplifies the clarity seen when a researcher is looking at existing taxonomic provenance of NPs as well as their location.[7] However, with so many untapped natural sources for new therapeutic compounds, there is plenty of space for new exciting discoveries by simply looking at new source organisms.[8]

(Sorokina et al., n.d.)
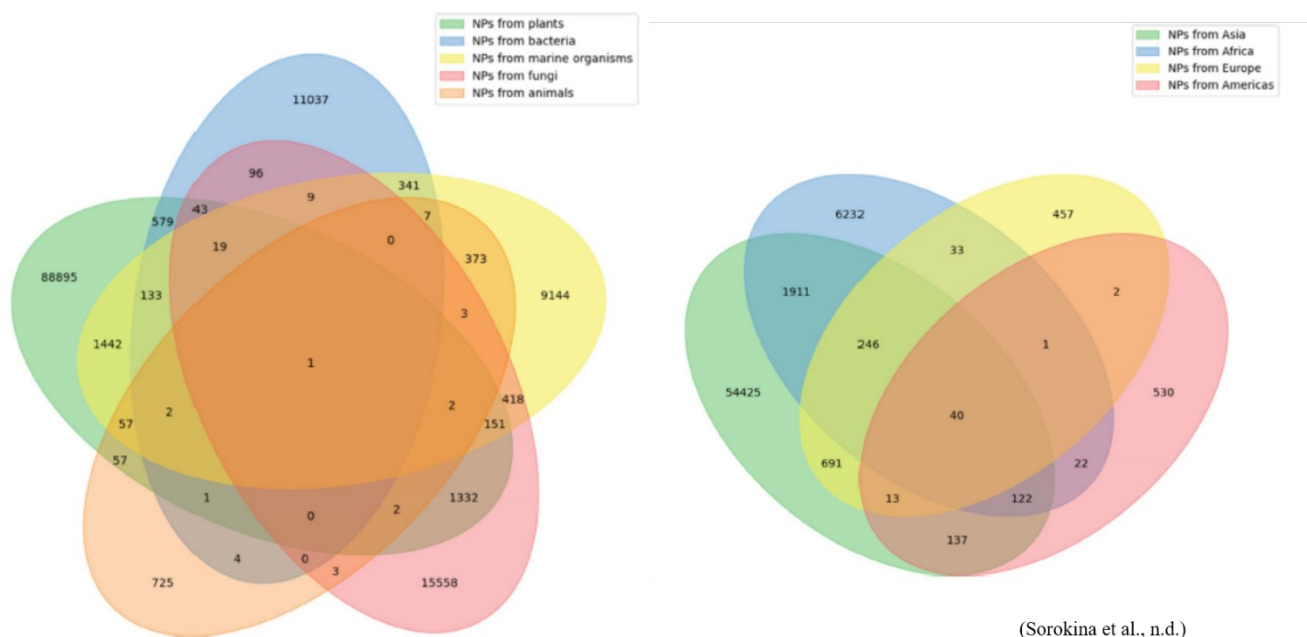
Figure 1.1 – NP taxonomic provenance (Left) and NP geographically location (Right).[7]

1.1.1.1 Plants

Terrestrial plants have been the source of many useful compounds and SMs with interesting biological and pharmacological properties. The most widely recognized NP-derived anticancer chemotherapeutic drugs have been sourced from terrestrial plants; these include topotecan, irinotecan, docetaxel, paclitaxel, etoposide, teniposide, vinblastine, vincristine, and vinorelbine.[9] Reserpine, **Figure 1.2**, needs mentioning for its contribution to alkaloid total

synthesis. Elucidation of the stereochemical configuration of reserpine in 1955 enabled studies

directed towards its total synthesis. The completion of this remarkable synthesis highlighted the

ability to build six-membered rings using the Diels-Alder reaction, as well as the substrate-

stereocontrolled reactions to build stereocenters around six-membered rings.[10] This synthesis

indirectly contributed to the total synthesis of camptothecin **(Figure 1.2),** which in turn gave us

the remarkable chemotherapeutic drugs topotecan and irinotecan. Exploration of the natural

products found in terrestrial plants has proven to be a fruitful endeavor and plant natural products

will continue to be explored further for their medicinal properties.
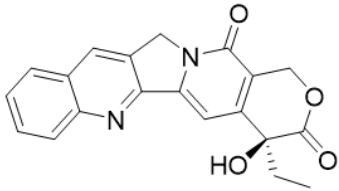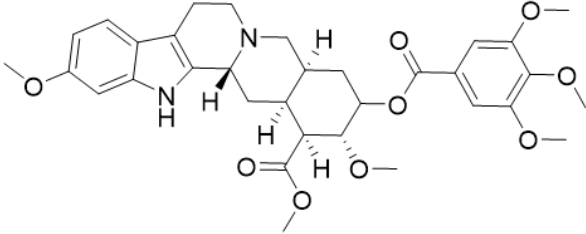
1.1 (±)-Camptothecin	1.2 (-)-Reserpine
• Topoisomerase inhibitor • Isolated from the bark and stem of the Chinese plant *Camptoteca acuminata* • Isolated in 1958 with structure determination in 1966 by M.E Wall and M.C. Wani • Total synthesis in 1971 by Stork and Schultz	• Antihypertensive • Extracted from the Indian snakeroot *Rauwolfia serpentina* • Isolated by Schlittler *et al.* in 1952 and the structure was determined in 1955 by Ciba group and number individual researchers • Total synthesis by R. B. Woodward in 1958

Figure 1.2 - Pharmaceutically active NPs from plant sources.

1.1.1.2 Animalia

The animal kingdom, where toxic defense mechanisms are common, has proven to be a rich source of NPs with medical relevancy. Snake venoms have shown great therapeutic benefits in small doses due to their toxic behavior. Captopril, an angiotensin-converting enzyme (ACE) inhibitor, is derived from the venom of the Brazilian pit viper snake *Bothrops jararaca*. Tirofiban and Eptifibatide are both antiplatelet drugs acting as glycoprotein IIb/IIIa inhibitors and can both be traced back to the venom of the saw scaled viper (*Echis carinatus)* and the pygmy rattlesnake *(Sistrurus miliarius),* respectively.[9]

1.1.1.3 Bacteria and Fungi

Bioactive SMs from microbial sources have become some of the most important drugs in clinical use. The door to antibiotic drug discovery in microorganisms was opened when penicillin was discovered in 1929. Subsequently, new related β-lactam antibiotics including norcardicin, imipenem, and aztreonam were discovered in fungal cultures. Other prominent microbial antibiotics that have saved countless lives are the glycopeptide vancomycin *(Amycolatopsis orientalis)* and the macrolide erythromycin *(Saccharopolyspora erythraea).*[9] Erythromycin (**Figure 1.3)** is an incredibly complex structure, whose aglycone erythronolide B contains 10 stereogenic centers, 5 consecutively, all present in a 14-membered ring lactone. This complex synthetic target saw the synthesis take place 29 years after the initial discovery by the Filipino scientist Abelardo B. Aguilar in 1952.[11] Other microbial NP drugs include doxorubicin (*Streptomyces peucetius)* and torreyanic acid *(Torreya taxifolia*), which have been used to treat acute leukemia, lung cancer, breast cancer, thyroid cancer, and Hodgkin's and non-Hodgkin's lymphomas.[9]
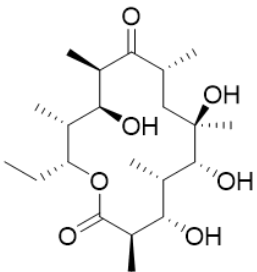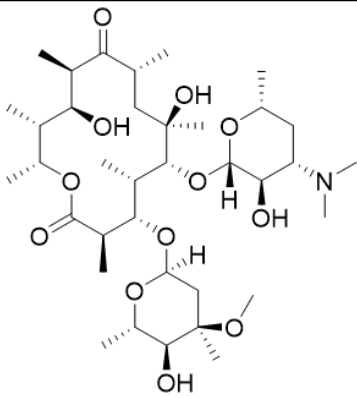
| 1.3 – Erythronolide B | 1.4 – Erythromycin A |

- Macrolide Antibiotic used to treat bacterial infection
- Isolated from metabolic products of *Saccharopolyspora erythraea,* formly *Stretomyces erythreus*
- Isolated and characterized in 1952 by Abelardo B. Aguilar and Eli Lilly and Company who cut the former out of the product discovery
- Total Synthesis of Erythronolide B was accomplished in 1978 by E. J. Corey
- Total Synthesis of Erythromycin A was accomplished in 1981 by R. B. Woodward

Figure 1.3 – Pharmaceutically relevant and active NPs from a bacterial source.

1.1.1.4   Marine Natural Products

The marine environment, which contains all of the above sources, was largely ignored as a NP source until the introduction of snorkeling and SCUBA in the 1960's. The ability to explore what covers roughly 70% of the earth has allowed the discovery of novel marine natural products (MNPs). The incredible size of the world's oceans means that only around 5% of all deep-sea life has been explored, which illustrates how many new MNPs may exist.[12] Interestingly, microorganisms seem to be the main bioactive NP source in marine environments, playing on their symbiotic relationship with marine invertebrate species including sponges, jellyfish, anemones, and corals. As of 2019, there have been 8 approved drugs (6 in the 21st century) derived from MNPs. The first two MNP drug leads to be discovered were nucleosides that came

from the Caribbean demosponge *Tectitethya crypta*, giving cytarabine for the treatment of leukemia and lymphoma, and the anti-viral agent vidarabine. The antineoplastic agent eribulin (**Figure 1.4**) used to treat breast cancer and liposarcoma, is a synthetic analog of halicondrin B that was isolated from sea sponge *Halicondria okadai*. It resulted from optimization of a key intermediate in the total synthesis of halicondrin B by Kishi and co-workers.[13] MNPs with the therapeutic potential to stop the proliferation of prostate cancer will be the focus of this thesis.

1.5 – Eribulin	**1.6 – Halichondrin B**

- Eribulin is an antineoplastic agent and is a NP derivative of Halichondrin B
- Halichondrin B was isolated from sea sponge *Halicondria okadai*
- Halichondrin B was isolated, characterized, and shown to have anti-cancer properties by Hirata and Uemura in 1986
- Total Synthesis of Halichondrin B was accomplished in 1992 by Yoshito Kishi and co-workers
- Total Synthesis of Eribulin was accomplished in 2001 by Eisai, who collaborated with Kishi using a remarkably active intermediate in Kishi's Synthesis

Figure 1.4 – Antineoplastic agents derived from MNPs.

1.2   Prostate Cancer

Prostate cancer (PC) is the most diagnosed cancer amongst men in the USA and Canada, with an estimated 248,530 and 24,000 new cases, respectively, expected for 2021. Survival rates have been improving due to early detection screening, but the expected mortality rates are estimated to be 34,130 and 4,500, respectively, for 2021.[14,15] Upon diagnosis, surgery

(prostatectomy) or radiation therapy can usually manage the malignancy, but advanced tumor progression requires more definitive treatment of androgen binding hormones. The androgen steroidal hormones play a key role in regulating prostate cancer tumor growth. Testosterone and dihydrotestosterone (DHT), the two most common androgens, are important for normal prostate function (**Figure 1.5**) and their tumor growth stimulating activities are mediated by the androgen receptor (AR). Without the presence of a ligand the AR typically associates with heat shock proteins (HSPs) that chaperone it into the cytoplasm of the cell allowing it combine with DHT. AR can then migrate to the cell nucleus and bind to specific enhancer regions of DNA known as androgen response elements (AREs). Recruitment of Coregulators completes the transcriptional complex, ultimately leading to gene expression and is the pathway in which PC leads to tumor growth. Utilizing a luteinizing-hormone-releasing hormone (LHRH) agonist for Androgen Deprivation Therapy (ADT) can typically cause a significant reduction in tumor growth, but in most cases the tumor will relapse to an androgen-refractory state. This assertion comes from rising serum prostate-specific antigen (PSA), suggesting the AR is reactivated, indicating the more potent phenotype, castration resistant prostate cancer (CRPC) has emerged.[16]
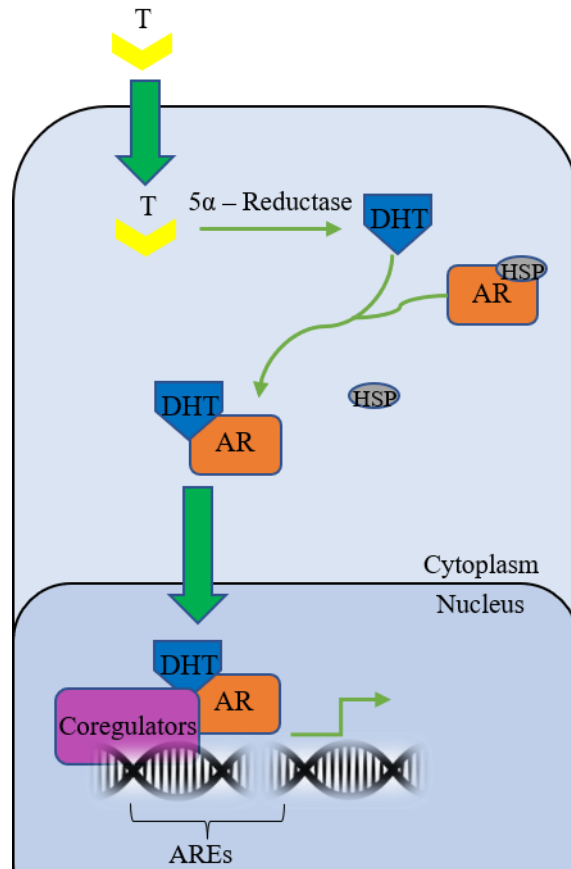
Figure 1.5 - Major androgen receptor signaling pathway in prostate cancer. Testosterone diffuses into the cell and is enzymatically converted to DHT. Upon binding to DHT, AR, which associates with HSPs translocates to the nucleus, binds to its target genes and regulates their expression, stimulating PC tumor growth.

1.2.1 The Androgen Receptor

The human AR is a nuclear transcription factor and an effector of androgen hormone biological activity. The AR gene is located on the X chromosome (q11-12) and consists of 8-exons. Full-length AR (FL-AR) can range in size from 910-919 amino acids due to the polymorphic nature of repeat units in the *N*-terminal domain (NTD). AR is comprised of 4

distinct regions (**Figure 1.6**), an intrinsically disordered NTD (547-556 residues), a folded DNA-binding domain (DBD, 65 residues), a disordered hinge region (HR; 49 residues), and a folded C-terminal ligand binding domain (249 residues; LBD).[17] Transcriptional activity is modulated through ligand independent (Tau 5) and dependent (Tau 1) activation function 1 (AF-1) within the NTD and ligand dependent activation function 2 (AF-2) within the LBD.[18] The LBD ligand binding pocket found along AF-2 is critical for the binding of androgens and is the direct and indirect target for all FDA-approved drugs currently in use against the AR.
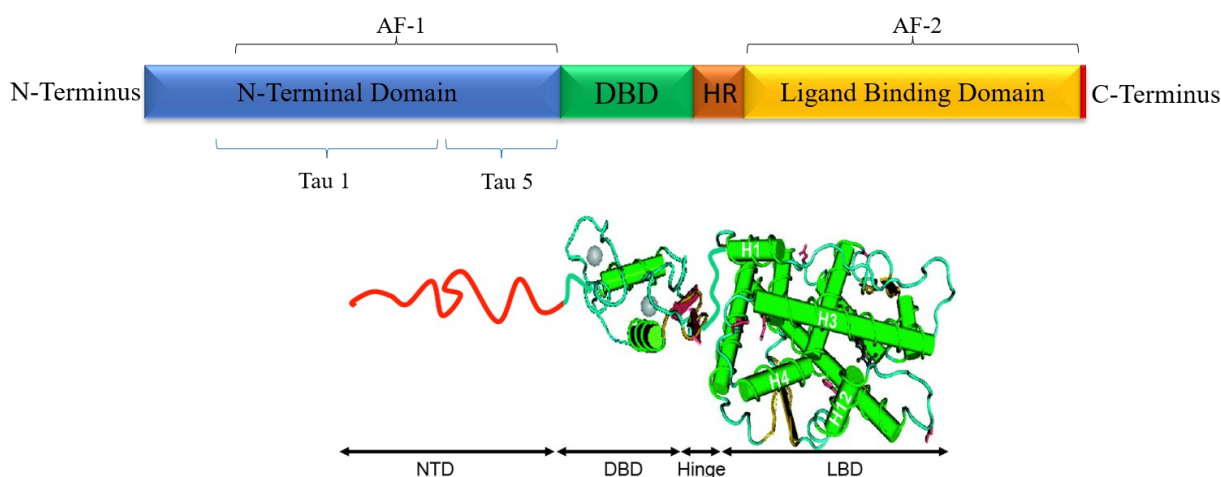
Figure 1.6 – The androgen receptor protein.

1.2.2   LBD-Therapies – Antiandrogens

If tumor progression persists upon first treatment (prostatectomy, radiation), then ADT will be enacted as a subsequent treatment. Prior to initiating antiandrogen drug treatment, patient's testicles are usually surgically (orchiectomy) or chemically (LHRH agonist) castrated in an effort to remove endogenous androgen production. If androgens continue to bind the AR, typically through adrenal gland steroid production, then CRPC phenotype has commenced and

the use of steroidal CYP17 inhibitor, abiraterone acetate, can be administered to prevent steroidogenesis. Eventually, androgens can overcome this blockage and non-steroidal antiandrogens (NSAAs) are required to out compete directly along the LBD ligand binding pocket. DHT has the highest endogenous androgen binding affinity (low nM) for the AR-LBD, meaning NSAAs must have a stronger binding affinity for the ligand binding pocket than DHT to be an efficacious option. By outcompeting androgens, a conformational change of the AR-LBD occurs, stopping transcriptional activity, alleviating tumor growth. Currently, NSAAs include first-generation drugs (**Figure 1.7)** bicalutamide, flutamide, and nilutamide, and second-generation drugs (**Figure 1.8**) enzalutamide, apalutamide, and darolutamide. Unfortunately, ADT only buys the patient time as resistance mechanisms can develop from these therapies which include: gain-of-function mutations of the AR which sees the antiandrogens begin behaving agonistically due to a transactivation of the LBD by other steroids, secondly, constitutively active AR splice variants (AR-V) occur that lack the LBD rendering current antiandrogens impotent with no ligand binding pocket to bind to. The net result is metastatic castration resistant prostate cancer (mCRPC), which once diagnosed gives men only 2-3 years to live. The AR is unique in that no transcriptional activity occurs in the LBD, but rather it resides in the NTD, so targeting this region is essential to effectively treat CRPC.[17]

1.2.2.1   First-Generation Drugs

1.2.2.1.1   Flutamide

Flutamide (**1.7**) (Figure 1.7) was the first FDA-approved NSAA drug to be used in conjunction with LHRH agonists for advanced mCRPC in 1989. The mechanism of action was

poorly understood and extensive clinical trials found no significant increase in life compared to steroidal antagonist alone (cyproterone acetate). It was also found that only 20% of patients receiving flutamide remained sexually active after 7 years. It's no longer considered a therapeutic due to efficacy and side-effect issues.[19]

1.2.2.1.2 Nilutamide

Nilutamide (**1.8**) is the successor to Flutamide. It increased metabolic stability, having a longer half-life in the body allowing for single daily dose administration. It's similar to Flutamide in structure, but the introduction of the N-substituted arylthiohydantoin (NATH) rendered a more metabolically stable compound. It unfortunately had similar efficacy issues seen in its predecessor (**1.7**), however, its discovery is significant as its NATH central structure became a focal point of subsequent second generation NSAAs.[20]

1.2.2.1.3 Bicalutamide

Bicalutamide (**1.9**) is the most investigated NSAA, with mixed results as a monotherapy. It currently shows a lower average life extension for mCRPC patients compared to ADT by 6 weeks. However, it has shown great benefit to a small population of patients that sees tumor regression from AR destabilization. It is still considered an alternative to the gold-standard ADT as a monotherapy without LHRH.[19]

1.7 - Flutamide   **1.8 - Nilutamide**   **1.9 - Bicalutamide**
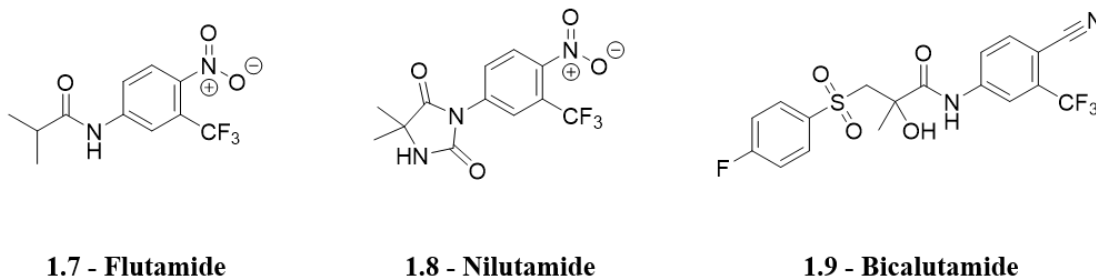
Figure 1.7 – First Generation NSAAs.

1.2.2.2   Second-Generation Drugs

1.2.2.2.1   Enzalutamide

Enzalutamide (**1.10**), a NATH, was discovered through structure activity relationships (SAR) optimization of first-generation NATH, RU-59063 (**1.11**).[21] RU-59063 was discovered through previous SAR studies of NATH candidate Nilutamide in an attempt to find a more AR selective NSAA than the first-generation candidate.[22] Although highly selective, its potency was insufficient which led to further SAR to increase potency culminating in the discovery of Enzalutmaide. Enzalutamide was found to have 5-8-fold increase (IC_{50} = 36 nM) in binding affinity to the AR-LBD compared to bicalutamide, closing the gap on DHT. Nuclear translocation of AR is repressed by enzalutamide, inhibiting DNA interaction through the use of co-activators. Most importantly it doesn't possess agonistic behavior and was found to be well-tolerated by patients. Unfortunately, enzalutamide is still fallible to AR mutation and AR-V and cannot be used effectively for advanced mCRPC.[23]

1.2.2.2.2   Apalutamide

Apalutamide (**1.12**) can be considered a successor to enzalutamide, as it has similar

properties and was produced through SAR to improve its potency and specificity. Binding

affinity for the LBD increased 7-10-fold (IC$_{50}$ = 16 nM) compared to bicalutamide and it was

shown to be more selective for the AR than other nuclear hormone receptors. Its lower dose

makes it more tolerable in patients and it doesn't easily permeate the blood-brain-barrier (BBB)

mitigating enzalutamide's propensity to trigger seizures in patients that require high doses.

Clinical trials have shown extension of life for patients with mCRPC on the order of 40 months,

an increase over two years without the use of NSAAs. However, just like other NSAAs that

target the AR-LBD, it is fallible to AR mutation to splice variants.[23]

1.10 Enzalutamide   **1.11 RU-59063**   **1.12 Apalutamide**
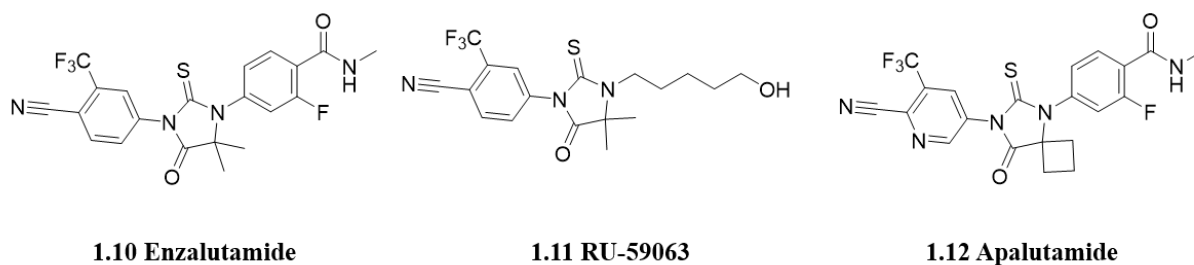
Figure 1.8 – Second Generation NSAAs.

1.2.3   AR-NTD – An Intrinsic Challenge

mCRPC shows the continued rise in PSA typical of earlier stages of PC. PSA is an

androgen-regulated gene specific to AR activation, meaning AR activity still exists despite the

blockage of androgens. Transcriptional activity still occurs via interleukin 6 (IL6) transduction

resulting in the binding of signal transducer and activator of transcription 3 (STAT3) and protein

kinase A (PKA) to the full-length AF-1 region of the NTD. This transactivation of the AR allows

14

for tumor growth proliferation despite the blockage of DHT to the AR. Blocking the full-length AF-1 and AR-V AF-1 is crucial to stopping mCRPC proliferation, although this is not trivial.[24] The NTD is a promiscuous target due its inherent lack of structure and limited secondary structure stability, making it an intrinsically disordered region (IDR). This means it can exist in a dynamic conformation with no stable binding site, so its conformation can vary depending on binding partner or protein environment. IDRs are a mixture of hydrophobic and charged amino acids, which allows for reversible non-covalent interactions with co-activating proteins, facilitating the signaling nature that is necessary for a transcription factor protein. Sequence similarity of the AR-NTD to other steroid hormone receptors is very low (<15%), meaning rational drug design will not be possible as very little structural information of the AR-NTD is known.[17]

1.2.4   AR-NTD – New Drug Candidates

In a joint effort that is specific to research done in Vancouver BC, the Sadar lab using the natural compound libraries of marine sponge and invertebrate extracts (Andersen lab) did an empirical study. A screening assay was developed that used an engineered lymph node Carcinoma of the Prostate (LNCaP) cell with a PSA gene linked to a luciferase reporter. LNCaP cells are androgen-sensitive human prostate adenocarcinoma cells, which inherently express endogenous AR that stimulate PSA expression. Upon castration, PSA mRNA continues to be up-regulated in an androgen-independent mechanism. By placing a luciferase reporter on the PSA promotor region, which contains AREs that depend on AR to promote induction, Sadar confirmed that PSA gene expression continued to increase upon binding synthetic androgen R1881 (**1.13**), **Figure 1.9**, or in the absence of androgen via forskolin (**1.14**) induced activation

of PKA or stimulation of the IL-6/Stat3 pathway. PKA transactivates the AR via the AR-NTD allowing for PC cell proliferation and, therefore, blocking the PSA-luciferase activity in the assay directly correlates to inhibiting the FL-AR function. Sadar used the assay to screen a large library of marine invertebrate extracts, which led to the discovery of three compound classes (Niphatenones, sintokamides, and ralaniten) that work by directly interacting with the AR-NTD.[17,25] These AR-NTD antagonists for CRPC are formally referred to as the "anitens". The work of this thesis will discuss the potential of new analogs of the sintokamides and ralaniten that were evaluated in animal studies as therapeutic agents or imaging agents to help understand the SAR for these compound families that bind to the AR-NTD.
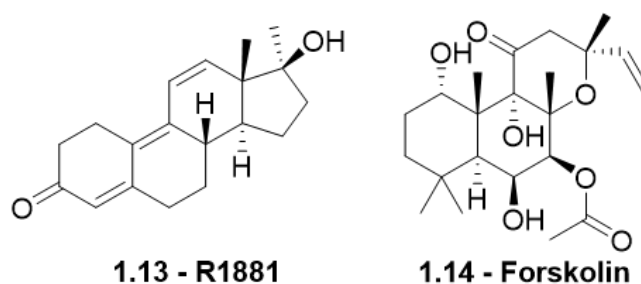
Figure 1.9 – AR Activator**s.**

Chapter 2: Therapeutic Potential of Fluorinated Ralaniten Analogs for Targeting the AR-NTD

2.1   Introduction

The ralaniten analog EPI-067 (**2.001**) (**Figure 2.1**) was discovered using assay guided fractionation of the crude MeOH extracts from the marine sponge *Geodia lindgreni,* which was collected off the coast of Papua New Guinea. It was found using the LNCaP cell-based assay screen, which identified its activity as an antagonist to the AR-NTD.[17,25] Its discovery is somewhat serendipitous, as the structure closely resembles an industrial chemical bisphenol A-diglycidyl ether (BADGE), which is used in the manufacturing of epoxy resin plastics. Retrosynthetic analysis can lead one to speculate how the glycidyl ethers became functionalized. The presence of the chloride ion rich ocean and the potential use of isopropanol as a cleaning agent leads to the speculation that EPI-067 (**2.001**) found its way into the ocean via a transport vessel being cleaned and was assimilated by a marine sponge. This "Catch-22" is an indictment of humanity's negligence within the environment, however this Bisphenol-A (BPA) scaffold would not have been discovered otherwise, leading to EPI-067's status as a 'nominal' natural product. It inspired SAR modifications leading to many AR-NTD antagonist candidates, which include the first generation racemic analog EPI-001 (**2.002**), its stereoisomers EPI-002 – EPI-005, and EPI-506, the first AR-NTD antagonist to enter clinical trials for treatment of mCRPC. The EPI-506 trial was halted due to pharmacokinetic issues and lack of potency despite clear indications of efficacy. This led to further development of the BPA scaffold to enhance the drug-like properties of new analogs. The thesis describes investigation of the fluorination of the BPA

bridge combined with addition of other substitutions aimed at increasing metabolic stability and compound solubility without comprising the compounds AR-NTD antagonist specificity and *in vivo* efficacy.
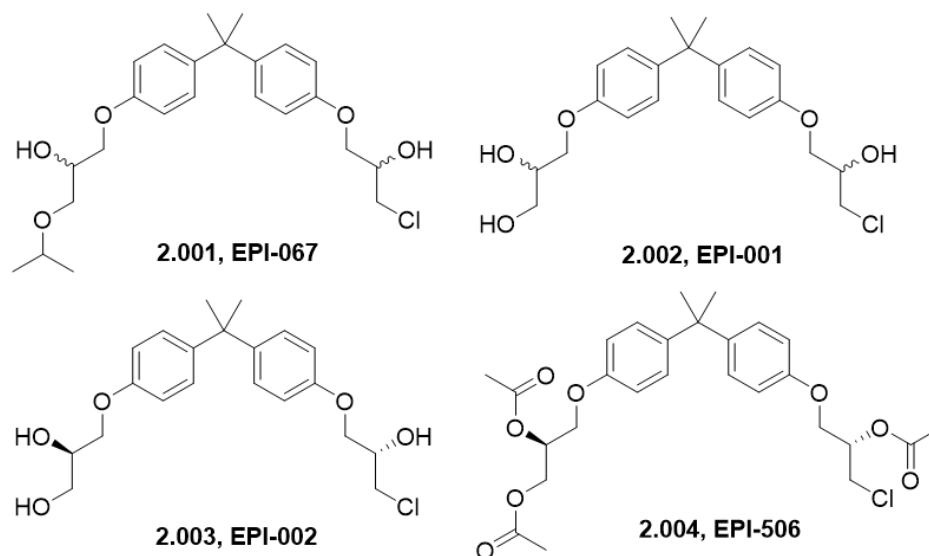
Figure 2.1 – First Generation EPI-compounds (EPI = ESSA Active Pharmaceutical Ingredient).

2.2 AR-NTD – EPI-001 the First Generation

The mutagenic nature of the AR in a cancerous environment prevents the LBD from being a viable option when seeking full remission of CRPC. Through the use of deletion experiments it has been proven that the AR-NTD is essential for transcriptional activity in both the absence and the presence of an androgen ligand. This has led researchers to deem the AR-NTD the "Achilles' Heel" of transcriptional activity. EPI-001 (**2.002**) was the first compound to test the viability of blocking the AR-NTD. It was found to inhibit AR transcriptional activity in a serum-free study in LNCaP cells using forskolin and IL6 to transactivate the AR.[17,26] EPI-001 demonstrated baseline reduction of transcriptional activity *in vitro* with an IC$_{50}$ of ~6 μM. Moreover, EPI-001 also inhibited the transcriptional activity of constitutively active AR-V that

18

lacks a LBD, demonstrating its mechanism of disrupting AR transcription doesn't depend on the presence of the LBD. For consistency, EPI-001 was also shown to exhibit no competitive behavior against androgen binding in a competitive ligand binding study.

Specificity for the AR was established by showing it to have no effect on other steroid hormone receptors, namely the progesterone receptor (PR) and glucocorticoid receptor (GR). These steroid receptors have very similar homology across their respective LBDs and DBDs with respect to the AR and use similar co-activators including CREB-binding protein (CBP). CBP attributes transcriptional activity through AF-1 with and without androgens and is expressed further with CRPC. EPI-001 was shown to inhibit CBPs interaction with AR. CBP is also an important co-activator of transcriptional activity for the PR and GR, so the fact that EPI-001 doesn't interact with these receptors shows its specificity for the AR-NTD rather than CBP itself, which was proven with *in vitro* studies. EPI-001 acts by destabilizing the interaction of CBP within the AF-1 region of the AR-NTD which which leads to inhibiting the expression of PSA.[26] This study lays the fundamental basis for continued study of the "aniten" class of CRPC therapeutics.
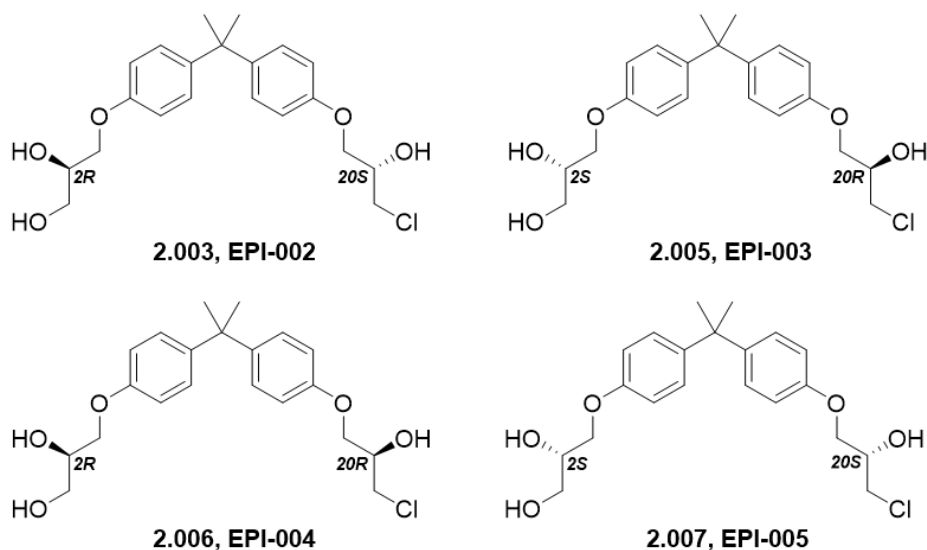
Figure 2.2 – Stereoisomers of EPI-001.

2.2.1 Initial SAR of EPI-001

The proven AR-NTD AF-1 antagonistic activity of the racemic EPI-001 compound, led to evaluation of its stereoisomers (**Figure 2.2**) EPI-002 – EPI-005 (**2.003, 2.005 – 2.007**). These compounds were compared with each other in an in vivo CRPC model using castrated mice (**Figure 2.3**). EPI-002 (**2.002**) with a *(2R)(20S)* configuration was found to be the most potent inhibitor of AR transcriptional activity, exhibiting a lower IC_{50} of 7.4 ± 1.5 μM compared to an IC_{50} of 12.6 ± 4.3 μM for EPI-001.[27] Interestingly, EPI-005 (**2.007**)) with the *(2S)(20S)* configuration showed comparable potency but EPI-003 and EPI-004 did not, suggesting that the configuration of the chlorohydrin C-20 alcohol may impact the binding affinity but that the glycol secondary C-2 alcohol did not. EPI-002 was chosen as the lead candidate due its increased potency, culminating in prodrug EPI-506 that contained acetate prodrug groups.
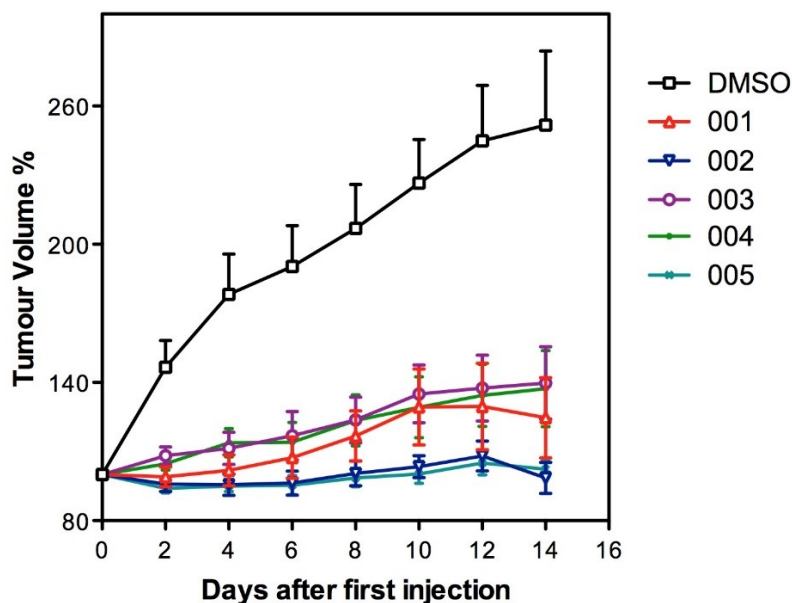
Figure 2.3 – Biological evaluation of EPI-001 and its constituent stereoisomers in castrated mice. Data generated in the Sadar lab at BCCA.[28]

2.2.2 EPI-Compounds– Potential Binding Mechanism

The chlorohydrin moiety on EPI-001 – EPI-005 seemed like a likely position for possible covalent binding to the AR-NTD AF-1 (**Figure 2.4**) as similar compounds that lack the chlorohydrin are inactive. The theory was put to the test using an alkyne modified **2.003,** EPI-054 (**2.008**) probe, by incubating it with LNCaP cells for 24 hours, followed by cell lysis and Click-chemistry to azide-biotin in a Streptavidin pull down experiment.[28] This probe (**Figure 2.5**) successfully pulled down a protein from a Streptavidin bead that corresponds to the FL-AR, proving EPI compounds covalently bind the AR-NTD. Furthermore, using an EPI-054 fluorescein-probe incubated with AF-1 protein, shows slow covalent binding in a dose-dependent manner, via a proposed epoxide forming rate determining step. EPI probe with no chlorohydrin, EPI-063 (**2.009**) or no secondary alcohol, EPI-096 (**2.010**) showed no covalent binding to the

21

AF-1 showing that the full chlorohydrin functionality may be necessary for AF-1 covalent

binding.[28]
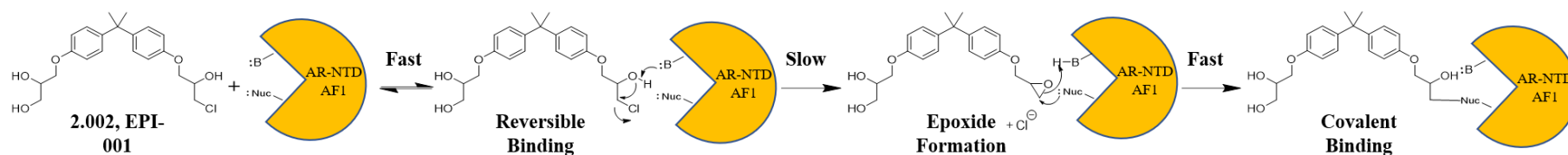
Figure 2.4 – Proposed covalent binding mechanism for EPI-001 (**2.002**) to the AR-NTD AF-1 region. First, there is a fast reversible interaction where the secondary alcohol of the chlorohydrin coordinates to a basic site of the AF-1 region. Secondly, an epoxide forms, in a slow rate-determining step, when the base removes the proton from the secondary alcohol. The reactive epoxide then rapidly forms an irreversible covalent bond to a nucleophilic amino acid side chain, binding EPI-001 to the AF-1 region.[28]
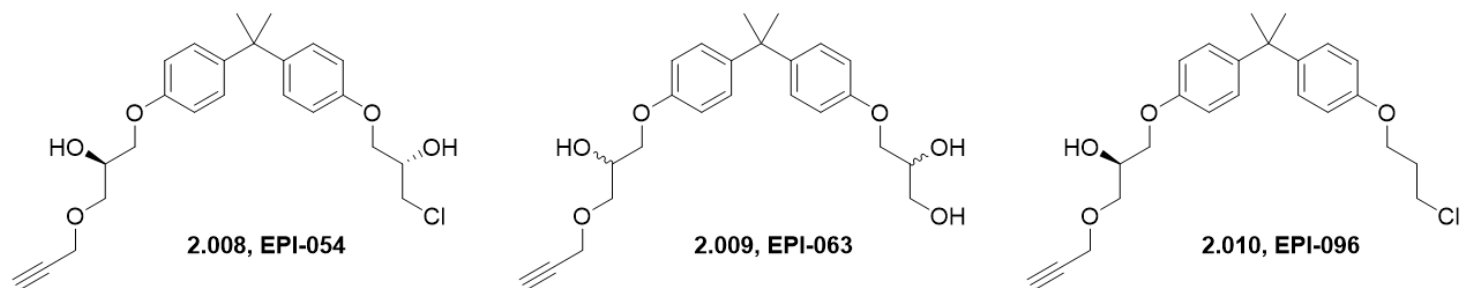
Figure 2.5 – EPI alkyne modified Click probes.[28]

2.3 EPI-002 Target Engagement

The binding of EPI-002 (**2.003**) to the AR AF-1 permitted imaging of the FL-AR and AR-Vs with ^{123}I radiolabeled analog ^{123}I-EPI-002 (**2.011**). ^{123}I-EPI-002 binds the same site as cold EPI-002 determined by a study with AF-1 protein preincubated with excess EPI-002 prior to ^{123}I-EPI-002 addition. Cold EPI-002 displaced ^{123}I-EPI-002, suggesting they bind the same site, allowing **2.011** to be an informative imaging agent.[27]

Biodistribution studies in castrated immunodeficient NOD/SCID mice was determined in LNCaP and PC3 xenografts. Selectivity for LNCaP that expresses FL-AR was exhibited, with off-target accumulation highest in the gallbladder, liver, and intestines.[27] ^{123}I-EPI-002 reached a maximum of $2.2\% \pm 0.5\%$ injected dose (ID)/g uptake in LNCaP tumors after 1 hour compared to $0.7\% \pm 0.4\%$ ID/g for PC3 tumors in the same animal; showing a 3.2 ratio for AR-rich tissue (LNCaP) compared to AR-deficient tissue (PC3). Blocking ^{123}I-EPI-002 with excess cold EPI-002 (50 mg/kg) caused a 74% decrease in ^{123}I-EPI-002 accumulation in LNCaP xenografts, however no change was exhibited in PC3 xenografts, suggesting the accumulation of ^{123}I-EPI-002 is specifically AR mediated.[27]

^{123}I-EPI-002 is great diagnostic tool and, therefore, the cold compound needed further study as a viable drug analog. Iodinating EPI-002 can alter pharmacokinetic properties, such as potency, biological activity, and off-target effects, meaning studies needed to be conducted on the cold compound I-EPI-002. Interestingly, I-EPI-002 has enhanced potency, nearly 10x, with an IC_{50} of 1.2 ± 0.2 μM, and maintains its activity inhibiting transcriptional activity with AR-Vs similar to EPI-002 but at concentrations nearly 10x lower. Furthermore, I-EPI-002 remained highly selective, having no inhibitory effect on the transcriptional activity of PR, GR, estrogen

receptor (ER). It also doesn't interact with the LBD making it feasible to be used in conjunction with current NSAAs.[27]

This proof-of-concept experiment determined the selectivity of I-EPI-002 (**2.011**) and confirmed its ability to block transcriptional activity in FL-AR and constitutively active AR-Vs. It also serendipitously found the importance of having a lipophilic bis-phenol core to enhance potency.[27] However, iodine is typically not used due to its poor metabolic stability, as there is potential for a key off-target effect of iodine uptake in the thyroid through enzymatic deiodination. This has been extensively studied with the iodine scavenging from iodotyrosine (**2.012**) through metabolic enzyme iodotyrosine deiodinases, or in cells from thyroxine (**2.013**) via iodothyronine deiodinases (**Figure 2.6**).[29,30]
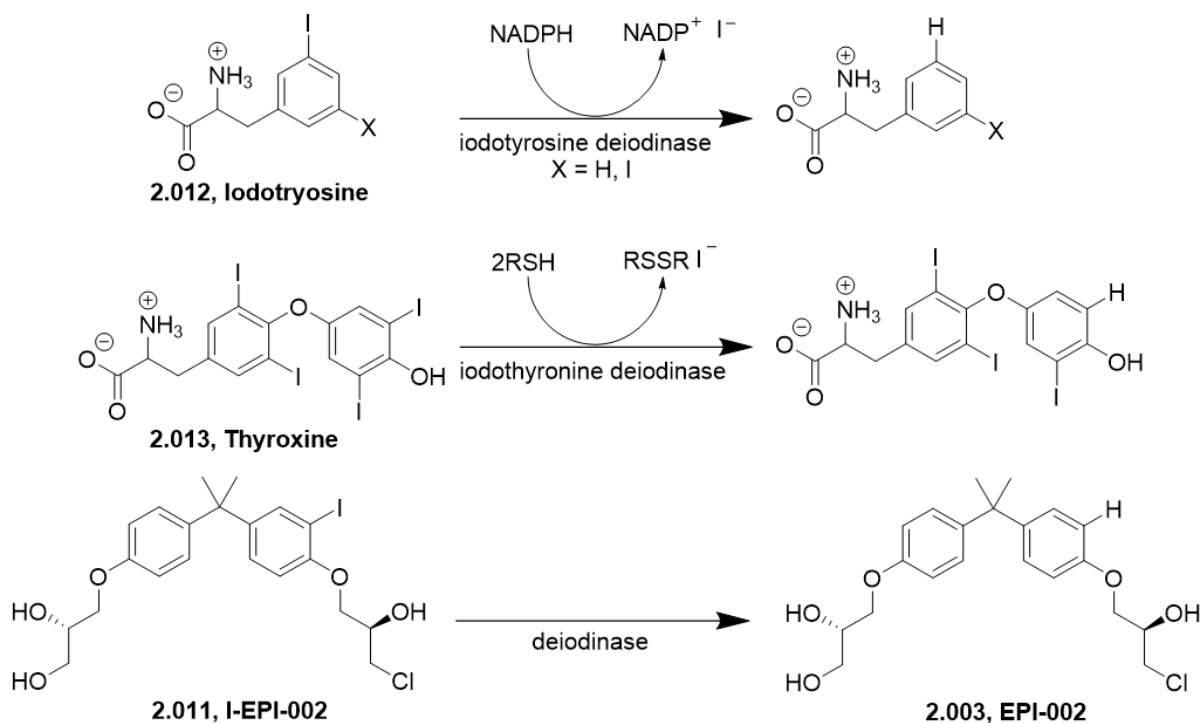
Figure 2.6 – Enzymatic deiodination pathways.[29,30]

2.3.1 EPI compounds inhibit transactivation of the AR-NTD

It was found that EPI-002 inhibits the transactivation of AR-NTD induced by IL6. The mechanism for IL6 transactivation is mediated through the transcription factor STAT3, which binds to and coactivates the AR. EPI-002 was shown to block STAT3 binding and thus inhibiting the transactivation of the AR-NTD induced by IL-6. Using NMR studies with EPI-001 it was demonstrated that it binds in the Tau5 region interacting with residues 353-364, 397-407, and 433-466.[31] Tau5 participates in the androgen independent activation of the FL-AR, lending to EPI compound's remarkable ability to inhibit tumor growth in AR-Vs, including those that lack a LBD. Its specificity is further illustrated in that it doesn't inhibit tumor growth in PC3 cells which don't depend on androgen activation (**Figure 2.7)**. Further SAR must be done to find a drug that is efficacious enough to treat mCRPC. The EPI compounds have been demonstrated to hit the target and effectively inhibit tumor growth in animal models, but potency, metabolic stability, and solubility have been limiting factors. This thesis will try to improve on a clinical candidate EPI-506 (**2.004**) that has already shown notable potential.[32]
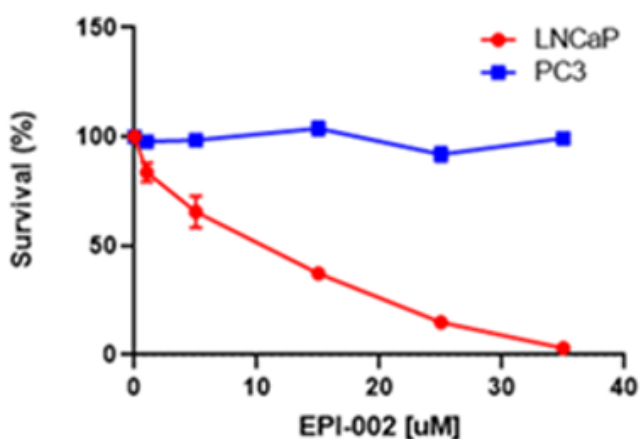
Figure 2.7 – EPI-002 is selective for androgen independent AR-NTD AF-1.[28] Data generated in the Sadar lab at BCCA.

2.4 Metabolism of Ralaniten Analogs

EPI-001, the mixture of stereoisomers, is the hydrolysis and hydrochlorination product of industrial epoxy resin Bis-phenol A diglycidal ether (BADGE). BADGE's industrial application included its use in lining food storage cans, which led to metabolic testing to evaluate its safety for human consumption due to its contact with food.[33] Furthermore, it was tested once again more rigorously upon new findings around the toxicity of the Bis-phenol A (BPA) in 1999 and 2002 by the European Food and Safety Authority (EFSA, 2004). The EFSA panel concluded that BADGE, its chlorohydrins and hydrates possess no carcinogenic or genotoxic behavior, allowing for its continued industrial use, and consequently EPI-002 was deemed safe for consumption. Climie published a proposed metabolic pathway for BADGE (**2.014**) in 1981 shown in **Figure 2.8**.[33,35] This logic can be extrapolated onto EPI compounds (**Figure 2.9**) with major metabolic byproducts identified for EPI-002 using high performance liquid chromatography (HPLC).[36]

27
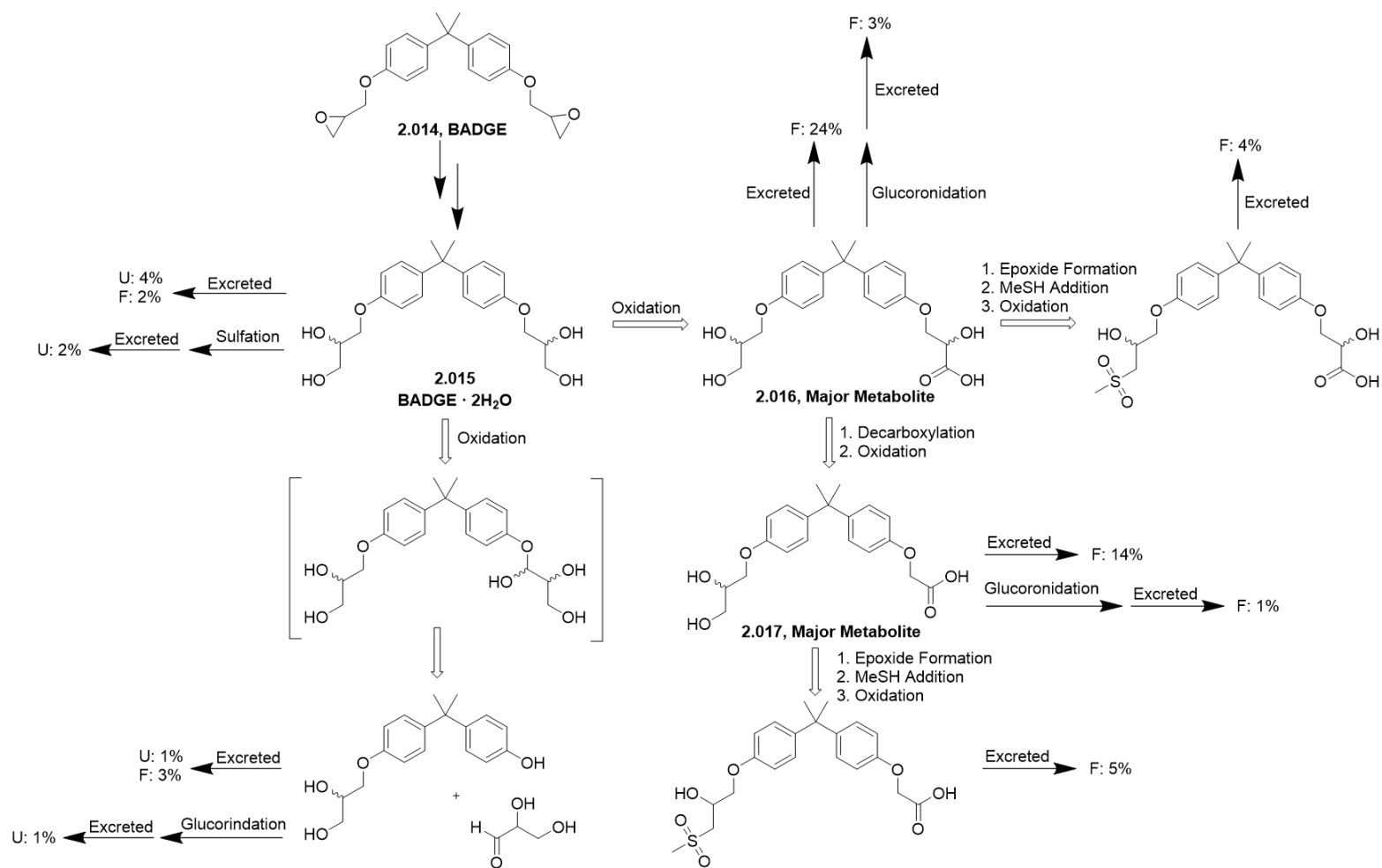
Figure 2.8 – The proposed degradation of the BADGE (reproduced directly from Climie et al.). U and F designations refer to

excretory fluid's urine and fecal respectively.[33]

Figure 2.9 – Proposed Degradation Pathway for EPI Chlorohydrin Compounds.[36]

EPI-002 (**2.003**) is prone to 3 major metabolic processes including oxidation, glucuronidation, and sulfation evidenced from the metabolism of hydrated BADGE (**2.015**) and its two major metabolic products **2.016** and **2.017**. The primary alcohol is the main culprit due to its inherent reactivity; it is prone to oxidation followed by decarboxylation, leading to major metabolite **2.018.** It can also likely be enzymatically glucuronidated to **2.019**, or sulfated to the sulfate ester that can then be readily excreted. The BADGE metabolism suggests the primary alcohol may be susceptible to sulfone formation through methyl mercaptan addition (MeSH), presumably mediated through an epoxide. However, this metabolite was most likely from a precursor of non-hydrated BADGE (**2.014**) as reforming the epoxide from the diol seems unreasonable. The chlorohydrin is also susceptible to cysteine binding to give **2.020**, mediated through a reactive epoxide that forms following dechlorination. However, the presence of an electrophilic chlorine is considered essential for binding to the AR.

This leads to the main synthetic goals to improve upon the current drug without losing potency and specificity. Removing the primary alcohol without losing a hydrogen bond donor (HBD) or hydrogen bond acceptor (HBA), which are important for solubility and stability in the binding pocket. Sterically hindering the secondary alcohols by making them tertiary alcohols, making them less prone to glucuronidation and eliminating the potential of oxidation, or removing them completely. These changes make the overall compound more lipophilic; this thesis will describe how these issues can be addressed while maintaining the core EPI compound attributes.

2.5 Fluorinated Ralaniten (EPI-002) Analogs

2.5.1 Overview

SAR driven improvement of EPI-001 led to EPI-002 (ralaniten) and the prodrug EPI-506 (ralaniten acetate) that was evaluated by ESSA Pharma in a phase I/II clinical trial for treatment of mCRPC. Several hundred analogs of ralaniten have been synthesized in the Andersen lab and ESSA Pharma and these have been tested by the Sadar lab to find an improved clinical candidate. This effort identified an analog designated 7386 that ESSA Pharma is currently evaluating in a phase I/II clinical trial for the treatment of mCRPC. The structure of EPI-7386 is still a trade secret so it cannot be discussed further.

EPI-506 (**2.004**) was well tolerated, however, due to poor pharmacokinetic performance leading to a large pill burden, the drug trial was halted. Analysis of blood samples from patients in this halted study revealed the metabolic transformations that rendered ralaniten acetate less effective than desired at preventing AR transcriptional activity. It was found that **2.004** treatment initiated the upregulation of UDP-glucuronosyltransferase (UGT2B) enzymes that coincided with loss of potency. Further investigation showed the susceptibility of ralaniten to O-glucuronidation by UGT2B enzymes. Glucuronidation of the primary alcohol (**Figure 2.10**) allows for the fast metabolism and clearance of ralaniten through major metabolic product **2.021**. This metabolic mechanism highlights the reactivity of primary and secondary hydroxyl groups during drug exposure time. Furthermore, the chlorohydrin is susceptible to glucuronidation, however it may be necessary for covalent binding the AR-NTD AF-1. This knowledge, along with metabolic processes previously described, led to a complete overhaul of the side-chains on

the BPA scaffold. Careful consideration must be taken when making modifications as it can drastically change the on-target binding characteristics of a potential drug candidate.
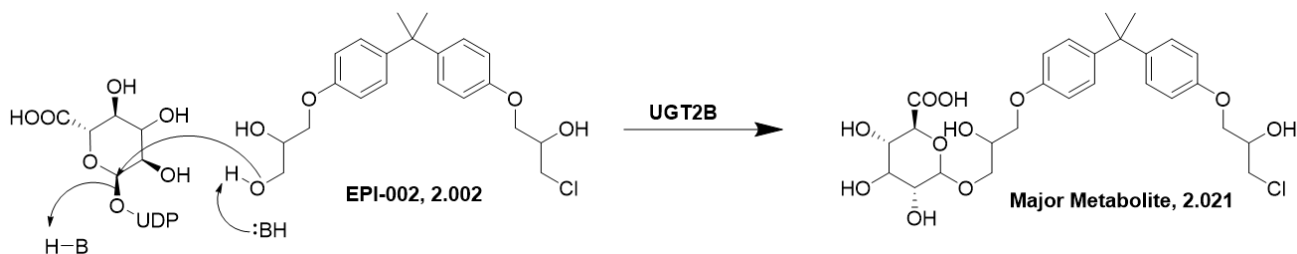
Figure 2.10 – Enzymatic glucuronidation of ralaniten that leads to drug metabolism.

2.5.1.1 Lipinski's Rule of Five

Medicinal chemists use Lipinski's Rule of Five (RO5) as a guide when exploring synthetic analogs to enhance the drug-like properties of a compound. Important factors to consider for good pharmacokinetics include absorption, distribution, metabolism, and excretion (ADME).[37] After rigorous SAR proving the relationship a compound has to its target, a compound's octanol-water partition coefficient (ClogP) becomes an important attribute and RO5 suggests this number should ideally be below five. Typically, a protein binding area is hydrophobic, but hydrophilicity is important for drug delivery. If a compound is too hydrophilic it can more easily by-pass the BBB and also be prone to off-target effects that can contribute to cytotoxicity. However, if it's too hydrophobic there can be solubility issues, making it difficult to determine pharmacokinetic data and administer the drug. The introduction of hydrogen bond acceptors (HBAs) and hydrogen bond donors (HBDs) are also important. Typically, it is suggested to have no more than ten HBAs and five HBDs. HBAs are important for ADME as increasing acceptors can enhance absorption and binding to the target protein. However, having

too many HBAs could lead to cytotoxic effects due to poor drug release, or lead to protein conformational changes impacting adsorption. HBDs play a similar role, but if too many exist on molecule it will typically lead to something too hydrophilic leading to cytotoxicity through off-target effects. Adhering to the RO5 is a great first place to start for drug development, however, drugs can sit outside the suggested lines, so the generation of good ADME data through SAR and synthetic modification is the only true way to determine drug efficacy.

2.5.2   Applying RO5 to Ralaniten

EPI-002 (**2.003**) has three HBDs and five HBAs and can be considered hydrophilic with a low ClogP of 2.80. After making synthetic adjustments to EPI-002 for metabolic stability (**Figure 2.11)** it becomes clear that the desired changes decrease the solubility. The enhanced potency of I-EPI-002 (**2.011)** is a remarkable find, but due to enzymatic metabolic instability the iodine atom needs to be replaced. Previous studies found by replacing the iodine with chlorine led to only a 2-fold increase in potency over **2.003**, however, putting two chlorines on one ring generated an 8-fold increased potency making the dichloro-analog comparable to **2.011**. However, this increased potency for **2.022** comes at the cost of solubility. By adding the fluorines to the BPA bridge **(2.023)**, it is evident that there would be increase in hydrophilicity, while at the same time adding two, although weak, HBAs. However, this doesn't address the metabolic problem of the primary alcohol that is directly susceptible to glucuronidation or as evidenced in the BADGE metabolism or sulfated to a sulfate ester then excreted. To avoid the putative reactivity of the primary alcohol and at the same time dampen the increase in CLogP and retain the HBD and HBA properties, the primary hydroxyl group was converted to a methyl sulfonamide which imparts metabolic stability while maintaining the same amount of HBDs and

HBAs. However, this change to **2.003** generates a relatively lipophilic compound **2.024**, which can be made more lipophilic with the fluorinated bridge methyls. This gives a comparable ClogP value to **2.003**, but with better metabolic stability, which identified compound BU-86 **(2.24)** as a synthetic target in this thesis. Another metabolic issue is the secondary alcohol, which can still reasonably be oxidized, glucuronidated, or sulfated similar to the primary alcohol. The addition of the methyl group sterically hinders the now tertiary alcohol, rendering it significantly less reactive and it completely prevents oxidation. Again, without the fluorines, **2.025** would be very lipophilic leading to solubility issues. Therefore, compound BU-170 **(2.46)** was an important synthetic target for this thesis. The last thing that needs to be determined is the impact the chlorohydrin has on biological activity, because previous work suggests it might be paramount for on-target binding to the AR-NTD AF-1. However, it is not known for certain whether the chlorohydrin is in fact necessary. If the secondary alcohol is removed it would impart greater metabolic stability eliminating the potential for reactive epoxide formation that is susceptible to previously discussed metabolic pathways and potential off-target covalent binding. Testing all the metabolic adjustments without the fluorines with **2.026** would just not be viable because it simply would possess very poor solubility. Adding the fluorines to the BPA bridge, allows all metabolic adjustments to be tested at once in the relatively lipophilic compound BU-130 **(2.45)**, that still adheres to the RO5.
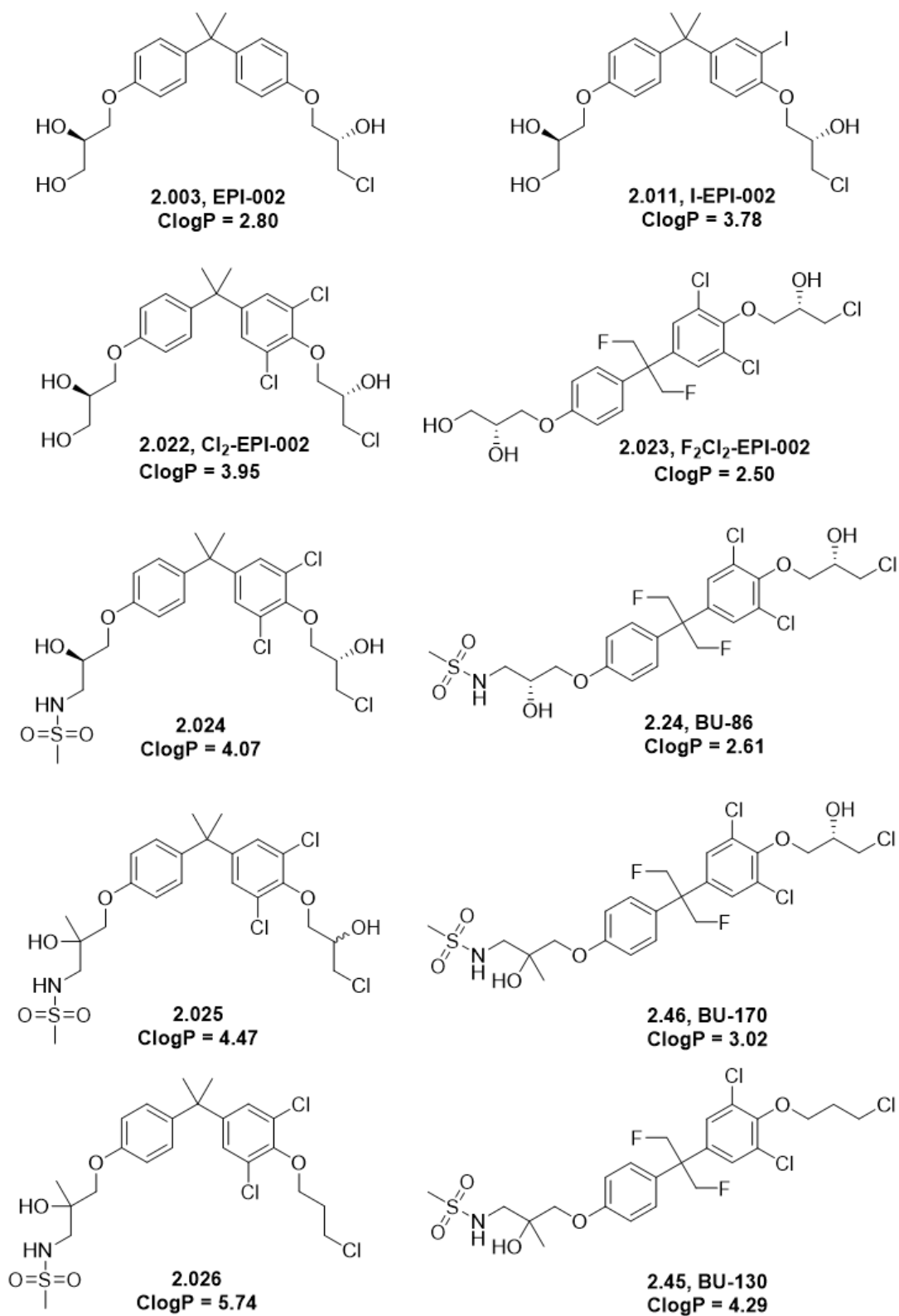
Figure 2.11 – Octanol-water partition coefficients for proposed ralaniten analogs.

2.5.3   Synthesis of Fluorinated Ralaniten Analogs

2.5.3.1   Synthesis of Common Intermediate 4-(1,3-difluoro-2-(4-(trityloxy)phenyl)propan-2-yl)phenol (2.12)

The addition of fluorines to the BPA bridge introduces another H-bond acceptor, albeit a weak one, from a low lying C-F σ* antibonding orbital.[38] It also decreases the ClogP rendering the molecule ~30-fold more water soluble, facilitating the tuning of the hydrophobicity of the molecule. This polarity change allows for more flexibility in using less-polar side chains that impart more metabolic stability. Lastly, its small size should not create steric interference when binding, as previous ralaniten analogs are already known to bind effectively to AR-NTD.

The synthetic strategy for ralaniten analogs typically starts from the inexpensive starting material of bisphenol A (BPA), but to put fluorines at the dimethyl bridge, a new strategy had to be implemented. We anticipated that this could be accomplished in one step from the inexpensive starting materials phenol, iron (III) chloride, and 1,3 difluoroacetone. Upon mixing starting materials **2.03** and **2.04** in the presence of the Lewis acid Iron (III) chloride, **2.11** was produced via a Friedel Crafts electrophilic aromatic substitution reaction as shown in **Scheme 2.1**. The yield was found to be far from efficient, but since it was the first step in a 7-9 step synthesis and the reagents were cheap, it didn't inhibit scale-up. Next mono-protection of the bis-phenol was accomplished via S_N1 electrophilic substitution reaction with trityl chloride to give **2.12** in moderate yield with starting material recovered and di-protected product recycled after simple deprotection in HCl.
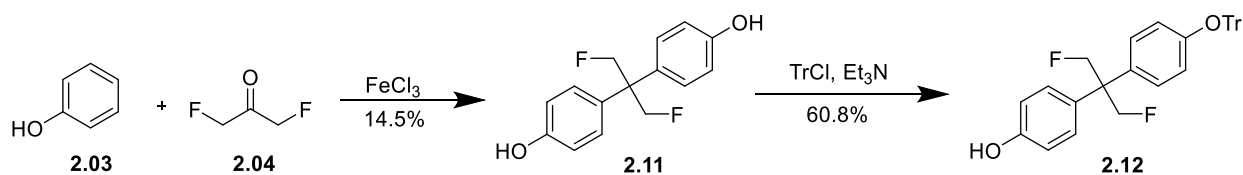
Scheme 2.1 – Synthesis of fluorinated BPA (**2.11**) and its subsequent protection to give **2.12**.

2.5.4   Synthesis of the Common Fluorinated Ralaniten Intermediate *(R)*-N-(3-(4-(2-(3,5-dichloro-4-hydroxyphenyl)-1,3-difluoropropan-2-yl)phenoxy)-2-hydroxypropyl)methanesulfonamide (2.23)

The common intermediate **2.12** (**Scheme 2.2**) was subsequently reacted with *(R)*-glycidol tosylate (**2.05**), through a S_N2 nucleophilic substitution reaction to produce **2.21** in 82.5% yield. The epoxide **2.21** was opened using methane-sulfonamide in the presence of cesium carbonate under reflux via S_N2 nucleophilic substitution reaction, followed by trityl-deprotection using 6M HCl to produce **2.22** in 62.3% yield (**Scheme 2.2**). The addition of the methane-sulfonamide enhances the water solubility over a primary hydroxyl group found in EPI-001, while also eliminating the potential for glucuronidation, as the sulfonamide is a weak nucleophile, that likely doesn't get deprotonated at physiological pH, but can still participate as a HBA. This change is critical for metabolic stability, but can still contribute to drug binding to the AR-NTD. Next, dichlorination of right-hand-side phenol was accomplished using sodium hypochlorite via an electrophilic aromatic substitution reaction yielding **2.23** in 62.6% yield. The introduction of the chlorines to the aromatic ring enhances molecular recognition, which can impart greater binding affinities with protein targets.[39] This is corroborated through previous work done in the Andersen group where halogenating the ring increases potency.[27]
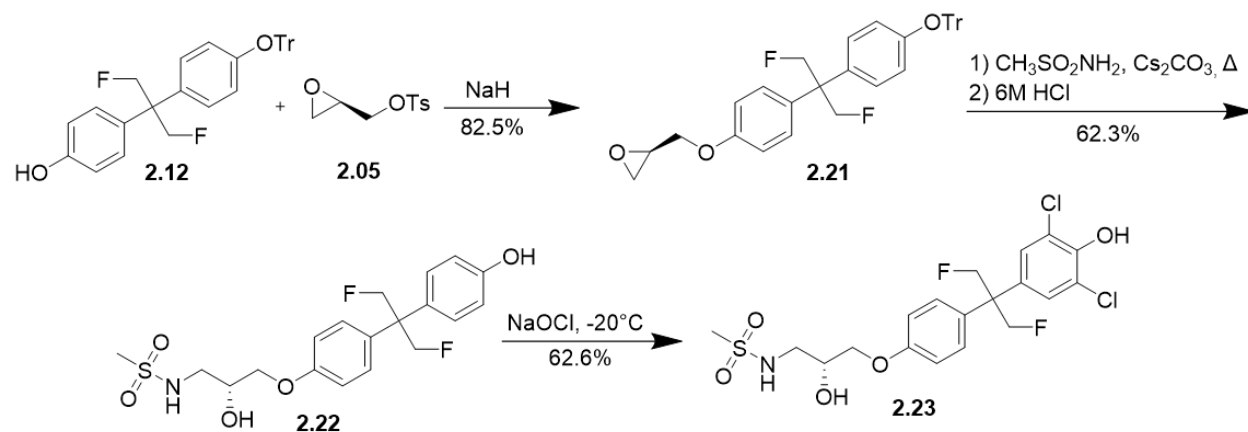
Scheme 2.2 – Synthesis of common intermediate **2.23**.

2.5.5 Synthesis of Fluorinated Ralaniten analogs BU-86 (2.24), BU-87 (2.25)

The common intermediate **2.23** was used to generate the final product drug candidates that were used in cell-based studies. **2.23** was reacted with *(R)*-glycidol tosylate in a S_N2 nucleophilic substitution reaction to give **2.21** as shown in **Scheme 2.3**. The glycidyl ether intermediate was subsequently reacted without further purification with Cerium (III) trichloride heptahydrate under reflux to open the epoxide via a nucleophilic substitution reaction to afford BU-86 **(2.24)** in 81.8% yield over two-steps. **2.23** was reacted with 1-bromo-3-chloropropane through a S_N2 nucleophilic substitution reaction to afford BU-87 **(2.25)** in 81.3% yield.

Scheme 2.3 – Synthesis of BU-86 (**2.24**), BU-87 (**2.25**).

2.5.5.1 Biological Evaluation of BU-86 (2.24) and BU-87 (2.25)

BU-86 (**2.24**) and BU-87 (**2.25**) block the AR-NTD, shown by inhibiting PSA-luciferase reporter in the LNCaP cells giving a half-maximal inhibitory concentration (IC$_{50}$) of 2.3 ± 0.1 and 2.9 ± 0.2 μM respectively, **Figure 2.12**. Both compounds show superior activity compared to EPI-002 (**2.003**) with an IC$_{50}$ of 9.8 ± 0.3 μM, but fall short of Enzalutamide (**1.10**) that has an IC$_{50}$ of 0.1 ± 0.004 μM. However, binding the AR-NTD allows for tumor inhibition in mCRPC, where enzalutamide is impotent.

Compound	PSA Luciferase Assay IC$_{50}$ (μM)
EPI-002 (2.003)	9.8 ± 0.3
Enzalutamide (1.10)	0.1 ± 0.004
BU-86 (2.24)	2.3 ± 0.1
BU-87 (2.25)	2.9 ± 0.2
BU-88 (2.26)	0.06 ± 0.002
BU-89 (2.33)	0.05 ± 0.002
BU-130 (2.45)	1.8 ± 0.1
BU-170 (2.46)	2.1 ± 0.2

Figure 2.12 – IC$_{50}$ values of AR-NTD Antagonists. Data generated in the Sadar lab at BCCA.

BU-86 **(2.24)** and BU-87 **(2.25)** target the LNCaP cells that depend on androgen, **Figure 2.13**, showing its specificity for AR. The limited off-target effect on PC3, that is androgen independent and not modulated by AR, by **2.25** could be due to the removal of the chlorohydrin in favor of the propyl chloride side-chain. However, more evidence would be needed to properly evaluate this claim.
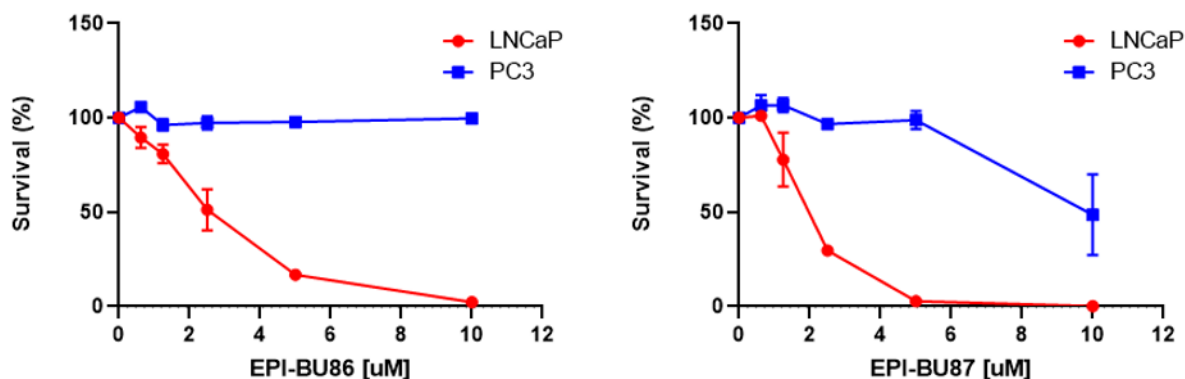
Figure 2.13 – BU-86 (**2.24**) and BU-87 (**2.25**) target LNCaP cells that are androgen dependent. Data generated in the Sadar lab at BCCA.

2.5.6 Synthesis of Fluorinated Ralaniten Ketone Analog BU-88 (2.26)

The Fluorinated ketone **2.26**, gives a potential site to form a reversible covalent bond with an amine or a thiol on an amino acid side chain. The ketone also represents a putative metabolic product of **2.25**. Common intermediate **2.25** was reacted with Dess–Martin periodinane as shown in **Scheme 2.4** to facilitate the oxidation of the secondary alcohol to give ketone product, BU-88 (**2.26**) in 48.1%, where the alcohol starting material (**2.25**) was recovered for further reactions or cell-based studies.

It was found through stability studies that the ketone was unstable in mildly basic conditions, similar to what is found in blood. When **2.26** was exposed to triethylamine at room temperature it degraded to the phenol **2.33.** The fragment formed from the cleaved side-chain remains to be found but we have proposed that it degrades in intramolecular fashion forming the azetidione sulfonamide, **2.27**. The azetidione **2.27** is a reasonable possibility due to its commercial availability that indicates it's relatively stable.[40] This led to the synthesis of BU-89 (**2.33)** as an interesting drug lead due to the significant biological activity of the ketone **2.26**.

Determining if the degradation product **2.33** is in fact the bioactive component upon *in vitro* and *in vivo* evaluation of **2.26** remains to be tested.
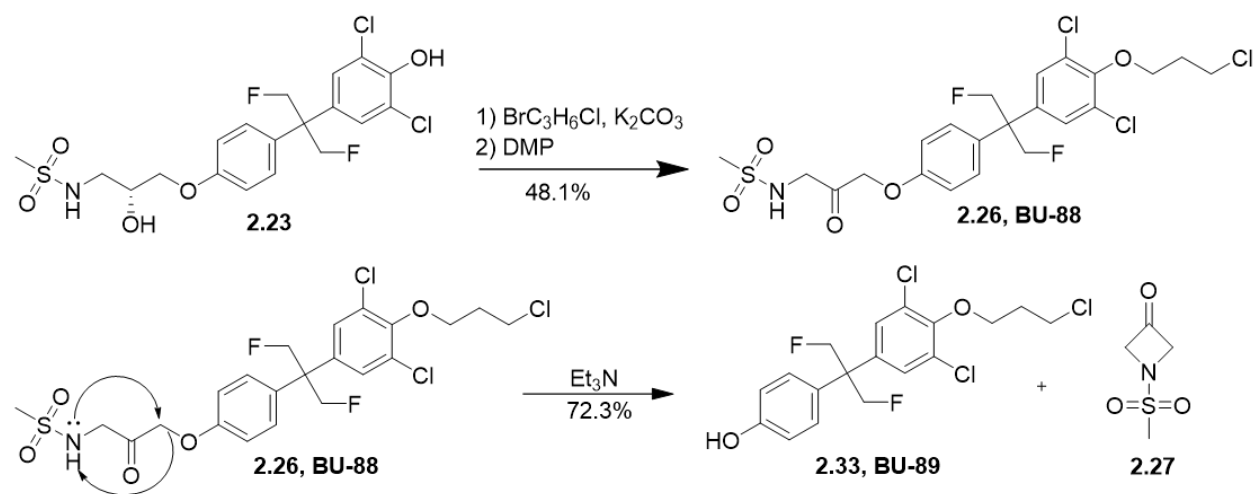
Scheme 2.4 – Synthesis of ketone BU-88 (**2.26**) and its potential chemical degradation mechanism to form BU-89 (**2.33**) and **2.27**.

2.5.7   Synthesis of Fluorinated Ralaniten Analog BU-89 (2.33)

After it was discovered that BU-89 **(2.33)** is the degradation product of BU-88 **(2.26)** (**Scheme 2.5**) a concerted effort was made to figure out if the ketone **2.26** or its degradation product **2.33** was responsible for the observed bioactivity**.** The synthesis of **2.33** uses the benzyl protecting group as the trityl protecting group would be unstable while chlorinating the ring in the subsequent step. Interestingly, hydrogenolysis of the benzyl protecting group could not be accomplished on the fluorinated analogs (yields >5%), although it can be done nearly quantitatively on the non-fluorinated analogs. However, the benzyl group was successfully removed with boron trichloride dimethyl sulfide complex to give BU-89 **(2.33)** in 61.8% yield over the last two steps.
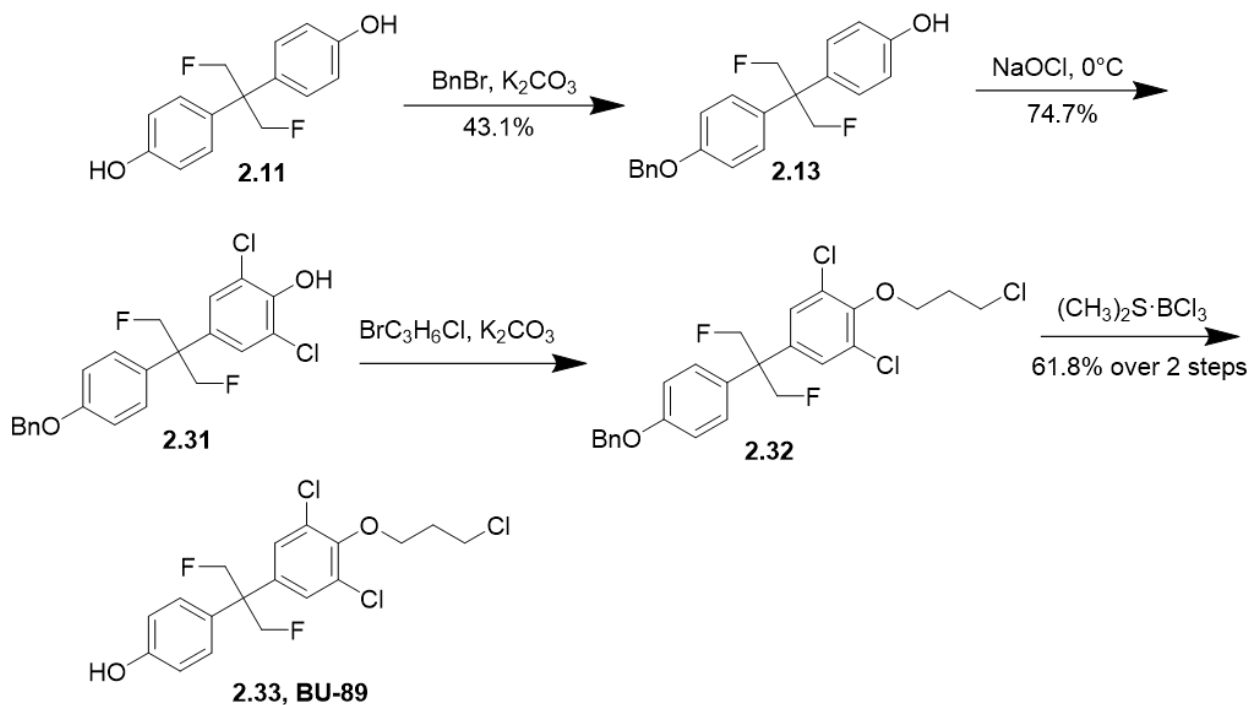
Scheme 2.5 – Synthesis of ketone degradation product BU-89 (**2.33**).

2.5.7.1   Biological Evaluation of BU-88 (2.26) and BU-89 (2.33)

BU-88 **(2.26)** and BU-89 **(2.33)** show low nanomolar IC_{50}'s in the PSA-luciferase screening assay for AR-NTD antagonists (**Figure 2.14**). Based on the similarities of the IC_{50} values for **2.26**, (0.05 ± 0.002 μM) and **2.33**, **(0.05 ± 0.002 μM)** it seems reasonable to conclude that the proposed degradation product **2.33** is responsible for the strong AR-NTD antagonist activity in LNCaP cells. **2.26** and **2.33** show stronger inhibition for AR than current industry standard enzalutamide by more than 2-fold. The downside is that preliminary studies have shown these compounds have an off-target effect with some interactions with the progesterone receptor, however more evidence is needed to properly evaluate this claim. This led to a halt for further studies, however their potent activity in the PSA-luciferase screening assay makes these analogs interesting candidates that deserve further evaluation.

Compound	PSA Luciferase Assay IC$_{50}$ (μM)
EPI-002 (2.003)	**9.8 ± 0.3**
Enzalutamide (1.10)	**0.1 ± 0.004**
BU-86 (2.24)	2.3 ± 0.1
BU-87 (2.25)	2.9 ± 0.2
BU-88 (2.26)	**0.06 ± 0.002**
BU-89 (2.33)	**0.05 ± 0.002**
BU-130 (2.45)	1.8 ± 0.1
BU-170 (2.46)	2.1 ± 0.2

Figure 2.14 – IC$_{50}$ values of AR-NTD Antagonists. Data generated in the Sadar lab at BCCA.

BU-88 **(2.26)** inhibits tumor growth in LNCaP xenografts grown in mice treated once per day orally at 30mg/kg, dosing started once tumors reached 100 mm^3 (**Figure 2.15)**. This *in vivo* data provides further evidence that **2.26** and its degradation product **2.33** deserve further study.
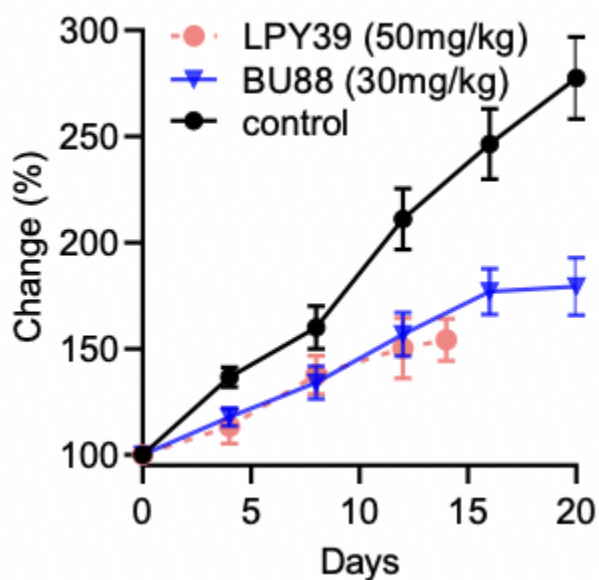
Figure 2.15 – BU-88 (**2.26**) inhibits tumor growth in LNCaP xenografts grown in mice. Data generated in the Sadar lab at BCCA.

2.5.8 Synthesis of Ralaniten Analogs BU-130 (2.45) and BU-170 (2.46)

The addition of the methyl group to give analogs **2.45** and **2.46,** imparts a tertiary center that sterically hinders the hydroxyl group, minimizing any nucleophilic potential it may have, potentially lowering the possibility of glucuronidation. It also prevents oxidation, making it more metabolically and chemically stable, as we know there is a facile degradation pathway that exists with the ketone functionality. Furthermore, adding the methyl leads to a net increase in ClogP, which imparts more lipophilicity to the side chain, without removing a HBA/HBD.
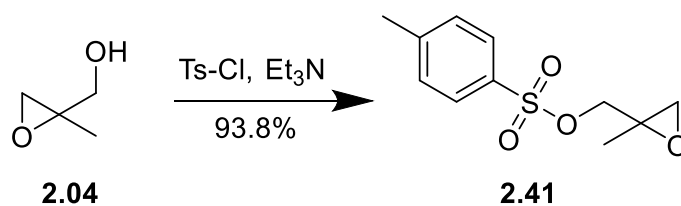
Scheme 2.6 – Synthesis of 2-methyl glycidol tosylate **2.41**.

Similar to previous analogs BU-86 **(2.24)** and BU-87 **(2.25)**, a methyl group was added using the racemic 2-methyl glycidol **(2.04)** **(Scheme 2.7)** that was first tosylated to give the alkylating agent **2.41**. **2.41** was then and added to the common intermediate **2.11 (Scheme 2.7)** via a S_N2 nucleophilic substitution reaction to afford **2.42** in 67.1% yield. The next two steps were done following the protocols previously mentioned in the synthesis of **2.23 (Scheme 2.2)**.
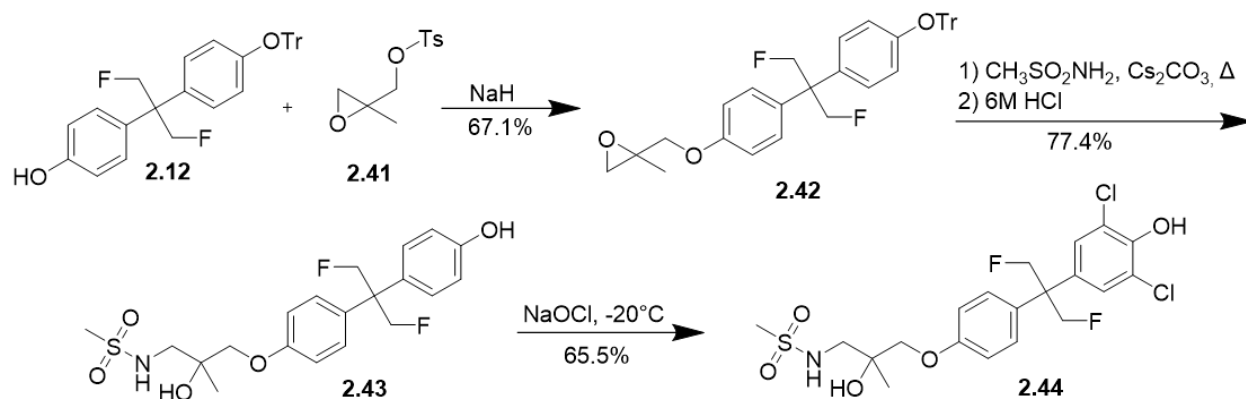
Scheme 2.7 – Synthesis of common intermediate **2.44**.

From common intermediate **2.44** the final side chains were added as shown in **Scheme 2.8**. **2.44** was reacted with 1-bromo-3-chloropropane in a base mediated S_N2 nucleophilic substitution reaction to yield BU-130 **(2.45)** in 86.7% yield. **2.44** to was also reacted with glycidol tosylate with via a base mediated S_N2 nucleophilic substitution reaction. The epoxide intermediate was subsequently opened by refluxing with cerium (III) trichloride heptahydrate giving BU-170 **(2.46)** in 93.0% yield.
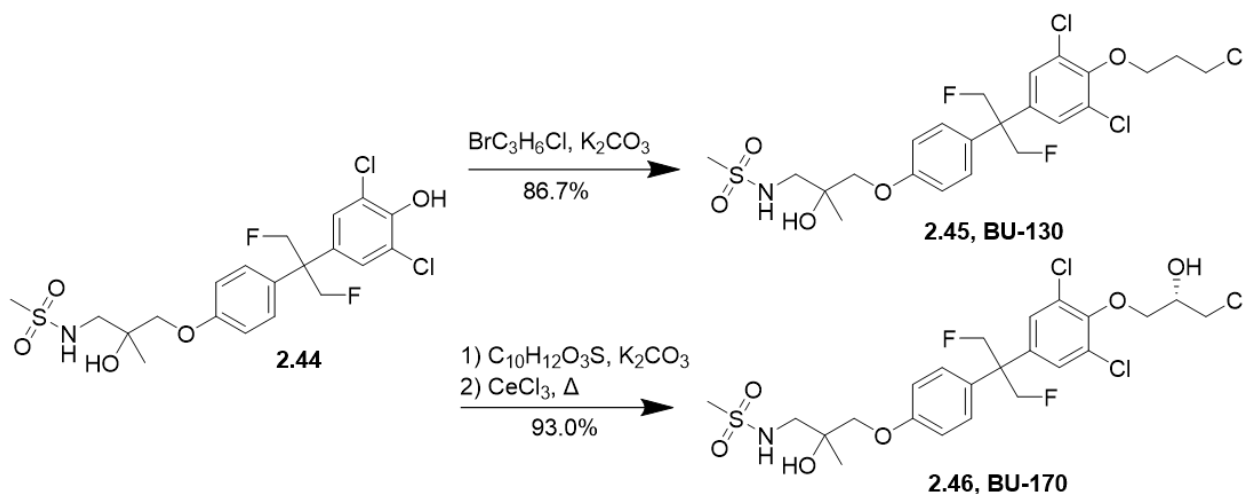
Scheme 2.8 – Synthesis of analogs BU-130 (**2.45**) and BU-170 (**2.46**).

2.5.8.1   Biological Evaluation of BU-130 (2.45) and BU-170 (2.46)

BU-130 **(2.45)** and BU-170 **(2.46)** should be the most metabolically stable EPI-001 analogs made to date and they still exhibit very good IC_{50} values of 1.8 ± 0.1 and 2.1 ± 0.2 μM, respectively (**Figure 2.16**). Interestingly, the blocking ability of the compound without the chlorohydrin is marginally better than with it, suggesting that the chlorohydrin may not be necessary for good AR binding. This also raises the more questions whether or not these

antagonists bind covalently as the metabolically stable **2.45** can't form a reactive epoxide and the alcohol cannot be oxidized.

Compound	PSA Luciferase Assay IC$_{50}$ (μM)
EPI-002 (2.003)	**9.8 ± 0.3**
Enzalutamide (1.10)	**0.1 ± 0.004**
BU-86 (2.24)	2.3 ± 0.1
BU-87 (2.25)	2.9 ± 0.2
BU-88 (2.26)	0.06 ± 0.002
BU-89 (2.33)	0.05 ± 0.002
BU-130 (2.45)	**1.8 ± 0.1**
BU-170 (2.46)	**2.1 ± 0.2**

Figure 2.16 - IC$_{50}$ values of AR-NTD Antagonists. Data generated in the Sadar lab at BCCA.

BU-130 **(2.45)** and BU-170 **(2.46)** inhibit tumor growth in LNCaP xenografts in the mice treated orally once per day at 30mg/kg (**Figure 2.17**). **2.45** and **2.46** show comparable activity fitting identically within error in both *in vitro* potencies and *in vivo* efficacies. This suggests that perhaps BU-130 **(2.45)** could be a superior clinical candidate due the lack of the chlorohydrin

which should impart greater metabolic stability. In fact, **2.45** and **2.46** currently show the best *in vivo* activity of any aniten NSAA to date making them prime candidates as a mono-therapeutics to treat mCPRC.
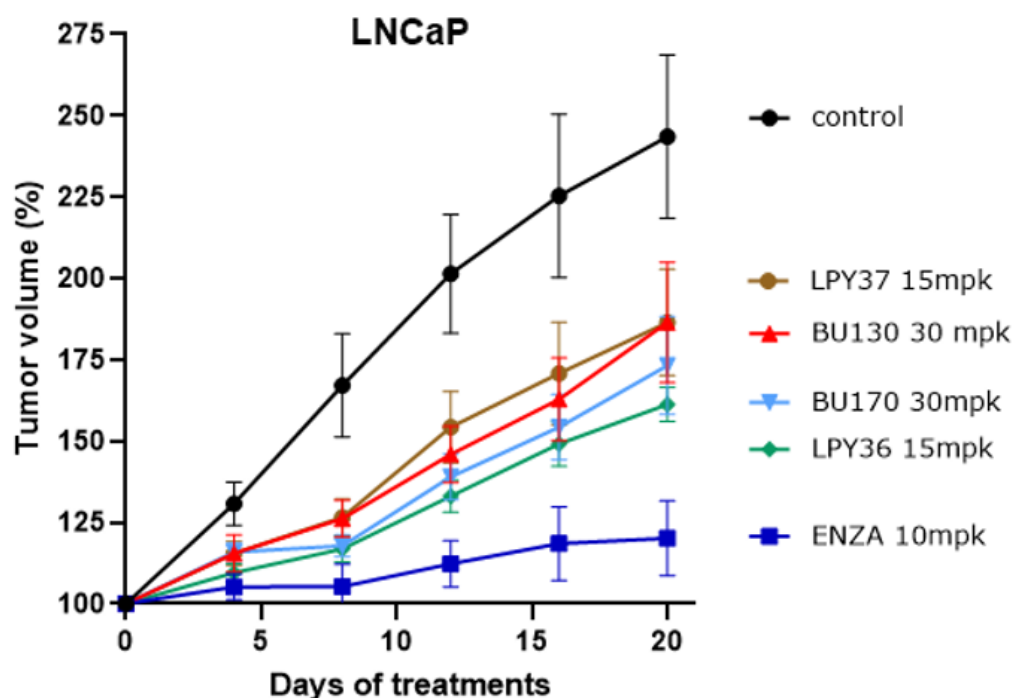
Figure 2.17 – BU-130 (**2.45**) and BU-170 (**2.46**) inhibit tumor growth in LNCaP xenografts grown in mice. Data was generated in Sadar lab at BCCA.

2.5.9   Fluorine Influence on ^{2}J Coupling in the ^{1}H NMR Spectra of Ralaniten Analogs

Upon forming the fluorinated BPA (**2.11**) we begin to see the ^{2}J$_{HF}$ coupling, **Figure 2.18**, where the geminal protons on the bridge methyls appear as singlets that are split by the fluorine atom by 48.5 Hz. Once a side chain containing a stereogenic center is added like in **2.21**, the geminal protons become diastereotopic and we begin to see ^{2}J$_{HH}$ geminal coupling because the

geminal protons are not chemically equivalent so they have different chemical shifts. The geminal proton chemical shift differences in **2.21** are small so the multiplet is highly second order. However, the coupling would be more apparent if the spectrum was recorded using a stronger field strength NMR spectrometer. Upon removing the protecting group, di-chlorinating the same ring, and functionalizing the free phenol, **2.45**, the AB portion of the ABX pattern becomes clear in the proton spectrum as shown in **Figure 2.19**. Each doublet of doublets pertains to one H_A/H_B pair as indicated by the splitting tree, with respective $^2J_{HH}$ and $^2J_{HF}$ coupling constants of 9.8Hz and 47.6Hz They have also been split by ^{19}F spin ½ nucleus, thus we see two doublet of doublet chemical shifts. This phenomenon becomes more resolved when increasing the NMR field strength from 400MHz to 600MHz, and the second order character of these resonances is evidenced by the "roofing effect" where the outer peaks are a smaller intensity relative to the inner peaks. This is confirmed by dividing the chemical shift difference, Δv, by the coupling constant J, represented by the form:

$$\frac{\Delta v}{J} = \frac{(5.1545 - 5.1018) \times 400MHz}{(5.1656 - 5.1411) \times 400MHz} = \frac{21.08}{9.8} = 2.15$$

Since $\Delta v/J$ for **2.45** is much less than 10, it is confirmed that the splitting is highly second order. Once two stereocenters are introduced to the molecule, **2.46**, the complexity of the geminal protons becomes even more complex and higher second order with the doublet of doublet patterns overlapping in the NMR, **Figure 2.20**. The phenomenon becomes clear when increasing the field strength from 600MHz to 850MHz.
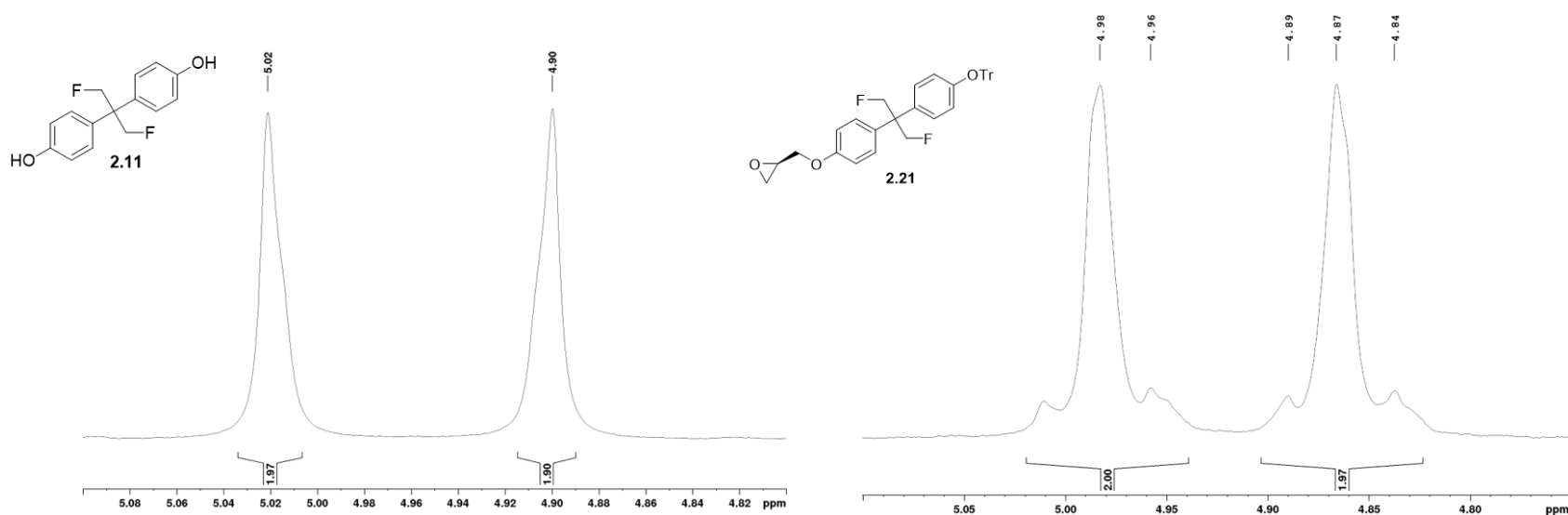
Figure 2.18 – ^{1}H NMR (400 MHz, DMSO-d6) of geminal protons on the fluorinated BPA gem-dimethyl bridge.
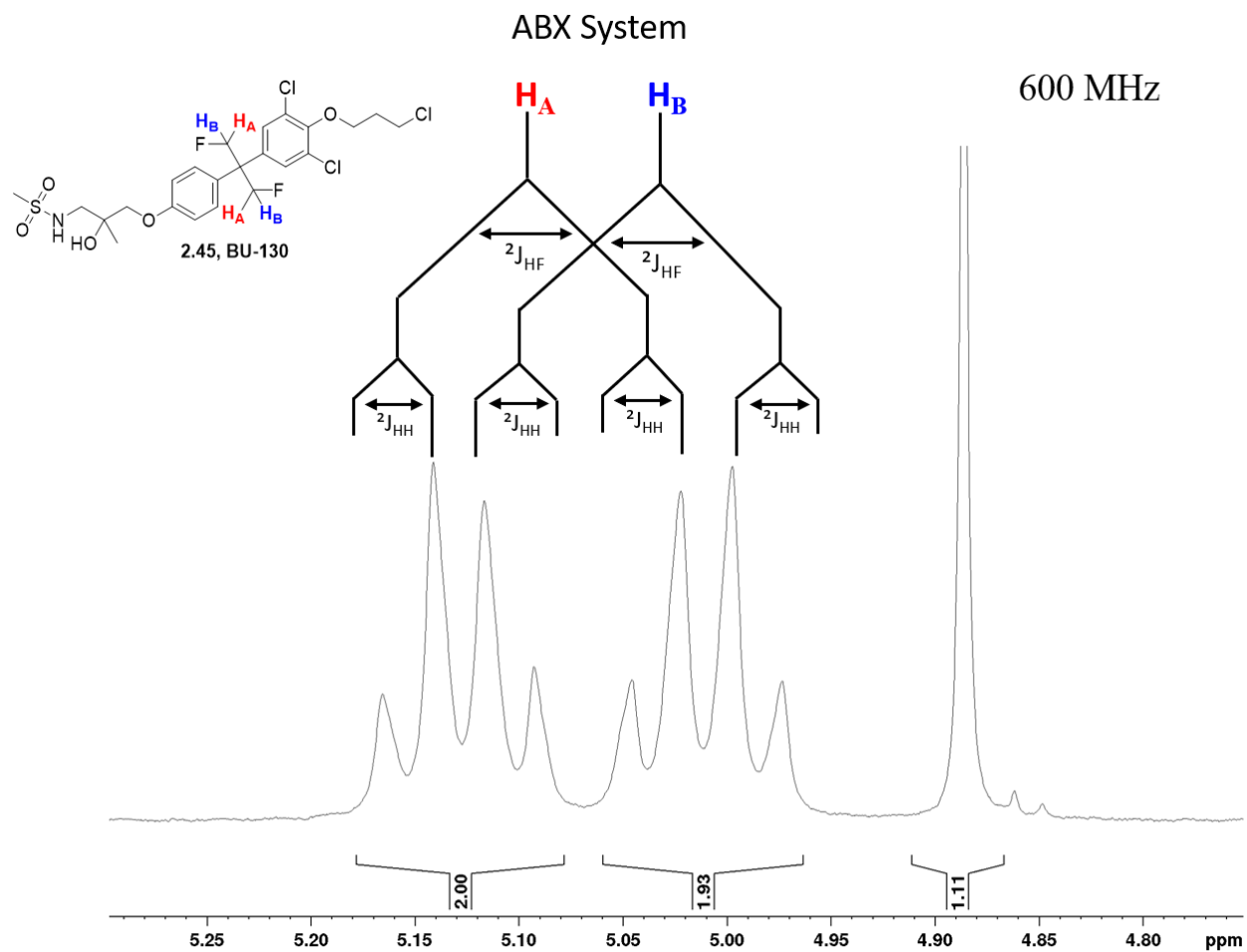
Figure 2.19 – Doublet of doublet splitting from adding a stereogenic center and losing ring symmetry and the corresponding ABX system for **2.45** (400 MHz, DMSO-d6).
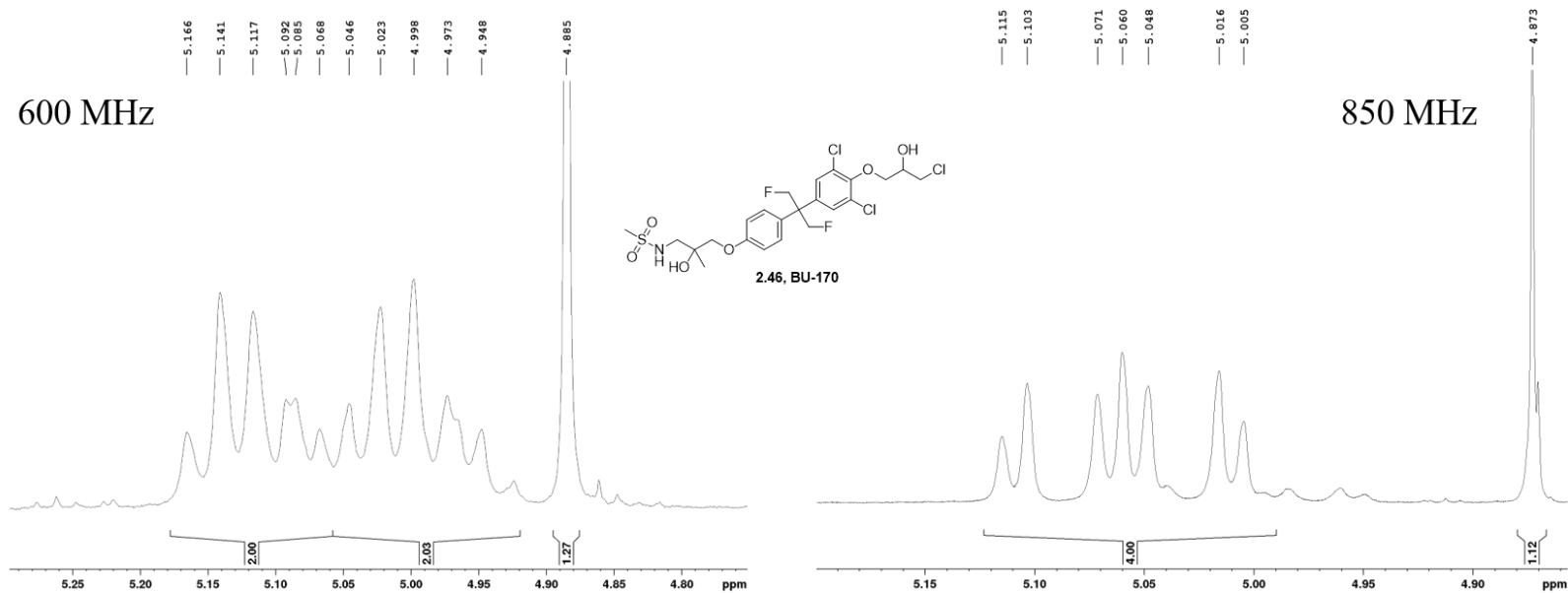
Figure 2.20 – NMR splitting of fluorinated analog **2.46** at different field strengths (600 MHz, DMSO-d6, 850 MHz, DMSO-d6) and the corresponding ABX system.

Chapter 3: Sintokamides – Animal Study and Imaging Agent Potential

3.1 Overview

Halogenated natural products (HNPs) are found across all natural product sources. There have now been well over 5,000 HNPs discovered, with the majority containing chlorine, followed by bromine, then very small amounts of the less abundant iodine. The majority of HNPs are formed biosynthetically using enzymes that operate through oxidative mechanisms, where haloperoxidases use hydrogen peroxide and halogenases use molecular oxygen.[41] Most HNPs are found in marine environments, where halide concentrations are higher, and biosynthetic incorporation by bacteria, macroalgae, phytoplankton, sponges, tunicates, worms, corals, and other invertebrates are more common.[42] Examples of HNPs include the antineoplastic agents β-lactone salinasporamide A, macrocylic lactone rebeccamycin, and the very potent enediyne calicheamicin γ.[1]

Sintokamides A to E **(3.001 – 3.005)** are HNPs (**Figure 3.1**) that were first described in 2008.[43] The small molecule AR-NTD inhibitory chlorinated dipeptides were isolated from the marine sponge *Dysidea sp.,* collected in Palau Sintok, Karimunjawa archipelago, Indonesia.[43] The compounds are derived from two leucine moieties that are connected via an amide linked tetramic acid. A to E analogs vary in the number of chlorine atoms incorporated into a side chain methyl group on either leucine moiety. Sintokamide A (SINT1) was the first small molecule compound that showed the inhibition of transcriptional activity related to the transactivation of AR-NTD in PC cells. It was found to bind the AR AF-1 region stopping transcriptional activity of both the FL-AR and enzalutamide resistant AR-V. The mechanism of the action is not currently understood, but is presumed to bind covalently, however more research needs to be done for confirmation. More importantly, its highly selective for the AR, as it shows no blocking

of transcriptional activity among similar steroid receptors PR and GR. Their potency and selectivity make the sintokamides both small molecule drug candidates and excellent imaging agent candidates to understand AR binding mechanisms. This chapter will discuss the synthesis of sintokamide analogs with potential for use as cell biology tools, therapeutic agents, or imaging agents.
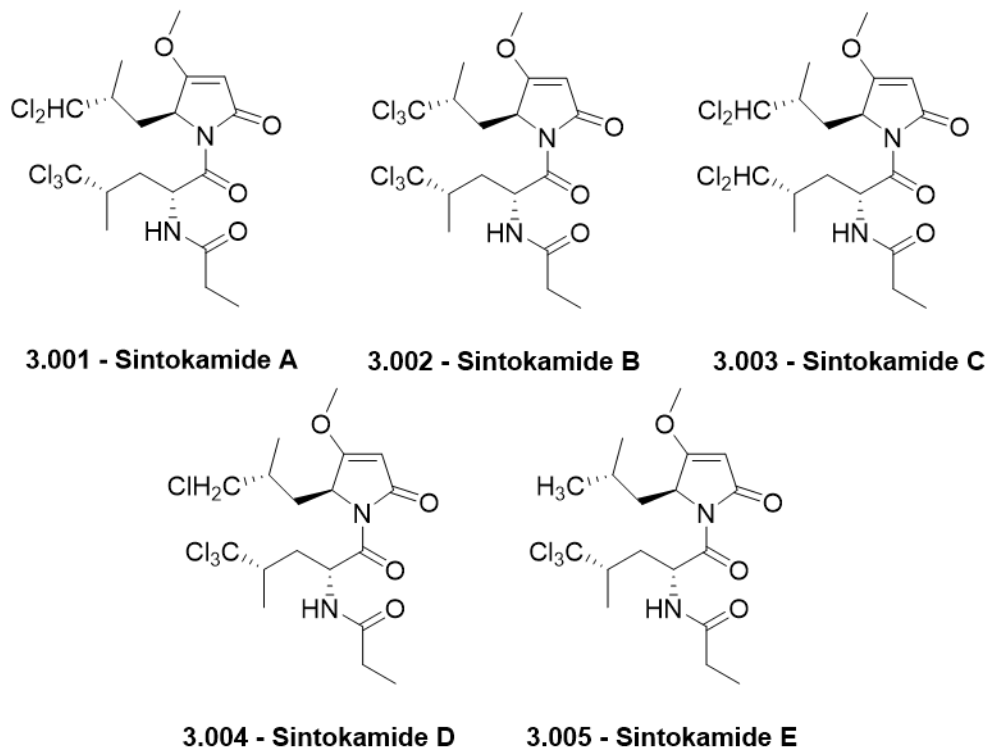
Figure 3.1 – Chlorinated Peptides Sintokamide A-E isolated from marine sponge *Dysidea sp.*

3.2 Therapeutic Potential for Modified Sintokamide Analogs

3.2.1 Sintokamide A and its Synthetic Analogs

SINT1 (**3.001**) has demonstrated *in vitro* AR-NTD antagonist bioactivities that make it a promising lead scaffold for elaboration to produce NP inspired clinical candidates for treatment

of mCRPC. This prompted total syntheses of sintokamides A, B, and E and a NP modification

program that yielded new synthetic analogs with increased potency and scale to get further *in*

vitro and *in vivo* data.[44,45] The most promising analogs found in the Andersen lab SAR

optimization study were LPY37 **(3.41)** and LPY36 **(3.42)**. These analogs differ from SINT1

(**Figure 3.2**) by removing the methyl groups on each chlorinated alkyl chain which also removes

two stereocenters from the molecule, giving chlorinated norleucine residues. An increase in

potency from making the synthesis more simplistic is a welcome attribute for any new analogs.

Additional modifications included the introduction of a pivaloyl amide functional group at the *N*-

terminal amine in exchange for a propyl amide, and epimerization at C-10 going from the natural

(S) configuration to the unnatural *(R)* configuration. These changes increased the potency for the

new analog, but they also decreased the aqueous solubility making it hard to dose animals. The

promising *in vitro* data for LPY36 **(3.42)** suggested further investigation with *in vivo* studies,

which required a scale-up of the synthesis for LPY36 **(3.42)** and related analogs.
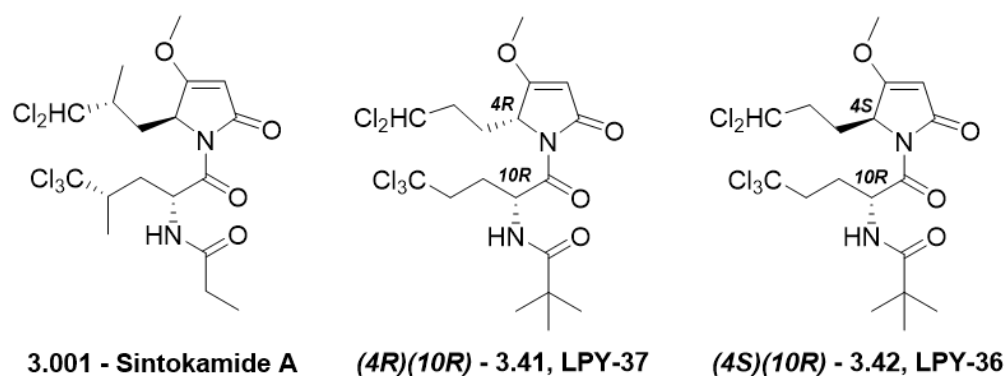
Figure 3.2 – Pharmacologically active MNP Sintokamide A (SINT1) and its most active

synthetic analogs.

3.2.2   Unique AR-NTD Activity of Sintokamides

In order to determine the unique binding to the AR-NTD FL-AR, SINT1 was exposed to a fluorescence polarization competition assay. Using a recombinant AR-LBD with known binding ligand Fluoromone, it was revealed that unlike synthetic androgen R1881, and NSAAs bicalutamide and enzalutamide, SINT1 did not compete with Fluoromone.[32] Full-length AR requires a bound ligand to signal AR nuclear translocation in the absence of androgens, however in SINT1 (**3.001**) treated LNCaP cells, AR remained in the cytoplasm. Three bioactive alkyne-modified sintokamide probes LPY30 (**3.006**) and LPY31 (**3.007**) the inactive probe LPY19 (**3.008**) as a negative control, and one ralaniten probe EPI-053 (**3.009**) as a positive control were evaluated in a Streptavidin pulldown experiment to look for binding to the AR-NTD (**Figure 3.3**). Using a purified recombinant AF-1 protein incubated with the alkyne containing probes followed by Click chemistry, addition of Streptavidin showed that LPY30 (**3.006**), LPY31 (**3.007**), and EPI-053 (**3.009**) were bound to the NTD AF-1 region. To show AF-1 binding inhibits the transactivation of the AR-NTD, LNCaP cells were transactivated by forskolin or IL-6 induction and were then subsequently shown be inhibited by SINT1 and the positive control, ralaniten compound EPI-002 (**2.003**). The interesting finding was that SINT1(**3.001**) inhibits transactivation induced by forskolin, but not IL6, whereas EPI-002 inhibits transactivation by both induction methods.[32] IL6 promotes transactivation using STAT3 to bind AR, showing that sintokamides may uniquely bind a different region of the AR-NTD AF-1 as it doesn't interact with STAT3. As described in chapter 2, ralaniten compounds have been found, through NMR studies, to bind the Tau5 region of the AF-1 in the AR-NTD.[31] This suggests that the sintokamides may interact with the Tau1 region of the AF-1, or perhaps in a region where Tau1 and Tau5 overlap along the AF-1.[32] This interesting finding shows the synergistic potential that

the sintokamide compounds can have with ralaniten analogs. Producing radiolabeled

sintokamide analogs can allow for the determination LNCaP tumor uptake allowing for the

monitoring of tumor progression and metabolism for sintokamides. The total synthesis of

sintokamide analogs will be discussed with minor improvements for ease of handling and scale-

up.
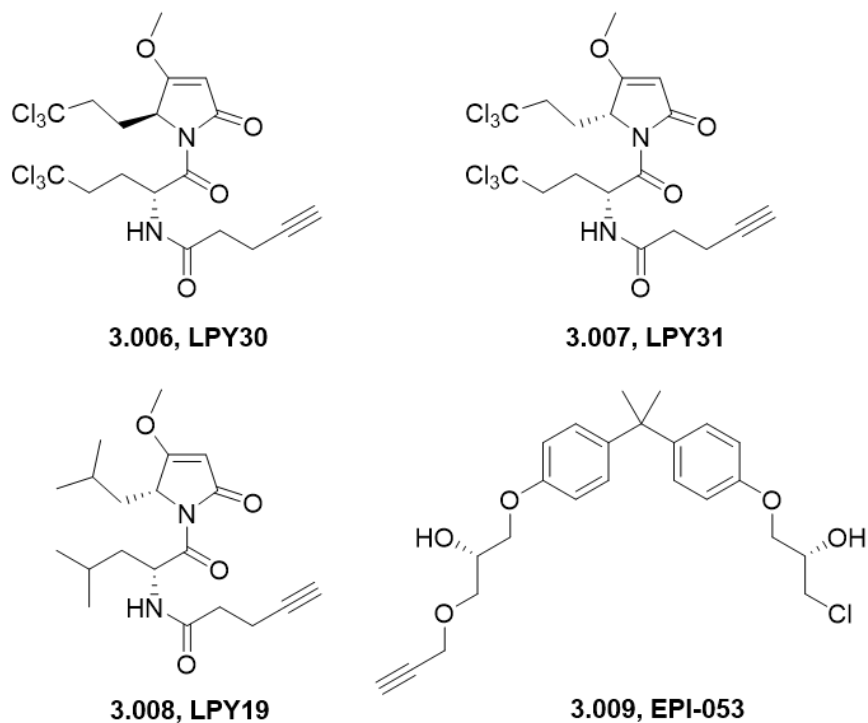
Figure 3.3 – Click probes for a Streptavidin pull down experiment.

3.2.3   Synthesis of Trichlorinated Norleucine Analog (R)-2-((tert-butoxycarbonyl)amino)-5,5,5-trichloropentanoic acid (3.16)

The synthesis of LPY36 and LPY37 (**Scheme 3.1**) begins with relatively inexpensive

reagents so the low yields in the first steps are remedied by the ease of access and cost. **3.10** is

added to a solution of chloroform, sodium hydroxide, and the phase transfer catalyst,

benzyldiethylammonium chloride, to facilitate the 1, 4 – Michael addition reaction. Distillation

was used to isolate the pure trichlorobutylmethylester, **3.11**, in 27.9% yield. Diisobutylaluminum

hydride reduction of **3.11** afforded the aldehyde **3.12**, which was used without further

purification due to the volatility of the product. Next an enantioselective Strecker reaction was

used to generate the amino acid functionality starting with the condensation of **3.12** with Ellman

sulfinamide *(R)-(+)*-2-methyl-2-propanesulfinamide gives the chiral imine, **3.13**, in 73.6% yield

over two steps formed under mild reaction conditions. **3.13** is then reacted with TMSCN in the

presence of a Lewis acid to activate the imine, facilitating the nucleophilic addition of the cyano

group. The reaction is quenched on the column to give **3.14** in 90.0% yield. **3.14** was suspended

in dry MeOH and HCl gas was bubbled in to complete the Strecker reaction forming the

chlorinated norleucine methyl ester analog. Refluxing the intermediate in 6 M HCl proved

elusive as degradation occurred and isolation of the compound was difficult. The formation of

the methyl ester allowed for the *in-situ* Boc protection reaction. HCl gas is formed by adding

concentrated HCl over $CaCl_2$, subsequent gas is passed through a Drierite column prior bubbling

into **3.14** dissolved in anhydrous MeOH. This reaction is followed by quenching with sodium

bicarbonate and removing MeOH and resuspending in THF/H_2O and adding $(Boc)_2O$ producing

3.15 in 83.1% yield over two steps. Hydrolysis of the methyl ester with lithium hydroxide gave

the final trichlorinated norleucine analog **3.16** in 97.7% yield.
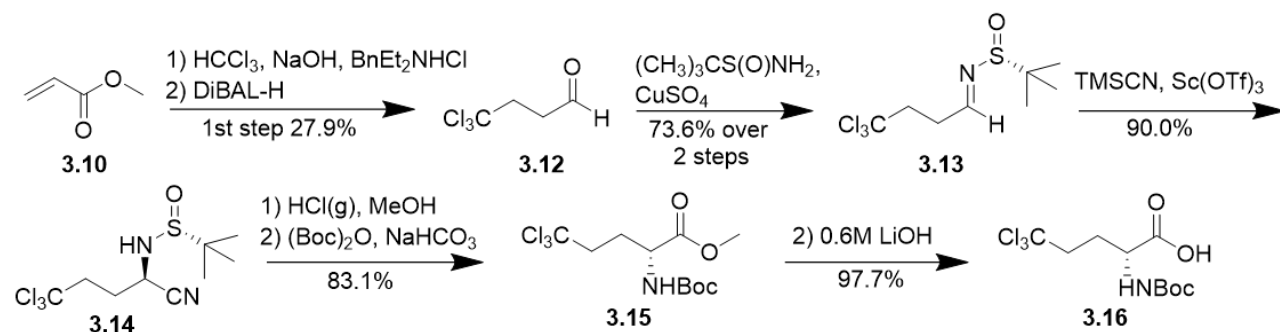
Scheme 3.1 – Synthesis of trichlorinated norleucine analog **3.16**.

3.2.4   Synthesis of gem-Dichlorinated Norleucine Analog Methyl 2-amino-5,5-dichloropentanoate (3.24)

The starting material for making the second chlorinated nor leucine residue was D-Glutamate (**3.03**), but the reaction could have been done with less expensive L-Glutamate because the final sintokamide amines **3.33** and **3.34** epimerize at C-4 during the tetramic acid formation steps giving two diastereomers. The synthesis (**Scheme 3.2**) begins with esterification of **3.20** to form the dimethyl ester mediated through the formation of an acid chloride to give **3.21**. The crude product was used without further purification, and excess sodium bicarbonate was added to **3.21** in the presence of (Boc)$_2$O to mono-Boc protect **3.21**. Subsequent Boc protection was done on the crude mono-Boc protected extract with stronger base DMAP to give the di-Boc protected analog, commenced in two separate reactions, via consecutive nucleophilic acyl substitution reactions with (Boc)$_2$O to produce **3.22** in 91.0% yield over 3 steps. Next, the δ-methyl ester of **3.22** was reduced using DIBAL-H to give **3.23** in 42.6% yield, with the starting material and corresponding alcohol recovered to be recycled for further formation of aldehyde **3.23** via Swern oxidation.
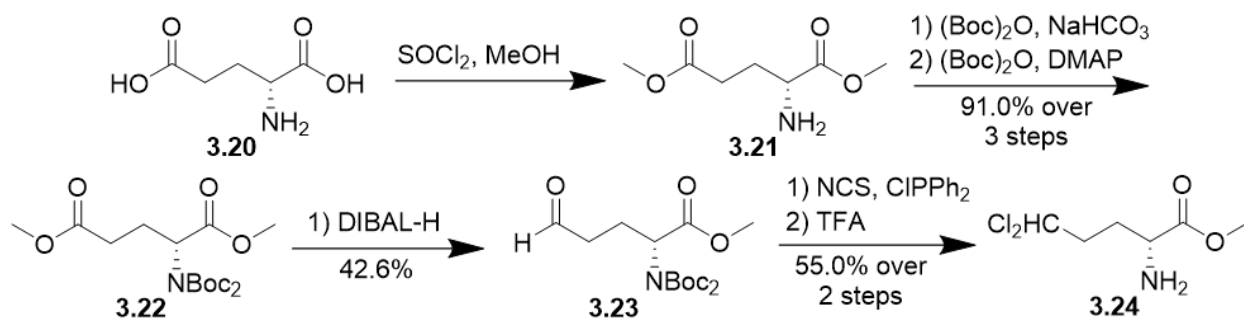
Scheme 3.2 – Synthesis of Gem-dichlorinated norleucine analog **3.24**.

The formation of the gem-dichloride was done previously by bubbling chlorine gas over triphenyl phosphite, however the process was tedious and required the use of chlorine gas, which is caustic and rusts metal making its storage and handling cumbersome. This reaction was replaced (**Figure 3.4)** with generating chloride anions *in situ* and adding **3.23** to generate the final gem-dichloride leucine analog **3.24** via successive nucleophilic reactions, followed by TFA deprotection of the di-Boc protecting group in a moderate yield of 55.0% over two steps
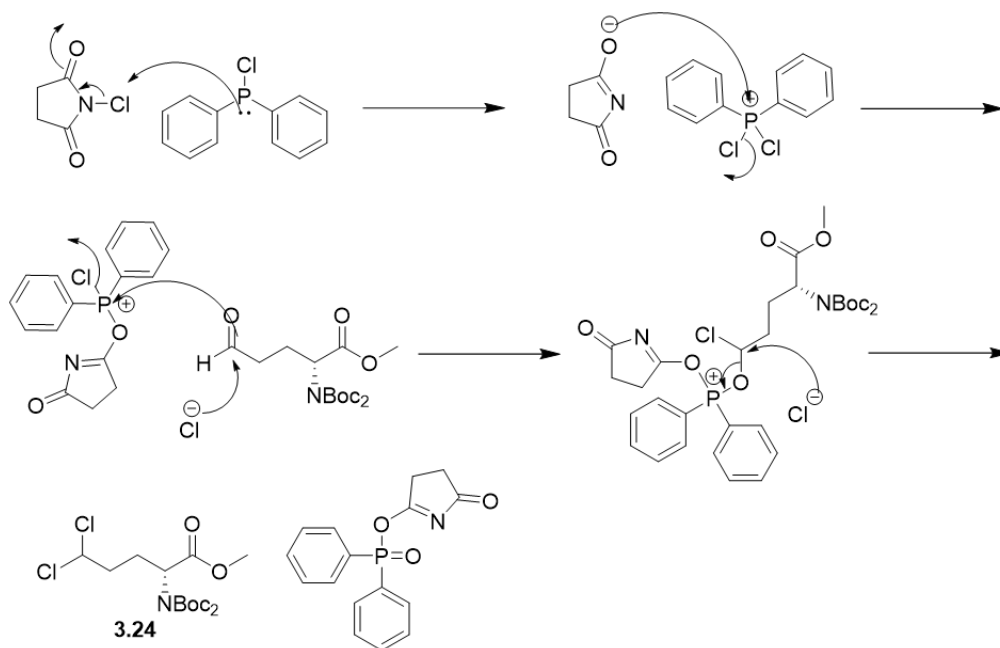
Figure 3.4 – Proposed mechanism of gem-dichloride product **3.24**.

3.2.5 Coupling Chlorinated Norleucine Analogs to Form Free Amine Sintokamide Core Intermediates

The coupling (**Scheme 3.3**) of acid **3.16** and amine **3.24** to form an amide bond was accomplished through the formation of the EDC activated ester with Oxyama Pure being a non-explosive alternative to HOBt, facilitating the cross-coupling without racemization to form dipeptide **3.31** in 91.5% yield.
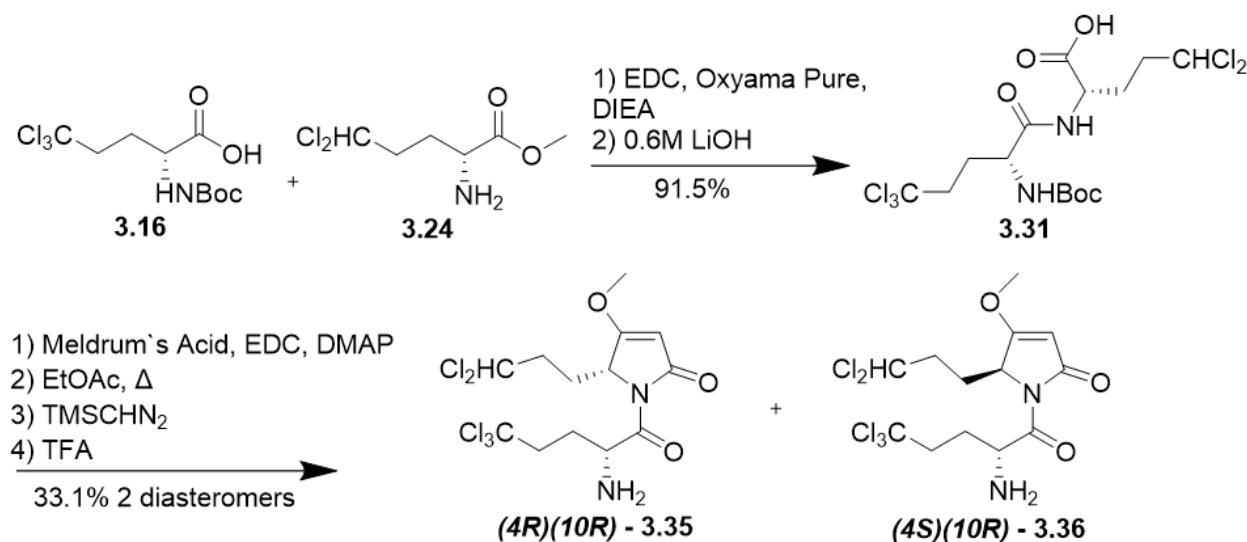
Scheme 3.3 – Coupling of chlorinated norleucine analogs to produce form free amine sintokamide intermediates *(4R)(10R) – 3.35* and *(4S)(10R) – 3.36*.

The formation of the tetramic acid to complete the sintokamide scaffold was originally carried out in 3 successive steps without purification. However, it was found that purifying after the first step to remove excess Meldrum's acid increased the overall yield 2-fold. Mechanistically (**Figure 3.5**), the activated ester is coupled with the Meldrum's acid, which when heated ring opens into a highly reactive ketene which allows for the intramolecular condensation reaction to commence. The solvent is removed and replaced with toluene/methanol

to facilitate the formation of the methyl ether with trimethylsilyldiazomethane. Finally, after

purification, the Boc protecting group is removed with TFA to give *(4R)(10R) – 3.35* and

(4S)(10R) – 3.36 in 33.1% yield across both diastereomers.
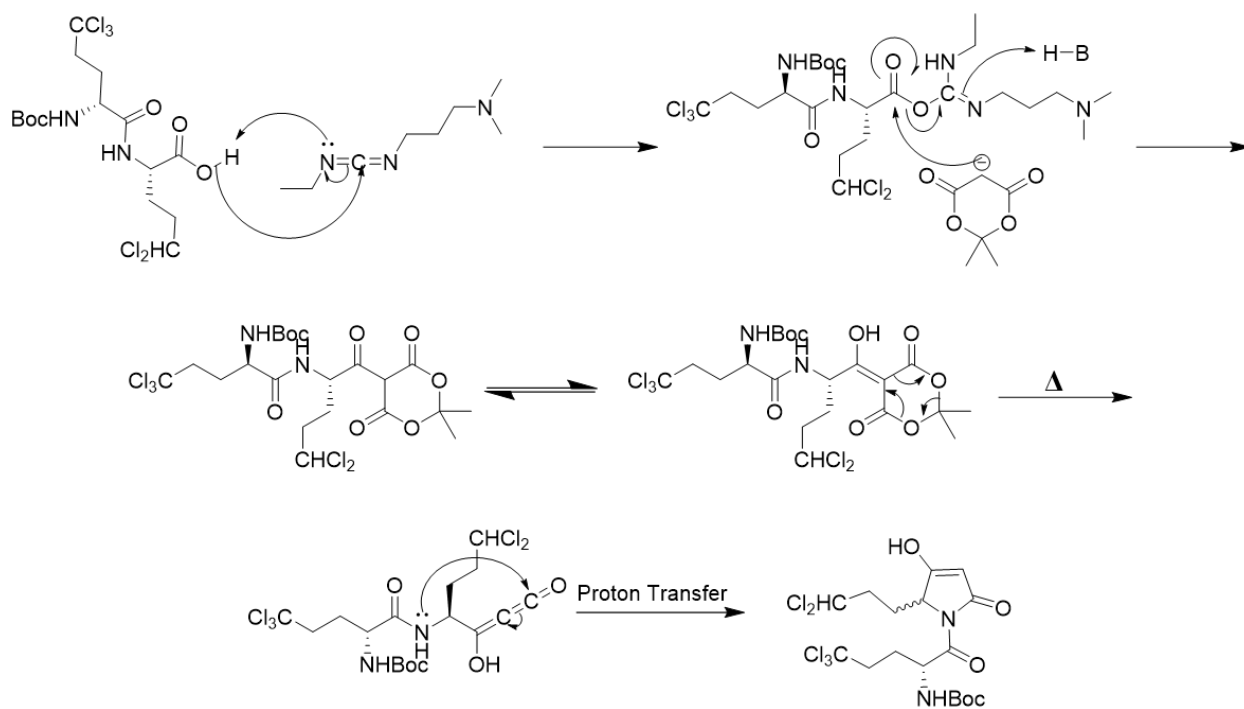
Figure 3.5 – Intramolecular condensation mechanism to form tetramic acid ring**.**

3.2.6   Synthesis and Biological Activity of Sintokamide Analogs LPY36 (3.42) and LPY37 (3.41)

From intermediates *(4R)(10R) – 3.35* and *(4S)(10R) – 3.36,* the synthesis of *(4R)(10R) –*

3.41 (LPY37) and *(4S)(10R) – 3.42* (LPY36) is a straightforward nucleophilic acyl substitution

reaction with pivaloyl chloride (**Scheme 3.4)** to the give the sintokamide analogs in 79.7% and

90.1% yield, respectively. Interestingly, the reaction of **3.41** seemed to generate a sintokamide

by-product to a much greater extent than **3.42**. More work is required to determine what is happening, and whether or not the configuration determines the impurity.
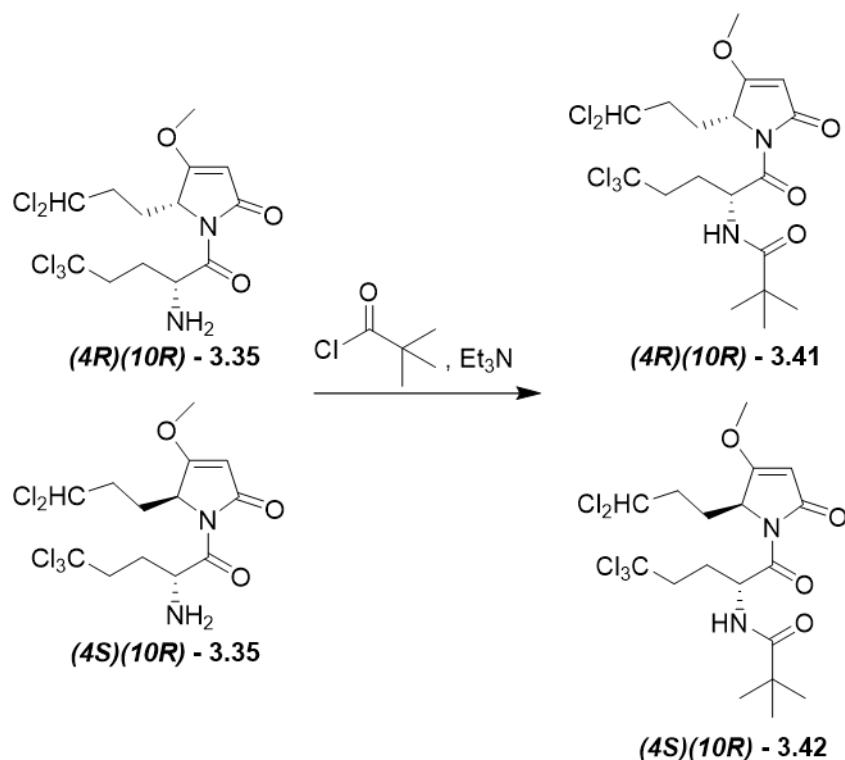
Scheme 3.4 – Synthesis of bioactive sintokamide pivaloyl analogs *(4R)(10R)* **- 3.41** and *(4S)(10R)* **- 3.42**.

(4R)(10R) – 3.41 (LPY37) (15 mg/kg) and *(4S)(10R) – 3.42* (LPY36) (15 mg/kg) were evaluated against LNCaP xenografts in castrated mice treated every other day via oral gavage. **Figure 3.6** shows the antitumor activity that both compounds possess, and at comparable concentrations to industry standard enzalutamide. *(4S)(10R) – 3.42* (LPY36) has superior tumor growth suppression, making it a very promising candidate as an AR-NTD antagonist. Interestingly *(4S)(10R) – 3.42* (LPY36) has the NP configuration, which clearly plays a significant role in the analog's *in vivo* potency.
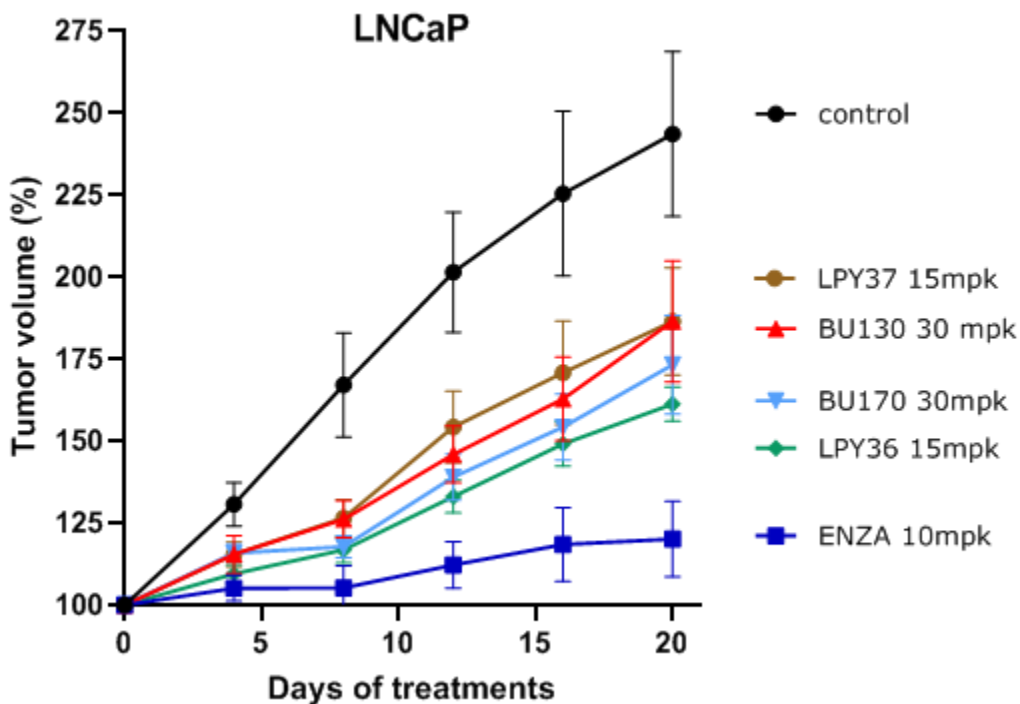
Figure 3.6 - (4R)(10R) – 3.61 (LPY37) (15mg/kg) and **(4S)(10R) – 3.62** (LPY36) (15mg/kg) have LNCaP antitumor activity in castrated mice. Data generated in the Sadar lab at the BCCA**.**

3.2.7   Synthesis and Biological Activity of Sintokamide Analogs LPY39 (3.51) and LPY80 (3.52)

From intermediates *(4R)(10R) – 3.35* and *(4S)(10R) – 3.36*, the synthesis is done in one step, (**Scheme 3.5**) via PyBop cross coupling reaction that proceeds as a nucleophilic acyl substitution reaction to form the sintokamide acetylpiperidine *(4R)(10R) – 3.51* (LPY39) and *(4S)(10R) – 3.52* (LPY80) in 88.3% and 78.9% yield, respectively.
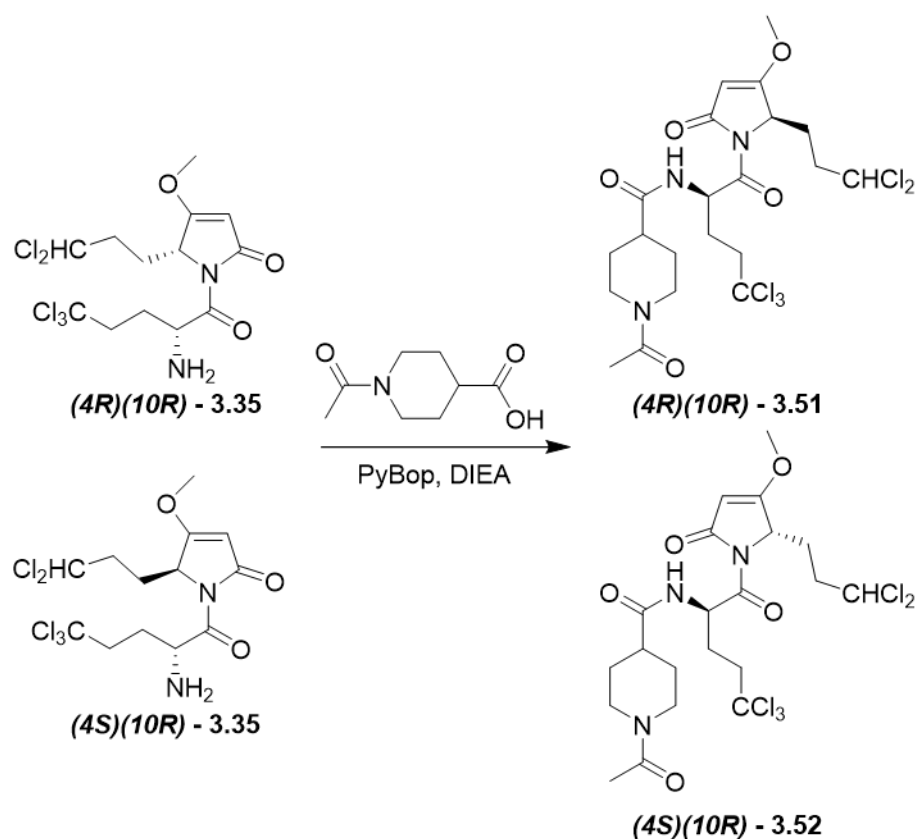
Scheme 3.5 – Synthesis of Sintokamide acetyl piperidines *(4R)(10R)* - **3.51** and *(4S)(10R)* - **3.52**.

The high ClogP of the *in vitro* optimized analogs LYP36 (**3.42**) and LPY37 (**3.41**) made it extremely challenging to evaluate these compounds in murine models of CRPC via either PO or IV administration. The introduction of the acetyl piperidine *N*-terminus cap in the place of pivaloyl brings down the ClogP significantly but still retains the steric hindrance required for metabolic stability. The increase in water solubility of **3.51** made the compound much more amenable to *in vivo* evaluation. Unfortunately, the *in vitro* data for LPY39 (**3.51**) and LPY80 (**3.52**) showed very little activity in the standard LNCaP luciferase transcription inhibition assay and some off-target effects on PC3 cells. The cause of these *in vitro* effects may be the increased

hydrophilic nature of the drug. However, in an *in vivo* human xenograft model of CRPC, **3.51** was the first sintokamide analog shown to effectively inhibit the growth of LNCaP tumors via oral administration at a dose of 50 mg/kg (**Figure 3.7)**. Further investigation of these analogs certainly must be done to corroborate the findings as the *in vivo* and *in vitro* data suggest two stories, demonstrating the fine line researchers walk on drug efficacy.
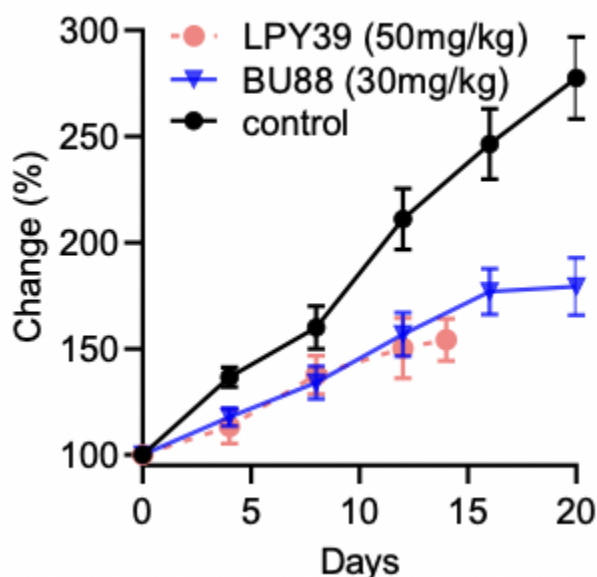
Figure 3.7 – LPY39 (**3.51**) inhibits tumor growth in LNCaP xenografts grown in mice. Data generated in the Sadar lab at the BCCA.

3.2.8   Synthesis of Fluorine Radiolabeled Probes

Radiolabeled probes are important for demonstrating protein target engagement *in vitro* and *in vivo*. The sintokamide target is known to be the AR-NTD, however information on how and where it binds *in vitro* is currently only speculation and there is no evidence that it binds the target *in vivo*. Good radiolabeled probes stay as close in structure as possible to an active analog, so our first attempt at making a radiolabeled probe was to elaborate on sintokamide A **(3.01)**

(**Scheme 3.6**) by incorporating a propionyl bromide moiety, *(4S)(10R) – 3.61* that can, in theory, be easily modified into a ^{18}F-probe. Unfortunately, the lability of the sintokamide core did not allow for the bromine to be selectively displaced. When doing the reaction in a flask, a small amount of "cold" ^{19}F-labeled material, *(4S)(10R) – 3.62*, was recovered using HPLC purification, but upon further review of the NMR spectrum, no olefinic proton could be found despite the compound containing a fluorine by ^{19}F NMR, thus suggesting that the sintokamide core was labile to fluoride anion exposure at elevated temperatures. A second attempt was made to make a *(4R)(10R) – 3.41* (**LPY37**) derivative (**Scheme 3.6**) by having a fluorine on one of the pivaloyl methyl groups. This attempt required the cross-coupling of 3-fluoro-2,2-dimethylpropanoic acid, however the cross-coupling reaction would not proceed, even after several attempts.
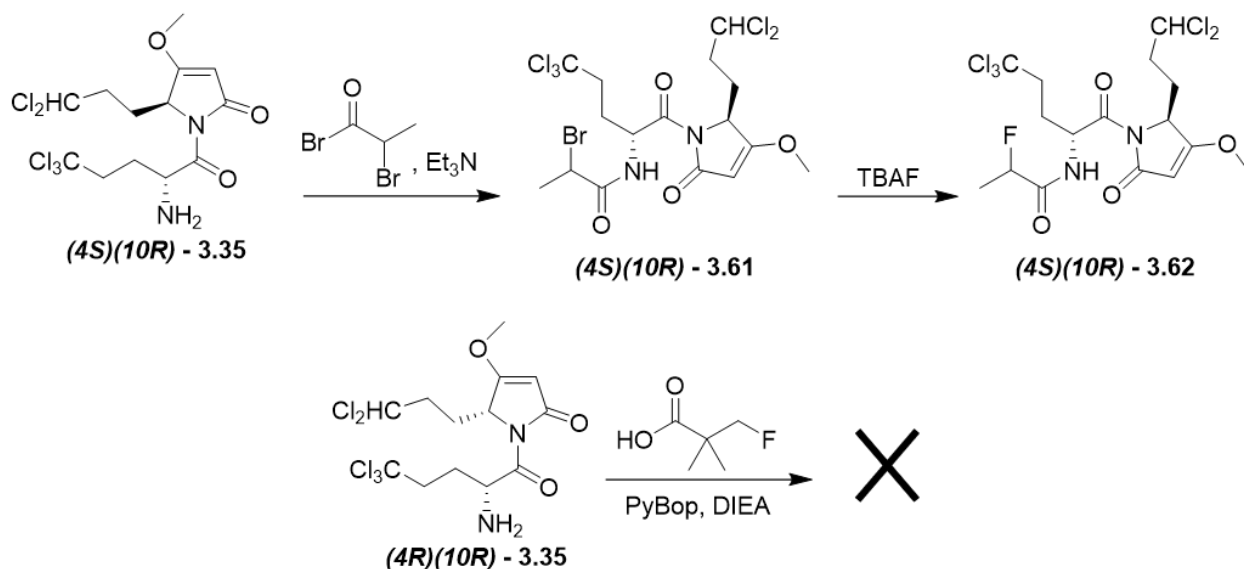
Scheme 3.6 – Fluorinated radiolabeled reaction attempts.

Another attempt was made using an alkyne modified derivative of sintokamide A, where the propyl amide was replaced with 4-pentyne amide. *(4S)(10R) – 3.65*, which was made by a previous researcher and was elaborated on (**Scheme 3.7**) by forming a 1-azido-3-propane tosylate, **3.64**, then "Clicking" that moiety to the sintokamide amide using the Copper (I) mediated 1,3-Huisgen dipolar cycloaddition. The triazole functionality imparts hydrophilicity to the molecule, giving it potential beyond just radiolabeling, while also providing a large UV-signature that allows for ease of purification when using HPLC methods. Furthermore, the triazole C-H proton has a very diagnostic chemical shift that can be used to fingerprint the products *(4S)(10R) – 3.66* and *(4S)(10R) – 3.67.* Ultimately the fluorination of *(4S)(10R) – 3.66* with TBAF was unsuccessful, presumably from the previously observed instability of the sintokamide core in presence of fluoride anions at elevated temperatures.
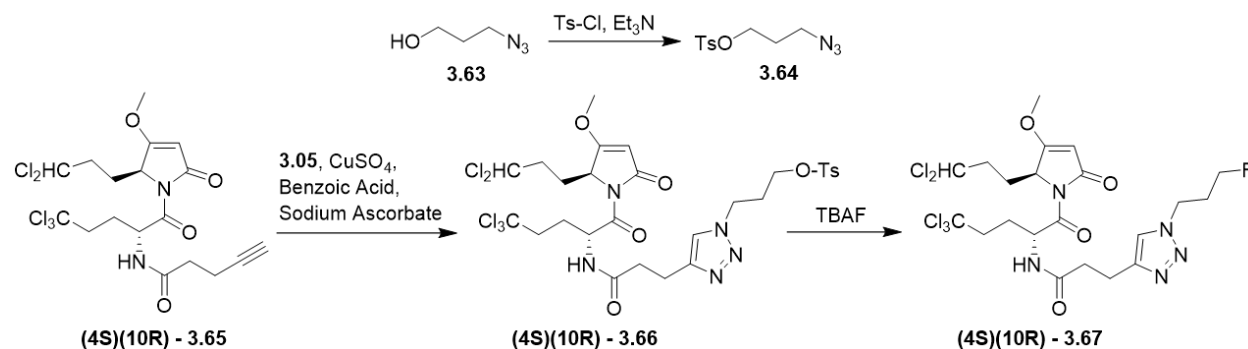
Scheme 3.7 – Synthesis of *(4S)(10R) – 3.66* via Cu(I) mediated 1,3 – Huisgen dipolar cycloaddition followed by TBAF fluorination.

Chapter 4: Experimental

4.1 General

All non-aqueous reactions were carried out in flame-dried glassware and under an argon atmosphere unless otherwise noted. Air and moisture sensitive liquid reagents were manipulated via a dry syringe. All dry solvents have been purchased from Sigma Aldrich protected under a Sure/Seal™. Other solvents and reagents were used as obtained from commercial sources without further purification. NMR spectra were obtained on Bruker Avance 400 direct, 400 inverse, Bruker Avance 600 CryoProbe, and Bruker Avance 850 NMR spectrometers at room temperature unless otherwise noted. Flash column chromatography was performed using Silicycle Ultra-Pure silica gel F60 (230-400 mesh). Analytical thin-layer chromatography (TLC) plates were aluminum-backed ultrapure silica gel 250 μm. Electrospray ionization low resolution mass spectrometry (ESI-LRMS) spectra were recorded on a Bruker HCT instrument. Electrospray ionization high resolution mass spectrometry (ESI-HRMS) spectra were recorded on an Agilent 6545 Q-TOF.

4.2 Experimental for Chapter 2

4.2.1 Preparation of 2.11

2.11
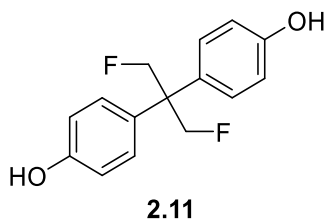
To a 100mL round-bottom flask containing phenol (2.20 g, 23.4 mmol) dissolved in DCM (40 mL) was added 1,3 difluoroacetone (1.00 g, 10.6 mmol). The flask was subsequently cooled to -10°C and Iron (III) chloride (1.72 g, 10.6 mmol) was added. The reaction was stirred overnight with the flask allowed to slowly warm to room temperature. DCM was removed *in vacuo* and the crude oil was taken up in 150 mL of ethyl acetate (EtOAc)/acetone (2:1) and washed with H_2O (25 mL) and brine (25 mL). The organic layer was dried over Na_2SO_4 and concentrated *in vacuo*. The crude extract was purified using silca gel flash chromatography eluting with hexanes/ethyl acetate (4:1) to afford 4,4'-(1,3-difluoropropane-2,2-diyl) diphenol (**2.11**) (406.1mg, 1.54mmol) as a yellow oil in 14.5% yield. ^{1}H NMR (400 MHz, DMSO-d6) δ: 9.40 (s, 2H), 7.01 (d, J = 8.7 Hz, 4H), 6.71 (d, J = 8.7 Hz, 4H), 5.01 (s, 2H), 4.89 (s, 2H). ^{13}C NMR (100 MHz, DMSO-d6) δ: 156.1, 131.2, 128.7, 115.0, 85.7, 83.9, 50.4. ^{19}F NMR (300 MHz, DMSO-d6) δ: -219.8.

4.2.2   Preparation of 2.12

2.12
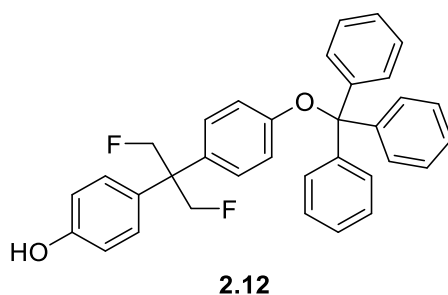
To a 100mL round-bottom flask containing **2.11** (460 mg, 1.74 mmol) in anhydrous DCM (20 mL) at 0°C was added in subsequent order Et_3N (0.25 mL, 1.74 mmol), Trityl chloride (325 mg, 1.17 mmol) in 4 mL DCM added dropwise, followed by a catalytic amount of 4-dimethylamino pyridine (DMAP). The reaction was allowed to proceed overnight, slowly warming to room

temperature. The reaction was diluted with 80 mL of EtOAc and washed with H_2O (15 mL) and brine (15 mL) and the organic layer was dried over Na_2SO_4 and concentrated *in vacuo*. The crude extract was purified using silica gel flash chromatography eluting with hexanes/EtOAc (9:1) to afford **2.12** (360 mg, 0.711 mmol) as a white solid in 60.8% yield. ^1H NMR (400 MHz, DMSO-d6) δ: 9.41 (s, 1H), 7.42 (d, J = 7.6Hz, 3H), 7.30 (m, 12H), 7.03 (d, J = 8.6Hz, 2H), 6.89 (dd, $J_{1,2}$ = 3.7, $J_{1,3}$ = 8.8Hz, 2H), 6.73 (d, J = 8.7Hz, 2H), 6.69 (d, J = 8.7Hz, 1H), 6.63 (d, J = 8.8Hz, 1H), 4.98 (d, J = 30.2Hz, 2H). ^{13}C NMR (100 MHz, DMSO-d6) δ: 156.1, 147.8, 143.7, 128.7, 128.6, 128.4, 127.9, 127.8, 127.5, 127.2, 126.6, 120.1, 115.0, 89.6, 80.5. ^{19}F NMR (300 MHz, DMSO-d6) δ: -219.8, -220.4.

4.2.3   Preparation of 2.13

2.13
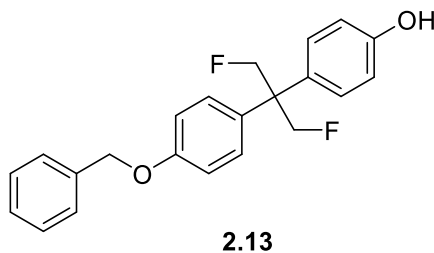
To a 50mL round-bottom flask containing **2.11** (690.8 mg, 2.61 mmol) in anhydrous DMF (20 mL) at 0°C was added K_2CO_3 (361.3 mg, 2.61 mmol) followed by benzyl bromide (300 mg, 1.75 mmol) in 3 mL of DMF. The reaction was stirred overnight and allowed to warm to room temperature. The reaction was diluted to 80mL of EtOAc and was washed with H_2O (3x 10 mL) and brine (3x 10 mL) and the organic layer was dried over Na_2SO_4 and concentrated *in vacuo*. The crude extract was purified using silica gel flash chromatography eluting with the hexanes/EtOAc (9:1) to afford **2.13** (267.6 mg, 0.755 mmol) as a white solid in the 43.1% yield. ^1H NMR (400 MHz, DMSO-d6) δ: 9.42 (s, 1H), 7.41 (m, 5H), 7.16 (d, J = 8.8Hz, 2H), 7.03 (d, J

= 8.6Hz, 2H), 6.99 (d, J = 8.9 Hz, 2H), 6.73 (d, J = 8.7Hz, 2H), 5.10 (s, 2H), 5.06 (s, 2H), 4.94

(s, 2H). ^{13}C NMR (100 MHz, DMSO-d6) δ: 1571., 156.2, 137.1, 128.8,128.7, 128.4, 127.7,

115.1, 114.5, 85.6, 83.9, 69.1. ^{19}F NMR (300 MHz, DMSO-d6) δ: -220.2.

4.2.4 Preparation of 2.21

2.21
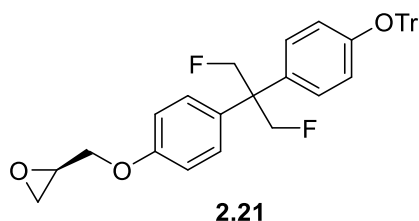
To a 100mL round-bottom flask containing **2.12** (1.14 g, 2.25 mmol) in anhydrous DMF (20

mL) cooled 0°C was added NaH 60% in mineral oil (108.1 mg, 2.70 mmol) portion-wise. After

stirring for 10 minutes, *(R)*-glycidol tosylate (565.3 mg, 2.48 mmol) was added in 5 mL of DMF

dropwise over 5 minutes. The reaction was allowed to stir overnight, slowly warming to room

temperature. The reaction was cooled back down to 0°C and was quenched with slowly with

1mL of saturated ammonium chloride followed by pouring in a further 15 mL and dilution with

80 mL of EtOAc. The organic layer was then washed with H$_2$O (3x 10 mL) and brine (3x 10 mL)

and dried over Na$_2$SO$_4$ then concentrated *in vacuo.* The crude extract was then purified by silica

gel flash chromatography eluting with Hexanes/EtOAc (7:3) to afford **2.21** (1.04 g, 1.86 mmol)

as a white solid in 82.5% yield. ^{1}H NMR (400 MHz, DMSO-d6) δ: 7.42 (d, J = 7.4Hz, 6H), 7.35

(t, J = 7.2Hz, 6H), 7.28 (t, J = 7.2Hz, 3H), 7.01 (d, J = 8.8Hz, 2H), 6.91 (d, J = 4.1Hz, 2H), 6.89

(d, J = 4.0Hz, 2H), 6.63 (d, J = 8.9Hz, 2H), 4.98 (s, 2H), 4.87 (s, 2H), 4.32 (dd, J = 11.4Hz, 1H),

3.83 (dd, J = 11.4Hz, 1H), 3.33 (m, 1H), 2.86 (dd, J = 4.9Hz, 1H), 2.72 (dd, J = 5.1Hz, 1H). ^{13}C

NMR (100 MHz, DMSO-d6) δ: 157.0, 154.5, 143.6, 128.8, 128.4, 127.9, 127.8, 127.2, 120.2,

114.3, 89.6, 68.9, 49.7, 43.7. ^{19}F NMR (300 MHz, DMSO-d6) δ: -220.8.

4.2.5 Preparation of 2.22
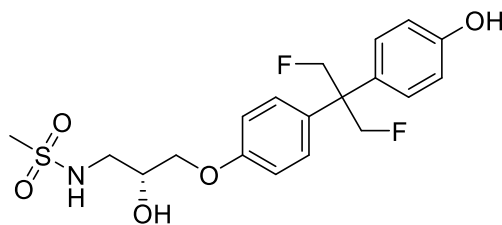
2.22

A 50 mL round-bottom flask containing **2.21** (370 mg, 0.658 mmol), methanesulfonamide (968 mg, 9.86 mmol), and Cs_2CO_3 (257 mg, 0.789 mmol) was dissolved in DMF (20 mL) and heated to 100°C for 3 hours. Upon the reaction cooling it was diluted with 60 mL of EtOAc and the pH was adjusted to PH ~7 with 6 M HCl and was washed with H_2O (3x 10 mL) and brine (3x 10 mL) and the organic layer was dried over Na_2SO_4 and concentrated *in vacuo.* The crude extract was dissolved in 15 mL of DCM and cooled to 0°C and ~3 mL of 6 M HCl was added followed by MeOH until a homogenous solution was formed and was stirred overnight. The reaction was diluted with 60 mL of EtOAc and was quenched with $NaHCO_3$ to pH ~6 and was washed with H_2O (10 mL) and brine (10 mL) and the organic layer was dried over Na_2SO_4 and concentrated *in vacuo.* The crude extract was purified by silica gel flash chromatography eluting with DCM/MeOH (95:5) to afford **2.22** (170 mg, 0.410 mmol) as a colorless oil in 62.3% yield. ^{1}H NMR (400 MHz, DMSO-d6) δ: 9.42 (s, 1H), 7.15 (d, J = 8.8Hz, 2H), 7.06 (t, J = 6.2Hz, 1H), 7.03 (d, J = 8.6Hz, 2H), 6.92 (d, J = 8.9Hz, 2H), 6.74 (d, J = 8.7Hz, 2H), 5.28 (d, J = 4.8Hz, 1H), 5.05 (s, 2H), 4.93 (s, 2H), 3.96 (quin, $J_{1,3}$ = 12.1Hz, $J_{2,3}$ = 5.0Hz, 1H), 3.90 (t, J = 5.0Hz, 2H), 3.16 (m, 1H), 3.05 (m, 1H), 2.94 (s, 3H). ^{13}C NMR (100 MHz, DMSO-d6) δ: 157.3, 156.2, 133.1, 131.0, 128.8, 128.7, 115.1, 114.3, 85.6, 83.8, 69.7, 68.1, 50.6, 45.6. ^{19}F NMR (300 MHz, DMSO-d6) δ: -220.1.

4.2.6 Preparation of 2.23

2.23
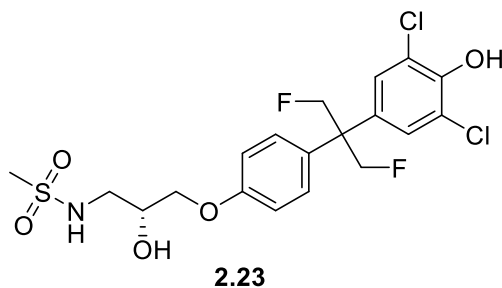
To a 50 mL round-bottom flask containing **2.22** (170 mg, 0.410 mmol) in Acetonitrile (15 mL) cooled to -20°C was added 10% solution NaOCl (762 mg, 1.02 mmol). The reaction was stirred for 10 minutes at -20°C before being quenched with a saturated solution of $NaHSO_3$ (10 mL). The mixture was diluted with 30mL of EtOAc and washed with H_2O (10 mL) and brine (10 mL) and the organic layer was dried over Na_2SO_4 and concentrated *in vacuo*. The crude extract was purified by silica gel flash chromatography eluting with Hexanes/EtOAC (2:3) to afford **2.23** (124 mg, 0.256 mmol) as a pale-yellow oil in 62.6% yield. ^1H NMR (400 MHz, DMSO-d6) δ: 10.24 (s, 1H), 7.21 (s, 2H), 7.18 (d, J = 8.8Hz, 2H), 7.05 (t, J = 6.1Hz, 1H), 6.95 (d, J = 8.9Hz, 2H), 5.28 (d, J = 4.8Hz, 1H), 5.11 (dd, $J_{1,2}$ = 6.4Hz, $J_{2,3}$ = 9.7Hz, 2H), 5.00 (dd, $J_{1,2}$ = 6.3Hz, $J_{2,3}$ = 9.4Hz, 2H), 3.97 (m, 1H), 3.91 (m, 2H), 3.16 (m, 1H), 3.06 (m, 1H), 2.94 (s, 3H). ^{13}C NMR (100 MHz, DMSO-d6) δ: 157.6, 148.1, 128.8, 128.0, 122.1, 114.5, 85.2, 83.5, 69.7, 68.1, 50.8, 45.6. ^{19}F NMR (300 MHz, DMSO-d6) δ: -221.4.

4.2.7　Preparation of 2.24 (BU-86)

2.24, BU-86
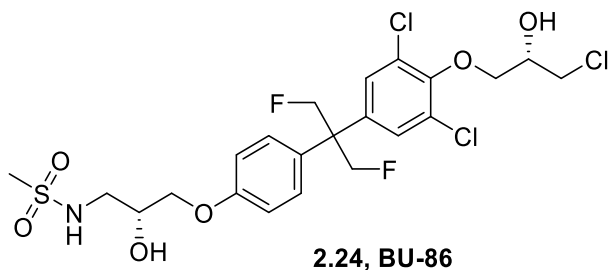
To a 50mL round-bottom flask containing **2.23** (64.8 mg, 0.138 mmol) in anhydrous DMF (6 mL) was added K_2CO_3 (20.0 mg, 0.145 mmol) at 0°C. To this flask was added *(R)*-glycidol tosylate (33.1 mg, 0.145 mmol) dropwise in 2 mL of DMF. The reaction was stirred at 0°C for 10 minutes before the ice bath was removed and the reaction was heated to 50°C and allowed to stir overnight. The reaction was quenched with water and diluted with EtOAc (60 mL) and washed with H_2O (2x 10 mL) and brine (3x 10 mL) and the organic layer was dried over sodium sulfate and concentrated *in vacuo*. The crude mixture was used without. further purification. The crude was re-dissolved in acetonitrile (40 mL) in a 50 mL round-bottom flask equipped a condenser, and cerium trichloride heptahydrate (66.8 mg, 0.179 mmol) was added before refluxing the reaction overnight. The reaction was filtered over celite and the celite was washed with acetonitrile (3x 50 mL). The solvent was removed *in vacuo* and the crude mixture was purified using silica gel flash chromatography eluting with hexanes/EtOAc (3:2) to afford **2.24** (63.1 mg, 0.109 mmol) as a white solid in a yield of 79.3%. ^{1}H NMR (400 MHz, DMSO-d6) δ: 7.34 (s, 2H), 7.17 (d, J = 7.6Hz, 2H), 7.05 (t, J = 6.1Hz, 1H), 6.95 (d, 8.5Hz, 2H), 5.58 (d, 5.2Hz, 1H), 5.27 (d, 4.4Hz, 1H), 5.15 (m, 2H), 5.02 (m, 2H), 4.07 (m, 1H), 4.01 (m, 2H), 3.96 (m, 1H), 3.88 (m, 3H), 3.73 (d, J = 5.3Hz, 1H), 3.14 (m, 1H), 3.04 (m, 1H), 2.93 (s, 3H). ^{13}C NMR (100 MHz, DMSO-d6) δ: 157.7, 128.8, 128.7, 128.0, 122.1, 114.6, 114.5, 74.2, 69.7, 69.1, 68.1, 46.6,

45.6. ^{19}F NMR (300 MHz, DMSO-d6) δ: -220.0. ESI-HRMS: *m/z* calculated for

$C_{22}H_{26}Cl_3F_2NO_5S$ [M-H]-, 559.0565; found, 559.0568.

4.2.8 Preparation of 2.25 (BU-87)

2.25, BU-87
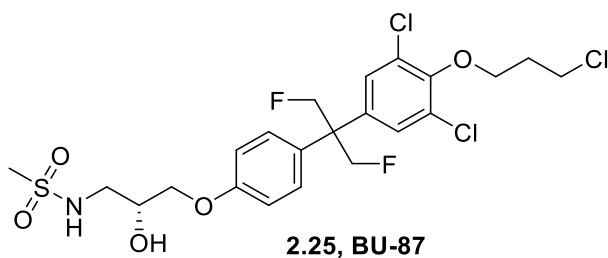
To a 50mL round-bottom flask containing **2.23** (320 mg, 0.715 mmol) in anhydrous DMF (10

mL) was added K_2CO_3 (103.8 mg, 0.751 mmol) at 0°C. To this flask was added 1-bromo-3-

chloropropane (118.3 mg, 0.751 mmol) dropwise in 2 mL of DMF. The reaction was stirred at

0°C for 10 minutes before the ice bath wave removed and reaction was heat to 50°C and allowed

to stir overnight. The reaction was quenched with H_2O and diluted with 60 mL of EtOAc and

washed with H_2O (2x 10 mL) and brine (3x 10 mL) and the organic layer was dried over Na_2SO_4

and concentrated *in vacuo.* The crude extract was purified by silica gel flash chromatography

eluting with hexanes/EtOAc (3:2) to afford **2.25** (326 mg, 0.581 mmol) as a white solid in a yield

of 81.3%. ^{1}H NMR (600 MHz, DMSO-d6) δ: 7.32 (s, 2H), 7.15 (d, J = 8.8Hz, 2H), 7.01 (t, J =

6.1Hz, 1H), 6.92 (d, J = 8.9Hz, 2H), 5.24 (d, J = 5.0, 1H), 5.09 (dd, $J_{1,2}$ = 16.6Hz, $J_{2,3}$ = 9.7Hz,

2H), 5.02 (dd, $J_{1,2}$ = 16.2Hz, $J_{2,3}$ = 9.5Hz, 2H), 4.10 (t, J = 5.9, 2H), 3.93 (m, 1H), 3.88 (m, 2H),

3.85 (t, J = 6.5Hz, 2H), 3.12 (m, 1H), 3.02 (m, 1H), 2.90 (s, 3H), 2.19 (quin, $J_{1,3}$ = 12.4Hz, $J_{2,3}$ =

6.2Hz, 2H). ^{13}C NMR (150 MHz, DMSO-d6) δ: 157.7, 149.4, 139.2, 131.3, 128.8, 128.7, 128.2,

114.6, 70.2, 69.6, 68.1, 51.2, 51.1, 51.0, 45.5, 41.7*, 41.7*, 32.6. ^{19}F NMR (300 MHz, DMSO-

d6) δ: -220.0. ESI-HRMS: *m/z* calculated for $C_{22}H_{26}Cl_3F_2NO_6S$ [M-H]-, 575.0514; found, 575.0518.

4.2.9   Preparation of 2.26 (BU-88)

2.26, BU-88
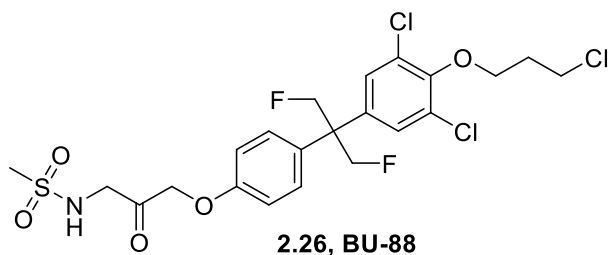
To a 50mL round-bottom flask containing **2.25** (580 mg, 1.03 mmol) dissolved in anhydrous DCM (15 mL) was added 0.3M Dess-Martin reagent (4.00 mL, 1.19 mmol) dropwise at 0°C, over 5 minutes. The reaction was stirred for 6 hours at 0°C before being quenched with saturated sodium thiosulfate and diluted with 60 mL EtOAc. The organic layer was washed with water (2x 10 mL) and brine (2x 10 mL) and dried over Na_2SO_4 and concentrated *in vacuo*. The crude extract was purified with silica gel flash chromatography eluting with hexanes/EtOAc (1:4) to afford ketone **2.26** (277 mg, 0.494 mmol) in a yield of 48.1%. ^{1}H NMR (600 MHz, DMSO-d6) δ: 7.43 (t, J = 3.8Hz, 1H), 7.33 (s, 2H), 7.14 (d, J = 5.9Hz, 2H), 6.90 (d, J = 5.9Hz, 2H), 5.11 (dd, $J_{1,2}$ = 6.5Hz, $J_{1,3}$ = 16.2Hz, 2H), 5.03 (dd, $J_{1,2}$ = 6.3Hz, $J_{1,3}$ = 16.1Hz, 2H), 4.93 (s, 2H), 4.11 (s, 2H), 4.09 (t, J = 3.8Hz, 2H), 3.85 (t, J = 4.3Hz, 2H), 2.93 (s, 3H), 2.19 (quin, $J_{1,3}$ = 8.4Hz, $J_{2,3}$ = 4.1Hz, 2H). ^{13}C NMR (150 MHz, DMSO-d6) δ: 202.1, 156.8, 149.4, 139.1, 131.8, 128.8, 128.7, 128.2, 114.6, 84.8, 83.6, 70.3, 51.1, 49.0, 41.7, 32.6. ^{19}F NMR (300 MHz, DMSO-d6) δ: -222.1. ESI-HRMS: *m/z* calculated for $C_{22}H_{24}Cl_3F_2NO_5S$ [M-H]-, 575.0409; found, 575.0411.

4.2.10 Preparation of 2.31

2.31
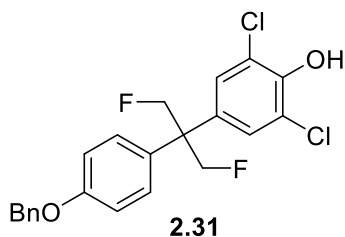
To a round-bottom flask containing **2.13** (160 mg, 0.451 mmol) dissolved in acetonitrile (40 mL) and cooled to 0°C was added 10% NaOCl (840 mg, 1.13 mmol). The reaction was stirred for 2 hours and allowed to warn to room temperature before being quenched with NaHSO$_3$ and diluted with 60 mL EtOAc. The organic layer was subsequently washed with H$_2$O (10 mL) and brine (10 mL) and dried over Na$_2$SO$_4$ and solvent was removed *in vacuo.* The crude product was purified by silica gel flash chromatography eluting with hexanes/EtOAc (4:1) to afford **2.31** (142 mg, 0.401 mmol) as a pale-yellow oil in 74.7% yield. ^{1}H NMR (400 MHz, DMSO-d6) δ: 10.24 (s, 1H), 7.42 (m, 5H), 7.22 (s, 2H), 7.19 (d, J = 8.8Hz, 2H), 7.03 (d, J = 8.9Hz, 2H), 5.12 (dd, J$_{1,3}$ = 13.9Hz, J$_{2,3}$ = 4Hz, 2H), 5.00 (dd, J$_{1,3}$ = 15.3Hz, J$_{2,3}$ = 5.8Hz, 2H). ^{13}C NMR (100 MHz, DMSO-d6) δ: 157.4, 148.1, 137.0, 133.8, 131.9, 128.9, 128.4, 128.0, 127.8, 127.7, 122.1, 114.7, 85.2, 83.5, 69.2, 50.8. ^{19}F NMR (300 MHz, DMSO-d6) δ: -221.5.

4.2.11 Preparation of 2.32

2.32
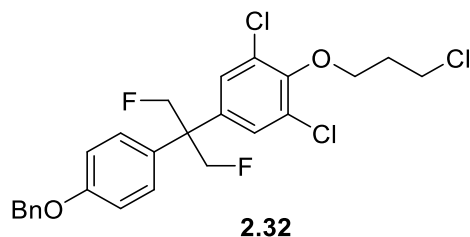
To a round-bottom flask cooled to 0°C containing **2.31** (690 mg, 1.63 mmol) in DMF (20 mL) was added K_2CO_3 (270 mg, 1.96 mmol) followed by 1-bromo-3-chloropropane (270 mg, 1.71 mmol). The reaction was stirred overnight and allowed to warm slowly to room temperature. The reaction was quench with 10mL of H_2O and diluted with 80mL of EtOAc. The organic layer was washed with H_2O (2x 15 mL) and brine (3x 15 mL) and then dried over Na_2SO_4 and concentrated *in vacuo.* The crude mixture was used in the next step without further purification. ^{1}H NMR (400 MHz, DMSO-d6) δ: 7.42 (m, 5H), 7.37 (s, 2H), 7.20 (d, J = 8.8Hz, 2H), 7.04 (d, J = 8.9Hz, 2H), 5.16 (dd, $J_{1,3}$ = 9.8Hz, $J_{2,3}$ = 8.4Hz, 2H), 5.12 (s, 2H), 5.05 (dd, $J_{1,3}$ = 9.5Hz, $J_{2,3}$ = 8.4Hz, 2H), 4.14 (t, J = 5.9Hz, 2H), 3.89 (t, J = 6.4Hz, 2H), 2.23 (quin, $J_{1,3}$ = 12.4Hz, $J_{2,3}$ = 6.2Hz, 2H). ^{13}C NMR (100 MHz, DMSO-d6) δ: 157.5, 149.4, 139.2, 137.0, 131.5, 128.9, 128.7, 128.4, 128.2, 127.9, 127.7, 114.8, 85.1, 83.3, 70.3, 69.2, 51.1, 41.7, 32.7. ^{19}F NMR (300 MHz, DMSO-d6) δ: -222.1.

4.2.12 Preparation of 2.33 (BU-89)

2.33, BU-89
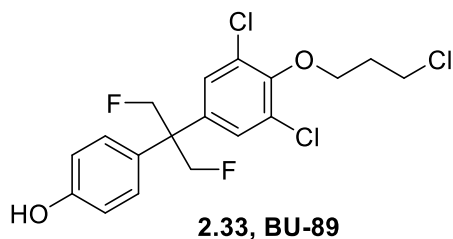
To a round-bottom flask containing **2.32** (670 mg, 1.34 mmol) in anhydrous DCM (30 mL) was added 2.0 M trichloroborane-methyl sulfide complex (3.35 mL, 6.70 mmol). The reaction was stirred for 5 hours before being quenched with $NaHCO_3$. The reaction was diluted further with 90mL of DCM and washed with $NaHCO_3$ (2x 15 mL), H_2O (1x 15 mL) brine (3x 15 mL) and dried over Na_2SO_4 and concentrated *in vacuo.* The crude extract was purified using silica gel flash chromatography eluting with hexanes/EtOAc (7:3) to afford **2.33** (413 mg, 1.01 mmol) as a pale-red/orange solid in 75.2% yield and 61.8% yield over 2-steps. ^{1}H NMR (600 MHz, DMSO-d6) δ: 9.49 (s, 1H), 7.31 (s, 2H), 7.02 (d, J = 8.7Hz, 2H), 6.73 (d, J= 8.8Hz, 2H), 5.07 (dd, $J_{1,2}$ = 9.6Hz, $J_{2,3}$ = 17.8Hz, 2H), 4.99 (dd, $J_{1,2}$ = 9.6Hz, $J_{2,3}$ = 17.8Hz, 2H), 4.09 (t, J = 6.1Hz, 2H), 3.85 (t, J = 6.5Hz, 2H), 2.22 (quin, $J_{1,3}$ = 12.4Hz, $J_{2,3}$ = 6.2Hz, 2H). ^{13}C NMR (150 MHz, DMSO-d6) δ: 156.5, 149.3, 139.4, 129.4, 128.7, 128.6, 128.2, 115.3, 84.8, 83.6, 70.2, 51.0, 41.7, 32.6. ^{19}F NMR (300 MHz, DMSO-d6) δ: -221.6. ESI-HRMS: *m/z* calculated for $C_{18}H_{17}Cl_3F_2O_2$ [M-H]- 408.0262; found, 408.0263.

4.2.13 Preparation of 2.41

2.41
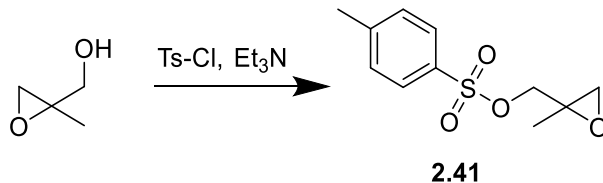
To a 100 mL round-bottom flask cooled to 0°C containing 2-methyl glycidol (1.00 g, 11.35 mmol) in anhydrous DCM (30 mL) was added Et₃N (3.19 mL, 22.70 mmol) followed by tosyl chloride (2.27 g, 11.92 mmol) in 10 mL of DCM added dropwise then a catalytic amount of DMAP was added. The reaction was stirred overnight and allowed to warm to room temperature slowly. The reaction was diluted with 120 mL of DCM and washed with H_2O (2x 20 mL) and brine (2x 20 mL) and dried over Na_2SO_4 and concentrated *in vacuo.* The crude extract was purified with silica gel flask chromatography using hexanes/EtOAc (4:1) to afford **2.41** (2.58g, 10.65mmol) as a colorless oil in 93.8% yield. ¹H NMR (400 MHz, DMSO-d6) δ: 7.81 (d, J = 8.3Hz, 2H), 7.51 (d, J = 8.0Hz, 2H), 4.25 (d, J = 10.9Hz, 1H), 3.87 (d, J = 10.9Hz, 1H), 2.70 (d, J = 4.8Hz, 1H), 2.65 (d, J = 4.8Hz, 1H), 2.44 (s, 3H), 1.23 (s, 3H).

4.2.14 Preparation of 2.42

2.42
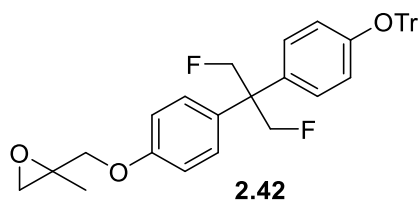
To a 250 mL round-bottom flask cooled to 0 °C containing **2.12** (3.17 g, 6.26 mmol) in anhydrous DMF (40 mL) was added 60% in mineral oil NaH (300 mg, 7.51 mmol). After stirring for 10 minutes **2.41** (1.60 g, 6.57 mmol) was added in 10 mL of DMF dropwise. The reaction was allowed to proceed overnight slowly warming to room temperature. The reaction was

quenched with 30 mL of saturated NH$_4$Cl and diluted with 120 mL of EtOAc and washed with

H$_2$O (3x 30 mL) and brine (3x 30 mL) and dried over Na$_2$SO$_4$ and concentrated *in vacuo.* The

reaction was purified using silica gel flash chromatography eluting with hexanes/EtOAc (8:2) to

afford **2.42** (2.41 g, 4.20 mmol) in 67.1% yield. ^{1}H NMR (400 MHz, DMSO-d6) δ: 7.42 (d, J =

7.4Hz, 6H), 7.35 (t, J = 7.2Hz, 6H), 7.29 (t, J = 7.1Hz, 4H), 7.00 (d, J = 8.8Hz, 2H), 6.90 (d, J =

1.9, 2H), 6.88 (d, J = 1.8Hz, 2H), 6.62 (d, J = 8.8Hz, 2H), 4.98 (s, 2H), 4.86, (s, 2H), 4.12 (d, J =

10.8Hz, 1H), 3.87 (d, J = 10.8Hz, 1H), 2.81 (d, J = 5.0Hz, 1H), 2.71 (d, J = 5.0Hz, 1H), 2.05 (s,

1H), 1.39 (s, 3H). ^{13}C NMR (100 MHz, DMSO-d6) δ: 143.6, 128.7, 128.4, 127.9, 127.2, 120.2,

114.3, 71.3, 55.2, 50.8, 18.2. ^{19}F NMR (300 MHz, DMSO-d6) δ: -220.8.

4.2.15 Preparation of 2.43

2.43
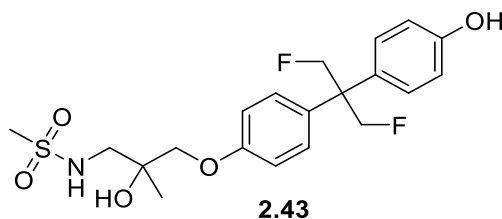
To a 100 mL round-bottom flask containing **2.42** (2.41 g, 4.20 mmol) dissolved in anhydrous

DMF (50 mL) was added methane-sulfonamide (6.18g, 63.0mmol) followed by Cs$_2$CO$_3$ (1.64 g,

5.04 mmol). The reaction mixture was equipped with a condenser and heated to 80°C overnight.

The reaction was diluted with 150 mL of EtOAc and washed with H$_2$O (3x 30 mL) and brine (3x

30 mL) and dried over Na$_2$SO$_4$ and concentrated *in vacuo.* The extract was then dissolved in 40

mL of DCM and ~6 mL of 6 M HCl was added, followed by the addition of methanol until the

solution became homogenous. The mixture was stirred for 4 hours at room temperature before

being concentrated *in vacuo*. The crude mixture was taken up in 150 mL of EtOAc and quenched with NaHCO$_3$ until pH 6, the organic layer was then washed with H$_2$O (1x 30 mL) and brine (1x 30 mL) and dried over Na$_2$SO$_4$ and concentrated *in vacuo*. The crude extract was then purified by silica gel flash chromatography eluting with DCM/MeOH (95:5) to afford **2.43** (1.35 g, 3.25 mmol) as a colorless oil in 77.4% yield. ^{1}H NMR (400 MHz, DMSO-d6) δ: 9.40 (s, 1H), 7.14 (d, J = 8.8Hz, 2H), 7.02 (d, J = 8.7Hz, 2H), 6.90 (d, J = 8.8Hz, 2H), 6.72 (d, J = 8.7Hz, 2H), 5.04 (s, 2H), 4.91 (s, 2H), 4.89 (s, 1H), 3.80 (d, J = 9.3Hz, 1H), 3.73 (d, J = 9.3Hz, 1H), 3.05 (m, 2H), 2.91 (s, 3H), 1.20 (s, 3H). ^{13}C NMR (100 MHz, DMSO-d6) δ: 158.1, 156.8, 129.4, 115.7, 115.0, 86.3, 73.1, 71.1, 51.2, 50.1, 23.1. ^{19}F NMR (300 MHz, DMSO-d6) δ: -220.1.

4.2.16 Preparation of 2.44

2.44
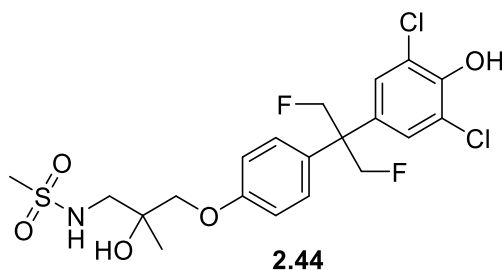
To a 100 mL round-bottom flask cooled to -20°C containing **2.43** (1.35 g, 3.25 mmol) dissolved in acetonitrile (40 mL) was added 10% NaOCl (6.05 g, 8.13 mmol). The reaction was stirred for 10 minutes before being quenched with saturated NaHSO$_3$ (30 mL) and diluted with 100mL of EtOAc and washed with H$_2$O (1x 20 mL) and brine (1x 20 mL) and dried over Na$_2$SO$_4$ then concentrated *in vacuo*. The crude extract was purified silica gel flash chromatography eluting with hexanes/EtOAc (2:3) to afford **2.44** (1.03 g, 2.13 mmol) as a pale-yellow oil in a yield of

65.5%. ¹H NMR (400 MHz, DMSO-d6) δ: 10.20 (s, 1H), 7.19 (s, 2H), 7.16 (d, J = 8.6Hz, 2H), 6.93 (d, J = 8.6Hz, 2H), 6.92 (t, J = 6.5Hz, 1H), 5.10 (dd, $J_{1,3}$ = 16.5Hz, $J_{2,3}$ = 6.7Hz, 2H), 4.98 (dd, $J_{1,3}$ = 16.4Hz, $J_{2,3}$ = 6.9Hz, 2H), 4.90 (s, 1H), 3.82 (d, J = 9.3Hz, 1H), 3.75 (d, J = 9.3Hz, 1H), 3.06 (m, 2H), 2.91 (s, 3H), 1.20 (s, 3H). ¹³C NMR (100 MHz, DMSO-d6) δ: 157.7, 148.0, 133.9, 128.8, 128.0, 122.1, 114.6, 72.5, 70.4, 50.8, 49.5, 22.6. ¹⁹F NMR (300 MHz, DMSO-d6) δ: -221.1.

4.2.17 Preparation of 2.45 (BU-130)

2.45
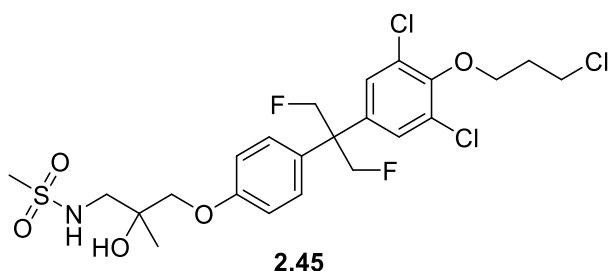
To a 50 mL round bottom flask cooled to 0°C containing **2.44** (400 mg, 0.826 mmol) in anhydrous DMF (12 mL) was added K_2CO_3 (120 mg, 0.868 mmol) followed by 1-bromo-3-chlorine propane (137 mg, 0.868 mmol) in 3 mL of DMF dropwise. The reaction was stirred at 0°C for 15 minutes before the ice bath was removed and the reaction was heated to 40°C overnight. The reaction was quenched with water (10 mL) and diluted with 80 mL of EtOAc and washed with H_2O (2x 20 mL) and brine (3x 20 mL) and dried over Na_2SO_4 and concentrated *in vacuo.* The crude extract was purified using silica gel flash chromatography eluting with hexanes/EtOAc (2:3) to afford **2.45** (412 mg, 0.717 mmol) as a white solid in 86.7% yield. ¹H NMR (400 MHz, DMSO-d6) δ: 7.33 (s, 2H), 7.15 (d, J = 8.8Hz, 2H), 6.92 (d, J = 8.9Hz, 2H), 6.90 (t, J = 6.5Hz, 1H), 5.13 (dd, $J_{1,2}$ = 9.8Hz, $J_{2,3}$ = 9.8Hz, 2H) 5.01 (dd, $J_{1,2}$ = 9.4Hz, $J_{2,3}$ = 9.9Hz, 2H), 4.89 (s, 1H), 4.11 (t, J = 6.0Hz, 2H), 3.86 (t, J = 6.5Hz, 2H), 3.80 (d, J = 9.3Hz, 1H),

3.74 (d, J = 9.3Hz, 1H), 3.04 (m, 2H), 2.89 (s, 3H), 2.20 (quin, $J_{1,3}$ = 12.4Hz, $J_{2,3}$ = 6.2Hz, 2H),

1.18 (s, 3H). ^{13}C NMR (150 MHz, DMSO-d6) δ: 146.5, 139.4, 130.5, 127.4, 127.2, 127.0, 126.7,

124.1, 122.3, 115.9, 113.5, 113.2, 111.6, 110.8, 77.3, 54.5, 40.8, 25.6, 22.7, 17.0 ^{19}F NMR (300

MHz, DMSO-d6) δ: -222.0. ESI-HRMS: *m/z* calculated for $C_{23}H_{28}Cl_3F_2NO_5S$ [M-H]-, 573.022;
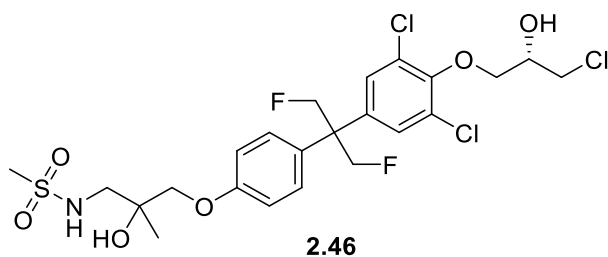
found, 573.023.

4.2.18 Preparation of 2.46 (BU-170)

2.46

To a 50 mL round bottom flask cooled to 0°C containing **2.44** (339 mg, 0.699 mmol) in

anhydrous DMF (12 mL) was added K_2CO_3 (102 mg, 0.734 mmol) followed by glycidyl tosylate

(168 mg, 0.734 mmol) in 3 mL of DMF dropwise. The reaction was stirred at 0°C for 15 minutes

before the ice bath was removed and the reaction was heated to 40°C overnight. The reaction

was quenched with water (10 mL) and diluted with 80 mL of EtOAc and washed with H_2O (2x

20 mL) and brine (3x 20 mL) and dried over Na_2SO_4 and concentrated *in vacuo*. The crude

mixture was used without purification and added to dry flask and dissolved in 40 mL of

acetonitrile followed by $CeCl_3 \cdot 7H_2O$ (339 mg, 0.909 mmol) and refluxed overnight. The reaction

was filtered for celite by vacuum filtration and the filter cake was washed with acetonitrile

(3x60mL) and then concentrated *in vacuo.* The crude mixture was purified by silica gel flask

chromatography eluting with hexanes/EtOAc (2:3) to afford **2.46** (384 mg, 0.650 mmol) as a

white solid in 93.0% yield. ^{1}H NMR (400 MHz, DMSO-d6) δ: 7.32 (s, 2H), 7.15 (d, J = 8.8Hz,

2H), 6.93 (d, J = 8.9Hz, 2H), 6.90 (t, J = 6.6Hz, 1H), 5.57 (d, J = 5.3Hz, 1H), 5.13 (dd, $J_{1,2}$ =

9.8Hz, $J_{2,3}$ = 9.8Hz, 2H) 5.01 (dd, $J_{1,2}$ = 9.3Hz, $J_{2,3}$ = 9.8Hz, 2H), 4.89 (s, 1H), 4.06 (m, 1H), 4.00

(d, J = 5Hz, 2H), 3.81 (m, 2H), 3.72 (m, 2H), 3.04 (m, 2H), 2.89 (s, 3H), 1.17 (s, 3H). ^{13}C NMR

(150 MHz, DMSO-d6) δ: 157.8, 149.4, 128.8, 128.7, 128.0, 122.1, 114.6, 114.5, 74.2, 72.4, 70.4,

69.1, 51.1, 49.4, 46.6, 22.6, 20.7. ^{19}F NMR (300 MHz, DMSO-d6) δ: -222.0. ESI-HRMS: *m/z*

calculated for $C_{23}H_{28}Cl_3F_2NO_6S$ [M-H]-, 589.0671; found, 589.0670.

4.3   Experimental for Chapter 3

4.3.1   Preparation of 3.11

3.11
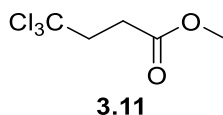
To a 250 mL round-bottom was added Chloroform (90 mL, 1.12 mol), methyl methacrylate (11

mL, 0.103 mol), BnEt₃NCl (500 mg, 2.19x10^{-4} mol) successively and cooled to 0°C. A solution

of sodium hydroxide (44.1 g, 1.12 mol) in H₂O (50 mL) was added dropwise over 10 minutes.

The solution was allowed to stir at 0°C for 1 hour then stirred for a further 2 hours at room

temperature. The solution was diluted with 120 mL of DCM and washed with H₂O (1x 40 mL)

and brine (1x 40 mL) and dried over Na₂SO₄ and concentrated *in vacuo*. The crude extract was

purified using vacuum distillation, distilling as the last fraction beginning at 90°C and ending at

122°C to afford **3.11** (5.85 g, 2.87x10^{-2} mol) as colorless liquid in 27.9% yield. ^{1}H NMR (400

MHz, CDCl₃) δ: 3.75 (s, 3H), 3.09 (m, 2H), 2.84 (m, 2H).

4.3.2 Preparation of 3.12

$$Cl_3C\underset{\textbf{3.12}}{\diagdown\diagup}\overset{\displaystyle O}{\underset{\displaystyle H}{\diagup}}$$
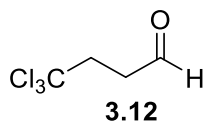
To a 250 mL round-bottom flask cooled to -78°C containing **3.11** (5.85 g, 28.8 mmol) dissolved

in of anhydrous THF (40 mL) was added 1.0 M DiBAL-H (30.2 mL, 30.2 mmol). The reaction

was stirred at -78°C for 1 hour before being quenched with a saturated solution of Rochelle's salt

(~40 mL) and EtOAc (~40 mL). Upon the solution becoming clear the reaction was diluted with

a further 80 mL of EtOAc and washed with H_2O (1x 30 mL) and brine (1x 30 mL). The product,

3.12 (4.00 g, 23.1 mmol) was recovered as a crude colorless liquid and used in the next step

without further purification. ^{1}H NMR (400 MHz, DMSO-d6) δ: 9.71 (s, 1H), 3.08 (t, J = 7.0Hz,

2H), 2.91 (t, J = 7.2Hz, 2H).

4.3.3 Preparation of 3.13

$$Cl_3C\underset{\textbf{3.13}}{\diagdown\diagup}\diagup$$
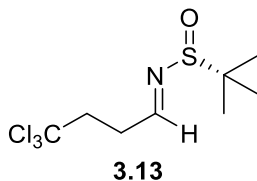
To a 100 mL round-bottom flask containing **3.12** (4.00 g, 23.1 mmol) in anhydrous DCM (20

mL) was added *(R)-(+)*-2-methylpropanesulfonamide (2.80 g, 23.1 mmol) followed by $CuSO_4$

(14.75 g, 92.4 mmol). The reaction was stirred at room temperature overnight. The reaction was

filtered over celite and the filtrate was concentrated *in vacuo.* The crude product was purified

using silica gel flash chromatography eluting with hexanes/EtOAc (7:3) to afford **3.13** (5.51 g,

21.2 mmol) as a yellow oil in 91.8% yield and 73.6% yield over 2-steps. ^{1}H NMR (400 MHz, CDCl$_3$) δ: 8.2 (t, J = 3.5Hz, 1H), 3.12 (m, 2H), 3.06 (m, 2H), 1.24 (s, 9H).

4.3.4 Preparation of 3.14

3.14
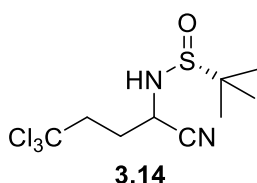
To a 100 mL round-bottom flask cooled to 0°C containing **3.13** (5.51 g, 21.2 mmol) dissolved in anhydrous DCM (15 mL) was added TMSCN (5.30 mL, 42.4 mmol) followed by Sc(OTf)$_3$ (1.04 g, 2.1 mmol). The reaction was stirred at 0°C for 2 hours then allowed to slowly warm to room temperature and stirred further overnight. The solvent was removed *in vacuo* and the crude mixture was purified using silica gel flash chronography eluting with hexanes/EtOAc (7:3) to afford **3.14** (5.48 g, 19.1 mmol) as white solid in 90.0% yield. ^{1}H NMR (400 MHz, CDCl$_3$) δ: 4.35 (m, 2H), 2.94 (m, 2H), 2.39 (m, 2H), 1.27 (s, 9H).

4.3.5 Preparation of 3.15

3.15
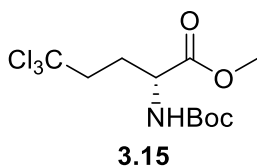
To a 100 mL round-bottom flask containing **3.14** (5.48 g, 19.1 mmol) dissolved in anhydrous MeOH was bubbled dry HCl gas that was formed by adding concentrated HCl over ~100 g of CaCl$_2$ then passed through Drierite™; The HCl gas was bubbled into solution for 1 hour before being removed, then the solution was stirred over night. The solution was cooled to 0°C and

quenched with sodium bicarbonate (19.26 g, 229 mmol). The solvent was concentrated *in vacuo*.

The crude product was resuspended in THF (120 mL) and cooled to 0°C before the addition of

H_2O (40 mL) and stirred for 5 minutes before the addition of $(Boc)_2O$ (4.57 g, 20.0 mmol) in

THF (20 mL). The reaction was allowed to stirred overnight warming to room temperature. The

mixture was diluted with EtOAc (60 mL) and quenched to pH 6 with 6 M HCl. The organic layer

was washed with H_2O (1x 30 mL) and brine (1x 30 mL) and concentrated *in vacuo*. The crude

was purified using silica gel flash chromatography eluting with hexanes/EtOAc (1:1) to afford
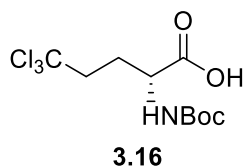
3.15 (5.31 g, 15.9 mmol) as colorless oil in 83.1% yield.

4.3.6   Preparation of 3.16

3.16

To a 100 mL round-bottom flask cooled to 0°C containing **3.15** (5.19 g, 15.5 mmol) in THF (40

mL) was added 0.6 M LiOH (25 mL) and the solution was stirred vigorously overnight and was

allowed to warm to room temperature. The mixture was diluted with EtOAc (80 mL) and

quenched to pH 3 and washed with H_2O (1x 20 mL) and brine (1x 20 mL) to afford **3.16** (4.97 g,

15.5 mmol) as white solid in 97.7% yield. ¹H NMR (400 MHz, $CDCl_3$) δ: 7.34 (d, J = 8.3Hz,

1H), 4.06 (ddd, $J_{1,3}$ = 8.6Hz, $J_{2,4}$ = 11.9Hz, 1H), 2.89 (m, 1H), 2.75 (m, 1H), 2.06 (m, 2H), 1.39

(s, 9H).

4.3.7 Preparation of 3.21
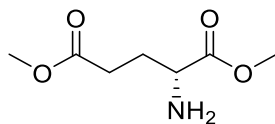
3.21

To a 100 mL round bottom flask cooled to 0°C containing D-Glutamic Acid (5.75 g, 39.1 mmol) dissolved in MeOH (40 mL) was added thionyl chloride (11.3 mL, 156.4 mmol) dropwise over 5 minutes. The solution was stirred overnight and allowed to warm to room temperature slowly. The solvent was removed *in* vacuo to afford crude product **3.21** (6.80 g, 38.8 mmol) as a green oil used without further purification in the next step.

4.3.8 Preparation of 3.22
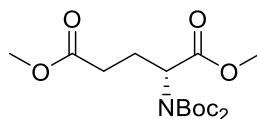
3.22

To a 250 mL round-bottom flask cooled to 0°C containing **3.21** (6.80 g, 38.8 mmol) dissolved in THF (60 mL) was added sodium bicarbonate (9.78 g, 116.4 mmol) followed by H_2O (30 mL) and allowed to stir for 5 minutes. To this solution (Boc)$_2$O (9.30 g, 40.7 mmol) was added in THF (20 mL) in one portion. The solution was allowed to stir overnight. The solution was diluted with 100 mL of ethyl acetate and quenched to pH 7 with 6 M HCl before washing with H_2O (1x 20 mL) and brine (1x 20 mL), dried over Na_2SO_4, and concentrated *in vacuo*. The crude oil colorless oil was re-dissolved in ACN (100 mL) and 4-dimethylamino pyridine (4.74 g, 38.8 mmol) was added followed by the addition of (Boc)$_2$O (9.30 g, 40.7 mmol) in ACN (20 mL) added in one portion. The mixture was allowed to stir overnight. The solution was diluted with

100 mL of EtOAc and quenched to pH 4 and washed with water (2x 20 mL) and brine (2x 20

mL), dried over Na$_2$SO$_4$, and concentrated *in vacuo*. The crude extract was purified using silica

gel flash chromatography eluting with hexanes/EtOAc (4:1) to afford **3.22** (13.30 g, 35.3 mmol)

as a colorless oil in 91.0% yield over 2 steps. ^{1}H NMR (400 MHz, DMSO-d6) δ: 4.88 (m, 1H),

3.65 (s, 3H), 3.59 (s, 3H), 2.33 (m, 2H), 2.28 (m, 1H), 2.06 (m, 1H), 1.44 (s, 18H).

4.3.9 Preparation of 3.23
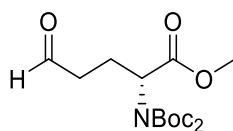
3.23

To a 250 mL round-bottom cooled to -78°C containing **3.22** (13.30 g, 35.3 mmol) in THF (60

mL) was added 1.0 M DiBAL-H (37.1 mL, 37.1 mmol) dropwise over 20 minutes. Once the

addition was complete the solution was stirred further for 1 hour. The reaction was then

quenched with a saturated solution of Rochelle's salt (40 mL) and EtOAc (40 mL) and stirred

until the solution cleared. The mixture was then diluted further with EtOAc (60 mL) and washed

with H$_2$O (1x 30 mL) and brine (1x 30 mL), dried over Na$_2$SO$_4$, and concentrated *in vacuo*. The

crude extract was purified using silica gel flash chromatography eluting with hexanes/EtOAc

(4:1) to afford **3.23** (5.72 g, 16.5 mmol) as a colorless oil in 42.6% yield. ^{1}H NMR (400 MHz,

CDCl$_3$) δ: 9.78 (s, 1H), 4.90 (m, 1H), 3.73 (s, 3H), 2.54 (m, 3H), 2.17 (m, 1H), 1.50 (s, 18H).

4.3.10 Preparation of 3.24

3.24
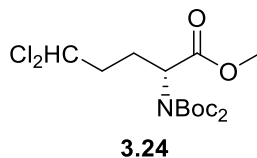
To a 100 mL round bottom flask cooled 0°C containing N-Chlorosuccinimide (1.20 g, 9.0 mmol) dissolved in anhydrous DCM (20 mL) was added Chlorodiphenylphosphine (1.66 mL, 9.0 mmol) dropwise over 5 minutes. The mixture was stirred for 5 minutes at 0°C before the ice bath was removed and **3.23** (2.08 g, 6.0 mmol) in anhydrous DCM (20 mL) was added via cannula over 15 minutes. The reaction was allowed to stir for 2 hours at room temperature before it was stopped and the solvent was concentrated *in vacuo*. The crude oil was purified using silica gel flash chromatography eluting with hexanes/EtOAc (4:1) to afford **3.24** (1.35 g, 3.4 mmol) as a pale-green oil in 56.7% yield. ^{1}H NMR (400 MHz, CDCl$_3$) δ: 5.82 (dd, J$_1$ = 5.2Hz, J$_2$ = 5.0Hz, 1H), 4.88 (m, 1H), 3.73 (s, 3H), 2.34 (m, 2H), 2.20 (m, 2H), 1.51 (s, 18H).

4.3.11 Preparation of 3.25

3.25
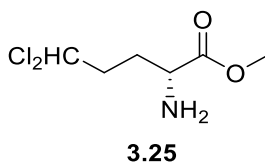
To a 50 mL round-bottom flask cooled to 0°C containing **3.24** (1.35 g, 3.4 mmol) in DCM (5 mL) was added TFA (5 mL) and the reaction was stirred for 5 minutes before the ice bath was removed. The reaction was stirred for a further 30 minutes until the TLC showed all the Boc had been removed and mixture concentrated *in vacuo* to yield **3.25** (663 mg, 3.3 mmol) as a yellow oil in 97.9% yield.

4.3.12   Preparation of 3.31

3.31
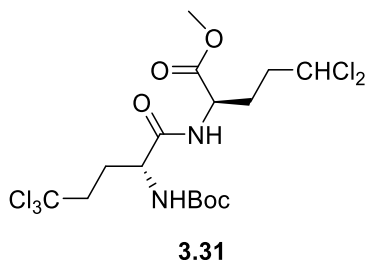
To a 100 mL round-bottom flask cooled to 0°C containing **3.16** (2.19 g, 6.85 mmol) in DMF (30 mL) was added EDC (1.31 g, 6.85 mmol), and Oxyma pure (969 mg, 6.85 mmol). The reaction was allowed to stir for 10 minutes before the addition of **3.25** (1.37 g, 6.85 mmol) pre-mixed with Diisopropylethylamine (1.72 mL, 10.27 mmol) in DMF (5 mL) was added dropwise over 5 minutes. The mixture was allowed to stir overnight slowly warming to room temperature. The reaction was diluted with EtOAc (150 mL) and washed with H_2O (3x 20 mL) and brine (3x 20 mL), dried over Na_2SO_4, and concentrated *in vacuo*. The crude extract was purified using silica gel flash chromatography eluting with hexanes/EtOAc (7:3) to afford **3.31** (3.15 g, 6.27 mmol) as a colorless oil in 91.5% yield. ^1H NMR (400 MHz, $CDCl_3$) δ: 6.75 (d, J = 7.4Hz, 1H) 5.80 (m, 1H), 5.08 (d, J = 7.8Hz, 1H), 4.65 (m, 1H), 4.23 (m, 1H), 3.79 (s, 3H), 2.80 (m, 2.80), 2.31 (m, 2H), 2.21 (m, 2H), 2.10 (m, 1H), 1.95 (m, 1H), 1.47 (s, 9H).

4.3.13   Preparation of 3.32

3.32
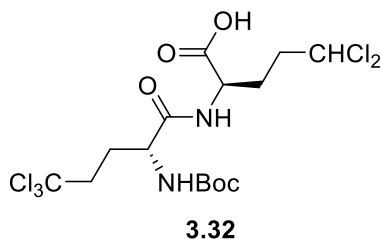
To a 100 mL round bottom flask cooled to 0°C containing **3.31** (3.15 g, 6.27 mmol) in THF (30 mL) was added 0.6 M LiOH (30 mL) and the reaction was stirred vigorously overnight and allowed to warm to room temperature slowly. The reaction was quenched to pH 3 using 6 M HCl and diluted with EtOAc (120 mL) and was washed with H_2O (1x 20 mL) and brine (1x 20 mL) to afford **3.32** (3.03 g, 6.20 mmol) as a white solid in 98.9% yield.

4.3.14   Preparation of *(4R)(10R)* – 3.33 and *(4S)(10R)* – 3.34

(4R)(10R) - **3.33**   *(4S)(10R)* - **3.34**
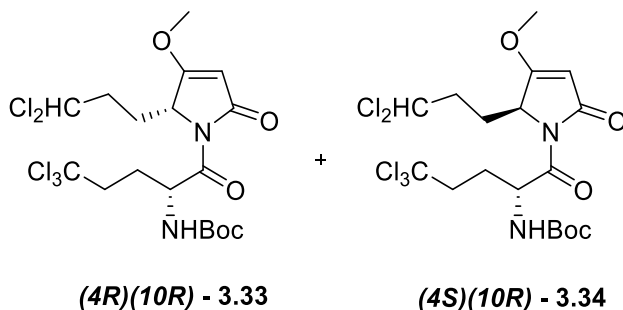
To a 100 mL round bottom flask containing Meldrum's acid (544.9 mg, 3.78 mmol) in DCM (15 mL) was added DMAP (1155.0 mg, 9.45 mmol). The mixture was stirred for 5 minutes before the addition of **3.32** (923.6 mg, 1.89 mmol) followed by the addition of EDC (1009.0 mg, 5.67 mmol). The mixture was stirred overnight and allowed to warm to room temperature slowly. The reaction was quenched with a 10% solution of citric acid (40 mL) and diluted with DCM and subsequently washed with brine (2x 20 mL) and 10% solution of citric acid (1x 40 mL). The

organic layer was dried over Na_2SO_4 and concentrate *in vacuo*. The crude material was purified using silica gel flash chromatography eluting with hexanes/EtOAc (1:1) to ensure the removal Meldrum's acid and DMAP. The purified product was then re-dissolved in anhydrous EtOAc (40 mL) and refluxed for 2 hours until the TLC spot showed consumption of the starting material. The solvent was concentrated *in vacuo*. The crude product was re-dissolved in the tolune/MeOH (4:1) before the addition of 0.6 M $TMSHCN_2$ (6.3 mL, 3.78 mmol). The reaction was stirred for 15 minutes before being quenched with water (2 mL) and the solvent was concentrated *in vacuo*. The crude product was then purified by silica gel chromatography eluting with hexanes/EtOAc (7:3) to afford **3.33** (172.1 mg, 0.371 mmol) in the (R)(R) configuration and **3.34** (118.2 mg, 0.254 mmol) in the *(S)(R)* configuration as white solids in a yield of 33.1% across both diastereomers. ^{1}H NMR – *(4R)(10R) -* **3.33** (400 MHz, $CDCl_3$) δ: 5.74 (dt, J_1 = 4.8Hz, J_2 = 4.2Hz, 1H), 5.34 (ddd, J = 3.0Hz, 1H), 5.19 (d, J = 8.4Hz, 1H), 5.15 (s, 1H), 4.71 (dd, J = 2.7Hz, 1H), 3.92 (s, 3H), 2.91 (m, 2H), 2.44 (m, 1H), 2.32 (m, 1H), 2.19 (m, 2H), 1.93 (m, 2H), 1.45 (s, 9H). *(4S)(10R) -* **3.34** (400 MHz, $CDCl_3$) δ: 5.76 (t, J = 5.6Hz, 1H), 5.48 (ddd, J = 3.4Hz, 1H), 5.30 (d, J = 8.8Hz, 1H), 5.16 (s, 1H), 4.77 (s, 1H), 3.93 (s, 3H), 3.00 (m, 1H), 2.83 (m, 1H), 2.39 (m, 2H), 2.18 (m, 1H), 2.06 (m, 3H), 1.47 (s, 9H).

4.3.15 Preparation of *(4R)(10R)* - **3.35**
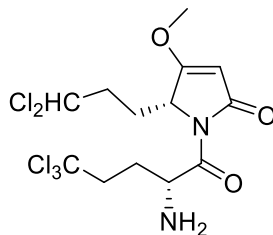
(4R)(10R) - **3.35**

To a 10 mL round-bottom flask cooled to 0°C containing *(4R)(10R)* – **3.33** (19.3 mg, 4.16×10^{-2} mmol) dissolved in DCM (2 mL) was added TFA (2 mL) and the reaction was stirred at for 2 hours (TLC shows complete removal of the Boc group). The solvent was removed *in vacuo*, to afford *(4R)(10R)* – **3.35** in quantitative yield.

4.3.16 Preparation of *(4S)(10R)* – **3.36**
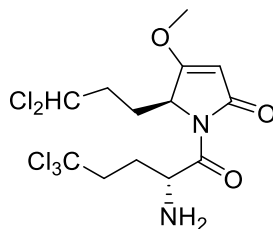
(4S)(10R) - **3.36**

Using a similar procedure described for **3.35** afforded *(4S)(10R)* – **3.36** in quantitative yield.

4.3.17 Preparation of *(4R)(10R) – 3.41*
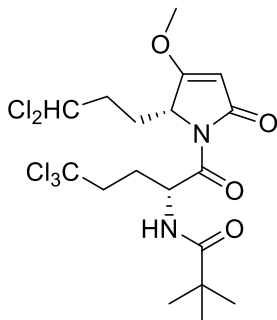
(4R)(10R) - **3.41, LPY37**

To a 25 mL round bottom flask containing **3.35** (44.0 mg, 0.084 mmol) dissolved in anhydrous DCM (5 mL) was added triethylamine (0.05 mL, 0.37 mmol) followed by propionyl chloride (0.04 mL, 0.37 mmol) at room temperature. The reaction mixture was stirred overnight before being quenched with water and 1 drop of 6 M HCl and was extracted into EtOAc and washed with H_2O (1x 10 mL) and brine (1x 10 mL). The organic layer was dried over sodium sulfate and purified by silica gel flash chromatrography eluting with hexanes/ethyl acetate (9:1 – 7:3) to give final product *(4R)(10R) – 3.41* (34.2 mg, 0.067 mmol) in 79.7% yield. ^{1}H NMR *(4S)(10R) –* **3.41** (400 MHz, $CDCl_3$) δ: 5.75 (t, J = 4.6Hz, 1H), 5.34 (ddd, J = 2.9Hz, 1H), 5.24 (d, J = 8.6Hz, 1H), 5.16 (s, 1H), 4.72 (t, J = 4.7Hz, 1H), 3.93 (s, 3H), 2.93 (m, 2H), 2.39 (m, 2H), 2.20 (m, 2H), 1.93 (m, 2H), 1.46 (s, 9H).

4.3.18 Preparation of (4S)(10R) – 3.42

(4S)(10R) - 3.42, LPY36

To a 25 mL round bottom flask containing **3.36** (49.0 mg, 0.093 mmol) dissolved in anhydrous DCM (5 mL) was added triethylamine (0.05 mL, 0.37 mmol) followed by propionyl chloride (0.04 mL, 0.37 mmol) at room temperature. The reaction mixture was stirred overnight before being quenched with water and 1 drop of 6 M HCl and was extracted into EtOAc and 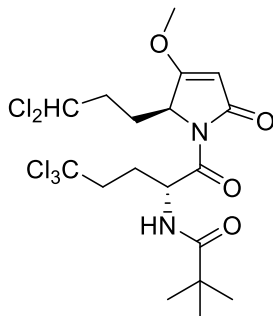washed with H_2O (1x 10 mL) and brine (1x 10 mL). The organic layer was dried over sodium sulfate and purified by silica gel flash chromatrography eluting with hexanes/ethyl acetate (9:1 – 7:3) to give final product **(4S)(10R) – 3.42** (42.8 mg, 0.084 mmol) in 90.1% yield. ^{1}H NMR **(4S)(10R) – 3.42** (400 MHz, CDCl$_3$) δ: 5.76 (t, J = 5.6Hz, 1H), 5.47 (ddd, J = 3.4Hz, 1H), 5.30 (d, J = 8.8Hz, 1H), 5.16 (s, 1H), 4.76 (t, J = 3.7Hz, 1H), 3.93 (s, 3H), 3.00 (m, 1H), 2.83 (m, 1H), 2.38 (m, 2H), 2.19 (m, 1H), 2.06 (m, 3H), 1.47 (s, 9H).
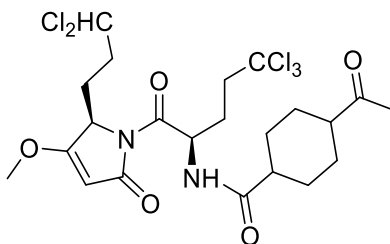
4.3.19 Preparation of *(4R)(10R) – 3.51*

(4R)(10R) - 3.51

To a 50 mL round bottom flask containing 1-acetylpiperidine-4-carboxylic acid (12.7 mg, 0.074 mmol) in anhydrous DMF (3 mL) cooled to 0°C was added PyBOP (41.8 mg, 0.080 mmol) followed by diisopropylethylamine (0.03 mL, 0.19 mmol). The reaction was stirred for 5 minutes before adding *(4R)(10R) – 3.35* (26.2 mg, 0.062 mmol). The reaction was allowed to proceed overnight, slowly warming to room temperature. The reaction was extracted into EtOAc (30 mL) and washed with H_2O (3x 5 mL) and brine (3x 5 mL) and the organic layer was dried over Na_2SO_4, filtered, and the solvent was removed *in vacuo*. The crude mixture was purified using silica gel flash chromatography eluting with 150 mL of hexanes/EtOAc (1:4) followed by DCM/MeOH (99:1) to give *(4R)(10R) – 3.51* (31.7 mg, 0.055 mmol) as a white solid in 88.3% yield. ^{1}H NMR *(4S)(10R) – 3.51* (400 MHz, DMSO-d$_6$) δ: 8.40 (d, J = 8.2Hz, 1H), 6.28 (t, J = 5.6Hz, 1H), 5.46 (s, 3H), 5.37 (m, 1H), 4.85 (dd, $J_{1,2}$ = 2.6Hz, $J_{2,3}$ = 2.3Hz, 1H), 4.30 (m, 1H), 3.91 (s, 3H), 3.80 (m, 1H), 3.03 (t, J = 13.5Hz, 1H), 2.84 (ddd, J = 5.3Hz, 2H), 2.13 (m, 1H), 1.98 (m, 1H), 1.98 (s, 3H), 1.70 (m, 2H), 1.50 (m, 1H).
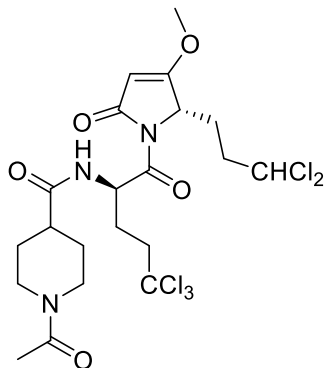
4.3.20 Preparation of *(4S)(10R)* – 3.52

(4S)(10R) - 3.52

To a 50 mL round bottom flask containing 1-acetylpiperidine-4-carboxylic acid (39.3 mg, 0.23

mmol) in anhydrous DMF (6 mL) cooled to 0°C was added PyBOP (129.4 mg, 0.25 mmol)

followed by diisopropylethylamine (0.10 mL, 0.57 mmol). The reaction was stirred for 5 minutes

before adding *(4S)(10R)* – **3.36** (81.1 mg, 0.19 mmol). The reaction was allowed to proceed

overnight, slowly warming to room temperature. The reaction was extracted into EtOAc (40 mL)

and washed with H_2O (3x 5 mL) and brine (3x 5 mL) and the organic layer was dried over

Na_2SO_4, filtered, and the solvent was removed *in vacuo*. The crude mixture was purified using

silica gel flash chromatography eluting with 250 mL of hexanes/EtOAc (1:4) followed by

DCM/MeOH (99:1) to give *(4S)(10R)* – **3.52** (86.8 mg, 0.15mmol) as a white solid in 78.9%

yield. ^{1}H NMR *(4S)(10R)* – **3.52** (600 MHz, DMSO-d_6) δ: 8.34 (dd, $J_{1,2}$ = 3.4Hz, $J_{2,3}$ = 2.1Hz,

1H), 6.38 (t, J = 3.9Hz, 1H), 5.54 (m, 1H), 5.49 (s, 3H), 4.89 (dd, $J_{1,2}$ = 3.2Hz, $J_{2,3}$ = 2.5Hz, 1H),

4.34 (d, J = 8.2Hz, 1H), 3.31 (s, 3H), 3.02 (m, 1H), 2.90 (m, 1H), 2.72 (m, 1H), 2.28 (m, 1H),

2.17 (m, 1H), 2.07 (m, 1H), 1.98 (s, 3H), 1.83 (m, 1H), 1.70 (m, 1H), 1.49 (m, 1H). ^{13}C NMR

(150 MHz, DMSO-d_6): 179.2, 174.4, 170.5, 169.4, 168.0, 99.5, 94.2, 74.1, 59.8, 57.4, 50.9, 45.3,

29.2, 28.0, 24.1, 21.3.

4.3.21 Preparation of *(4S)(10R) – 3.61*
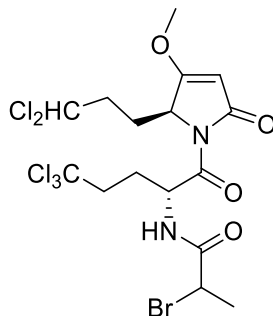
(4S)(10R) - 3.61

To a 25 mL round bottom flask containing *(4S)(10R) – 3.36* (31.7 mg, 0.074 mmol) dissolved in anhydrous DCM (5 mL) was added triethylamine (20 µL) followed by bromo-propionyl bromide (8 µL, 0.074 mmol) at room temperature and was allowed to stir overnight. The solvent was removed *in vacuo* and the crude product was purified using silica gel flash chromatography eluting with hexanes/EtOAc (7:3) to give product *(4S)(10R) – 3.61* (33.1 mg, 0.059 mmol) as a colorless oil in 79.6% yield. . ^{1}H NMR *(4S)(10R) – 3.61* (400 MHz, CDCl$_3$) δ: 7.66 (d, J = 7.8Hz, 1H), 5.75 (t, 5.6Hz, 1H), 5.71 (m, 1H), 5.17 (s, 1H), 4.78 (dd, J$_{1,2}$ = 3.5Hz, J$_{2,3}$ = 2.3Hz, 1H), 3.93 (s, 3H), 2.99 (m, 1H), 2.76 (m, 1H), 2.65 (s, 3H), 2.55 (m, 1H), 2.40 (m, 1H), 2.19 (m, 2H), 2.07 (m, 3H).

4.3.22 Preparation of *(4S)(10R) – 3.62*

(4S)(10R) - 3.62

To a 10 mL round bottom flask containing *(4S)(10R) – 3.61* (18 mg, 0.032 mmol) heated to

reflux in anhydrous THF (4 mL) was added tetrabutylammonium fluoride (62 μL, 0.064 mmol).

The reaction was reflux for 5 minutes before the solvent was removed *in vacuo.* The crude

mixture was purified by high performance liquid chromatography eluting with acetonitrile/water

(65/35) to give *(4S)(10R) – 3.62* (1.1 mg, 0.003 mmol) in 7.0% yield. NMR shows degradation,

compound recovered with the fluorine, but has no olefinic proton.

4.3.23 Preparation of *(4S)(10R) – 3.66*
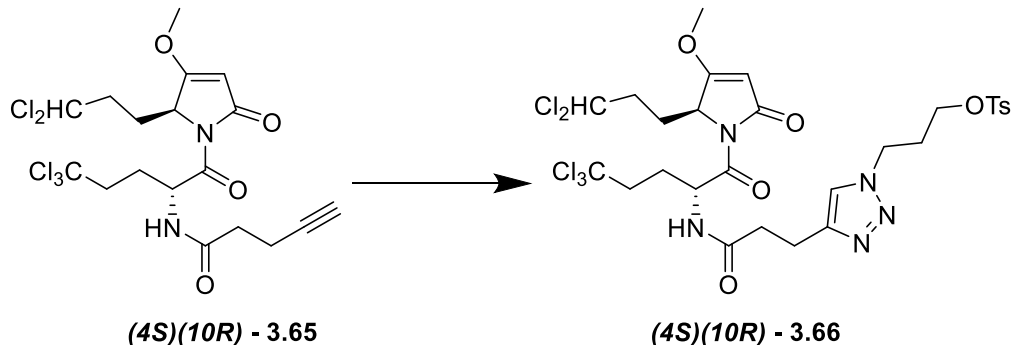
(4S)(10R) **- 3.65**   *(4S)(10R)* **- 3.66**

To a 10 mL round bottom flask containing *(4S)(10R) – 3.65* (10.8 mg, 0.021 mmol) dissolved in 4 mL of THF/H_2O/*t*-BuOH (1:2:1) was added **3.05** (5.5 mg, 0.021 mmol) followed by coupling reagents $CuSO_4$ (1 mg, 0.006 mmol), benzoic acid (1 mg, 0.008mmol), ascorbic acid (1.4 mg, 0.008mmol). The reaction was allowed to stir overnight before being extracted into ethyl acetate (20 mL) and washed with H_2O (1x 5 mL) and brine (1x 5 mL). The organic layer was dried over Na_2SO_4, filtered, and the solvent was removed *in vacuo* and was purified by silica gel flash chromatography eluting with hexanes/EtOAc (1:4) to give *(4S)(10R) – 3.66* (14.4 mg, 0.019 mmol) as a colorless oil in 88.6% yield. . ^{1}H NMR *(4S)(10R) – 3.66* (400 MHz, CDCl$_3$) δ: 8.13 (d, J = 6.2Hz, 1H), 7.78 (d, J = 8.2Hz, 2H), 7.38 (m, 3H), 6.68 (d, J = 8.1Hz, 1H), 5.76 (t, J = 6.1Hz, 1H), 5.73 (m, 1H), 5.15 (s, 1H), 4.74 (dd, J$_{1,2}$ = 3.4Hz, J$_{2,3}$ = 1.9Hz, 1Hz), 4.40 (m, 2H), 4.02 (t, J = 5.4Hz, 2H), 3.92 (s, 3H), 3.06 (t, J = 6.2Hz, 2H), 2.91 (m, 1H), 2.67 (m, 3H), 2.48 (s, 3H), 2.48 (s, 3H), 2.38 (m, 3H), 2.05 (3H).
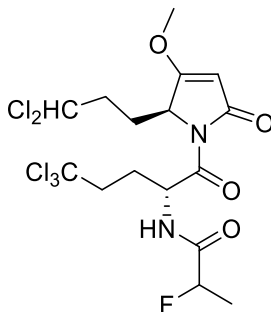
4.3.24 Preparation of *(4S)(10R) – 3.67*
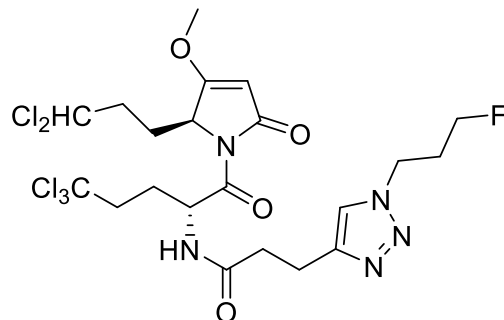
(4S)(10R) - 3.67

To a 10 mL round bottom flask containing *(4S)(10R) – 3.66* (7.4 mg, 0.010 mmol) dissolved in anhydrous THF (3 mL) was added 0.1 M TBAF (0.11 mL, 0.011 mmol). The reaction was then refluxed for 2 hours before the solvent was removed *in vacuo*. The crude mixture was purified with silica gel flash chromatography eluting with hexanes/EtOAc (3:2) to give product *(4S)(10R) – 3.67* (2.7 mg, 0.0044 mmol) as a yellow oil in 44.2% yield. NMR shows degradation, compound recovered with the fluorine, but has no olefinic proton.

Chapter 5: Conclusion

This thesis describes the synthesis and biological evaluation of derivatives of ralaniten and the sintokamides, two AR-NTD antagonist scaffolds that have previously been isolated and identified in the Andersen Lab. The "aniten" class of therapeutic candidates target the AR-NTD as a means to inhibit tumor growth in PC and mCRPC.

In Chapter 2, synthesis and biological evaluation of fluorinated ralanitens was discussed. The fluorination of the gem-dimethyl bridge decreased the ClogP of the scaffold allowing for more lipophilicity to be introduced, allowing for the elaboration of EPI-002 **(2.003)**. I-EPI-002 **(2.011)** showed that halogenating the phenyl rings increased potency, but it has a potential metabolic lability due to iodine scavenging enzymes. Comparable potency increases were found by dichlorinating one of the phenyl rings, and the lipophilicity from this substitution was circumvented by fluorinating the gem-dimethyl BPA bridge. Next the metabolic liability of the primary hydroxyl group was addressed by replacing the alcohol with a methyl sulfonamide group that was assumed to be resistant to oxidation or glucuronidation. This led to the synthesis of BU-86 **(2.24)** and BU-87 **(2.25)** that were designed to test the necessity of the chlorohydrin side chain and its importance for bioactivity, as the reactive epoxide that can form from the chlorohydrin has the potential to undergo off-target covalent binding. Interestingly, both these candidates target the androgen receptor effectively with IC_{50} values of 2.3 ± 0.1 and 2.9 ± 0.2 µM, respectively, in an *in vitro* screening assay for AR-NTD antagonists. Both compounds are shown to have a significant increase in potency relative to EPI-002 **(2.003)** in the assay. The bioactivity of these compounds is comparable *in vitro*, but BU-87 **(2.25)** shows some off-target effects against PC3, making the chlorohydrin candidate BU-86 **(2.24)** superior in that regard. *In*

vivo data will be needed to determine their clinical potential in decreasing CRPC LNCaP xenograft growth.

The synthesis of the ketone BU-88 (**2.26**), a putative metabolite of BU-87 **(2.25)**, was also accomplished. Ketone **2.26** showed impressive *in vitro* activity with an IC_{50} of 0.056 ± 0.002 μM in the PSA luciferase screening assay. As such, BU-88 (**2.26**) is the most potent analog made to date in the EPI series, even exceeding the potency of the current industry standard drug enzalutamide **(1.10).** The dramatic increase in the potency of BU-88 **(2.26)** might be explained by reversible covalent bonding to the AR-NTD via the ketone. *In vivo* data shows that **2.26** effectively decreases tumor growth in LNCaP xenografts grown in mice. However, its selectivity came into question because it showed evidence of binding to the PR as well as AR. The high potency of BU-88 **(2.26)** coupled with evidence of binding to PR may suggest off-target cytotoxicity. However, further work will be needed to make this determination. Furthermore, BU-88 **(2.26)** has chemical stability issues, where the ketone bearing side-chain decomposed at physiological pH. Investigation of the degradation pathway revealed that the side chain fell off at basic pHs to produce BU-89 **(2.33).** This led to the synthesis of **2.33** and its IC_{50} value in the PSA luciferase assay was 0.05 ± 0.002 μM, which is identical to that to the parent compound BU-88 **(2.26)**. This suggests that the degradation product might actually be the active compound and therefore, the enhanced potency of BU-88 **(2.26)** probably does not involve reversible covalent binding to the AR via the ketone. The incredible activity of these compounds cannot be ignored and these scaffolds need further SAR to determine if the same activity can be achieved without potential off-target cytotoxic behaviour.

The last EPI-002 analogs BU-130 **(2.45)** and BU-170 **(2.46)** address all the metabolic issues on the ralaniten scaffold. The primary hydroxyl group is removed in the favor of the

methyl sulfonamide, chlorines are added to the ring for increased potency, and finally the secondary alcohol is changed in favor of a sterically hindered tertiary alcohol. All these adjustments are possible due to the fluorination of the gem-dimethyl BPA bridge maintaining the H_2O solubility of the new analogs. Again, determining the potency with and without the chlorohydrin was tested. **2.45** and **2.46** have comparable IC_{50} values of 1.8 ± 0.1 and 2.1 ± 0.2 μM, respectively. Both compounds are highly specific for AR with no activity in the androgen independent PC3 cell lines. Interestingly, these most metabolically stable compounds are also the most potent. Both compounds show *in vivo* activity inhibiting tumor grown in LNCaP xenografts grown in mice. At first glance the chlorohydrin **2.46** responds better *in vivo*, however their difference is not statistically significant. This concludes that **2.45** may be the best candidate synthesized in this chapter with its superior metabolic stability and the lowest IC_{50} value *in vitro.* There is no question these fluorinated ralaniten analogs are active AR-NTD inhibitors, but more animal studies will need to be done to determine if they are efficacious enough and have adequate pharmacokinetic ADME properties to be clinical candidates.

In Chapter 3, synthesis and biological evaluation of the sintokamide analogs is discussed, including their potential as therapeutics and imaging agents. LPY37 **(3.41)** and LPY36 **(3.42)** had previously shown promising dose response curves *in vitro*, which demanded an animal study to determine their ability to inhibit tumor growth *in vivo*. The synthesis of **3.41** and **3.42** needed to be scaled up to get enough material for the animal study. This led to one synthetic modification in the formation of the gem-dichloride **(3.24)**. The previous synthesis of **3.24** used chlorine gas bubbled over triphenyl phosphite, which was subsequently added to the aldehyde **3.23.** This reaction proved tedious, requiring heavy attention, corrosive gas cylinders, and poor yields. This step was optimized by premixing *N*-chlorosuccinimide and chlorodiphenylphosphine

followed by aldehyde **(3.23)** addition and stirring for 2 hours to give **3.24** cleanly in 55.0% yield over 2 steps. This increase in yield and shortened time enabled synthesis of **3.41** and **3.42** on a gram-scale. At this scale, the formation of the tetramic acids **3.35** and **3.36** was challenging. It was found that purifying after the first step to remove excess Meldrum's acid increased yields 2-fold, which helped achieve the material goal, but at some expense of time and purification effort. In the end, we were able to show for the first time both compounds **3.41** and **3.42** inhibit tumor growth in LNCaP xenografts in mice via oral administration of a daily dose of 15 mg/kg. This dosage is half of what is administered with ralaniten analogs, making analogs **3.41** and **3.42** the most effective *in vivo* AR-NTD antagonists known to date. The natural (*4S*)(*10R*) sintokamide scaffold configuration present in **3.41** showed superior activity of the two analogs evaluated in the *in vivo* assays. Due to the possibility that the sintokamides and ralaniten bind to different region to the AR-NTD, it would be reasonable to suggest that co-dosing animals with both compounds may lead to stronger tumor growth inhibition. A synergistic study with LPY36 **(3.41)** and BU-170 **(2.46)** is currently underway.

LPY37 **(3.41)** and LPY36 **(3.42)** are quite lipophilic due to having only one HBD and a pivaloyl amide making the compound hard to solubilize for *in vivo* administration. This led to the synthesis of LPY39 *(4S)(10R)* **- 3.51** and LPY80 *(4R)(10R)* **- 3.52** which drastically decreased the ClogP by introducing an acetyl piperidine amide in favour of the pivaloyl amide. LPY39 **(3.51)** was the first sintokamide compound to show tumor inhibition in LNCaP xenografts in mice, however, *in vitro* PSA-luciferase assays didn't show transcription inhibition, which led to the belief that these compounds may have non-selective cytotoxicity. Further evaluation of these compounds needs to be done to determine their efficacy as AR-NTD antagonists.

Sintokamides are known binders to the AR-NTD and thus can be used to image splice variant tumor progression in mCRPC. This led to the attempted synthesis of radiolabelled imaging agents **3.61** and its fluorinated cold compound counterpart **3.62**. The natural sintokamide (SINT1) has a propyl amide at the *N*-terminus. The potential imaging agent **3.61** is an analog of SINT1 with a propionyl bromide that could be reasonably displaced with ^{18}F to give a potential imaging agent. However, displacing the bromine with fluorine proved to be challenging and the sintokamide core seems to be labile in the presence of fluorine anions at elevated temperatures. Next the synthesis of a fluorinated sintokamide **3.41** was attempted, using a 3-fluro-2,2-dimethylpropanoic acid to cross-couple to free amine sintokamide core **3.35**, however, the cross-coupling reaction was unsuccessful. Lastly, using the copper mediated 1,3 Huisgen dipolar cycloaddition reaction the 4-pentyne amide sintokamide analog **3.65** and a tosylated propyl azide **(3.64)** was Clicked to give **3.66**. The attempted conversion of **3.66** to the cold fluorinated compound **3.67** was unsuccessful, presumably also due to the sintokamide core being labile to exposure to fluorine anions as was seen with the attempted synthesis of **3.61.**

Bibliography

(1)   Solecki, R. S. Shanidar IV, a Neanderthal Flower Burial in Northern Iraq. *Science.* **1975**, *190* (4217), 880–881. https://doi.org/10.1126/science.190.4217.880.

(2)   Poduri, R. Historical Perspective of Drug Discovery and Development. *Drug Discov. Dev.* **2021**, 1–10. https://doi.org/10.1007/978-981-15-5534-3_1.

(3)   Wang, J.; Xu, C.; Wong, Y. K.; Li, Y.; Liao, F.; Jiang, T.; Tu, Y. Artemisinin, the Magic Drug Discovered from Traditional Chinese Medicine. *Engineering* **2019**, *5* (1), 32–39. https://doi.org/10.1016/J.ENG.2018.11.011.

(4)   Cragg, G. M.; Newman, D. J. Natural Products: A Continuing Source of Novel Drug Leads. *Biochim. Biophys. Acta - Gen. Subj.* **2013**, *1830* (6), 3670–3695. https://doi.org/10.1016/J.BBAGEN.2013.02.008.

(5)   Kanda, Y.; Nakamura, H.; Umemiya, S.; Puthukanoori, R. K.; Murthy Appala, V. R.; Gaddamanugu, G. K.; Paraselli, B. R.; Baran, P. S. Two-Phase Synthesis of Taxol. *J. Am. Chem. Soc.* **2020**, *142* (23), 10526–10533. https://doi.org/10.1021/JACS.0C03592/SUPPL_FILE/JA0C03592_SI_001.PDF.

(6)   Ojima, I.; Habus, I.; Zhao, M.; Zucco, M.; Park, Y. H.; Sun, C. M.; Brigaud, T. New and Efficient Approaches to the Semisynthesis of Taxol and Its C-13 Side Chain Analogs by Means of β-Lactam Synthon Method. *Tetrahedron* **1992**, *48* (34), 6985–7012. https://doi.org/10.1016/S0040-4020(01)91210-4.

(7)   Sorokina, M.; Merseburger, P.; Rajan, K.; Yirik, A.; Steinbeck, C. COCONUT Online: Collection of Open Natural Products Database. https://doi.org/10.1186/s13321-020-00478-9.

(8)   Ntie-Kang, F.; Svozil, D. An Enumeration of Natural Products from Microbial, Marine and Terrestrial Sources. *Phys. Sci. Rev.* **2020**, *5* (8). https://doi.org/10.1515/PSR-2018-0121.

(9)   Dias, D. A.; Urban, S.; Roessner, U. A Historical Overview of Natural Products in Drug Discovery. *Metabolites* **2012**, *2*, 303–336. https://doi.org/10.3390/metabo2020303.

(10)   K. C. Nicolaou, E. J. S. *Classics in Total Synthesis: Targets, Strategies, Methods*. Wiley-VCH. **1996**.

(11)   Florence F. Hibionada. Remembering the battle of Dr. Abelardo Aguilar:Cure for millions, deprived of millions http://www.thenewstoday.info/2005/05/03/iloilonews3.htm (accessed Oct 27, 2021).

(12)   Jiménez, C. Marine Natural Products in Medicinal Chemistry. *ACS Med. Chem. Lett.* **2018**, *9* (10), 959–961. https://doi.org/10.1021/acsmedchemlett.8b00368.

(13)   Pereira, F. Have Marine Natural Product Drug Discovery Efforts Been Productive and How Can We Improve Their Efficiency? *Expert Opin. Drug Discov.* **2019**, *14* (8), 717–722. https://doi.org/10.1080/17460441.2019.1604675.

(14)   Siegel, R. L.; Miller, K. D.; Fuchs, H. E.; Jemal, A. Cancer Statistics, 2021. *CA. Cancer J. Clin.* **2021**, *71* (1), 7–33. https://doi.org/10.3322/CAAC.21654.

(15)   Brenner, D.; Poirier, A.; Smith, L.; Aziz, L. S.; Ellison, L.; Fitzgerald, N.; Saint-Jacques, N.; Turner, D.; Weir, H. K.; Woods, R.; Demers, A.; Billette, J.-M.; Statistics, ; Yao, C. C.; Shary, C.; Zhang, X.; Canada, S.; Dixon, M. Members of the Canadian Cancer Statistics Advisory Committee Analytic Leads Additional Analysis Project Management. **2021**.

(16)   Lonergan, P.; Tindall, D. Androgen Receptor Signaling in Prostate Cancer Development and Progression. *J. Carcinog.* **2011**, *10*. https://doi.org/10.4103/1477-3163.83937.

(17)   Sadar, M. D. Discovery of Drugs That Directly Target the Intrinsically Disordered Region of the Androgen Receptor. *Expert Opin. Drug Discov.* **2020**, *15* (5), 551–560. https://doi.org/10.1080/17460441.2020.1732920.

(18)   Heinlein, C. A.; Chang, C. Androgen Receptor in Prostate Cancer. *Endocrine Reviews*. 2004, pp 276–308. https://doi.org/10.1210/er.2002-0032.

(19)   Helsen, C.; Broeck, T. Van den; Voet, A.; Prekovic, S.; Poppel, H. Van; Joniau, S.; Claessens, F. Androgen Receptor Antagonists for Prostate Cancer Therapy. *Endocr. Relat. Cancer* **2014**, *21* (4), 105–118. https://doi.org/10.1530/ERC-13-0545.

(20)   Harris, M. G.; Coleman, S. G.; Faulds, D.; Chrisp, P. Nilutamide. A Review of Its Pharmacodynamic and Pharmacokinetic Properties, and Therapeutic Efficacy in Prostate Cancer. *Drugs Aging* **1993**, *3* (1), 9–25. https://doi.org/10.2165/00002512-199303010-00002.

(21)   Tran, C.; Ouk, S.; Clegg, N. J.; Chen, Y.; Watson, P. A.; Arora, V.; Wongvipat, J.; Smith-Jones, P. M.; Yoo, D.; Kwon, A.; Wasielewska, T.; Welsbie, D.; Chen, C. D.; Higano, C. S.; Beer, T. M.; Hung, D. T.; Scher, H. I.; Jung, M. E.; Sawyers, C. L. Development of a Second-Generation Antiandrogen for Treatment of Advanced Prostate Cancer. *Science*. **2009**, *324* (5928), 787–790. https://doi.org/10.1126/science.1168175.

(22)   Teutsch, G.; Goubet, F.; Battmann, T.; Bonfils, A.; Bouchoux, F.; Cerede, E.; Gofflo, D.; Gaillard-Kelly, M.; Philibert, D. Non-Steroidal Antiandrogens: Synthesis and Biological Profile of High-Affinity Ligands for the Androgen Receptor. *J. Steroid Biochem. Mol. Biol.* **1994**, *48* (1), 111–119. https://doi.org/10.1016/0960-0760(94)90257-7.
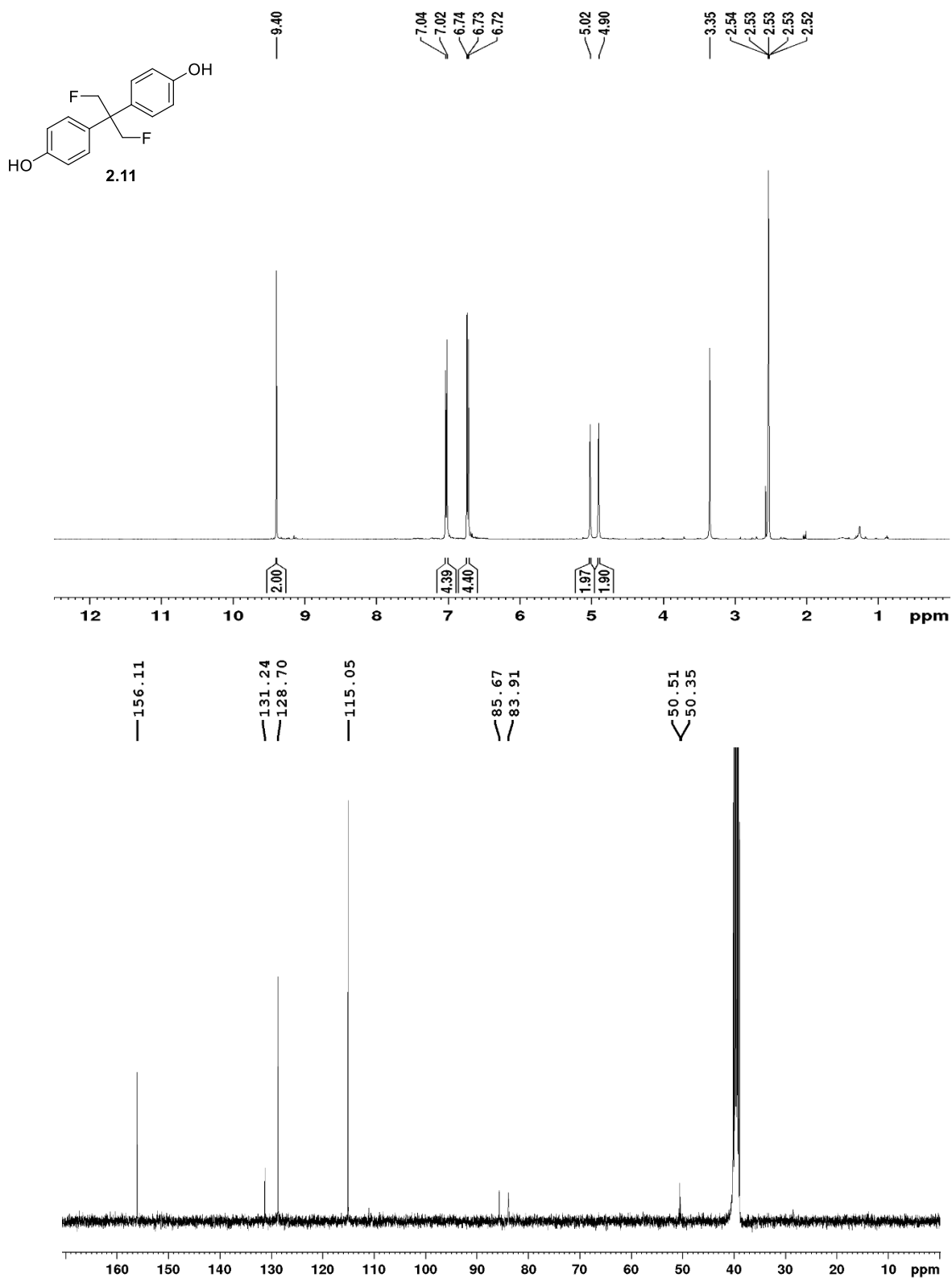
(23)   Rice, M. A.; Malhotra, S. V.; Stoyanova, T. Second-Generation Antiandrogens: From Discovery to Standard of Care in Castration Resistant Prostate Cancer. *Front. Neurol.* **2019**, *10* (AUG). https://doi.org/10.3389/fonc.2019.00801.

(24)   Antonarakis, E.; Armstrong, A.; Dehm, S.; Luo, J. Androgen Receptor Variant-Driven Prostate Cancer: Clinical Implications and Therapeutic Targeting. *Prostate Cancer Prostatic Dis.* **2016**, *19* (3), 231. https://doi.org/10.1038/PCAN.2016.17.

(25)   Andersen, R. J. Sponging off Nature for New Drug Leads. *Biochem. Pharmacol.* **2017**, *139*, 3–14. https://doi.org/10.1016/J.BCP.2017.04.012.

(26)   Sadar, M. D. Small Molecule Inhibitors Targeting the "Achilles'' Heel" of Androgen Receptor Activity." *Cancer Res.* **2011**, *71* (4), 1208–1213. https://doi.org/10.1158/0008-5472.CAN_10-3398.

(27)   Imamura, Y.; Tien, A. H.; Banuelos, C. A.; Wang, J.; Mawji, N. R.; Jian, K.; Fernandez, J. G.; Andersen, R. J.; Sadar, M. D.; Imamura, Y.; Tien, A. H.; Pan, J.; Leung, J. K.; Banuelos, C. A.; Jian, K.; Wang, J.; Mawji, N. R.; Fernandez, J. G.; Lin, K.-S.; Andersen, R. J.; Sadar, M. D. An Imaging Agent to Detect Androgen Receptor and Its Active Splice Variants in Prostate Cancer. *JCI Insight* **2016**, *1* (11), 87850. https://doi.org/10.1172/JCI.INSIGHT.87850.

(28)   Myung, J. K.; Banuelos, C. A.; Fernandez, J. G.; Mawji, N. R.; Wang, J.; Tien, A. H.; Yang, Y. C.; Tavakoli, I.; Haile, S.; Watt, K.; McEwan, I. J.; Plymate, S.; Andersen, R. J.; Sadar, M. D. An Androgen Receptor N-Terminal Domain Antagonist for Treating Prostate Cancer. *J. Clin. Invest.* **2013**, *123* (7), 2948–2960. https://doi.org/10.1172/JCI66398.

(29) Rokita, S. E.; Adler, J. M.; McTamney, P. M.; Watson, J. A. Efficient Use and Recycling of the Micronutrient Iodide in Mammals. *Biochimie* **2010**, *92* (9), 1227–1235. https://doi.org/10.1016/J.BIOCHI.2010.02.013.

(30) Bianco, A. C.; Kim, B. W. Deiodinases: Implications of the Local Control of Thyroid Hormone Action. *J. Clin. Invest.* **2006**, *116* (10), 2571. https://doi.org/10.1172/JCI29812.

(31) De Mol, E.; Fenwick, R. B.; Phang, C. T. W.; Buzón, V. B.; Szulc, E.; De La Fuente, A.; Escobedo, A.; García, J. J.; Bertoncini, C. W.; Estébanez-Perpiñ, E.; Mcewan, I. J.; Riera, A.; Salvatella, X. EPI-001, A Compound Active against Castration-Resistant Prostate Cancer, Targets Transactivation Unit 5 of the Androgen Receptor. *ACS Chem. Biol.* **2016**, *11*, 2499–2505. https://doi.org/10.1021/acschembio.6b00182.

(32) Banuelos, C. A.; Tavakoli, I.; Tien, A. H.; Caley, D. P.; Mawji, N. R.; Li, Z.; Wang, J.; Yang, Y. C.; Imamura, Y.; Yan, L.; Wen, J. G.; Andersen, R. J.; Sadar, M. D. Sintokamide A Is a Novel Antagonist of Androgen Receptor That Uniquely Binds Activation Function-1 in Its Amino-Terminal Domain. *J. Biol. Chem.* **2016**, *291* (42), 22231–22243. https://doi.org/10.1074/JBC.M116.734475.

(33) Climie, I. J. G.; Hutson, D. H.; Stoydin, G. Metabolism of the Epoxy Resin Component 2,2-Bis[4-(2,3-Epoxypropoxy)Phenyl]Propane, the Diglycidyl Ether of Bisphenol a (DGEBPA) in the Mouse.; Part I. A Comparison of the Fate of a Single Dermal Application and of a Single Oral Dose of 14c-DGEBPA. *Xenobiotica* **1981**, *11* (6), 391–399. https://doi.org/10.3109/00498258109045850.

(35) Opinion of the Scientific Panel on Food Additives, Flavourings, Processing Aids and Materials in Contact with Food (AFC) on a Request from the Commission Related to 2,2-Bis(4-Hydroxyphenyl)Propane Bis(2,3-Epoxypropyl)Ether (Bisphenol a Diglycidyl Ether, B. *EFSA J.* **2004**, *2* (7). https://doi.org/10.2903/j.efsa.2004.86.

(36) Obst, J. K.; Wang, J.; Jian, K.; Williams, D. E.; Tien, A. H.; Mawji, N.; Tam, T.; Yang, Y. C.; Andersen, R. J.; Chi, K. N.; Montgomery, B.; Sadar, M. D. Revealing Metabolic Liabilities of Ralaniten To Enhance Novel Androgen Receptor Targeted Therapies. *ACS Pharmacology and Translational Science*. **2019**, *2* (6), 453–467. https://doi.org/10.1021/acsptsci.9b00065

(37) Lipinski, C. A. Lead- and Drug-like Compounds: The Rule-of-Five Revolution. *Drug Discov. Today Technol.* **2004**, *1* (4), 337–341. https://doi.org/10.1016/J.DDTEC.2004.11.007.

(38) Hunter, L. The C–F Bond as a Conformational Tool in Organic and Biological Chemistry. *Beilstein J. Org. Chem.* **2010**, *6* (38). https://doi.org/10.3762/BJOC.6.38.

(39) Wilcken, R.; Zimmermann, M. O.; Lange, A.; Joerger, A. C.; Boeckler, F. M. Principles and Applications of Halogen Bonding in Medicinal Chemistry and Chemical Biology. *J. Med. Chem.* **2013**, 56 (4), 1363−1388. https://doi.org/10.1021/jm3012068.

(40) Wuitschik, G.; Carreira, E. M.; Wagner, orn; Fischer, H.; Parrilla, I.; Schuler, F.; Rogers-Evans, M. Oxetanes in Drug Discovery: Structural and Synthetic Insights. *J. Med. Chem* **2010**, *53 (8)*, 3227-3246. https://doi.org/10.1021/jm9018788.

(41)   Neumann, C. S.; Fujimori, D. G.; Walsh, C. T. Halogenation Strategies In Natural Product
Biosynthesis. *Chem. Biol.* **2008**, *15* (2), 99–109.
https://doi.org/10.1016/J.CHEMBIOL.2008.01.006.

(42)   Bidleman, T. F.; Andersson, A.; Jantunen, L. M.; Kucklick, J. R.; Kylin, H.; Letcher, R.
J.; Tysklind, M.; Wong, F. A Review of Halogenated Natural Products in Arctic,
Subarctic and Nordic Ecosystems. *Emerg. Contam.* **2019**, *5*, 89–115.
https://doi.org/10.1016/J.EMCON.2019.02.007.

(43)   Sadar, M. D.; Williams, D. E.; Mawji, N. R.; Patrick, B. O.; Wikanta, T.; Chasanah, E.;
Irianto, H. E.; Van Soest, R.; Andersen, R. J. Sintokamides A to E, Chlorinated Peptides
from the Sponge Dysidea Sp. That Inhibit Transactivation of the N-Terminus of the
Androgen Receptor in Prostate Cancer Cells. *Org. Lett.* **2008**, *10* (21), 4947–4950.
https://doi.org/10.1021/ol802021w.

(44)   Yan, L.; Banuelos, C. A.; Mawji, N. R.; Patrick, B. O.; Sadar, M. D.; Andersen, R. J.
Structure-Activity Relationships for the Marine Natural Product Sintokamides: Androgen
Receptor N-Terminus Antagonists of Interest for Treatment of Metastatic Castration-
Resistant Prostate Cancer. *J. Nat. Prod.* **2020**¸ 84 (3), 797-813.
https://doi.org/10.1021/acs.jnatprod.0c00921.

(45)   Gu, Z.; Zakarian, A. Concise Total Synthesis of Sintokamides A, B, and e by a Unified,
Protecting-Group-Free Strategy. *Angew. Chemie - Int. Ed.* **2010**, *49* (50), 9702–9705.
https://doi.org/10.1002/anie.201005354.

Appendix - ¹H and ¹³C NMR of Select Compounds in Chapters 2 and 3

2.11

9.40

7.04
7.02
6.74
6.73
6.72

5.02
4.90

3.35
2.54
2.53
2.53
2.53
2.52

2.00

4.39
4.40

1.97
1.90

12 11 10 9 8 7 6 5 4 3 2 1 ppm

156.11

131.24
128.70

115.05

85.67
83.91

50.51
50.35

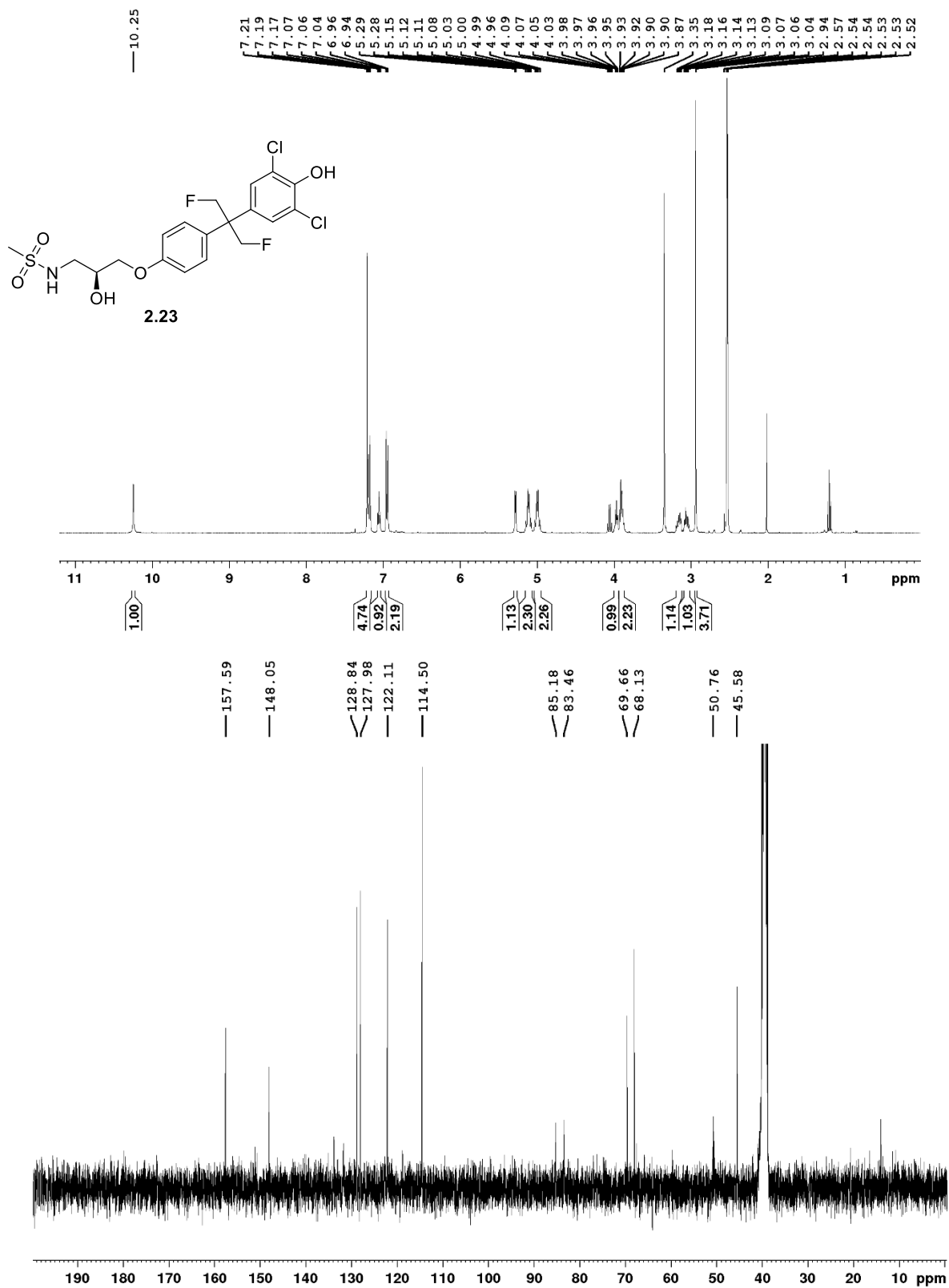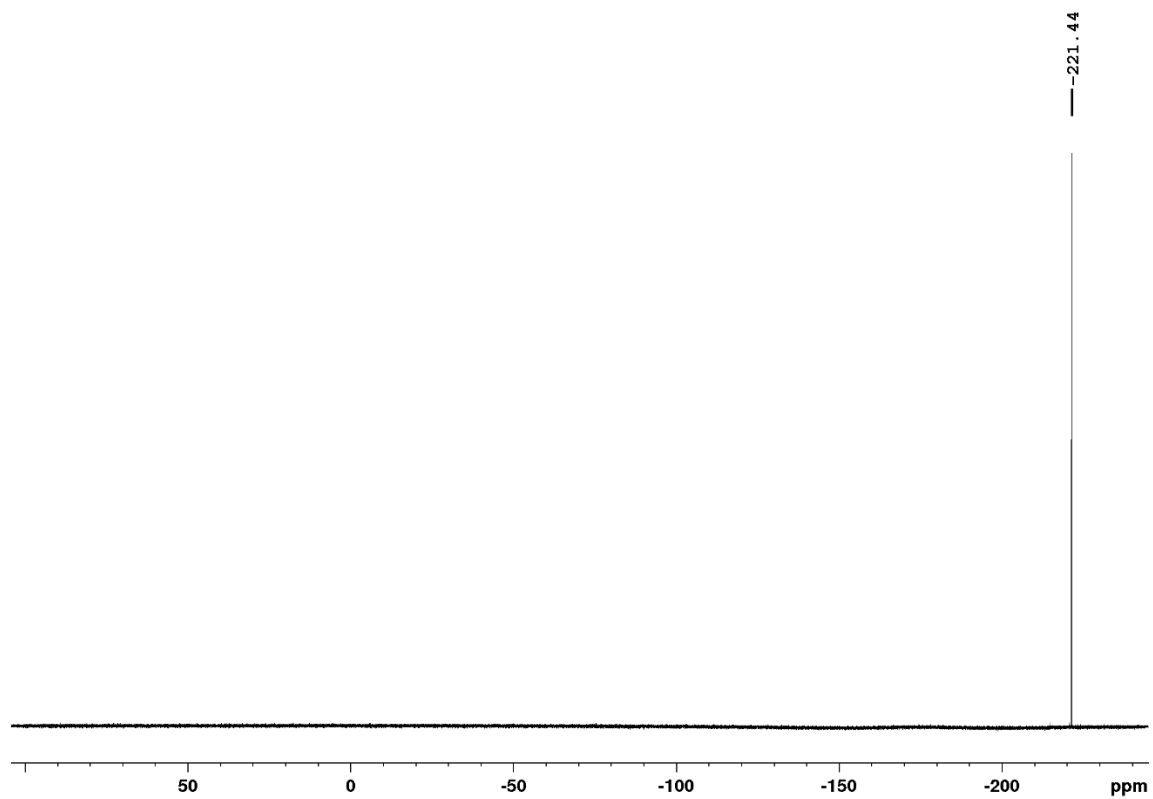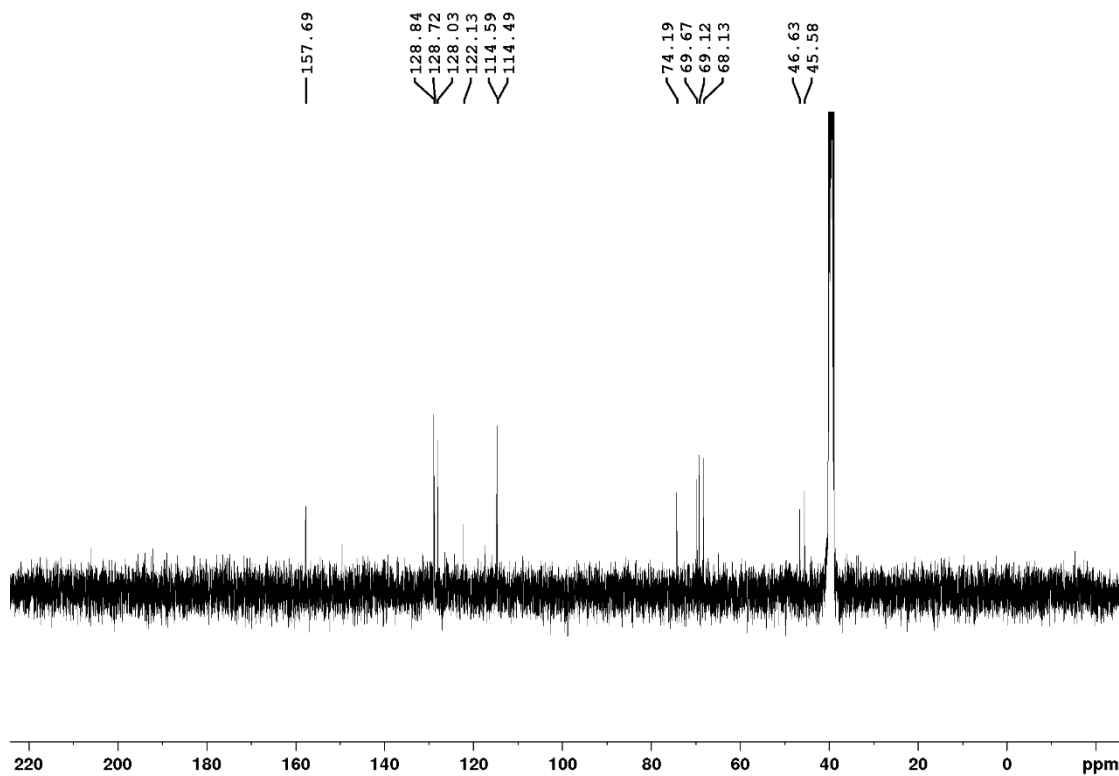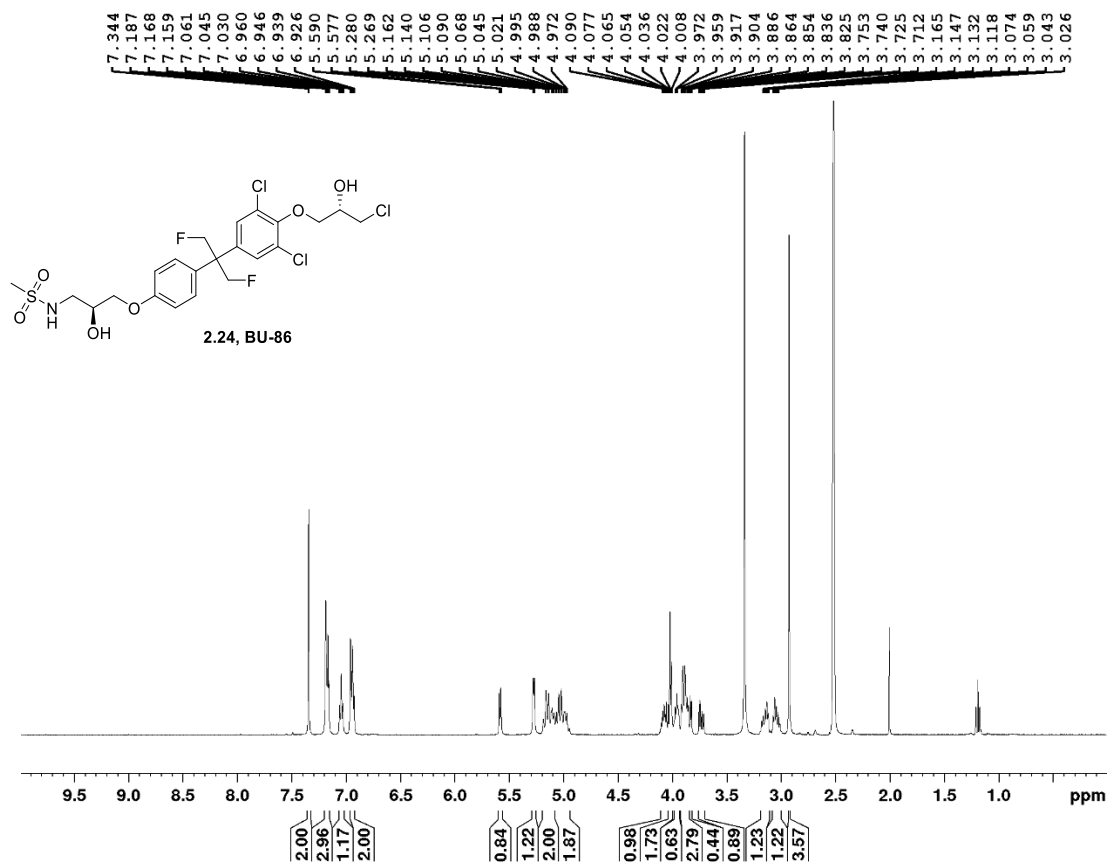160 150 140 130 120 110 100 90 80 70 60 50 40 30 20 10 ppm

119
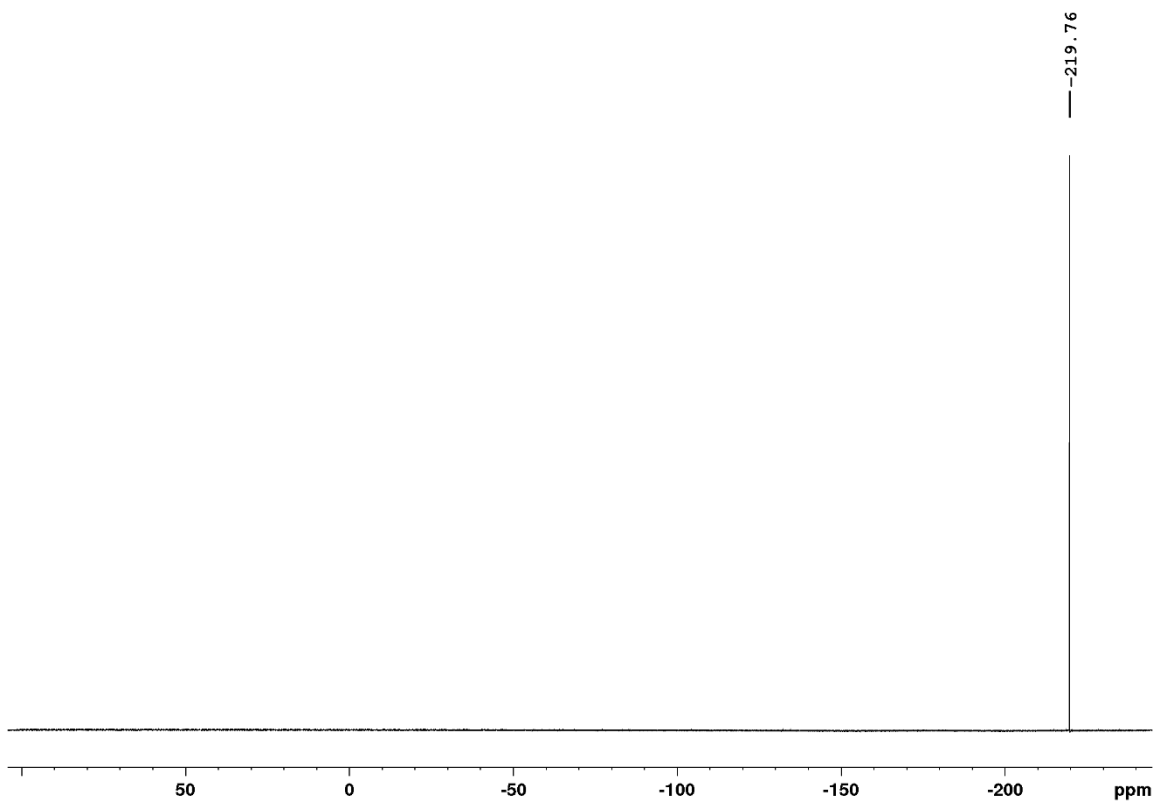
Figure A.1 – ^{1}H, ^{13}C, and ^{19}F NMR Spectra of **2.11** recorded in DMSO-d$_6$ at 400 MHz and 100 MHz, and 300 MHz respectively.

¹H NMR peaks (ppm): 9.41, 7.44, 7.42, 7.37, 7.35, 7.33, 7.31, 7.29, 7.28, 7.27, 7.26, 7.25, 7.24, 7.23, 7.04, 7.02, 6.90, 6.89, 6.88, 6.87, 6.74, 6.72, 6.71, 6.70, 6.68, 6.64, 6.62, 6.47, 5.02, 4.98, 4.95, 4.90, 4.85, 4.83, 3.36, 2.57, 2.54, 2.53, 2.53, 2.52, 2.05, 2.04, 2.01, 1.26

2.12

Integrations: 1.00, 2.76, 11.89, 1.87, 1.52, 2.69, 0.74, 0.44, 3.72

ppm axis: 9.5 9.0 8.5 8.0 7.5 7.0 6.5 6.0 5.5 5.0 4.5 4.0 3.5 3.0 2.5 2.0 1.5 1.0 ppm

¹³C NMR peaks (ppm): 156.12, 154.42, 147.76, 143.66, 131.24, 128.70, 128.62, 128.37, 127.87, 127.76, 127.51, 127.22, 126.62, 120.13, 115.05, 115.02, 89.60, 80.54, 40.15, 38.89

ppm axis: 190 180 170 160 150 140 130 120 110 100 90 80 70 60 50 40 30 20 ppm

121

Figure A.2 – ^{1}H, ^{13}C, and ^{19}F NMR Spectra of **2.12** recorded in DMSO-d$_6$ at 400 MHz and 100 MHz, and 300 MHz respectively
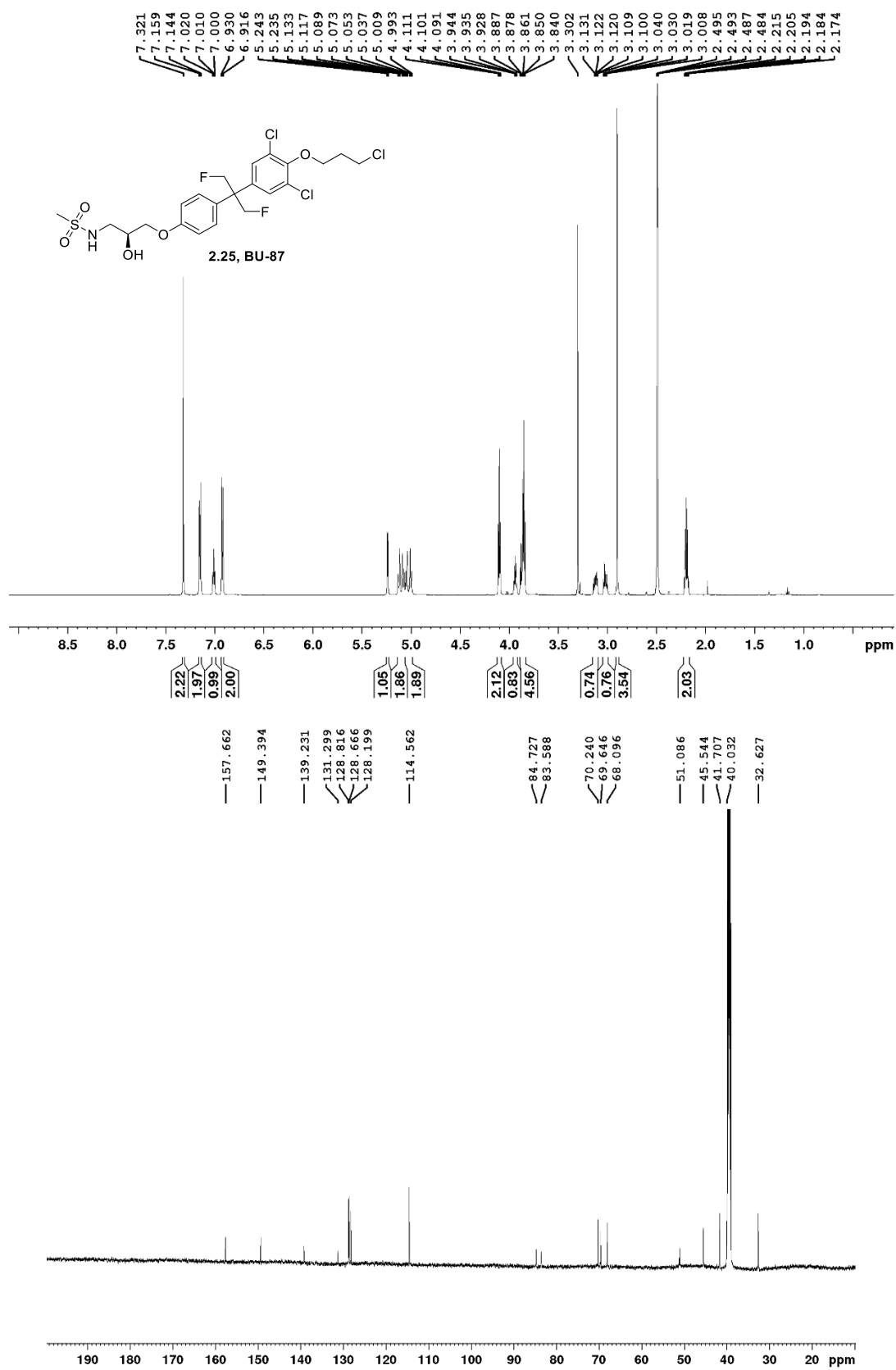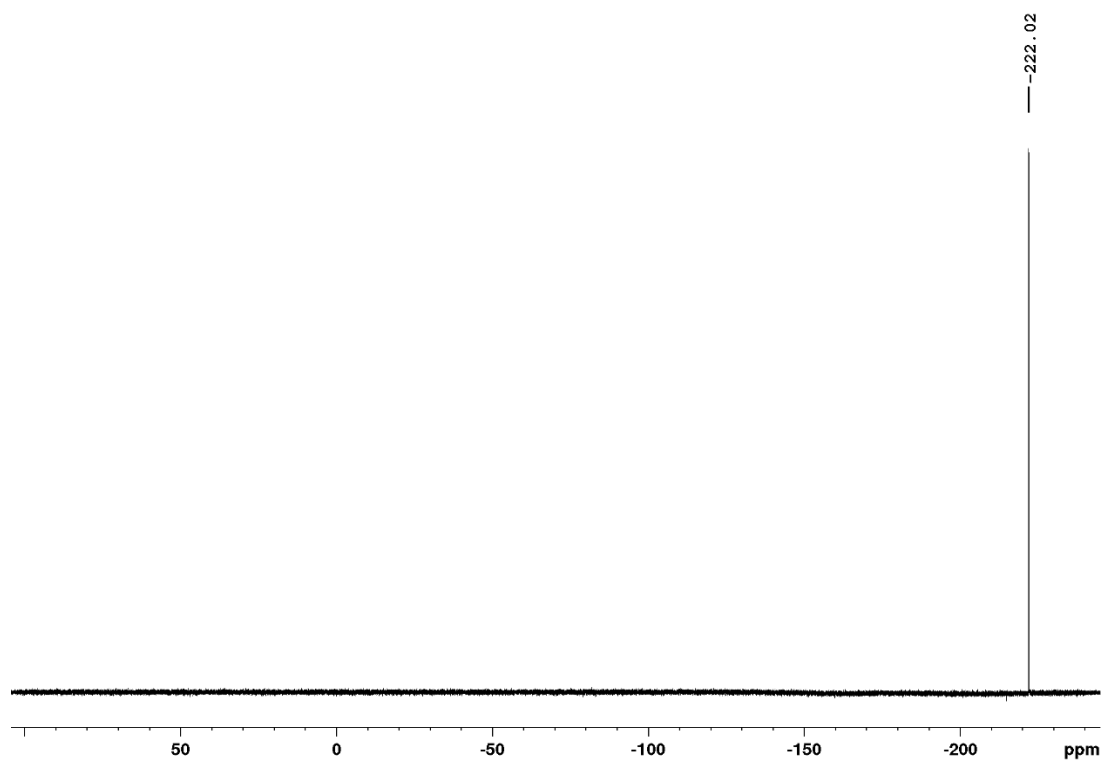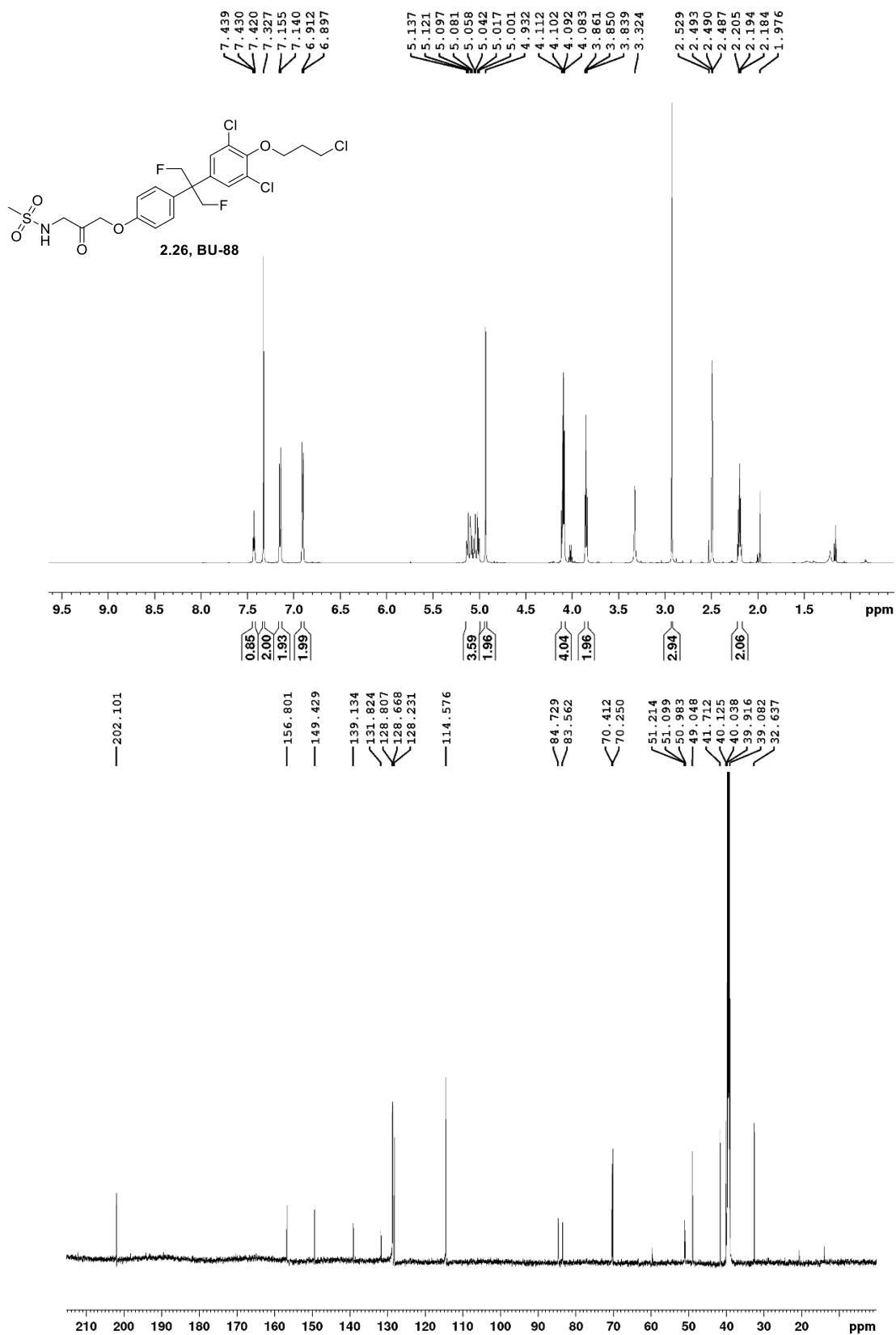
2.21

¹H NMR peaks (ppm): 7.44, 7.43, 7.41, 7.37, 7.35, 7.33, 7.30, 7.28, 7.27, 7.26, 7.02, 7.00, 6.91, 6.90, 6.89, 6.88, 6.64, 6.62, 4.98, 4.96, 4.89, 4.87, 4.84, 4.33, 4.33, 4.30, 4.07, 4.05, 3.85, 3.84, 3.82, 3.81, 3.35, 3.34, 3.33, 3.32, 3.31, 2.87, 2.86, 2.85, 2.73, 2.72, 2.71, 2.54, 2.53, 2.53, 2.52, 2.02, 1.22

Integrations: 6.75, 9.92, 1.80, 3.92, 1.93, 2.00, 1.97, 0.88, 1.03, 0.83, 1.06, 1.04

¹³C NMR peaks (ppm): 157.01, 154.49, 143.64, 128.77, 128.36, 127.88, 127.81, 127.24, 120.18, 114.26, 89.61, 68.87, 50.57, 49.66, 43.74, 40.15, 38.90
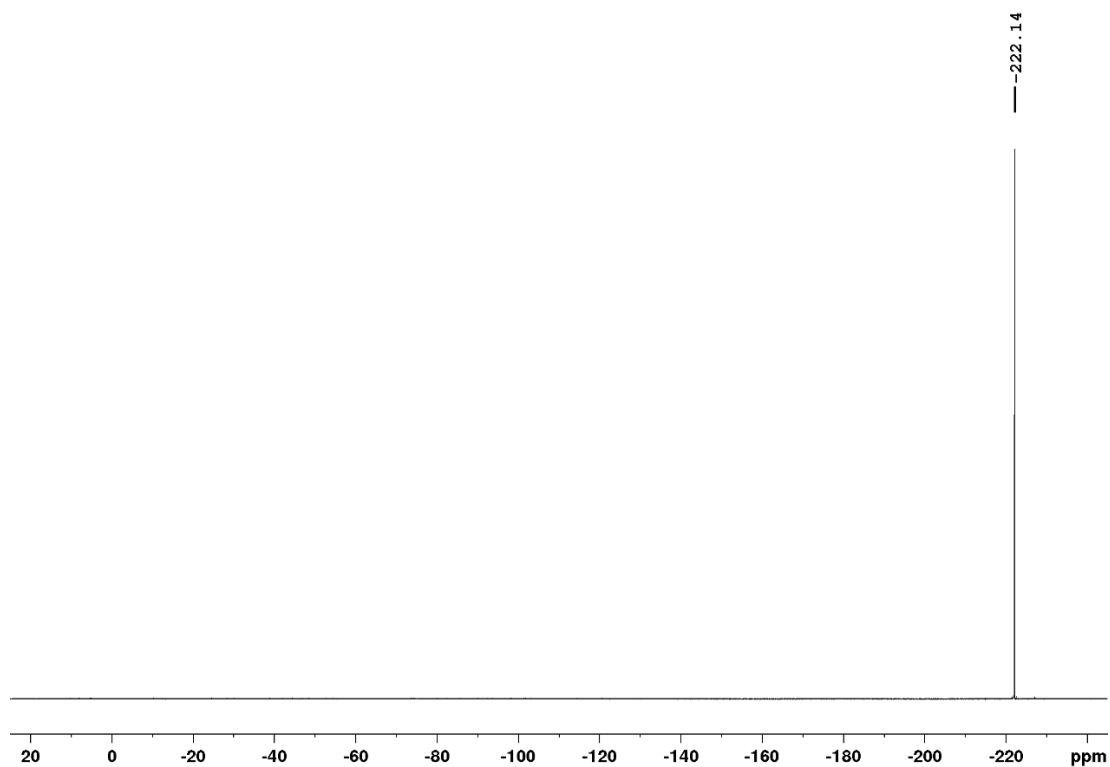
123
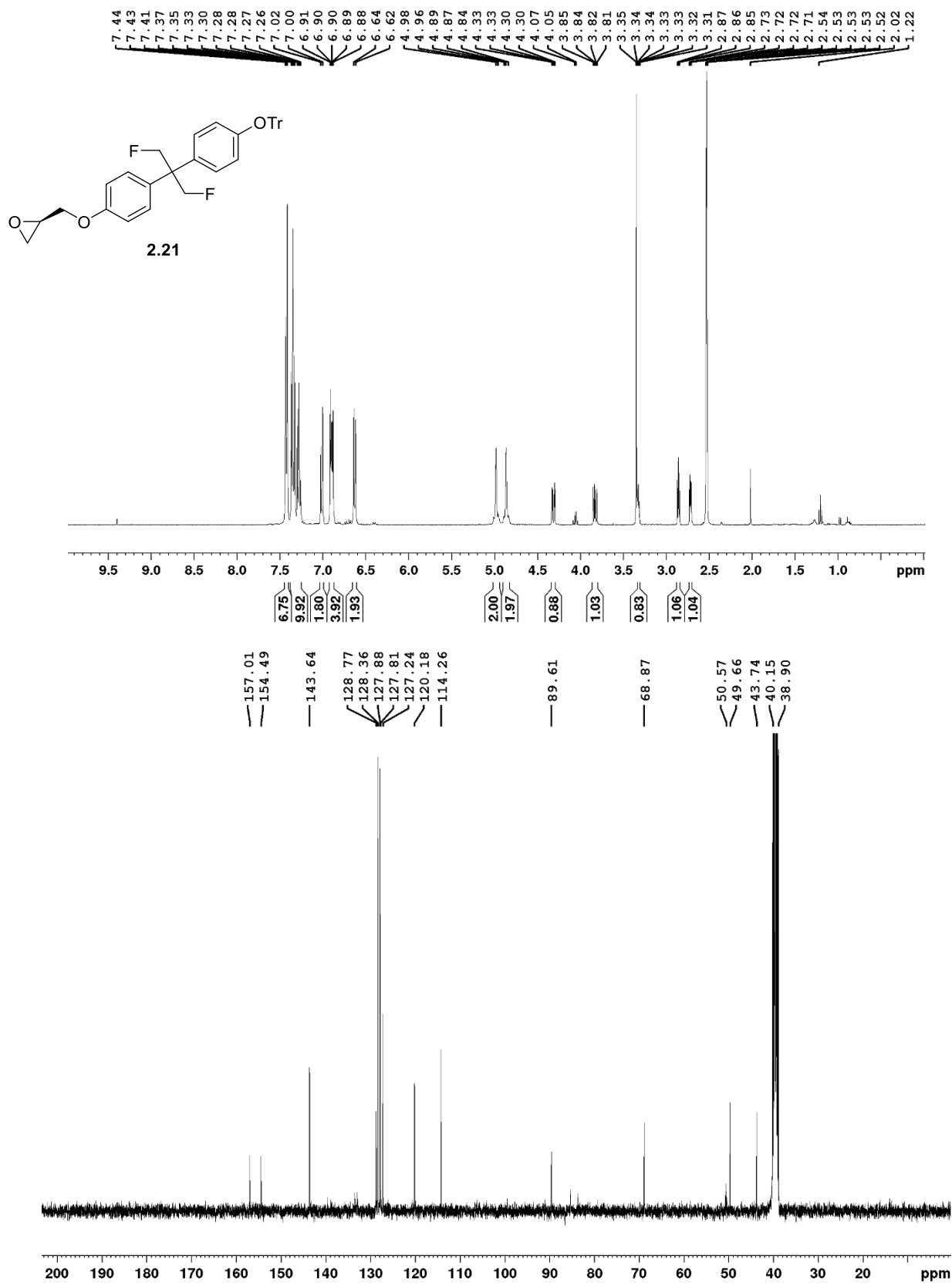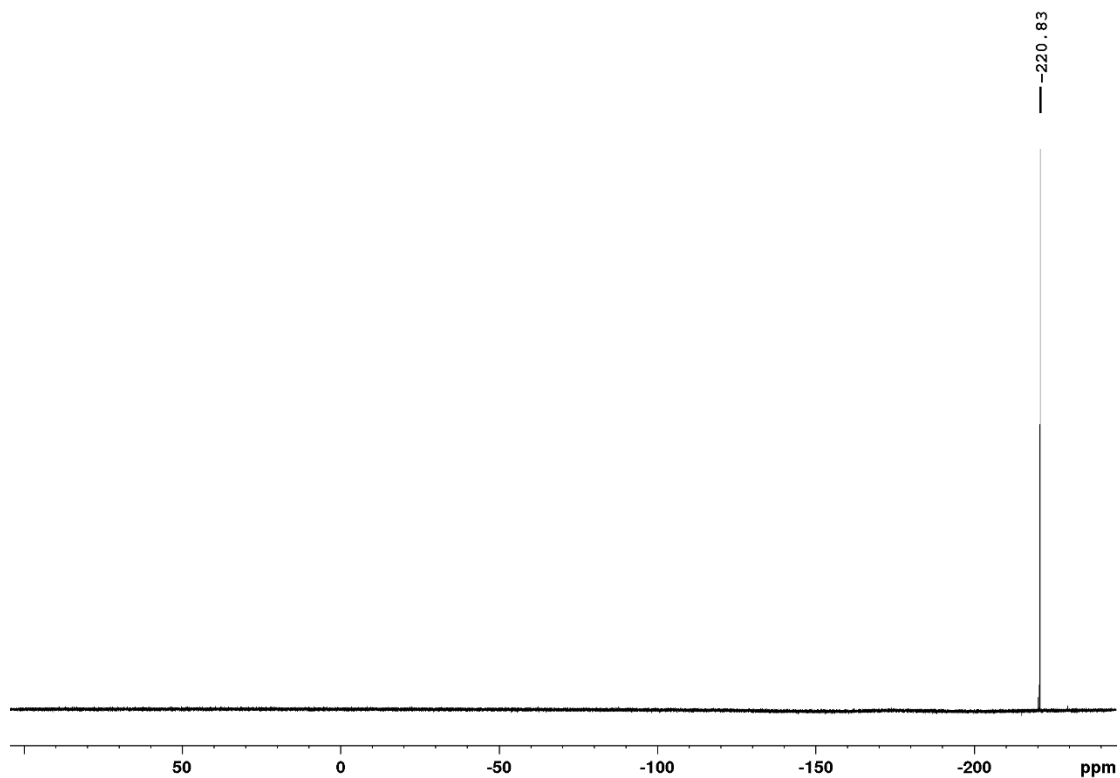
Figure A.3 – ^{1}H, ^{13}C, and ^{19}F NMR Spectra of **2.21** recorded in DMSO-d$_6$ at 400 MHz and 100 MHz, and 300 MHz respectively
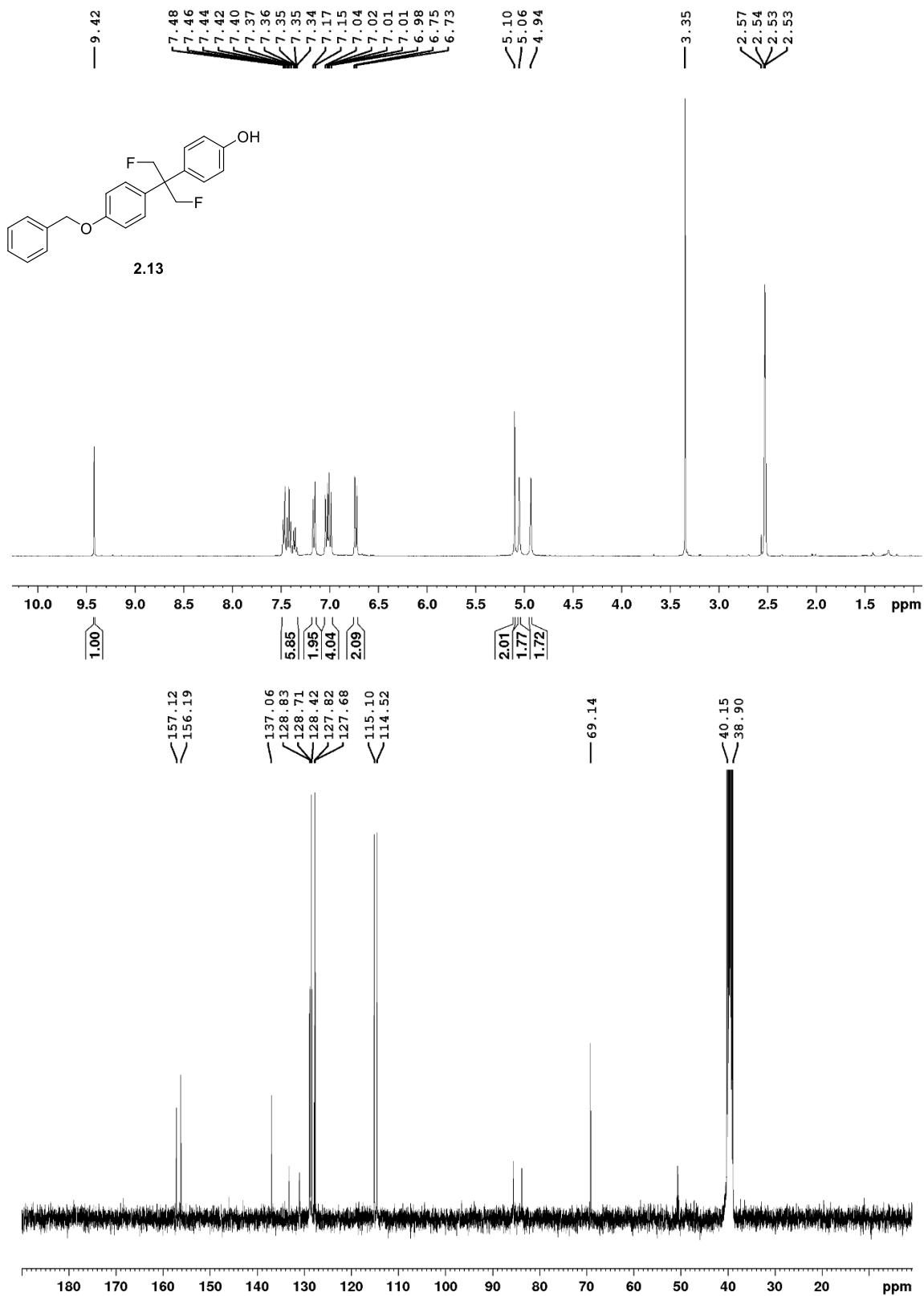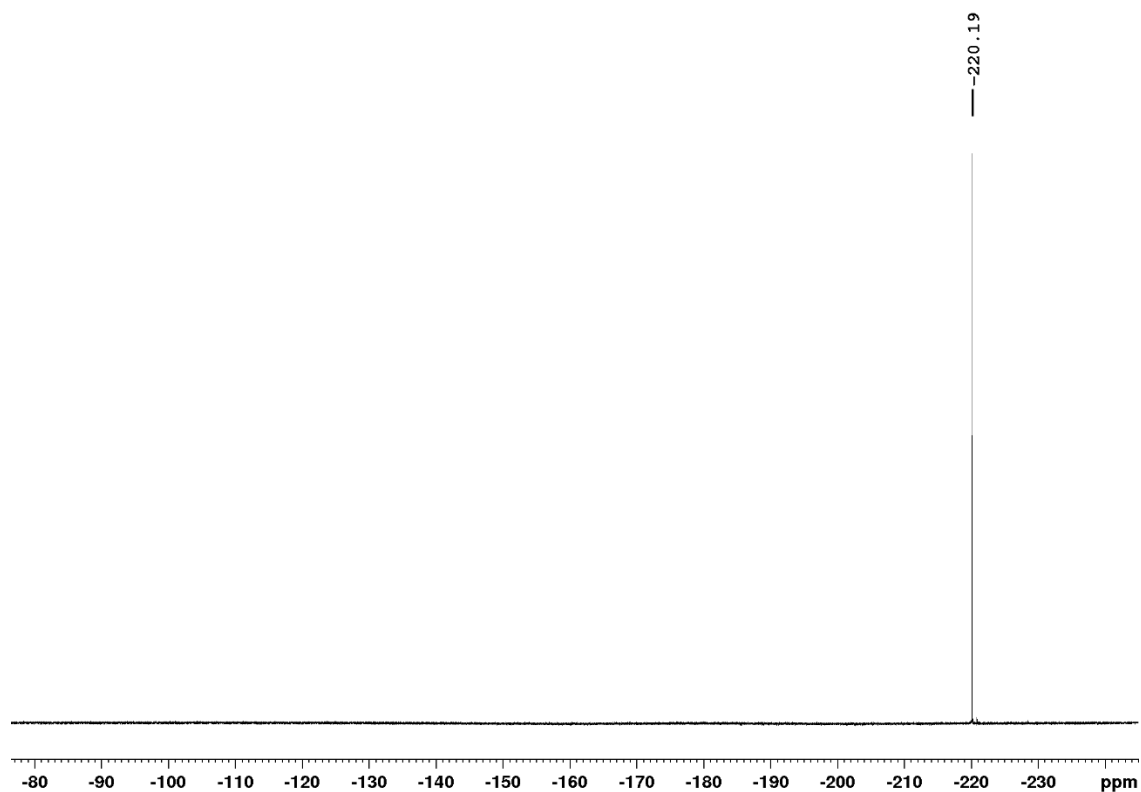
2.22

^{1}H NMR peaks: 9.42; 7.17, 7.15, 7.07, 7.05, 7.04, 7.02, 6.93, 6.91, 6.75, 6.74, 6.72; 5.28, 5.27, 5.06; 4.93, 4.07, 4.05, 3.97, 3.96, 3.94, 3.91, 3.90, 3.88, 3.35, 3.19, 3.17, 3.16, 3.14, 3.13, 3.08, 3.07, 3.05, 3.04, 3.02, 2.94, 2.57, 2.54, 2.53, 2.53, 2.52, 2.02; 1.22, 1.20, 1.19

Integrations: 1.00; 2.14, 3.03, 2.14, 1.91; 1.06, 1.98, 2.01; 0.94, 1.97; 1.14, 1.14, 3.72

^{13}C NMR peaks: 157.31, 156.19; 133.12, 131.03, 128.80, 128.72; 115.10, 114.29; 85.64, 83.84; 69.66, 68.14; 50.62, 50.45, 45.59
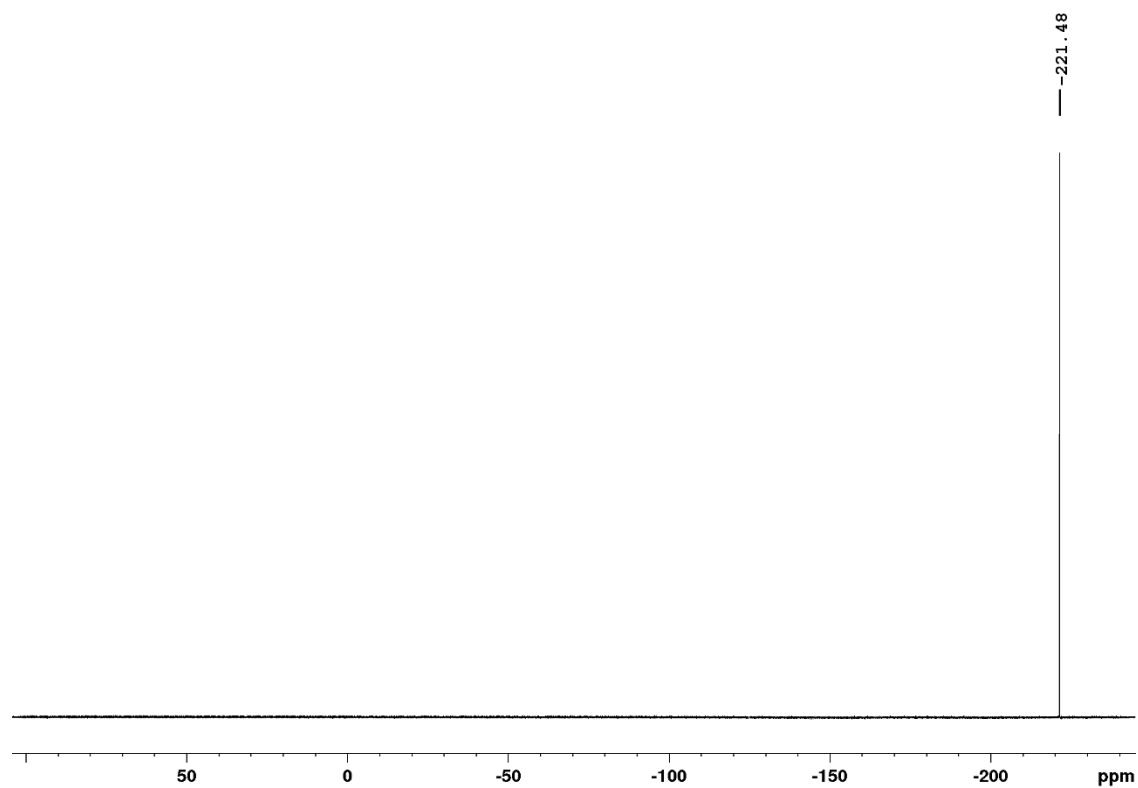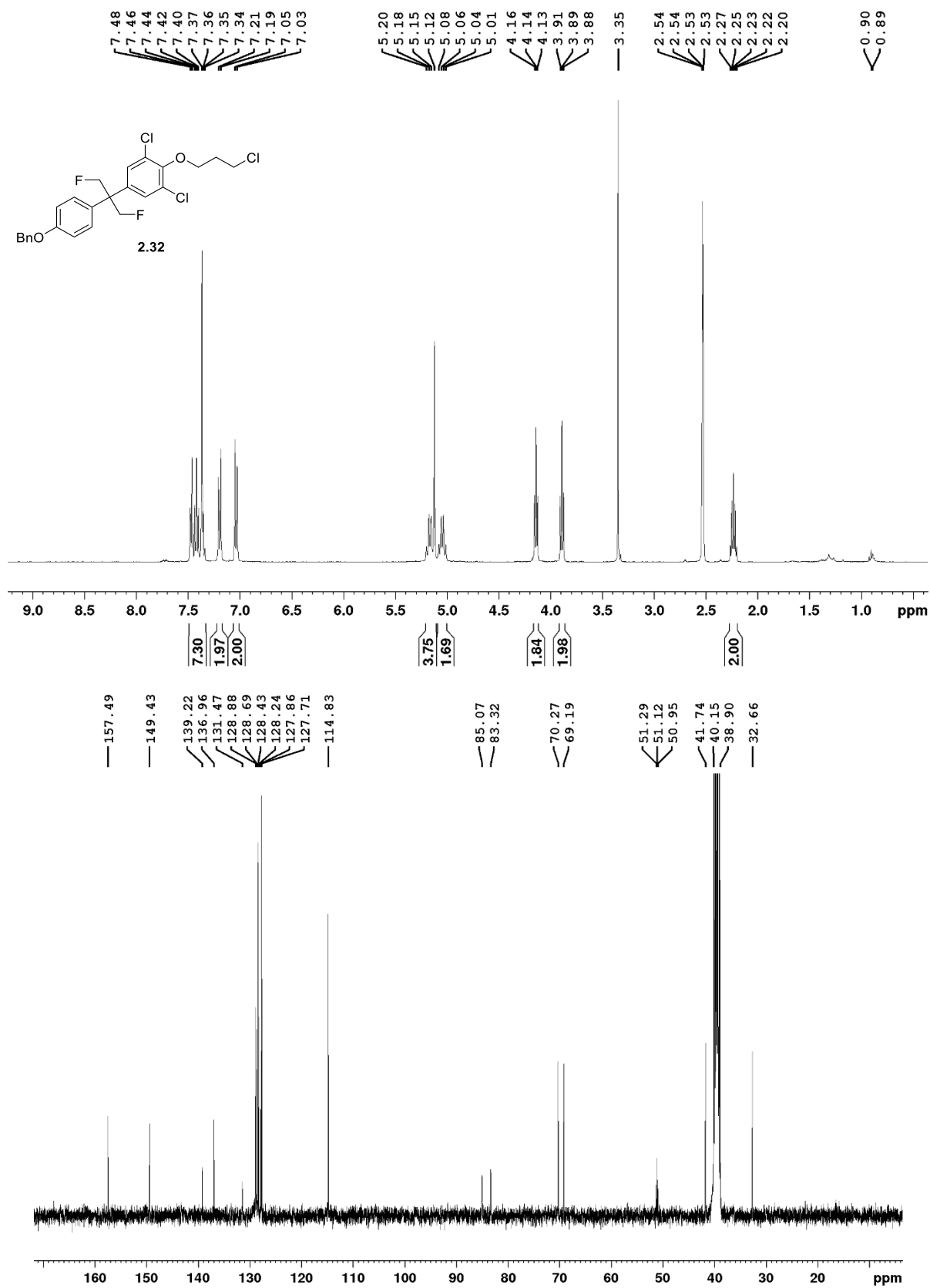
125
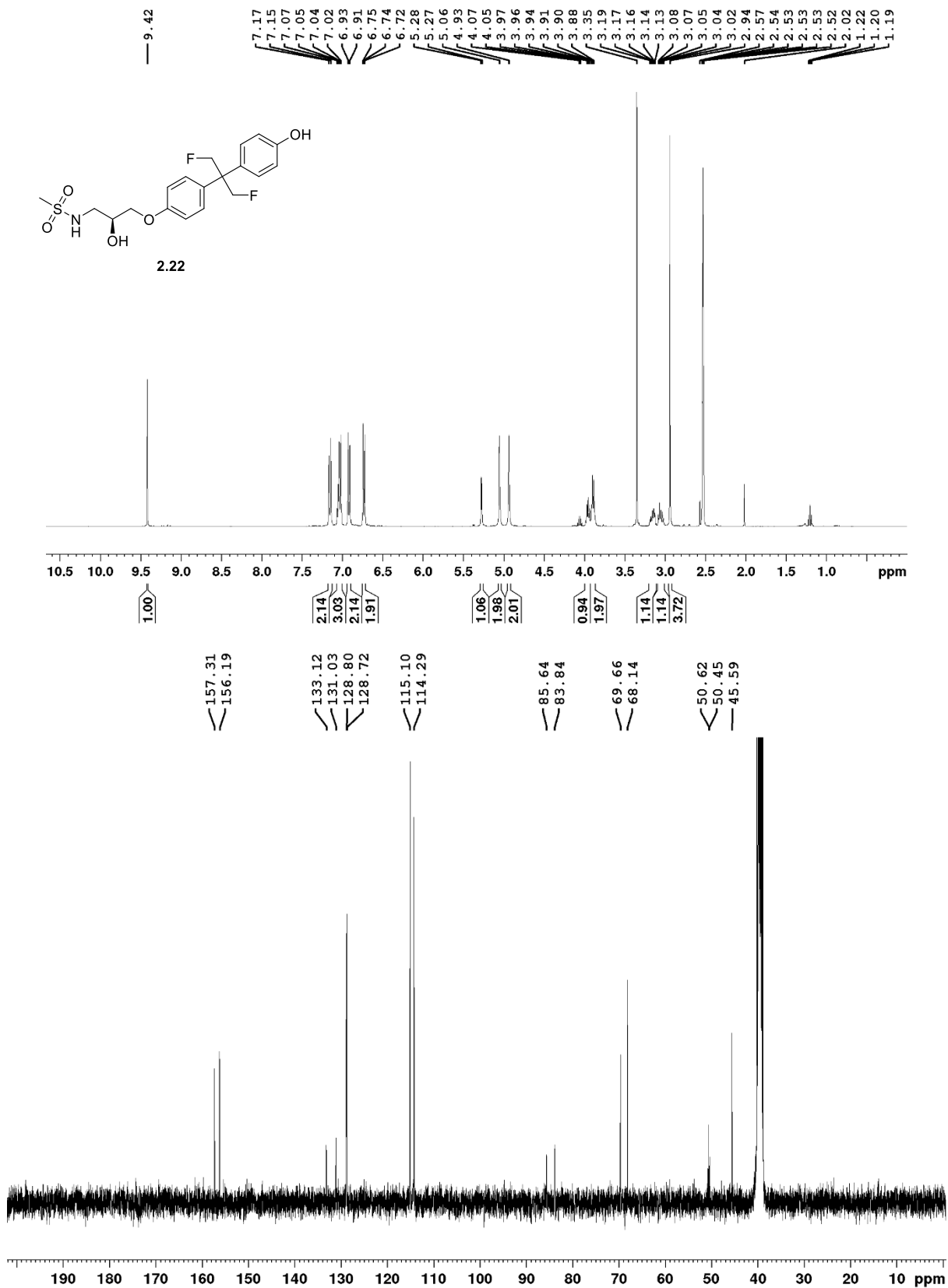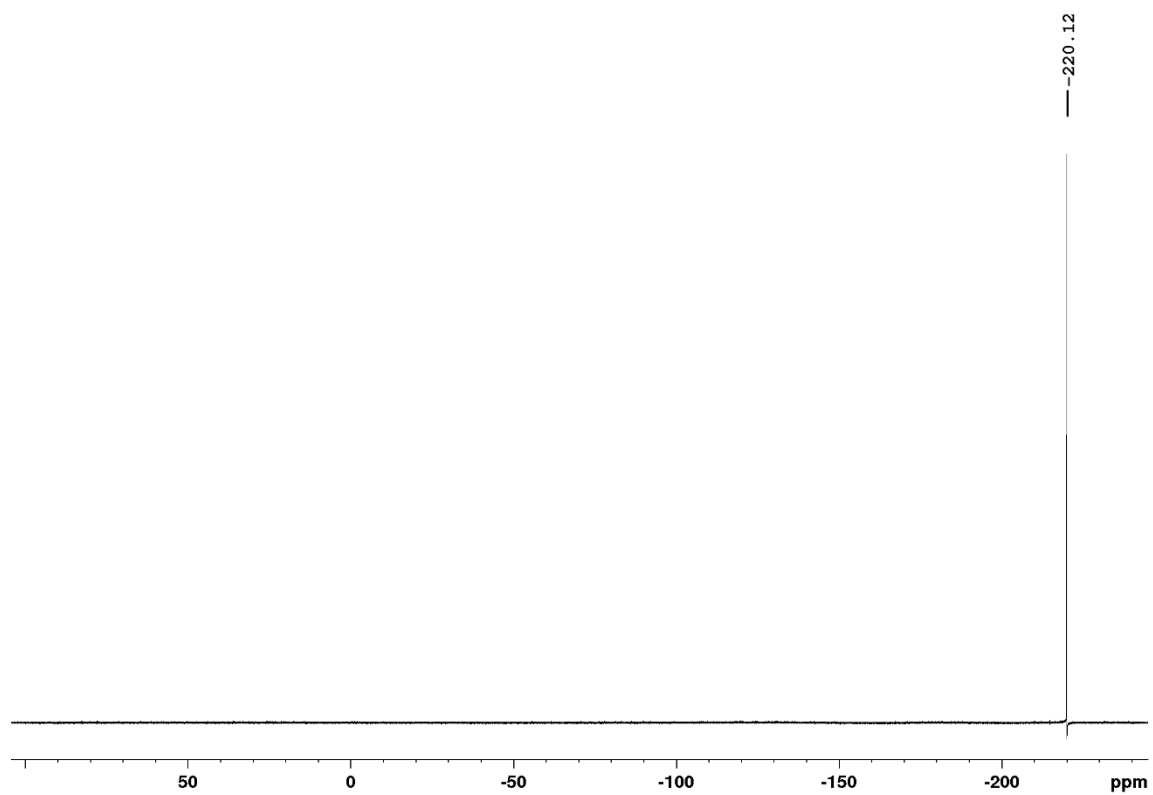
Figure A.4 – ^{1}H, ^{13}C, and ^{19}F NMR Spectra of **2.22** recorded in DMSO-d_6 at 400 MHz and 100 MHz, and 300 MHz respectively

2.23

Figure A.5 – ¹H, ¹³C, and ¹⁹F NMR Spectra of **2.23** recorded in DMSO-d₆ at 400 MHz and 100 MHz, and 300 MHz respectively
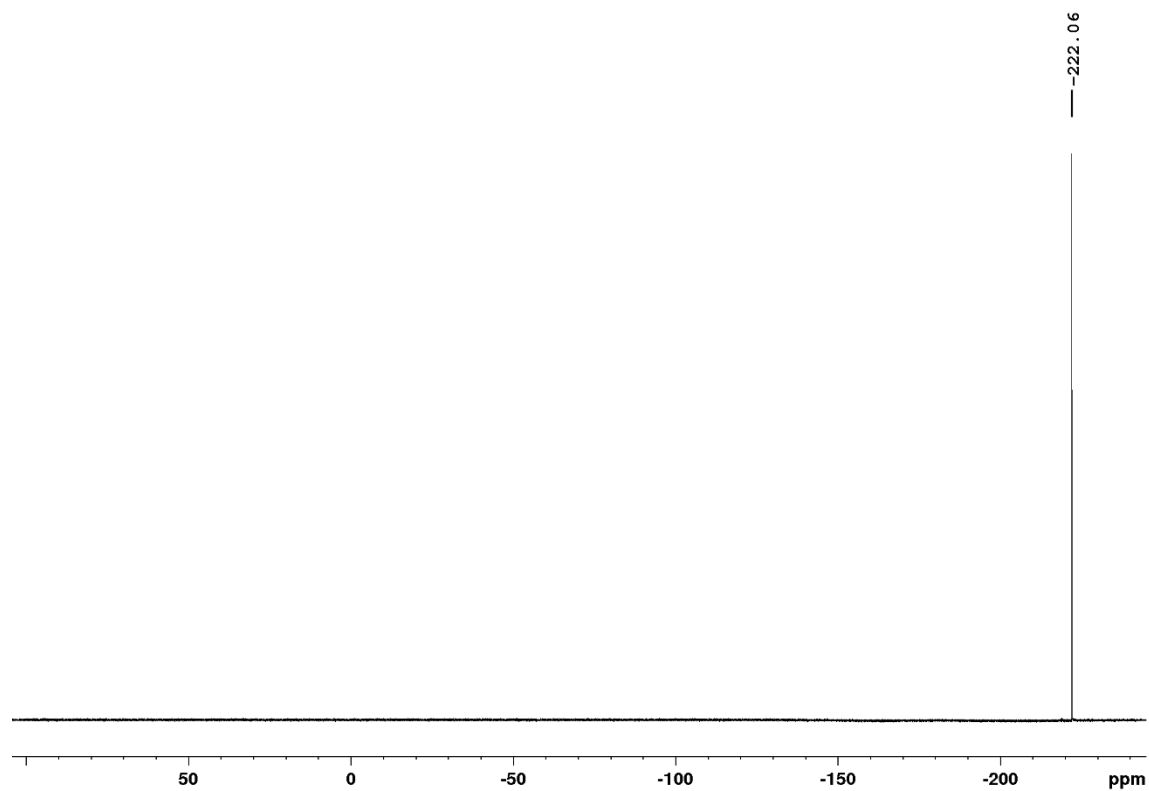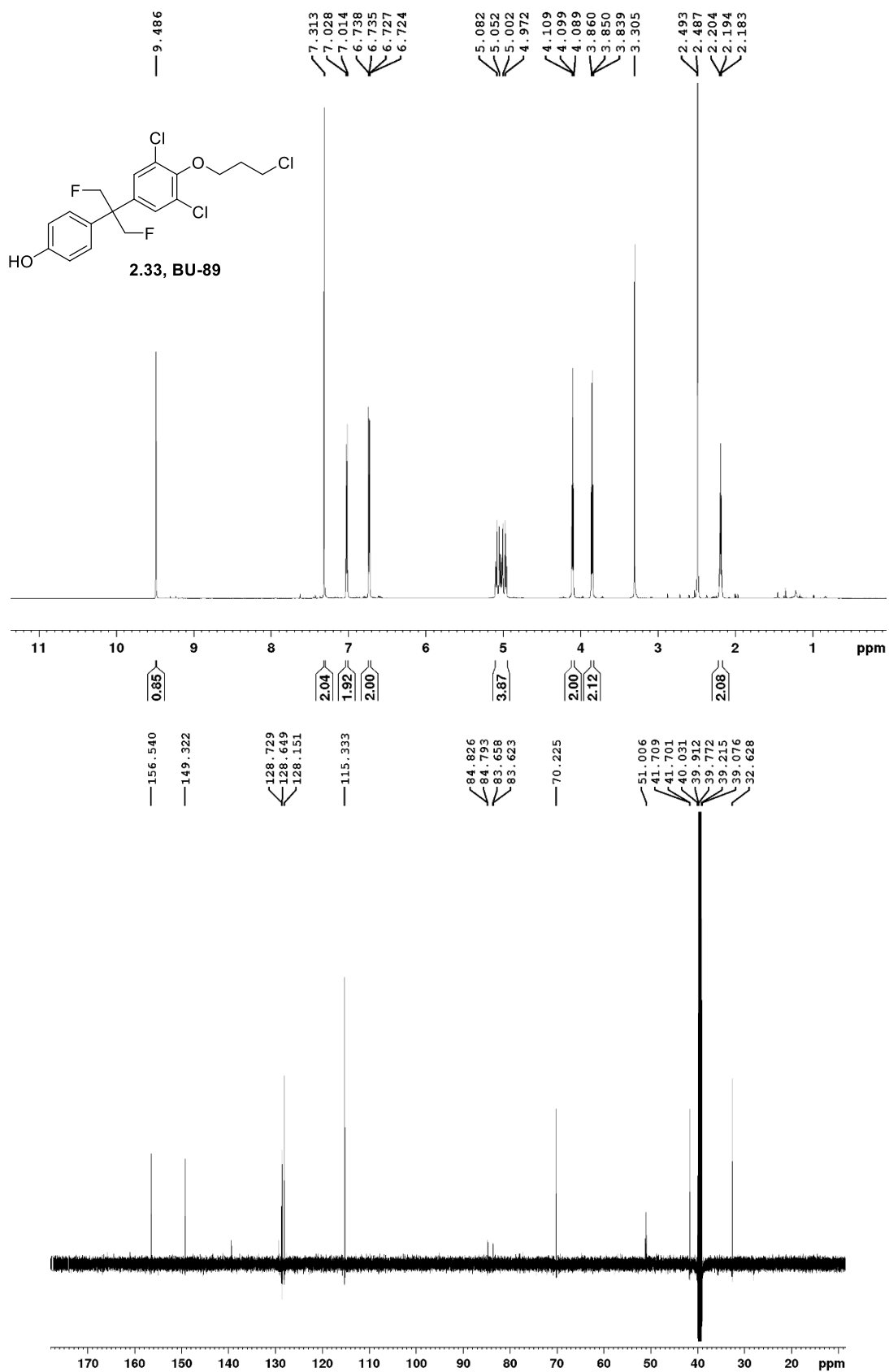
2.24, BU-86
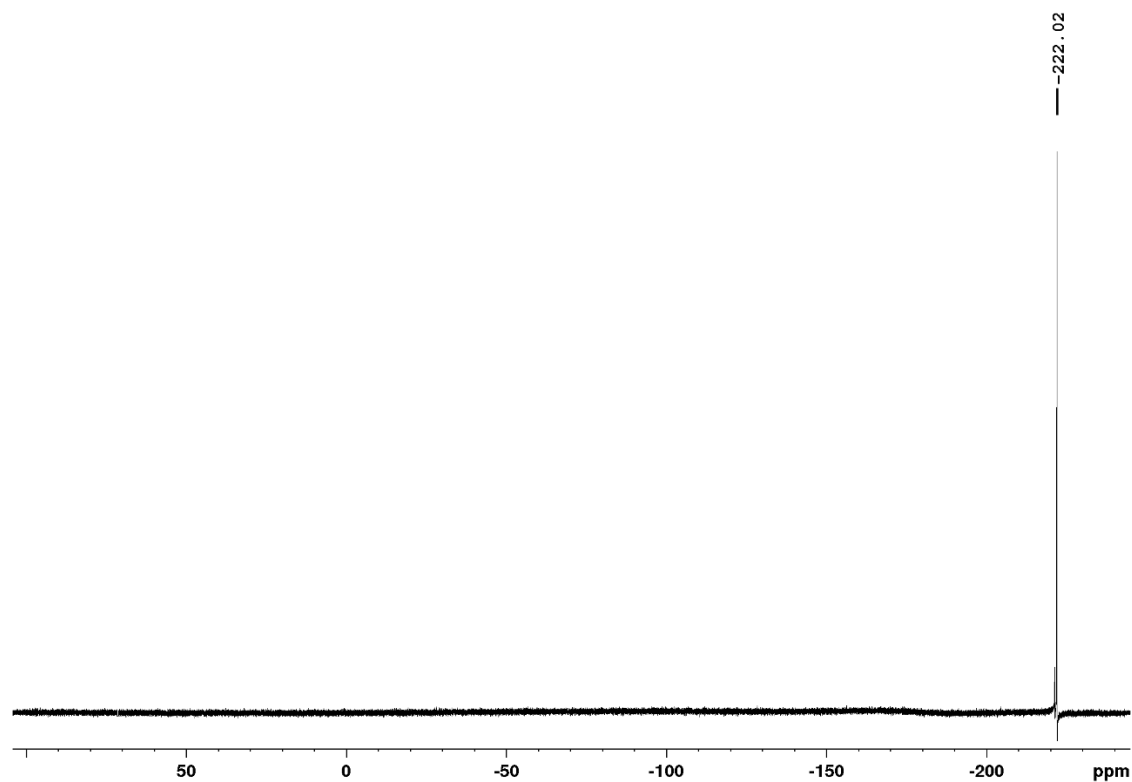
Figure A.6 – ^{1}H, ^{13}C, and ^{19}F NMR Spectra of **2.24** recorded in DMSO-d$_6$ at 400 MHz and 100 MHz, and 300 MHz respectively

2.25, BU-87
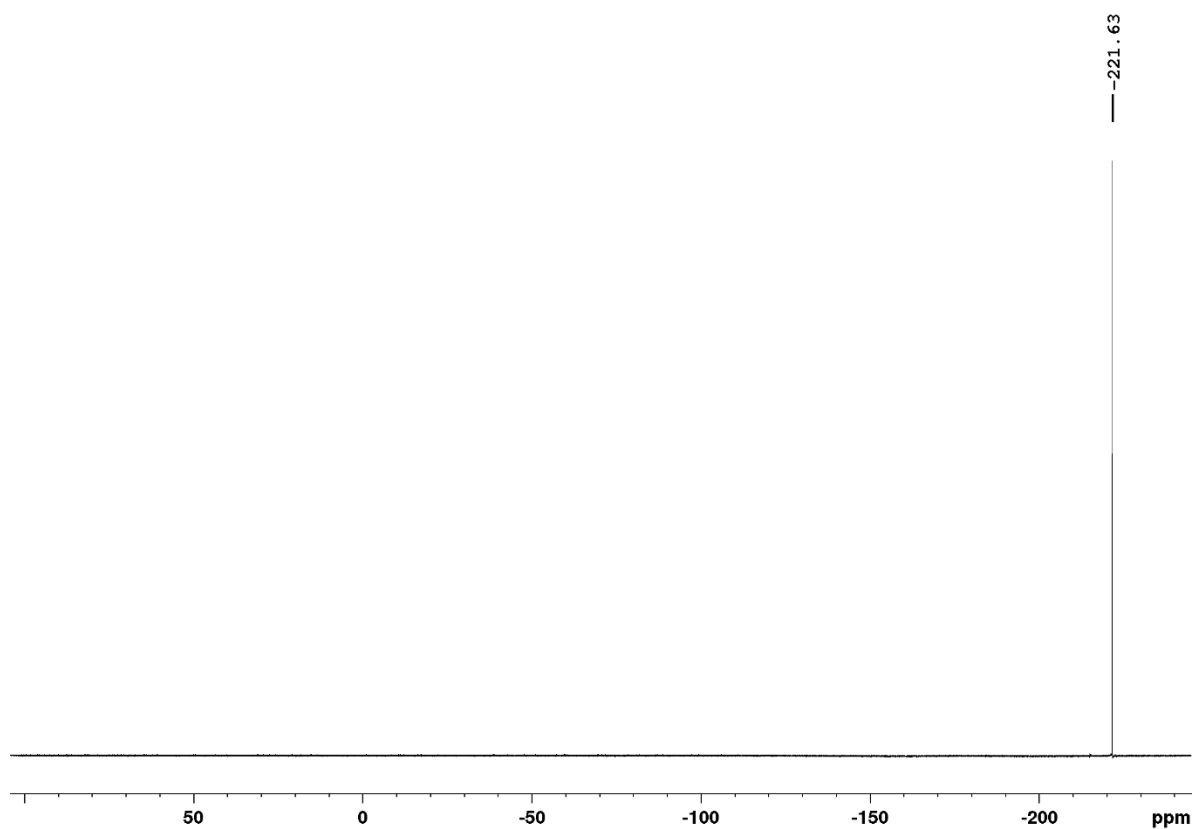
7.321, 7.159, 7.144, 7.020, 7.010, 7.000, 6.930, 6.916, 5.243, 5.235, 5.133, 5.117, 5.089, 5.073, 5.053, 5.037, 5.009, 4.993, 4.111, 4.101, 4.091, 3.944, 3.935, 3.928, 3.887, 3.878, 3.861, 3.850, 3.840, 3.302, 3.131, 3.122, 3.120, 3.109, 3.100, 3.040, 3.030, 3.019, 3.008, 2.495, 2.493, 2.487, 2.484, 2.215, 2.205, 2.194, 2.184, 2.174

2.22, 1.97, 0.99, 2.00, 1.05, 1.86, 1.89, 2.12, 0.83, 4.56, 0.74, 0.76, 3.54, 2.03

157.662, 149.394, 139.231, 131.299, 128.816, 128.666, 128.199, 114.562, 84.727, 83.588, 70.240, 69.646, 68.096, 51.086, 45.544, 41.707, 40.032, 32.627

Figure A.7 – ^{1}H, ^{13}C, and ^{19}F NMR Spectra of **2.25** recorded in DMSO-d$_6$ at 600 MHz and 150 MHz, and 300 MHz respectively

2.26, BU-88
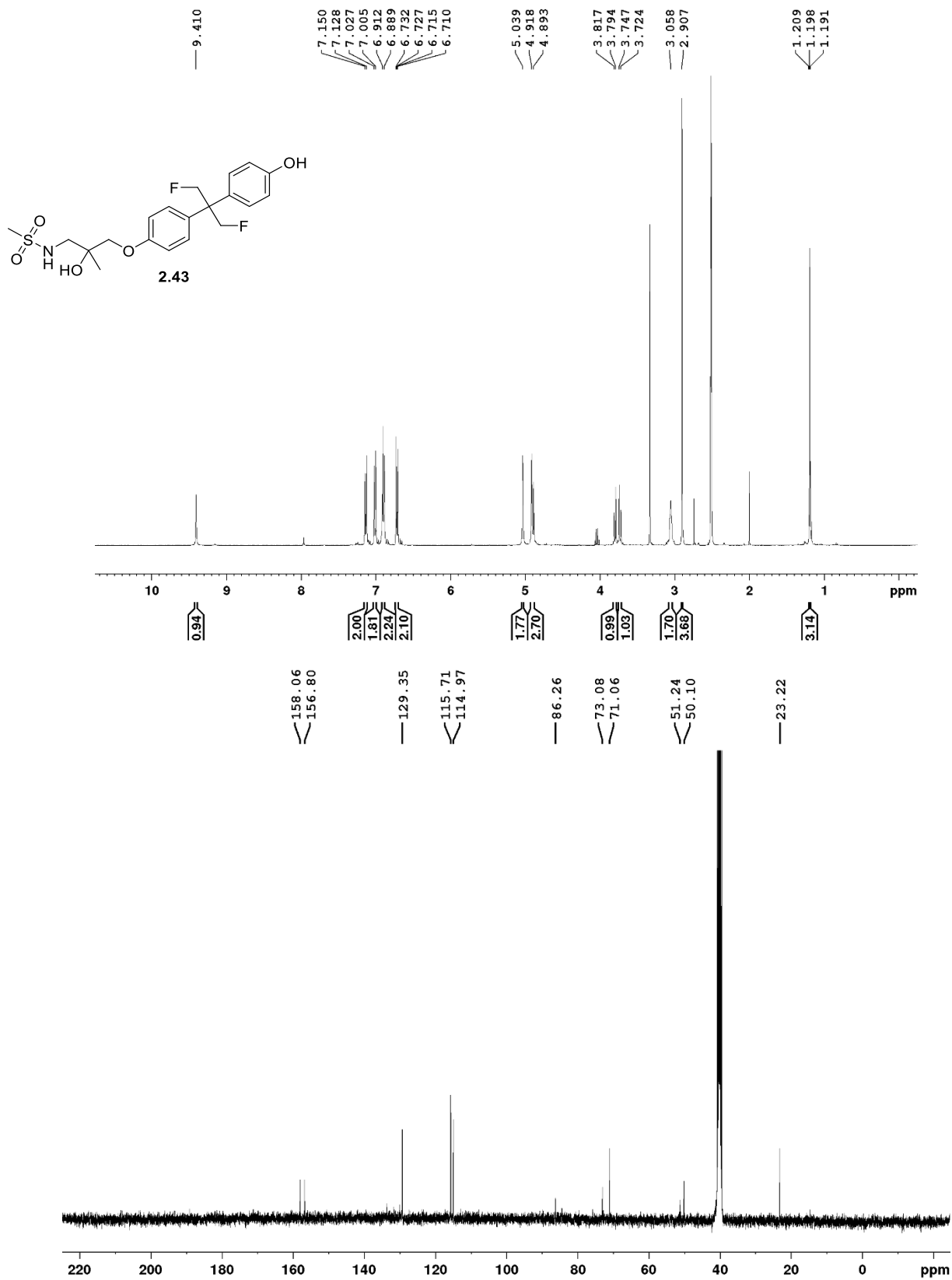
1H NMR peaks (ppm): 7.439, 7.430, 7.420, 7.327, 7.155, 7.140, 6.912, 6.897, 5.137, 5.121, 5.097, 5.081, 5.058, 5.042, 5.017, 5.001, 4.932, 4.112, 4.102, 4.092, 4.083, 3.861, 3.850, 3.839, 3.324, 2.529, 2.493, 2.490, 2.487, 2.205, 2.194, 2.184, 1.976

Integrations: 0.85, 2.00, 1.93, 1.99, 3.59, 1.96, 4.04, 1.96, 2.94, 2.06

13C NMR peaks (ppm): 202.101, 156.801, 149.429, 139.134, 131.824, 128.807, 128.668, 128.231, 114.576, 84.729, 83.562, 70.412, 70.250, 51.214, 51.099, 50.983, 49.048, 41.712, 40.125, 40.038, 39.916, 39.082, 32.637

—222.14

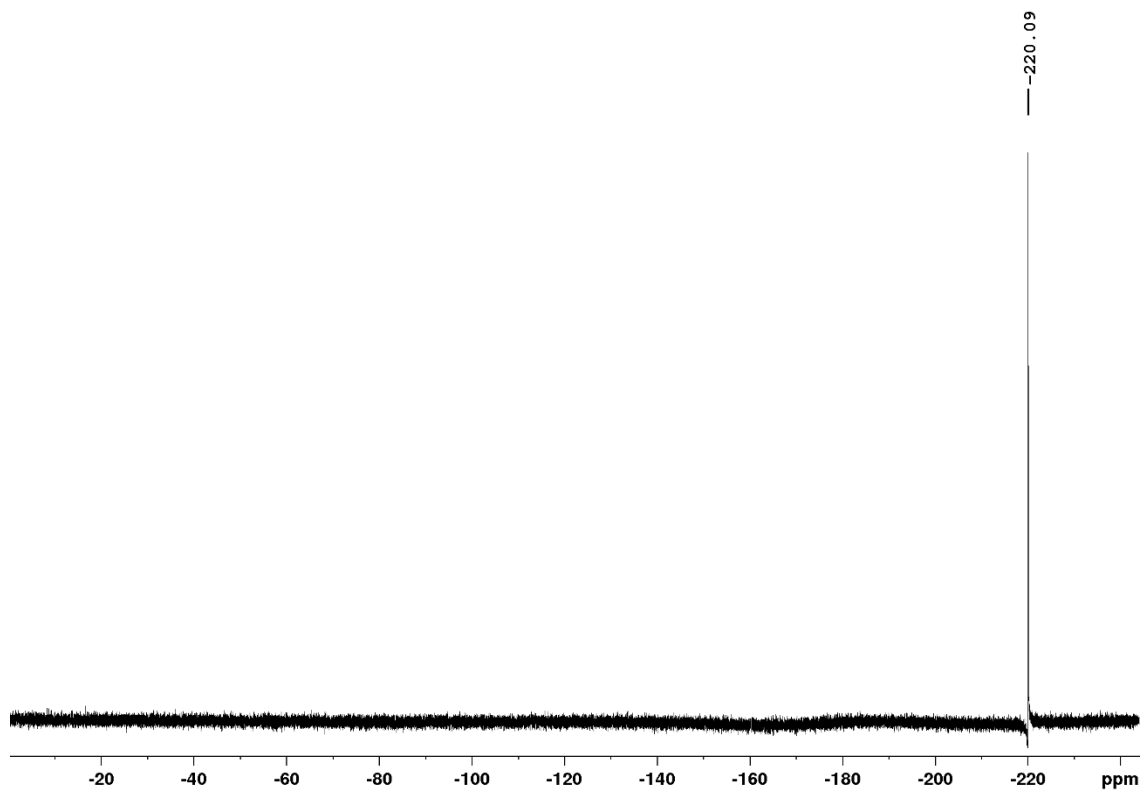|													
20	0	-20	-40	-60	-80	-100	-120	-140	-160	-180	-200	-220	ppm

Figure A.8 – ^{1}H, ^{13}C, and ^{19}F NMR Spectra of **2.26** recorded in DMSO-d$_6$ at 600 MHz and 150 MHz, and 300 MHz respectively
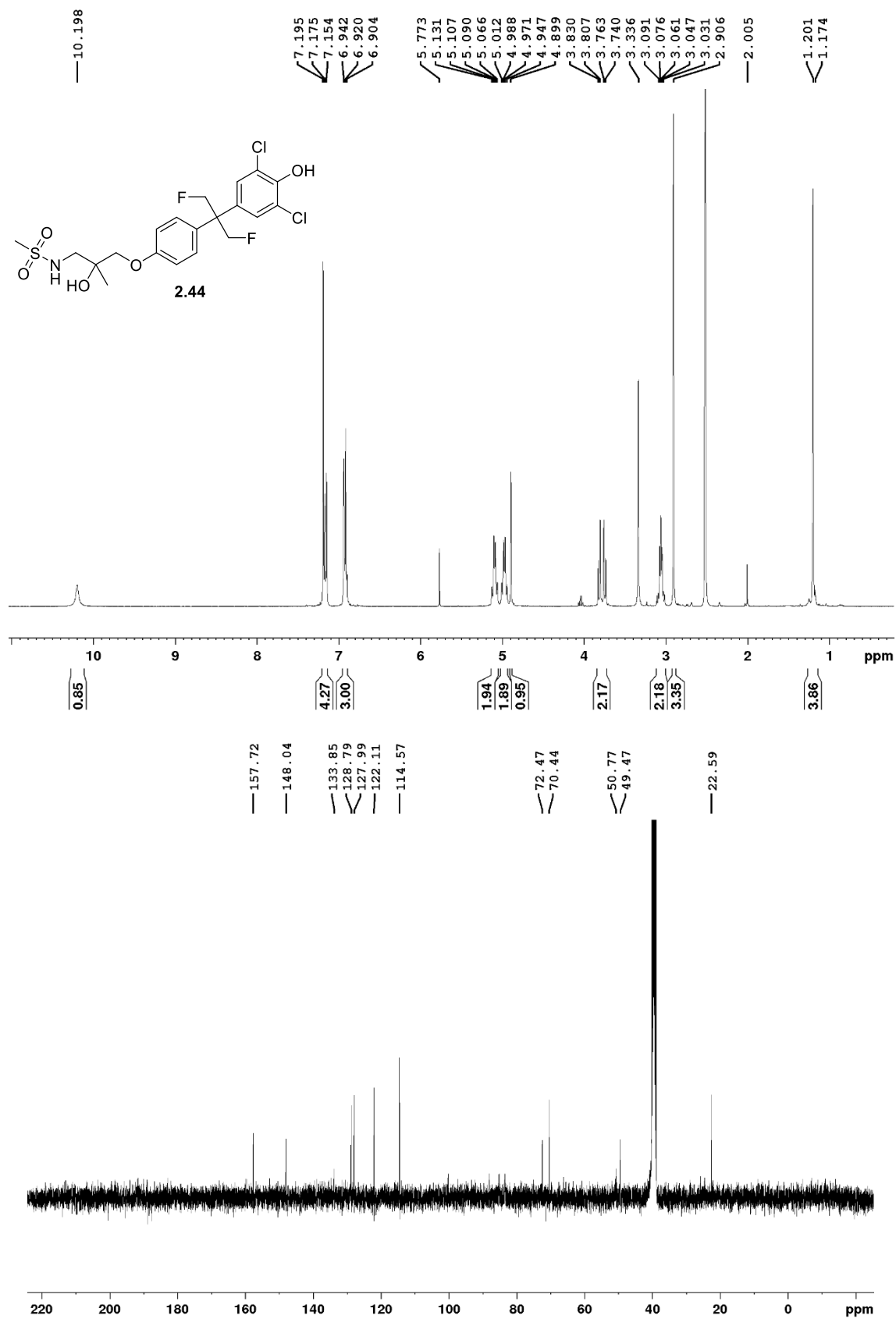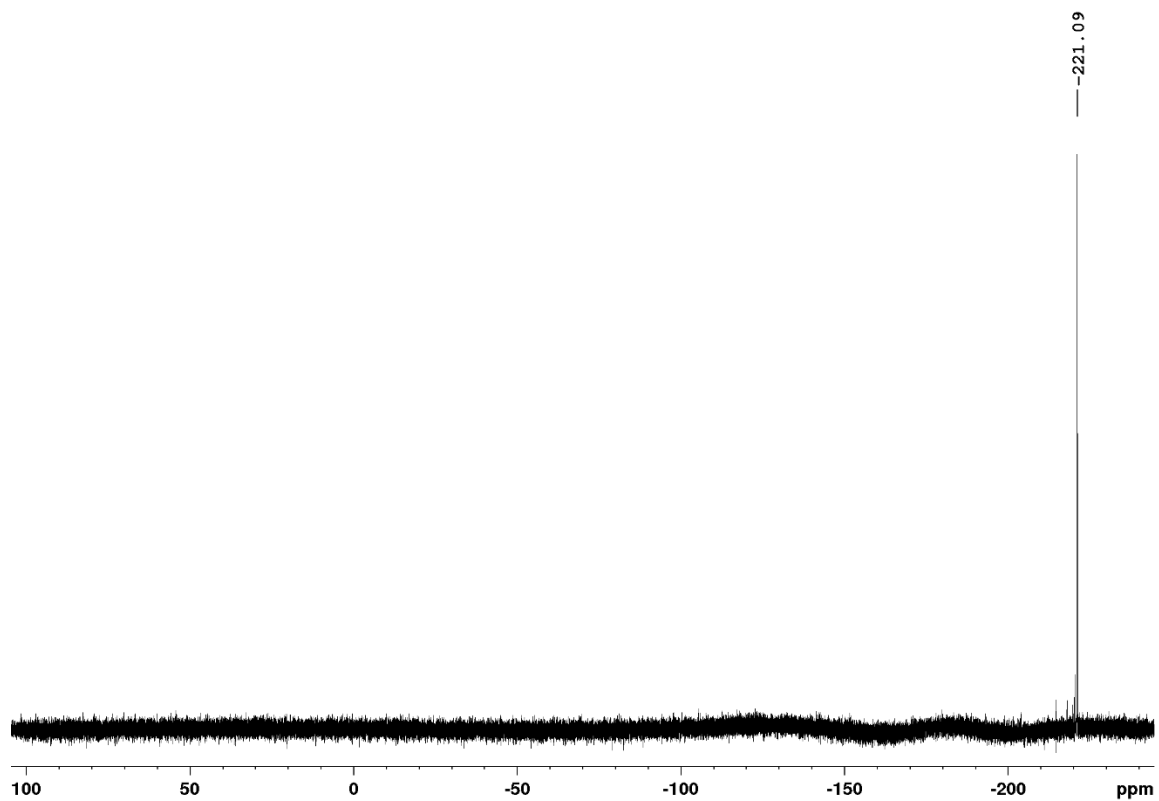
2.13

9.42

7.48 7.46 7.44 7.42 7.40 7.37 7.36 7.35 7.34 7.17 7.15 7.04 7.02 7.01 6.98 6.75 6.73

5.10 5.06 4.94

3.35

2.57 2.54 2.53 2.53

1.00

5.85 1.95 4.04 2.09

2.01 1.77 1.72

157.12 156.19

137.06 128.83 128.71 128.42 127.82 127.68

115.10 114.52

69.14

40.15 38.90

135

Figure A.9 – ^{1}H, ^{13}C, and ^{19}F NMR Spectra of **2.13** recorded in DMSO-d$_6$ at 400 MHz and 100 MHz, and 300 MHz respectively

137

—221.48

50	0	-50	-100	-150	-200	ppm
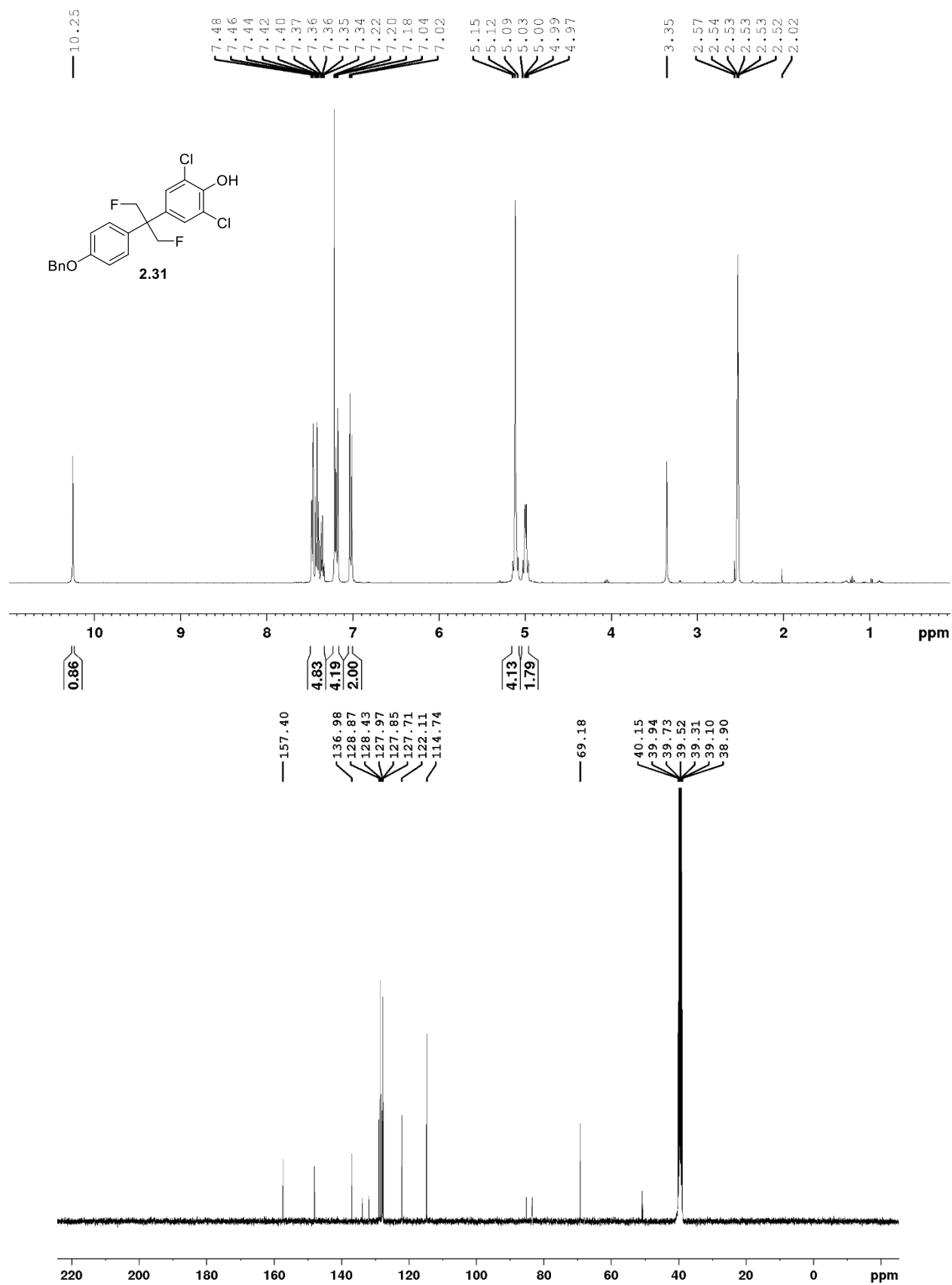
Figure A.10 – ^{1}H, ^{13}C, and ^{19}F NMR Spectra of **2.31** recorded in DMSO-d$_6$ at 400 MHz and 100 MHz, and 300 MHz respectively

2.32

139

−222.06

Figure A.11 – ^{1}H, ^{13}C, and ^{19}F NMR Spectra of **2.32** recorded in DMSO-d$_6$ at 400 MHz and 100 MHz, and 300 MHz respectively

2.33, BU-89

9.486

7.313
7.028
7.014
6.738
6.735
6.727
6.724

5.082
5.052
5.002
4.972

4.109
4.099
4.089
3.860
3.850
3.839

3.305

2.493
2.487
2.204
2.194
2.183

11 10 9 8 7 6 5 4 3 2 1 ppm

0.85

2.04
1.92
2.00

3.87

2.00
2.12

2.08

156.540
149.322

128.729
128.649
128.151

115.333

84.826
84.793
83.658
83.623

70.225

51.006
41.709
41.701
40.031
39.912
39.772
39.215
39.076
32.628

170 160 150 140 130 120 110 100 90 80 70 60 50 40 30 20 ppm

141

Figure A.11 – ^{1}H, ^{13}C, and ^{19}F NMR Spectra of **2.33** recorded in DMSO-d$_6$ at 600 MHz and 150 MHz, and 300 MHz respectively
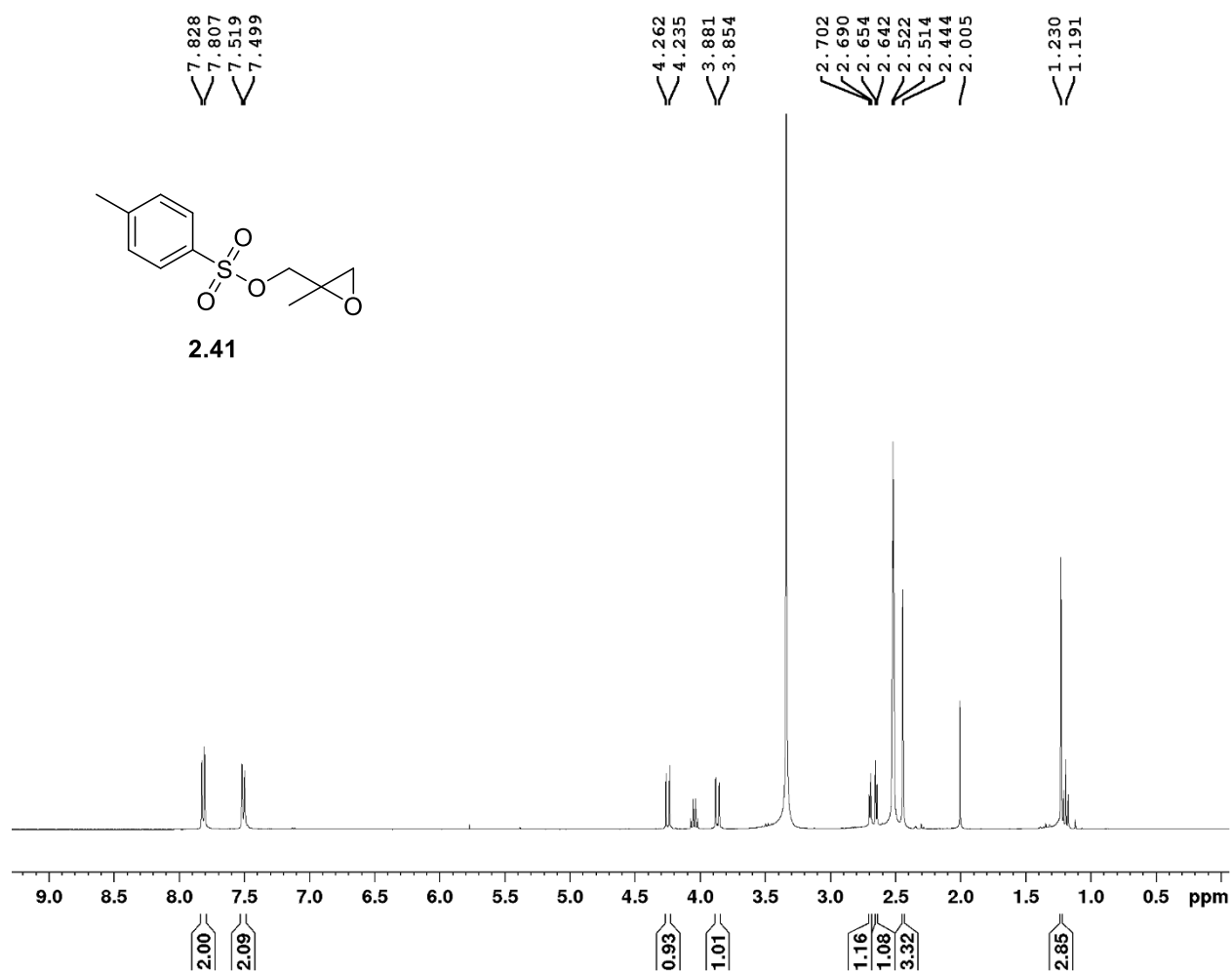
**Figure A.12** – ^{1}H NMR Spectra of **2.41** recorded in DMSO-d$_6$ at 400 MHz

144
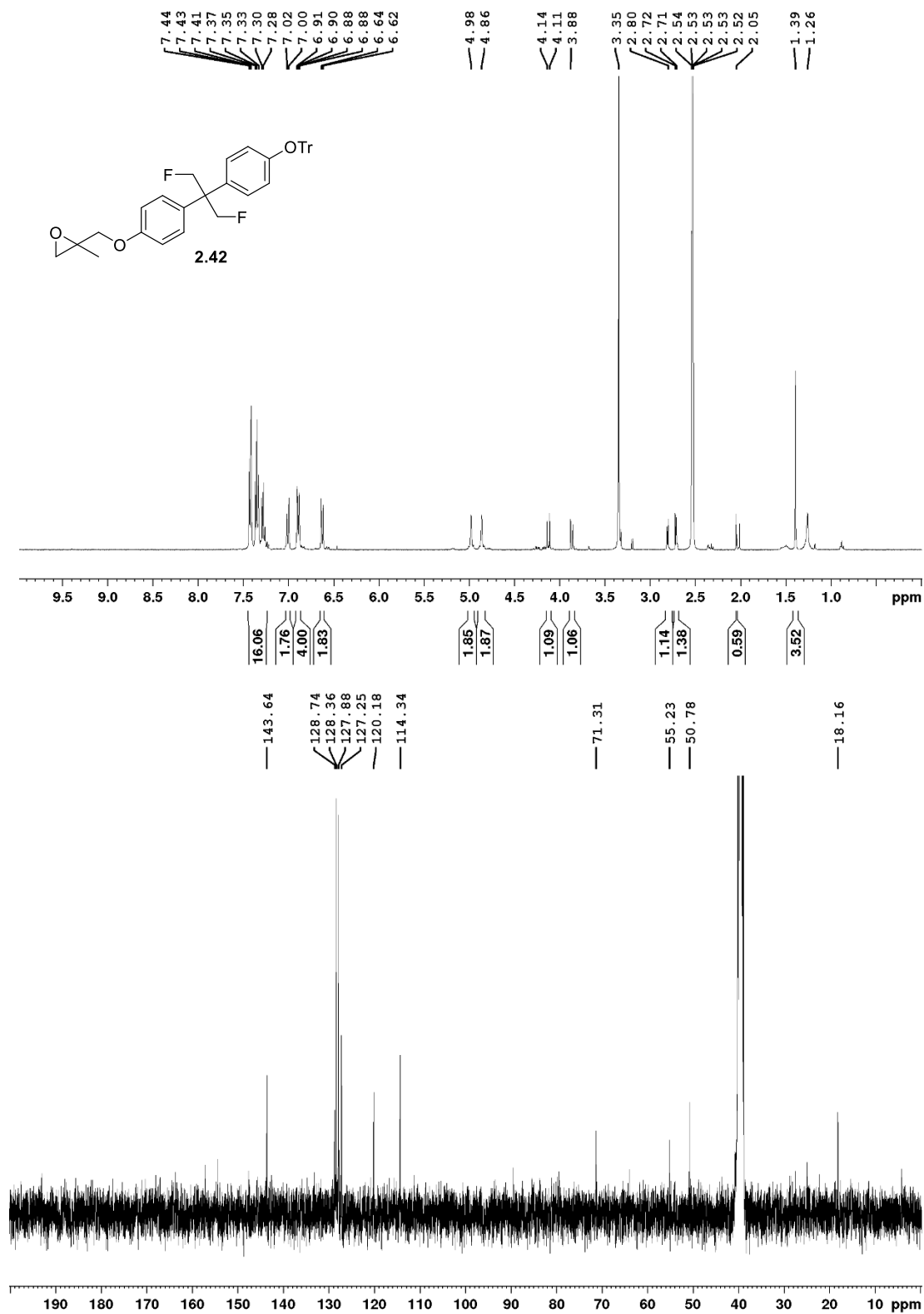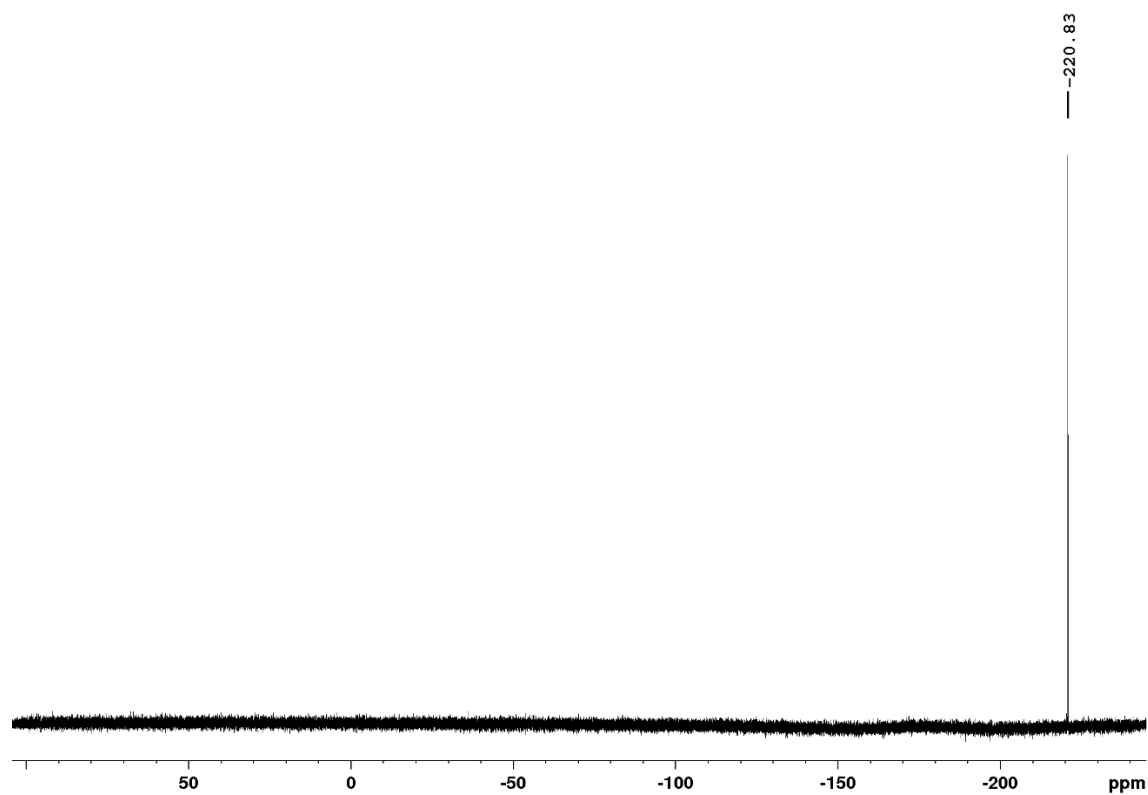
Figure A.13 – ^{1}H, ^{13}C, and ^{19}F NMR Spectra of **2.42** recorded in DMSO-d$_6$ at 400 MHz and 100 MHz, and 300 MHz respectively

2.43

9.410

7.150
7.128
7.027
7.005
6.912
6.889
6.732
6.727
6.715
6.710

5.039
4.918
4.893

3.817
3.794
3.747
3.724

3.058
2.907

1.209
1.198
1.191

0.94

2.00
1.81
2.24
2.10

1.77
2.70

0.99
1.03

1.70
3.68

3.14

158.06
156.80

129.35

115.71
114.97

86.26

73.08
71.06

51.24
50.10

23.22

10   9   8   7   6   5   4   3   2   1   ppm

220   200   180   160   140   120   100   80   60   40   20   0   ppm

146

Figure A.13 – ^{1}H, ^{13}C, and ^{19}F NMR Spectra of **2.43** recorded in DMSO-d$_6$ at 400 MHz and 100 MHz, and 300 MHz respectively

2.44

10.198

7.195
7.175
7.154
6.942
6.920
6.904

5.773
5.131
5.107
5.090
5.066
5.012
4.988
4.971
4.947
4.899
3.830
3.807
3.763
3.740
3.336
3.091
3.076
3.061
3.047
3.031
2.906
2.005

1.201
1.174

0.85

4.27
3.00

1.94
1.89
0.95

2.17

2.18
3.35

3.86

157.72
148.04
133.85
128.79
127.99
122.11
114.57

72.47
70.44

50.77
49.47

22.59

148

Figure A.14 – ^{1}H, ^{13}C, and ^{19}F NMR Spectra of **2.44** recorded in DMSO-d$_6$ at 400 MHz and 100 MHz, and 300 MHz respectively

2.45
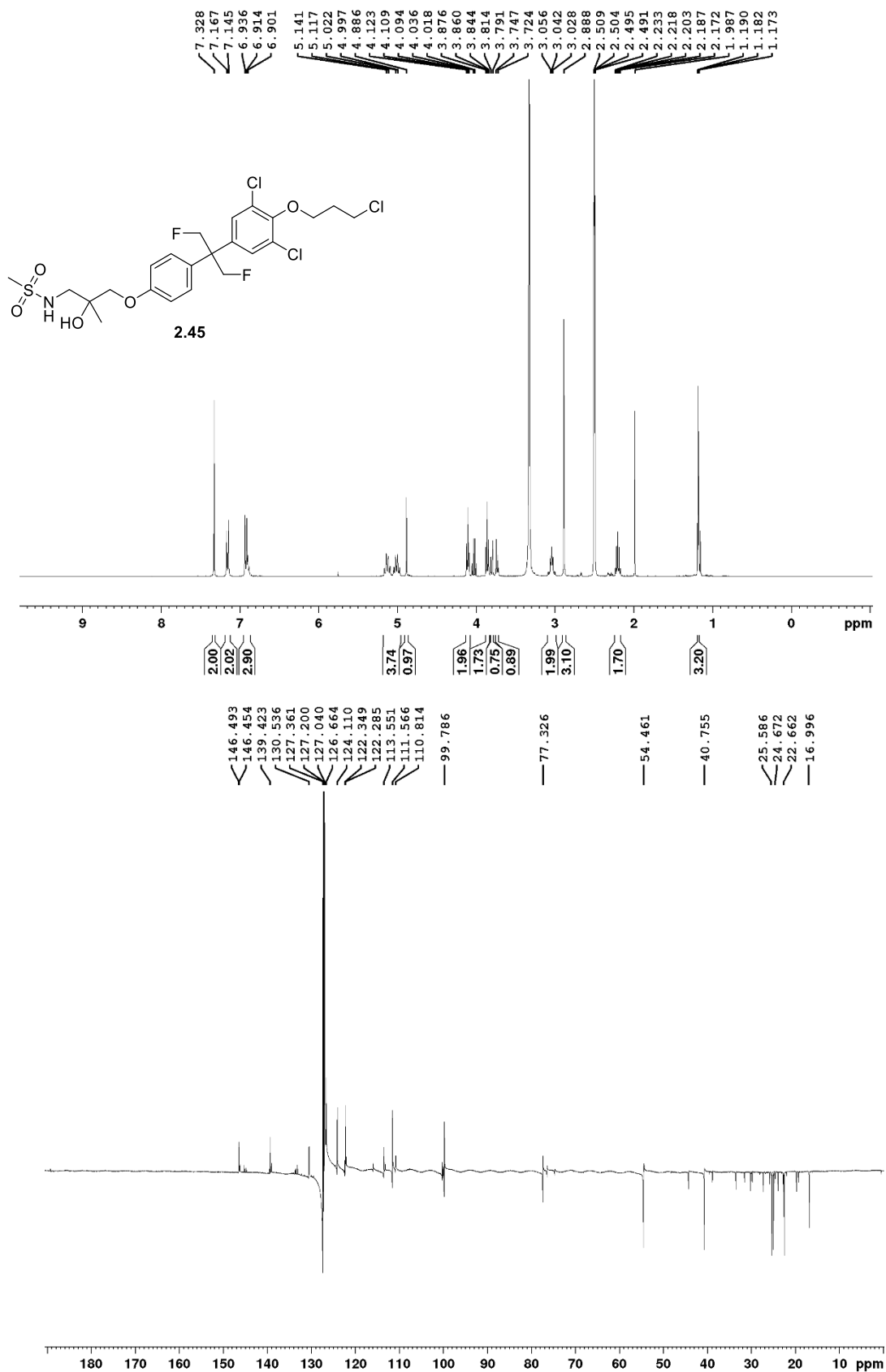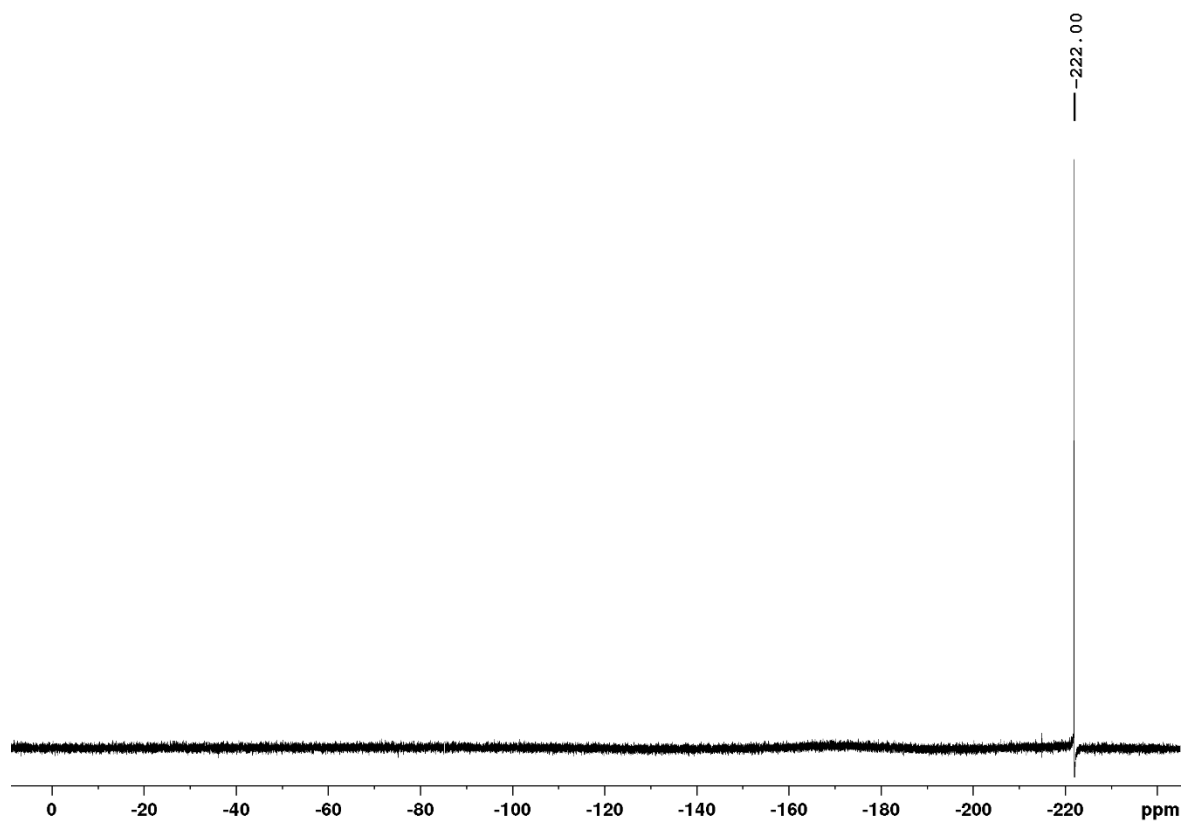
Figure A.15 – ^{1}H, ^{13}C, and ^{19}F NMR Spectra of **2.45** recorded in DMSO-d$_6$ at 600 MHz and 150 MHz, and 300 MHz respectively

2.46
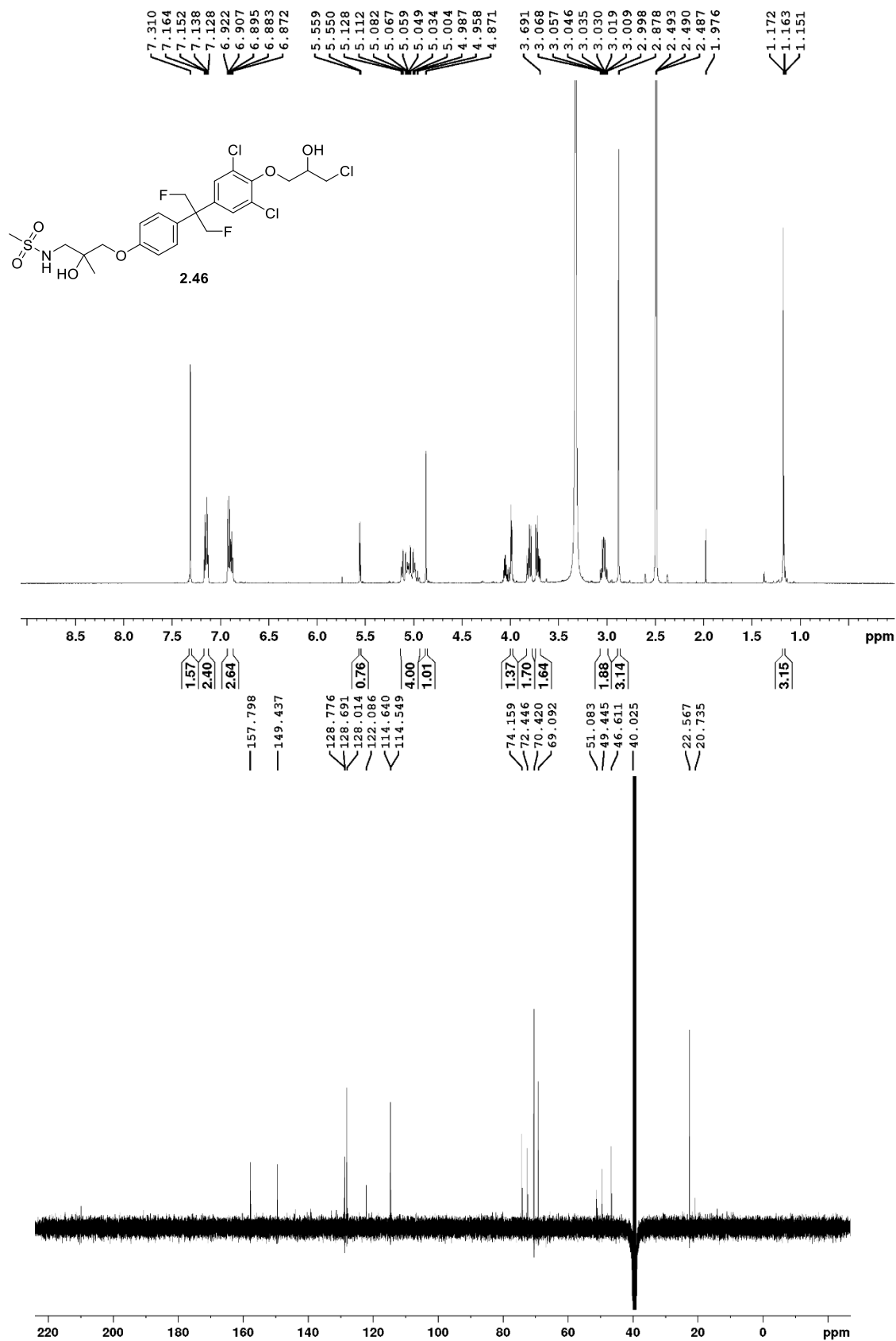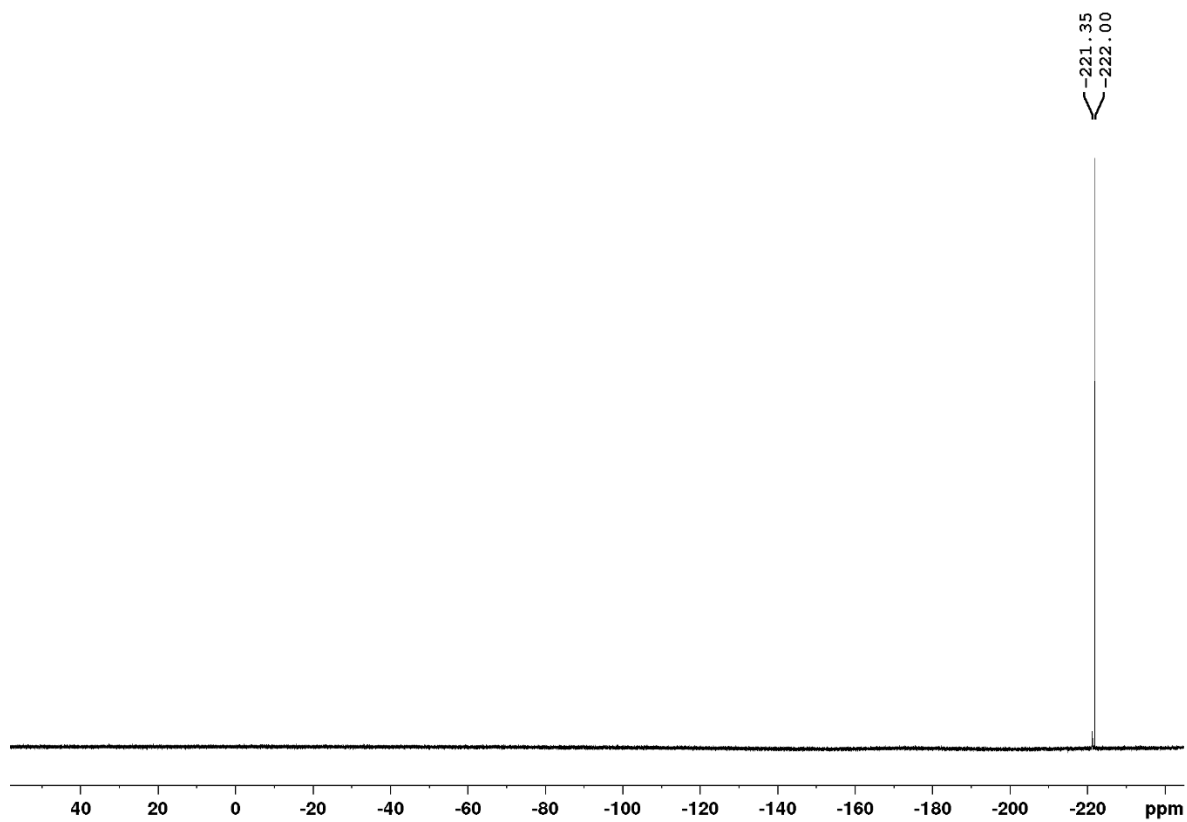
Figure A.16 – ^{1}H, ^{13}C, and ^{19}F NMR Spectra of **2.46** recorded in DMSO-d$_{6}$ at 600 MHz and 150 MHz, and 300 MHz respectively
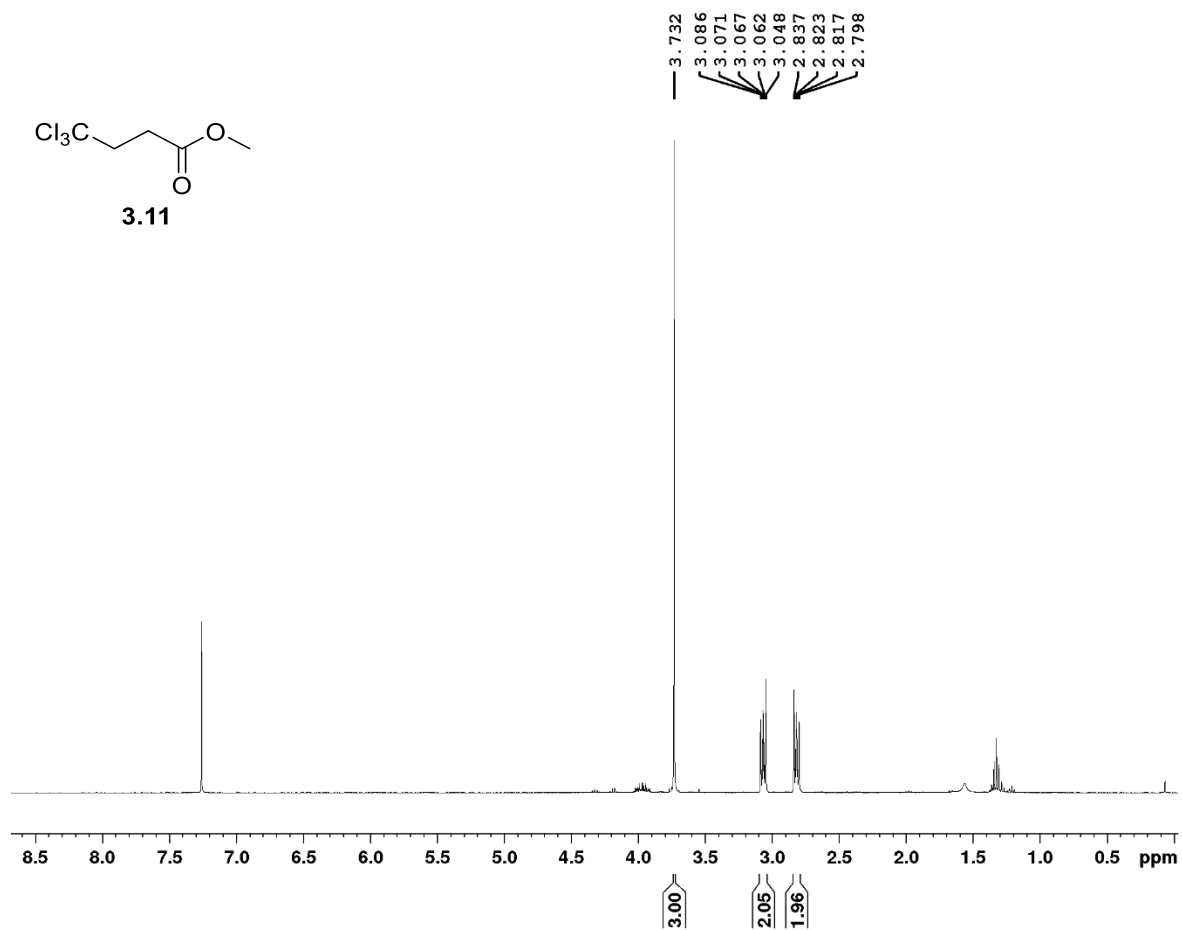
Figure A.17 – ^{1}H NMR of **3.11** recorded in CDCl$_3$ at 400 MHz
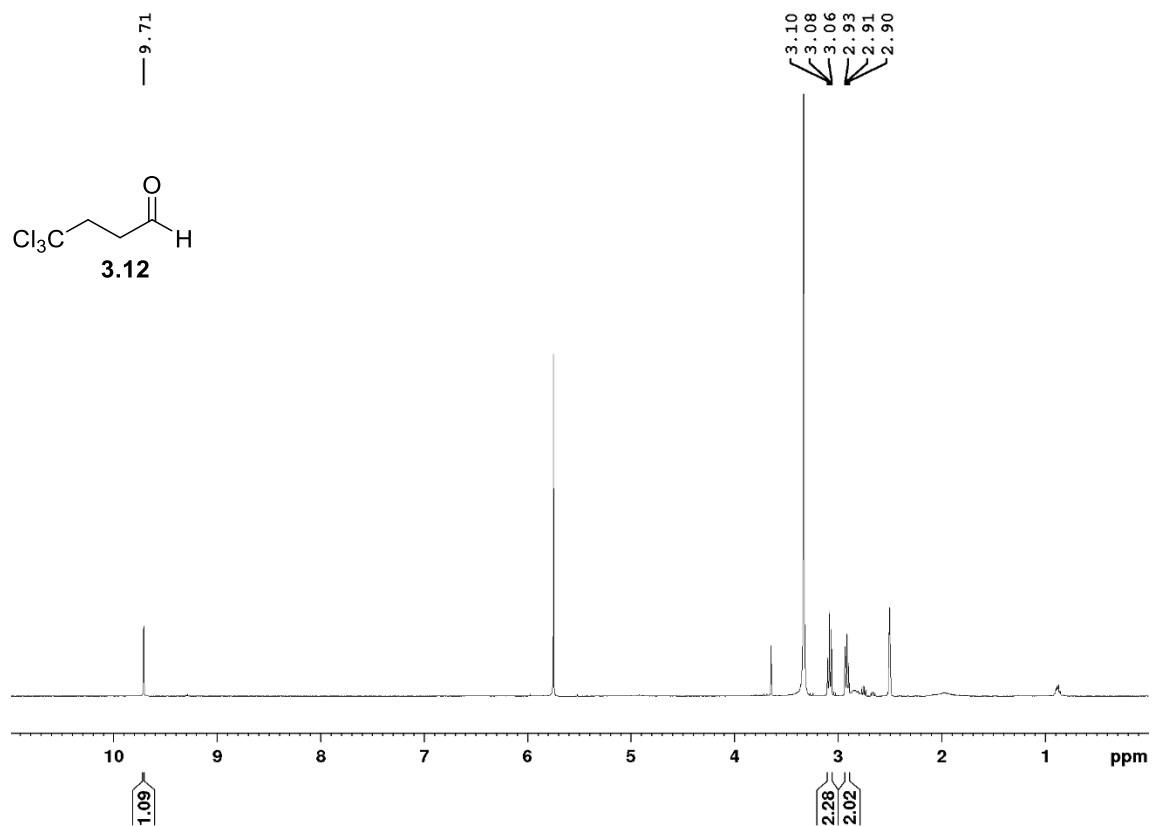
Figure A.18 – ^{1}H NMR of **3.12** recorded in DMSO-d$_6$ at 400 MHz
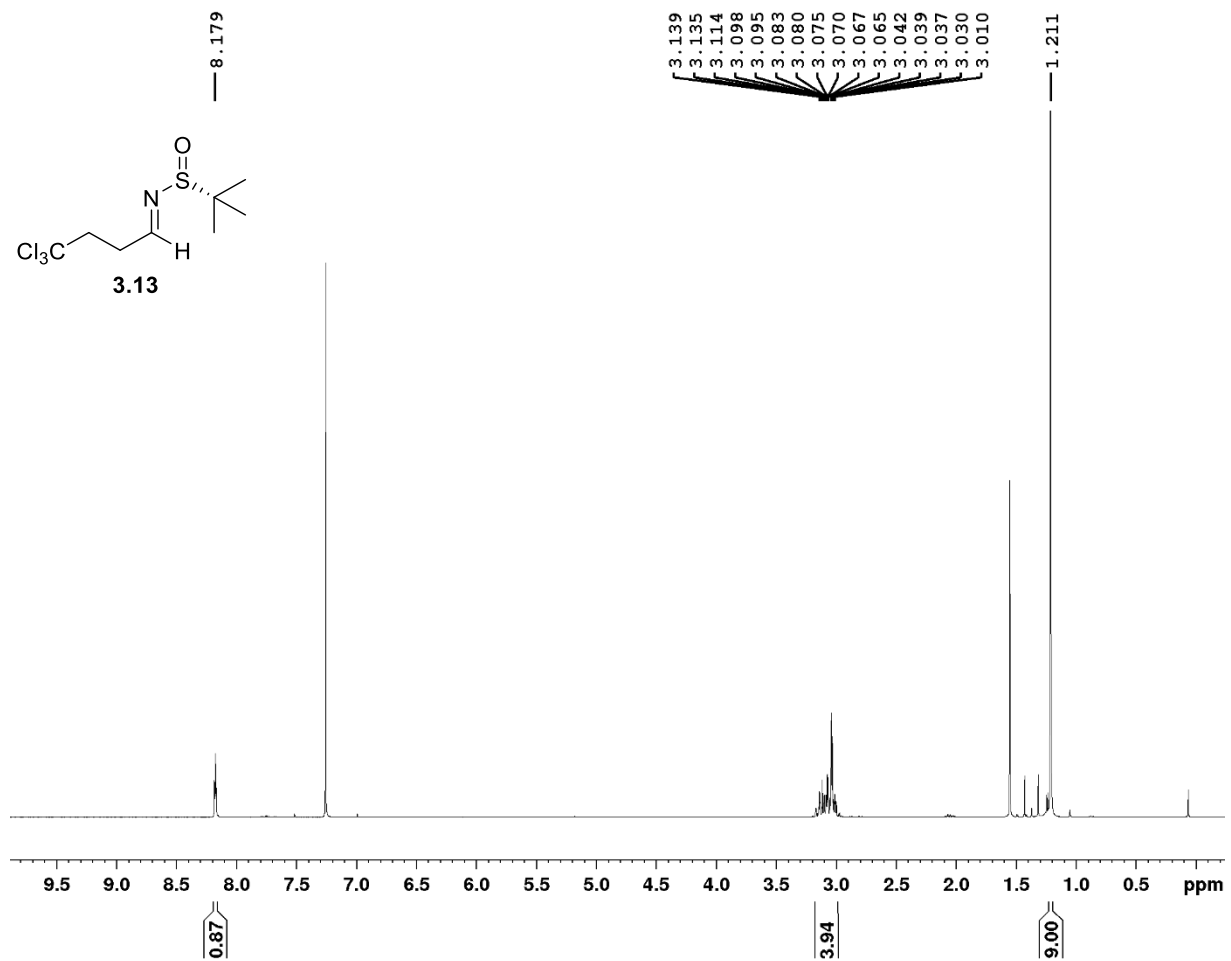
Figure A.19 – ^{1}H NMR of **3.13** recorded in CDCl$_3$ at 400 MHz
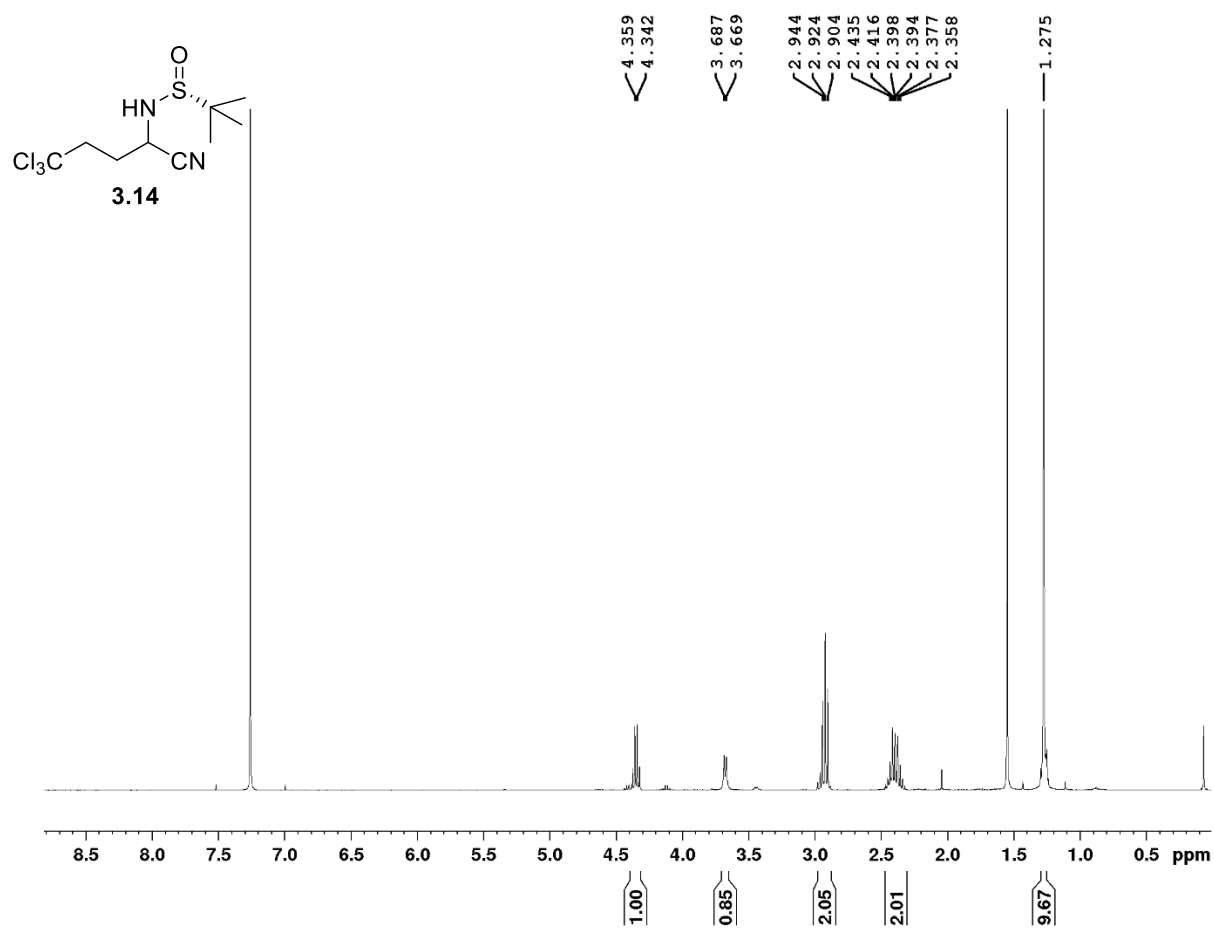
Figure A.20 – ^{1}H NMR of **3.14** recorded in CDCl$_3$ at 400 MHz
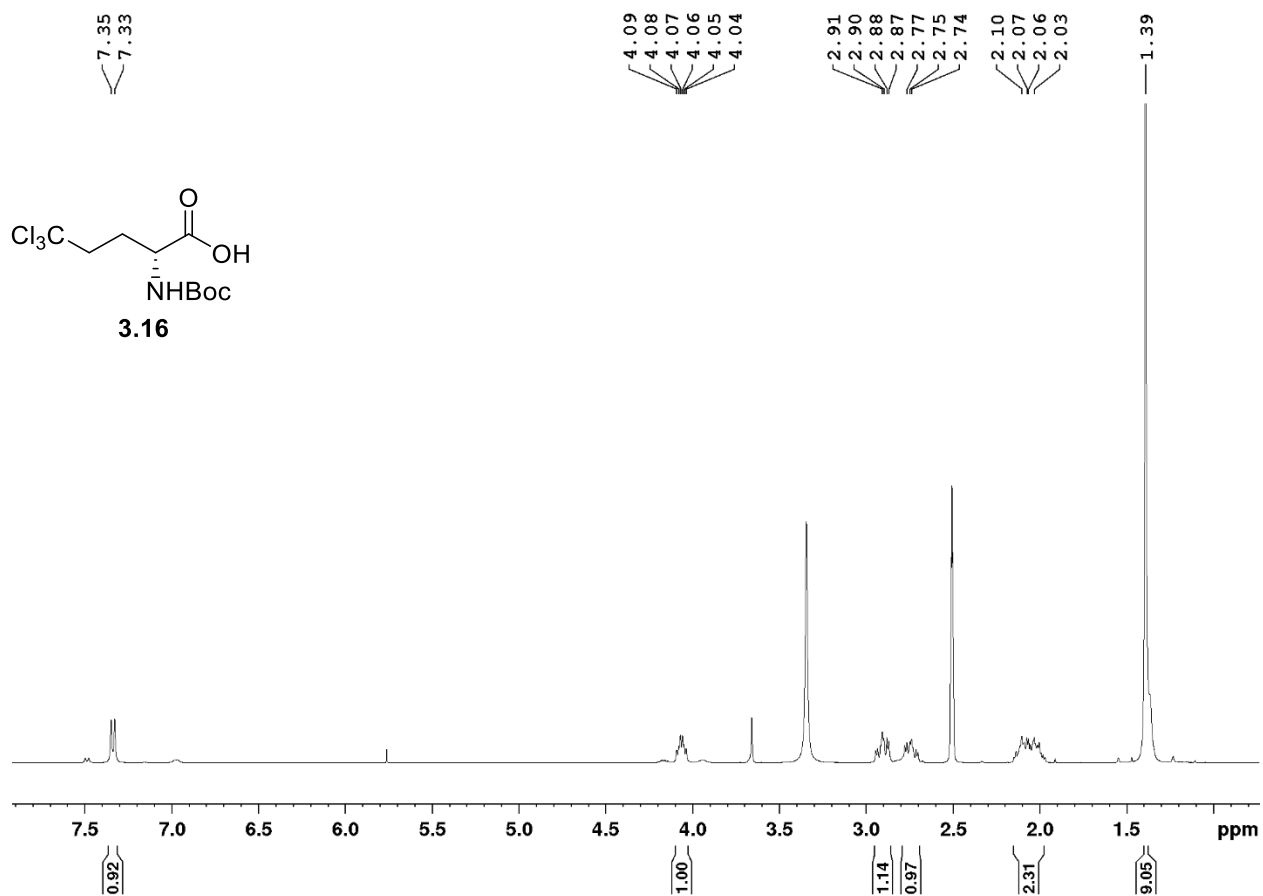
Figure A.21 – ^{1}H NMR of **3.16** recorded in DMSO-d$_6$ at 400 MHz
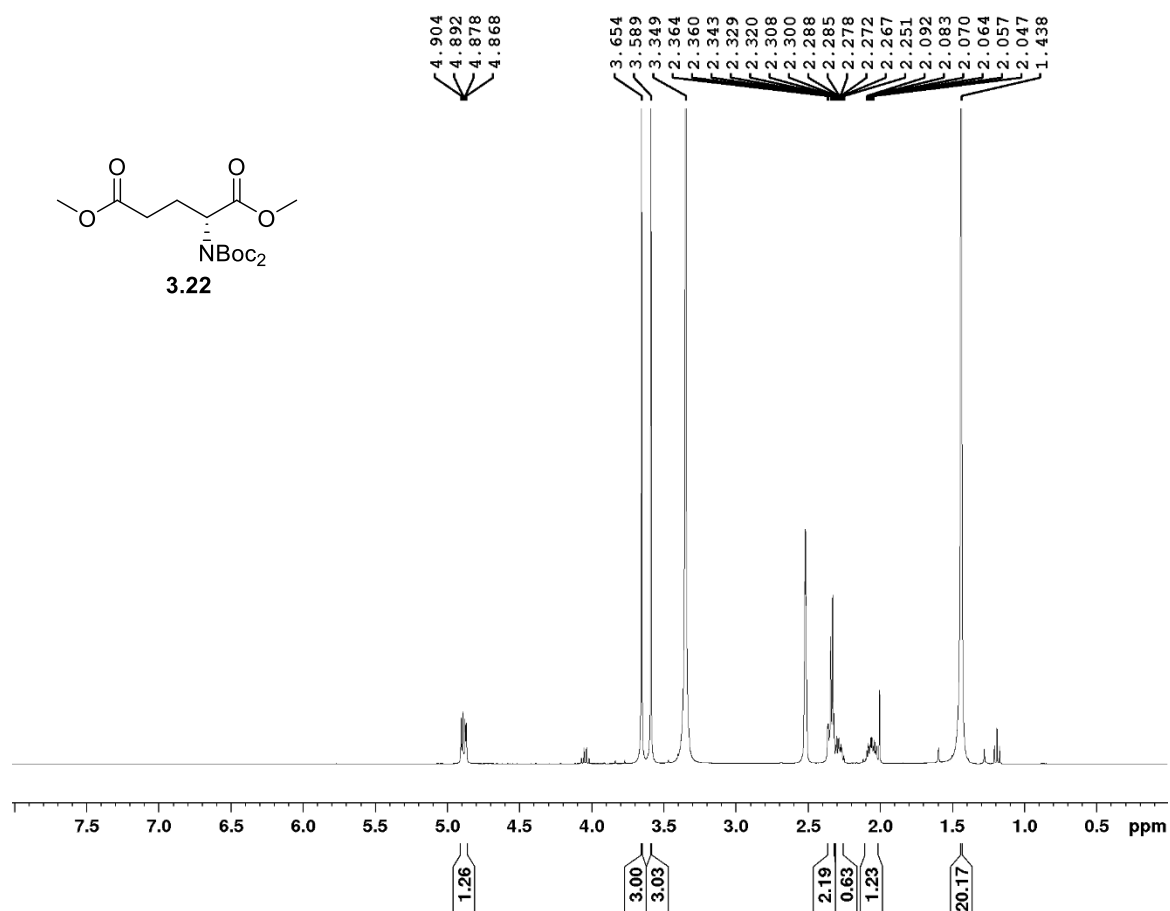
Figure A.22 – ^{1}H NMR of **3.22** recorded in DMSO-d$_6$ at 400 MHz
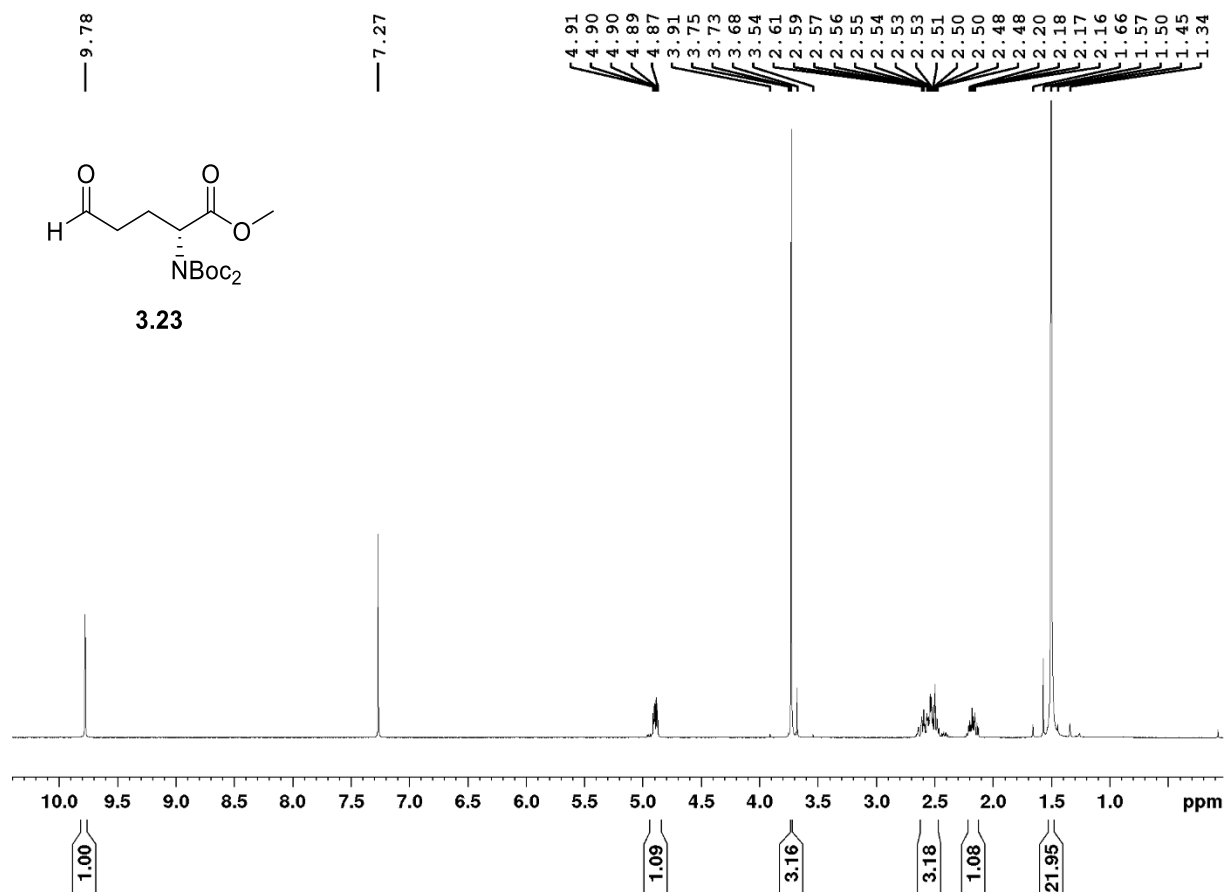
Figure A.23 – ^{1}H NMR of **3.23** recorded in CDCl$_3$ at 400 MHz
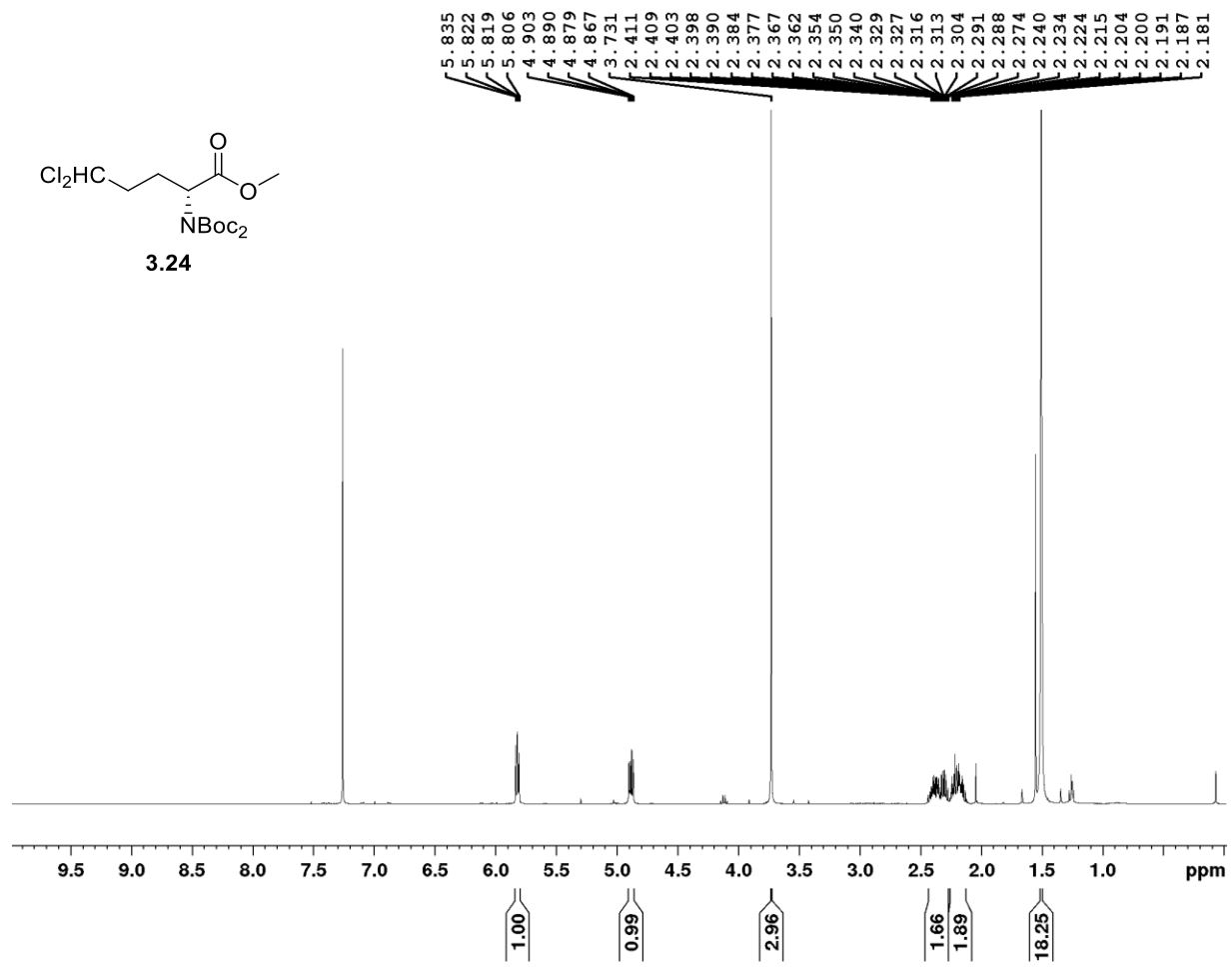
Figure A.24 – ^{1}H NMR of **3.24** recorded in CDCl$_3$ at 400 MHz
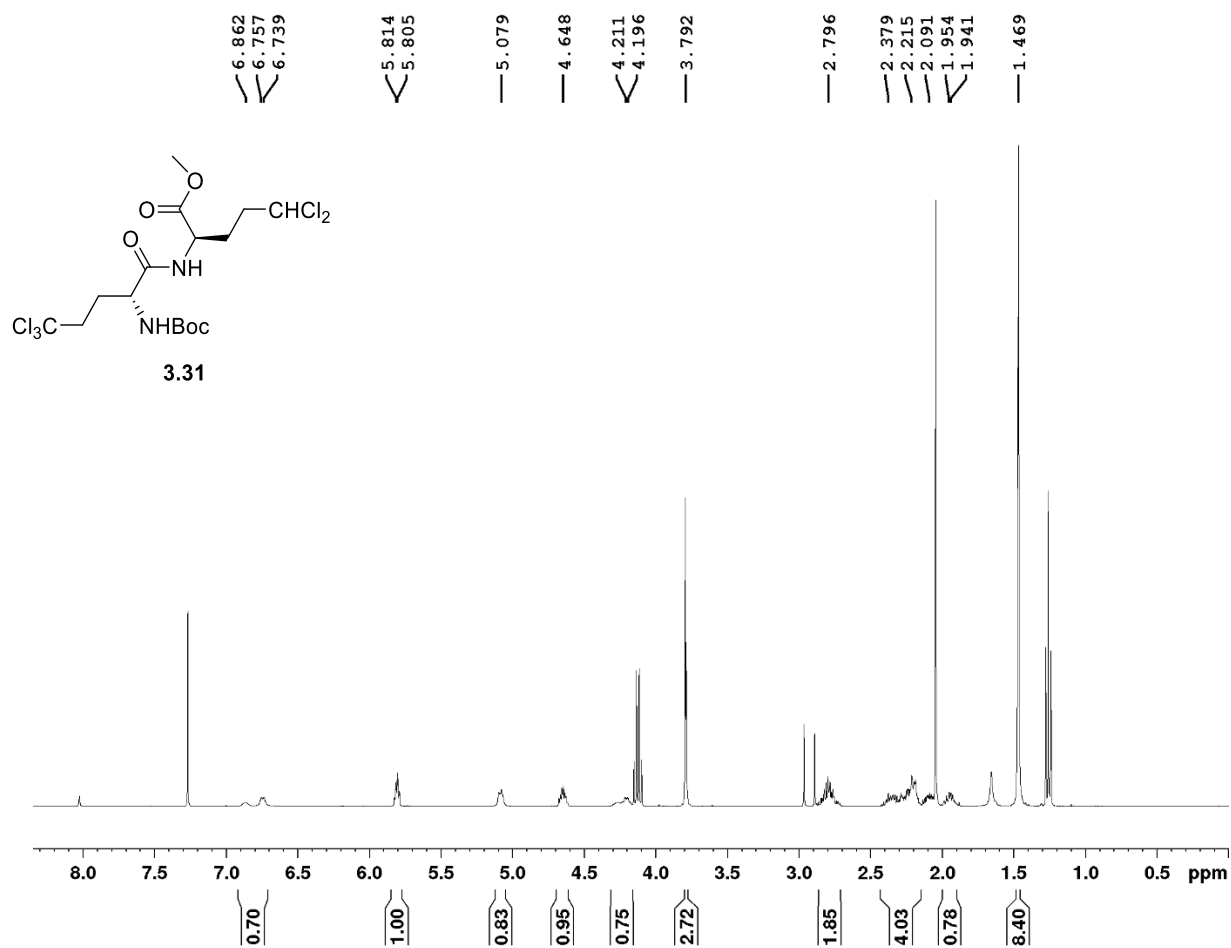
Figure A.25 – ^{1}H NMR of **3.31** recorded in CDCl$_3$ at 400 MHz
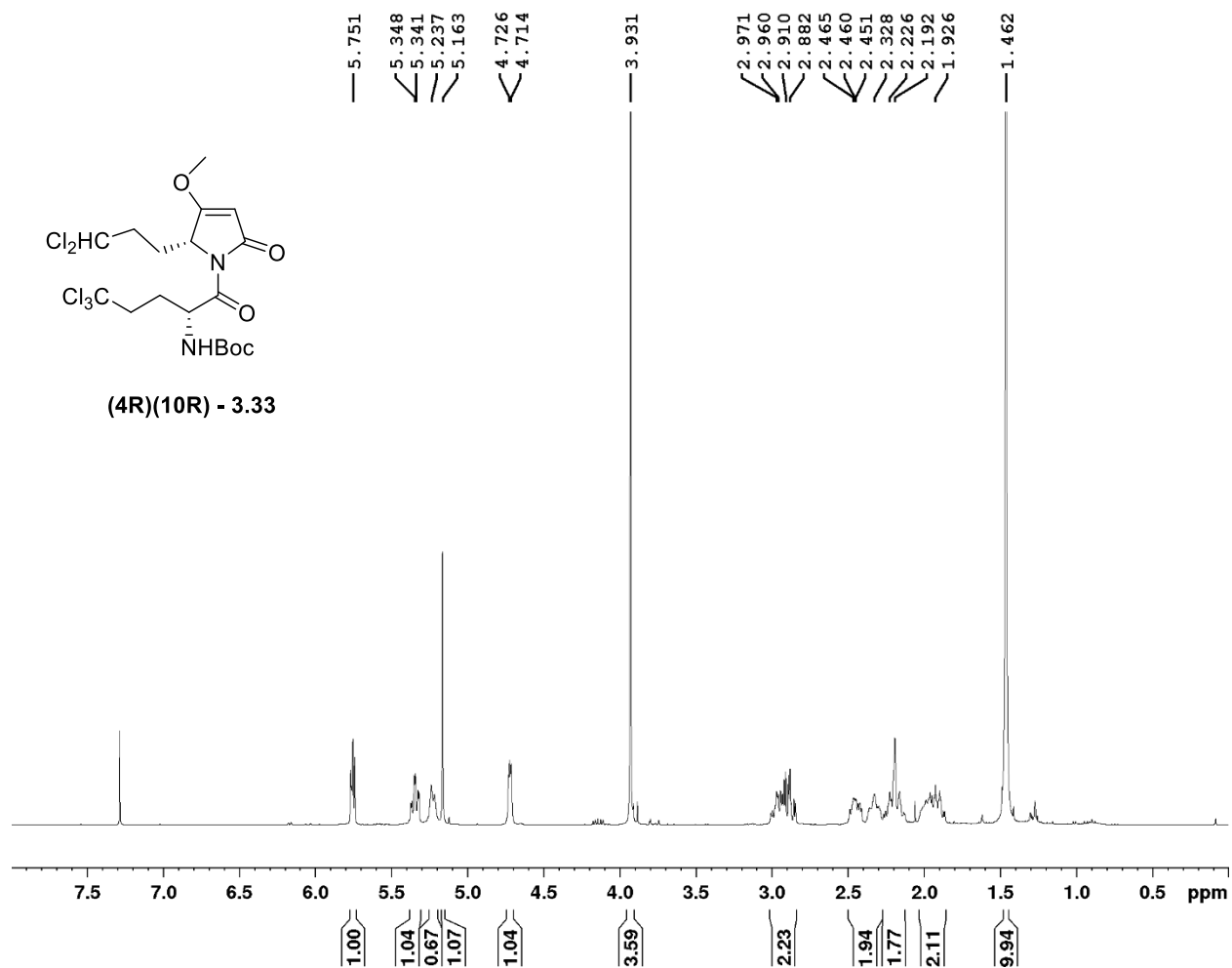
Figure A.26 – ^{1}H NMR of **3.33** recorded in CDCl$_3$ at 400 MHz
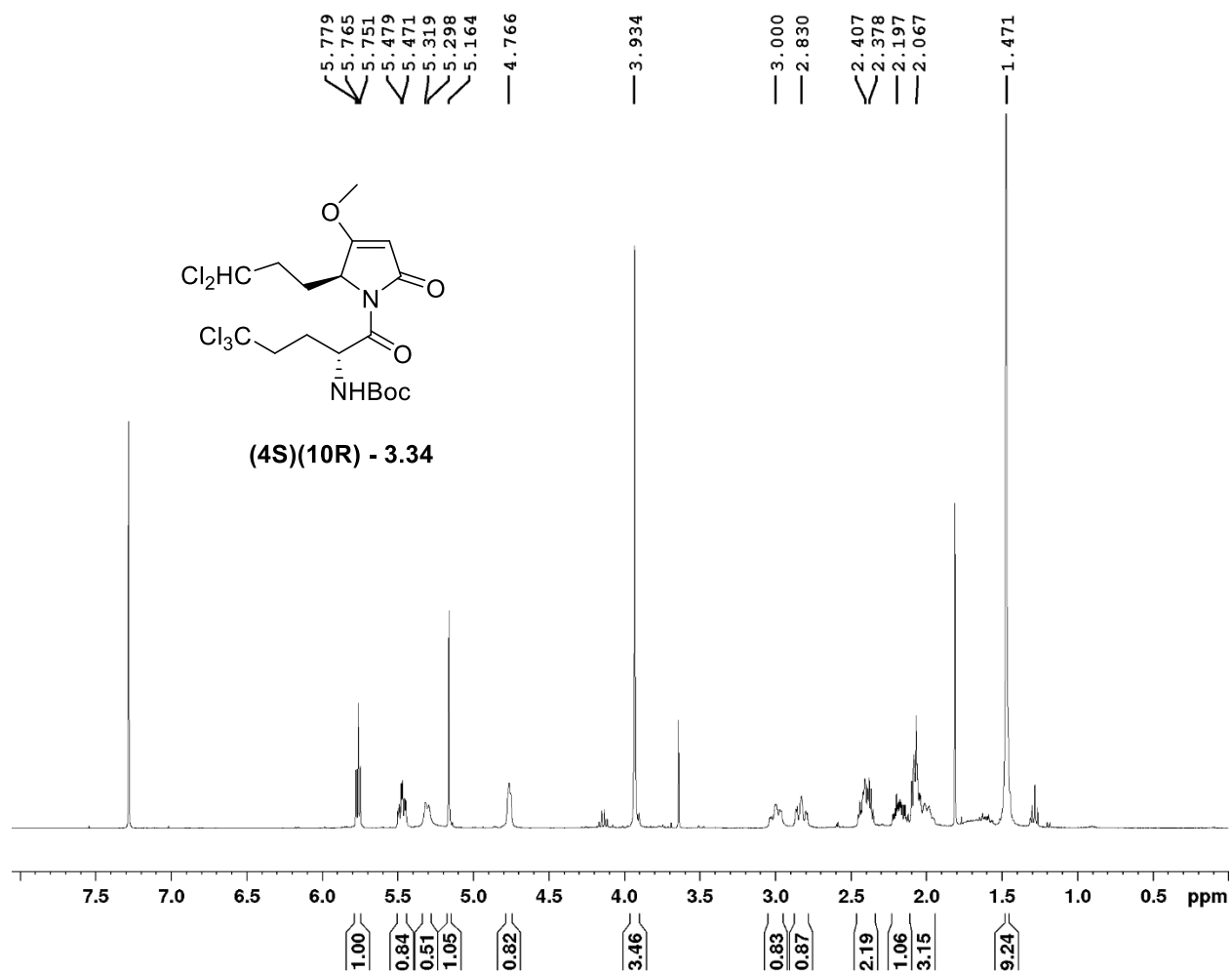
Figure A.27 – ^{1}H NMR of **3.34** recorded in CDCl$_3$ at 400 MHz
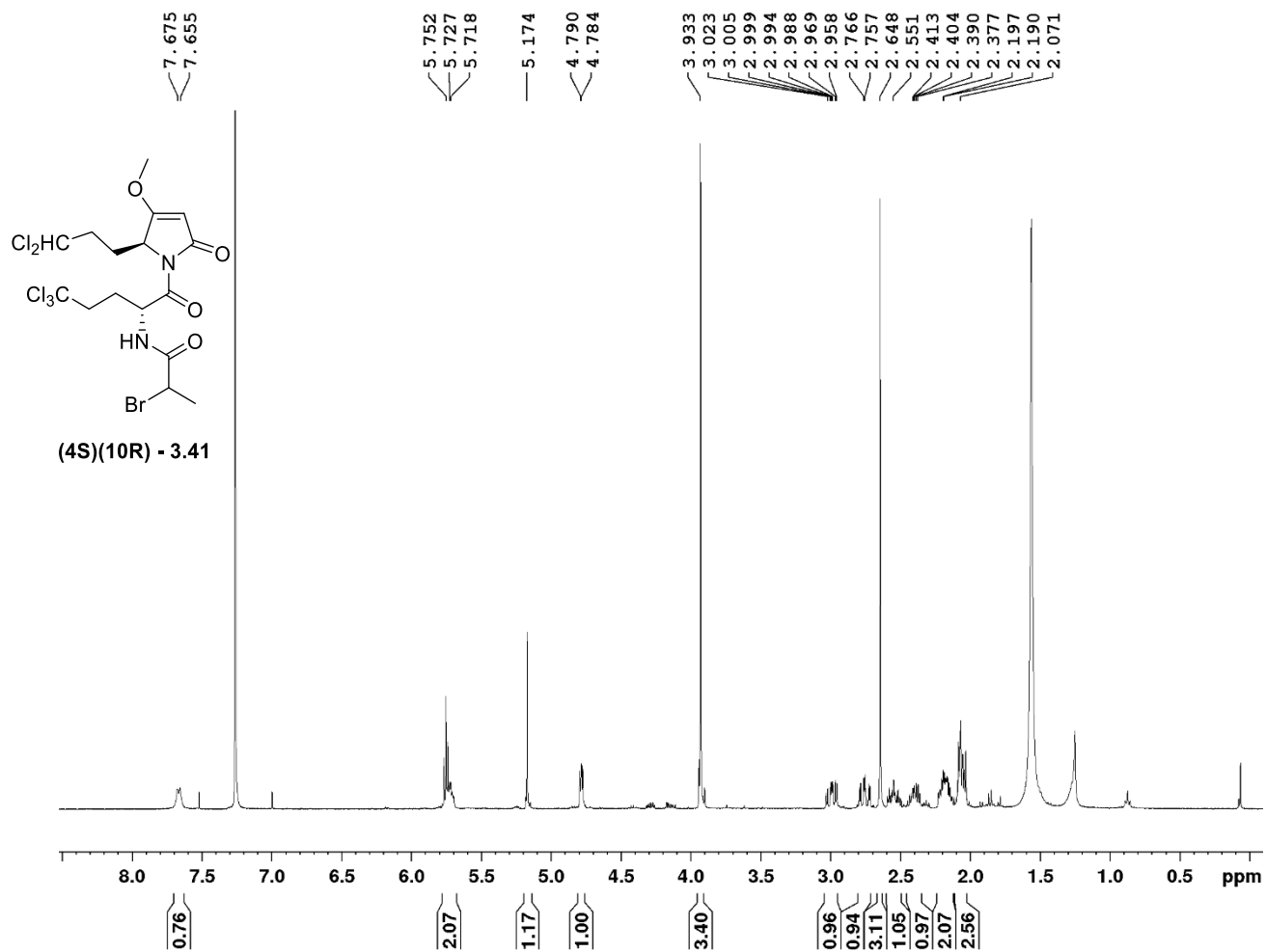
Figure A.28– ^{1}H NMR of **3.41** recorded in CDCl$_3$ at 400 MHz
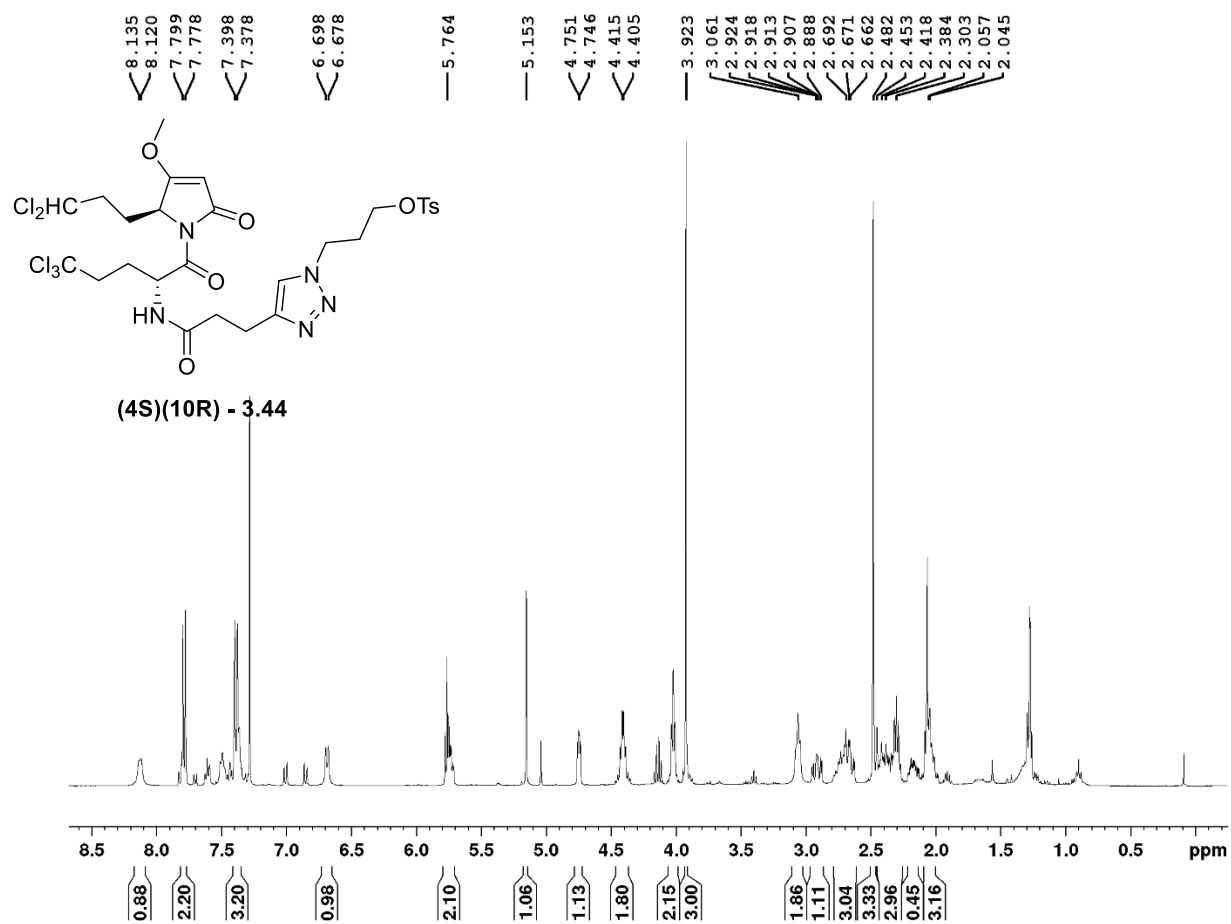
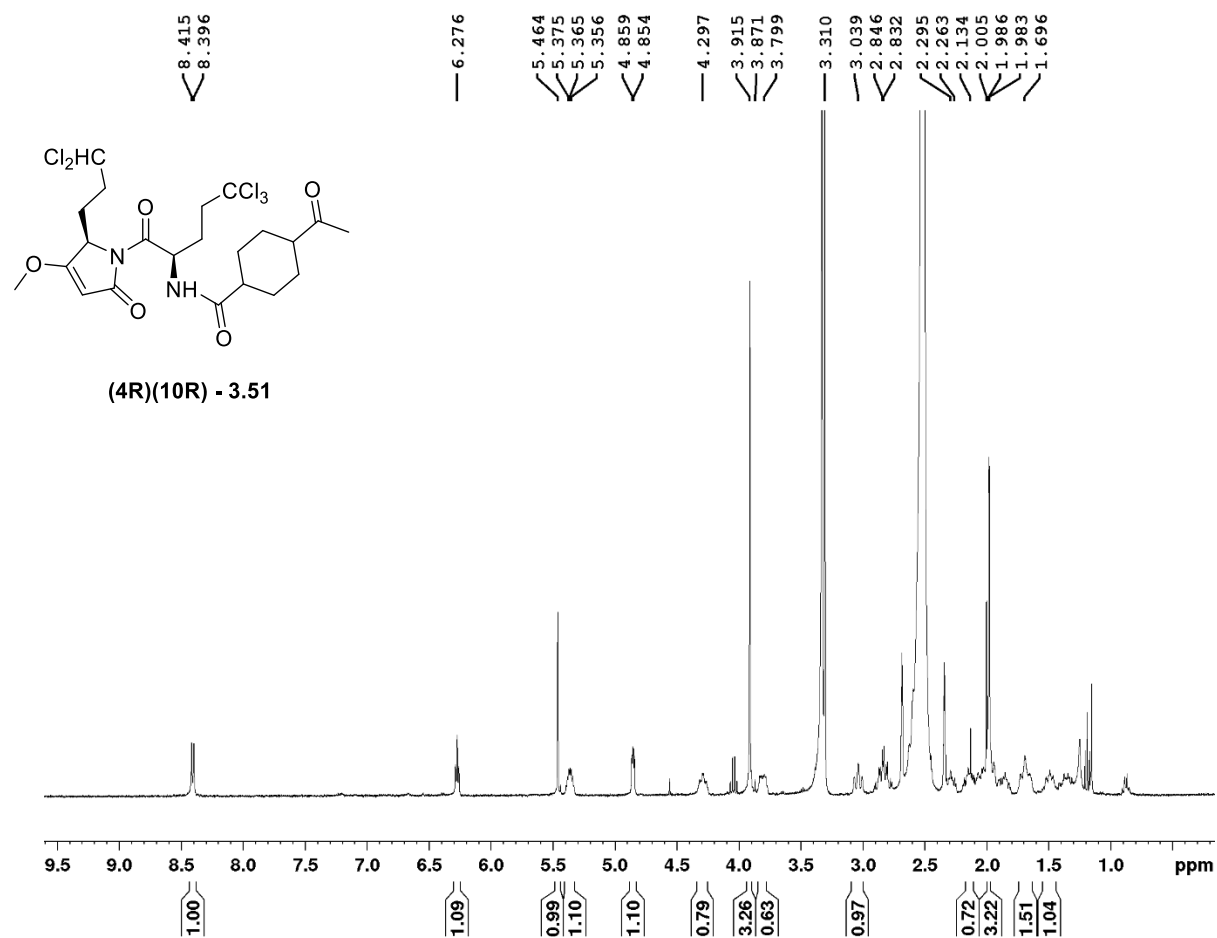**Figure A.29**– ^{1}H NMR of **3.44** recorded in CDCl$_3$ at 400 MHz

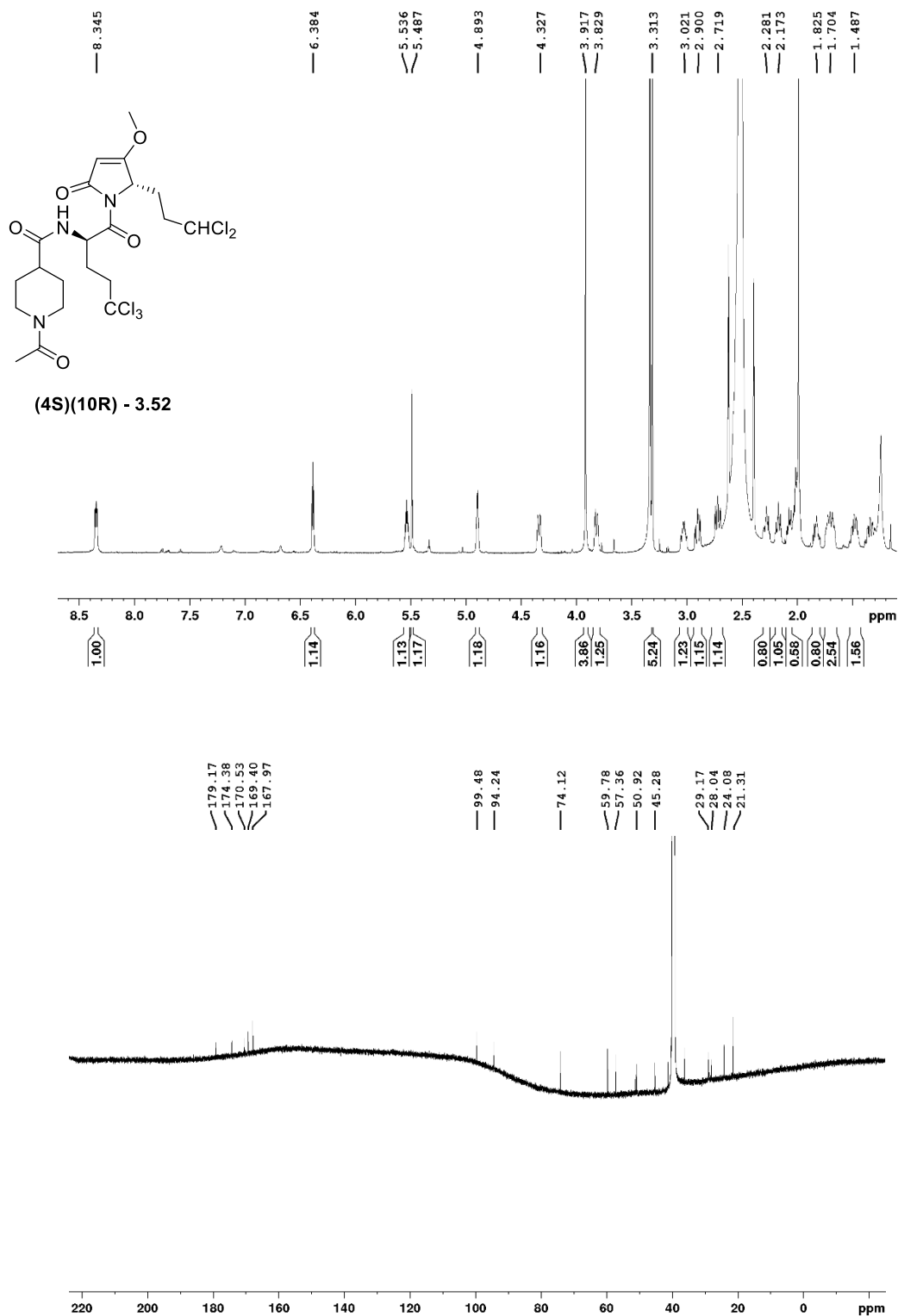**Figure A.30–** ^{1}H NMR of **3.51** recorded in DMSO-d$_6$ at 400 MHz

Figure A.31– ¹H, ¹³C NMR of **3.52** recorded in DMSO-d$_6$ at 600 MHz and 150 MHz respectively
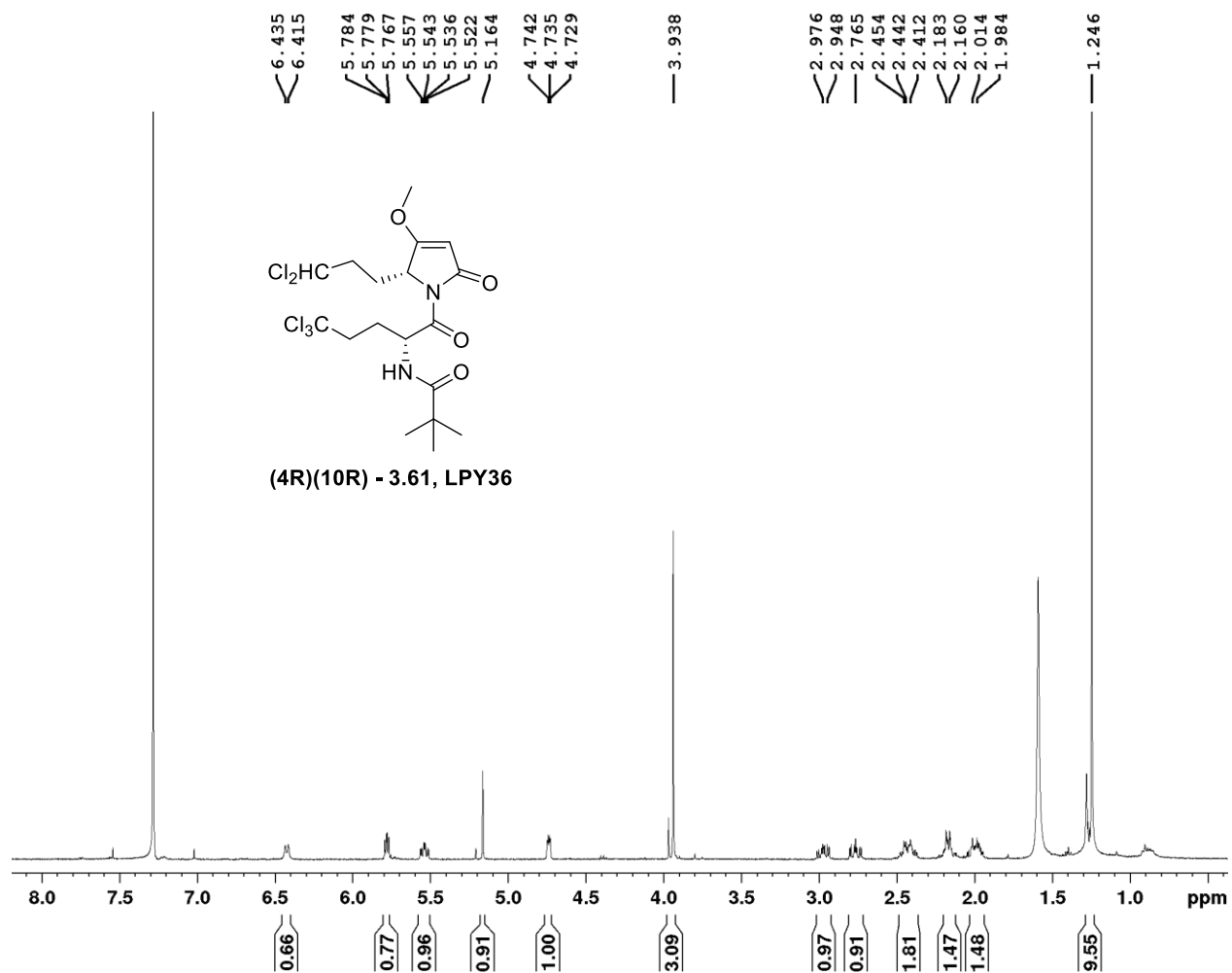
168

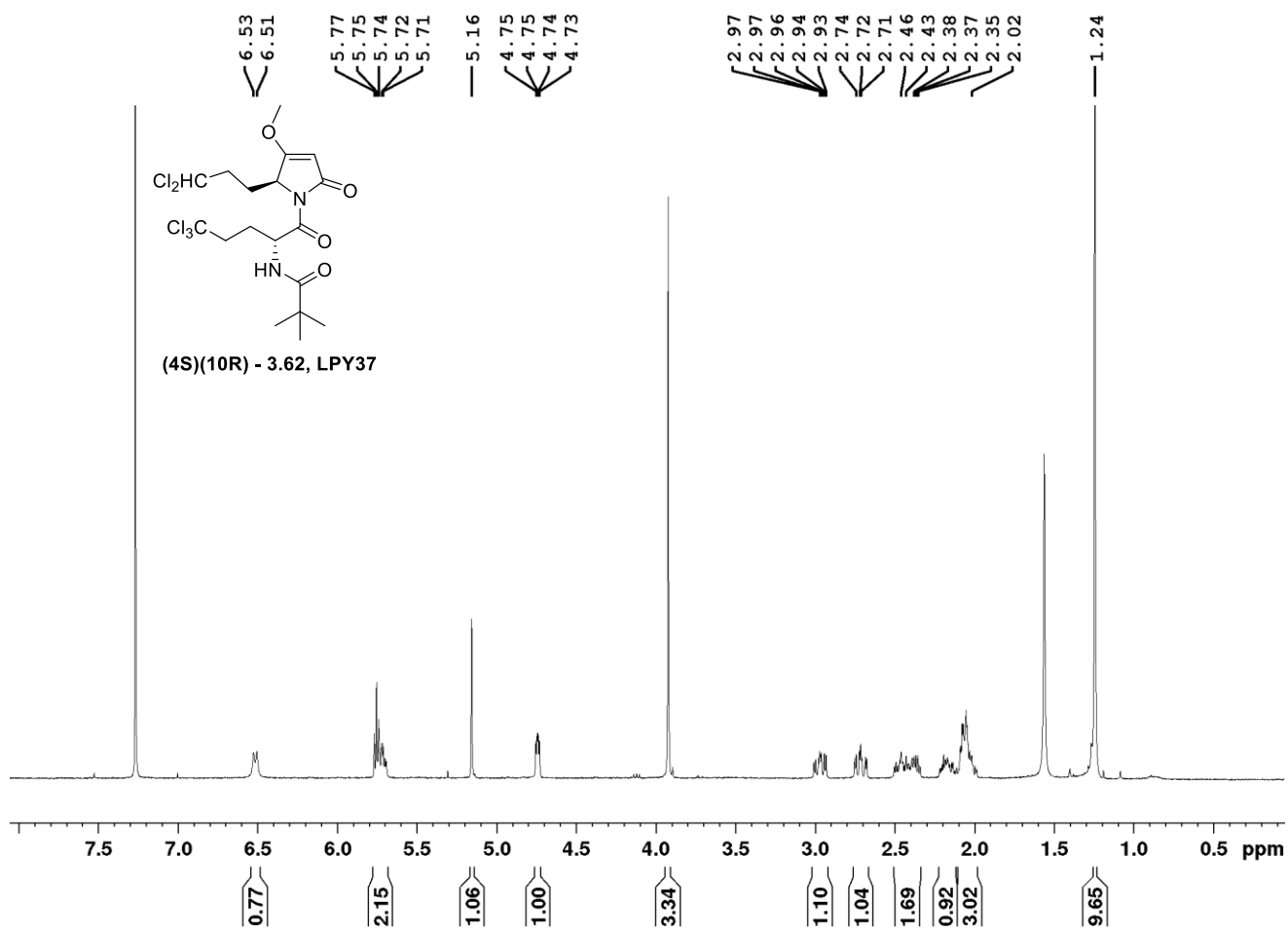**Figure A.32–** ^{1}H NMR of **3.61** recorded in CDCl$_3$ at 400 MHz

Figure A.33– ^{1}H NMR of **3.62** recorded in CDCl$_3$ at 400 MHz